

University of Southampton Research Repository ePrints Soton

Copyright © and Moral Rights for this thesis are retained by the author and/or other copyright owners. A copy can be downloaded for personal non-commercial research or study, without prior permission or charge. This thesis cannot be reproduced or quoted extensively from without first obtaining permission in writing from the copyright holder/s. The content must not be changed in any way or sold commercially in any format or medium without the formal permission of the copyright holders.

When referring to this work, full bibliographic details including the author, title, awarding institution and date of the thesis must be given e.g.

AUTHOR (year of submission) "Full thesis title", University of Southampton, name of the University School or Department, PhD Thesis, pagination

UNIVERSITY OF SOUTHAMPTON

FACULTY OF ENGINEERING AND THE ENVIRONMENT

Fluid Structure Interactions Research Group

**Identifying race time benefits of best practice in freestyle swimming
using simulation**

by

Angus Webb

Thesis for the degree of Doctor of Philosophy

June 2013

UNIVERSITY OF SOUTHAMPTON

ABSTRACT

FACULTY OF ENGINEERING AND THE ENVIRONMENT

Fluid Structure Interactions

Thesis for the degree of Doctor of Philosophy

Identifying race time benefits of best practice in freestyle swimming using simulation

Angus Webb

In the preparation of a swimmer for a race, it is not currently possible to determine the race time impacts of changes to equipment or technique. This study addresses this problem, by modelling the resistive and propulsive forces experienced by a swimmer, throughout the various phases of a race, to predict race time.

Swimming resistance is quantified for surface and underwater swimming, across a population of swimmers, using computational methods and bespoke measurement equipment. Due to the low repeatability, when measuring swimming resistance, statistical methods are utilised to quantify confidence in the measured data. For five repeat tests a 1.8% difference in swimming resistance can be resolved with 95% confidence. Arm propulsion is modelled, treating the arm as a single element moving through the water, producing drag. Leg propulsion is modelled using Large Amplitude Elongated Body Theory originally derived by Lighthill to predict the propulsion generated by fish. This enables freestyle flutter kick, when swimming on the surface, and underwater undulatory swimming, after the start and turn, to be modelled. Input motion for both arm and leg propulsion is determined from manual digitisation of video data, providing the body kinematics of a kick and the time accurate arm speed. Accurate swimming speed for a given stroke rate is achieved by comparing the simulated output with experimental data and scaling the arm and leg parameters. Using a race phase algorithm, the swimming speed for each phase of a swimming race is simulated.

To simulate fatigue, metabolic energy sources are considered. Both maximum power and energy capacity, for aerobic and anaerobic energy sources, are determined from literature. Using PI control of stroke rate, swimming fatigue is simulated by ensuring the propulsive power does not exceed the total available power from the energy model. Therefore, as a swimmer progresses through a race, the available power depletes, causing stroke rate and hence swimming speed to decay.

Combining these models, enables simulation of swimming speed and fatigue throughout a race, from which race time is predicted. The race time impact of changes to swimming resistance and propulsion are investigated. Resistance and propulsion changes from equipment, drafting and technique are quantified experimentally. A 9.5% reduction in swimming resistance, affecting the whole race or underwater phases only, has been found to improve a 100 m race time by 2.75s or 0.99s respectively.

Table of Contents

ABSTRACT.....	iii
Table of Contents.....	i
List of Tables	v
List of Figures	vii
DECLARATION OF AUTHORSHIP.....	xv
Acknowledgements.....	i
Glossary	iii
Nomenclature	v
1 Introduction	1
1.1 Background and Motivation	1
1.2 Aims and Objectives	2
1.2.1 Currently Unanswered Questions.....	2
1.2.2 Objectives	3
1.2.3 Limitations	3
1.3 Project SwimSIM	3
1.4 The Sport of Swimming.....	7
1.4.1 A Typical Swimming Race	7
1.4.2 Swimming Equipment.....	7
1.5 Parameterisation and Constraints of Human Swimming	8
1.6 Current Publications	11
1.7 Structure of Thesis	12
2 Literature Review.....	15
2.1 Introduction	15
2.2 Hydrodynamic Resistance Theory	16
2.2.1 Wave Resistance.....	17
2.2.2 Skin Friction Resistance	20
2.2.3 Viscous Pressure Resistance	22
2.2.4 Added Mass	24
2.3 Resistance of a Human Swimmer	25
2.3.1 Passive Resistance.....	25
2.3.2 Resistance Components in swimming.....	28
2.3.3 Active Resistance.....	33

2.4	Propulsion of a Human Swimmer.....	37
2.4.1	Overview of Propulsion	37
2.4.2	Arm Propulsion.....	37
2.4.3	Leg Propulsion.....	40
2.5	Swimming Fatigue.....	46
2.5.1	Race Analysis.....	46
2.5.2	Bioenergetics Theory	46
2.5.3	Exhaustion Studies	48
2.6	Simulation	50
2.6.1	Swimmer Force Model.....	51
2.6.2	Modelling and Simulation - Validation and Verification	52
2.7	Summary	54
3	Race Simulation	57
3.1	Introduction.....	57
3.2	Model Requirements and Aims	58
3.3	Modelling a swimming race.....	58
3.4	Modelling Motion	61
3.4.1	Time Step Model.....	61
3.4.2	Motion in Surge	62
3.5	Computational Approach	63
3.6	Resistance Model	65
3.7	Arm Propulsion	65
3.7.1	Model	65
3.7.2	Input Motion.....	68
3.7.3	Numerical Implementation.....	70
3.7.4	Stroke Imbalance	72
3.8	Implementation of Large Amplitude Elongated Body Theory.....	75
3.8.1	Numerical Interpretation of LAEBT	75
3.8.2	Capturing the motion of the body.....	78
3.9	Modelling Fatigue	82
3.10	Summary	84
4	Methods of measuring Resistance and Propulsion	87
4.1	Introduction.....	87
4.2	Tow System	88
4.2.1	Design.....	88
4.2.2	Calibration	92
4.2.3	Tow Procedure.....	92
4.3	Predicting Resistance from Deceleration Measurements	94

4.3.1	System Design and Measurement Procedure.....	95
4.4	Measuring changes in Resistance.....	98
4.4.1	Drag Shorts Repeatability Study.....	98
4.4.2	Statistical Analysis of Measurements	99
4.4.3	Drag Shorts Study Results	102
4.5	Summary.....	107
5	Swimming Resistance Model.....	109
5.1	Introduction	109
5.2	Total Passive Resistance	110
5.2.1	Results	110
5.3	Wave Resistance	113
5.3.1	Thin Ship Theory for Swimmer Wave Resistance.....	113
5.3.2	Results	115
5.3.3	Submersion Model.....	117
5.4	Skin Friction Resistance	118
5.5	Viscous Pressure Resistance	119
5.6	Passive Resistance Prediction.....	121
5.6.1	Resistance Uncertainty	121
5.6.2	Comparison with experimental data	122
5.7	Active Resistance Model.....	124
5.7.1	Velocity Perturbation Method	124
5.7.2	Naval Architecture Based Approach to Predict Active Drag	125
5.7.3	Results	127
5.8	Added Mass.....	129
5.9	Summary.....	129
6	Simulation Setup and Validation.....	131
6.1	Introduction	131
6.2	Simulation Convergence	132
6.2.1	Time Step Convergence.....	132
6.2.2	Strip Length Convergence.....	133
6.3	Simulating a tow.....	133
6.4	Comparison of Simulated and Experimental R-T.....	134
6.5	Arm Model Setup and Validation	137
6.6	LAEBT Setup and Validation	141
6.6.1	Underwater Undulatory Swimming.....	141
6.6.2	Freestyle Flutter Kick.....	146
6.7	Stroke Reconstruction.....	150
6.8	Free swim Speed.....	155

6.9	Effect of a resistance augment on speed	159
6.10	Race Reconstruction	164
6.11	Simulation Uncertainty.....	167
6.12	Energy Model.....	168
6.13	Summary	173
7	Simulation Case Studies	175
7.1	Introduction.....	175
7.2	Question 1: Resistance Reduction	176
7.2.1	Simulated Resistance Reduction.....	176
7.2.2	Hair Removal	179
7.2.3	Suit Testing	181
7.2.4	Good Cap – Bad Cap	185
7.3	Question 2: Technique	186
7.3.1	Simulated Imbalances	186
7.4	Question 3: Pacing strategy	188
7.5	Question 4: The Effect of Drafting.....	190
7.6	Summary	193
8	Conclusions	197
8.1	Simulation	197
8.2	Simulation Setup and Validation.....	201
8.3	Simulation Case Studies	204
8.4	Closing Remarks	205
	Appendices	207
	Appendix 1	207
	Appendix 2.....	233
	Appendix 3.....	241
	Appendix 4.....	243
	Appendix 5.....	245
	References	253

List of Tables

Table 2.1. Passive Drag determined from CFD (Bixler et al., 2007).....	27
Table 2.2. Drag results presented for 40 male swimmers in the prone position at a range of depths and speeds.	29
Table 2.3. Summary of Metabolic Energy Systems used to create muscle contraction	48
Table 4.1. Mean resistance coefficient data determined for male participants, with and without drag shorts for both push-off glide and passive tow experiments.....	102
Table 4.2. Mean resistance coefficient data determined for female participants, with and without drag shorts for both push-off glide and passive tow experiments.....	102
Table 5.1. Geometry dimensions used to determine wave resistance from Thin Ship Theory.	114
Table 5.2. Passive and Active drag prediction results using the NABA and VPM.	128
Table 6.1. Comparison of experimental and simulated mean R-T data for freestyle over speed tows.....	151
Table 6.2. Results of a timed free swim test at maximum effort with and without the chute.....	160
Table 6.3. Simulated free swim velocity with and without a 41.4% increase in total resistance.	161
Table 6.4. Simulated free swim velocity, with increased simulated resistance, with and without a 41.4% increase in total resistance.	163
Table 7.1. Mean resistance coefficient data determined for hirsute and glabrous conditions for both push-off glide and passive tow experiments	180
Table 7.2. Simulated race time and work done for a 10000 m freestyle race.	193

List of Figures

Figure 1.1. 50m Freestyle World Record Progression	1
Figure 1.2. Data acquisition of an athlete performing freestyle.....	6
Figure 1.3. Feedback of data being presented to athlete and coach by Jonty Skinner, minutes after the end of a run.....	6
Figure 1.4. FINA approved equipment used in competition.....	8
Figure 1.5. Histogram of heights and masses for participants involved in this study.....	9
Figure 1.6. Anthropometric data related to height (Winter, 1979).	10
Figure 1.7. Human planes and directions of movement (NASA, 1978).....	11
Figure 2.1. Resistance component breakdown of body moving at a constant speed on the free surface (Molland et al., 2011).....	16
Figure 2.2. Numerically predicted Kelvin Wave System using Thin Ship Theory	17
Figure 2.3. Boundary layer separation due to adverse pressure gradient (Anderson, 1985).....	22
Figure 2.4. Viscous pressure drag for elliptical sections of varying aspect ratio (Hoerner, 1965)	23
Figure 2.5. Compiled passive tow data (Kolmogorov and Duplishcheva, 1992)	26
Figure 2.6. Passive drag data (Mason et al., 2010).	26
Figure 2.7. Passive drag data (Takagi, 1998).	27
Figure 2.8. Drag results for a mannequin towed at a range of depths and speeds (Vennell et al., 2006).....	28
Figure 2.9. Effect of sinkage on the wave pattern resistance speed relationship (Taunton et al., 2012).	30

Figure 2.10. Effect of surface penetration on wave resistance (Taunton et al., 2012).....	31
Figure 2.11. Wave resistance decay with sinkage (Taunton et al., 2012).	31
Figure 2.12. CFD study of a submerged swimmer in the prone streamlined position, displaying the components of resistance (Bixler et al., 2007).....	33
Figure 2.13. Categories of fish kinematics (Hoar and Randall, 1978).....	41
Figure 2.14. Axis System and velocity calculation for Large amplitude elongated body theory (Lighthill, 1971).....	43
Figure 2.15. Rate of change of momentum is calculated in volume surrounding fish bounded by plane Π (Lighthill, 1971).....	44
Figure 2.16. Race strategy for sprint and long distance male freestyle events. Fatigue is dominant in the 100m event, while race tactics appear dominant in 400m event.	46
Figure 2.17. Fluid forces acting on each segment in SWUM (Nakashima et al., 2007).....	51
Figure 2.18. Simulation Model Verification and Validation in the Modelling Process(Robinson, 1997a)	53
Figure 3.1. Male freestyle race phase contributions. Race distance is displayed above each pie chart.	59
Figure 3.2. Race Phase Algorithm..	60
Figure 3.3. Race Simulation Process.....	64
Figure 3.4. Arm free body diagram.....	66
Figure 3.5. Generating two dimensional arm motion data from manual digitisation of video data footage.....	68
Figure 3.6. Fitting process to determine the arm motion in the <i>out of water</i> phase which is not captured by video data.	69

Figure 3.7. Rate of change of arm angle throughout a stroke cycle.....	70
Figure 3.8, Defined arm angle, from interpolation of the arm angle data, and back calculated arm angle; confirming the correct implementation of arm angle.....	71
Figure 3.9. Arm motion graphics display how an imbalance is modelled without changing the stroke rate. In both cases the red arm rotates at the same speed.	74
Figure 3.10. Motion and orientation of an infinitely thin strip of length da and width S , extending latterly through the swimmer (into the page), used to describe the motion of a swimmer during UUS	76
Figure 3.11. Definition of strip orientation	76
Figure 3.12. Body segments in the sagittal plane.....	78
Figure 3.13. Manual Digitisation to determine body segment motion during UUS.	79
Figure 3.14. Raw and filtered $x_{a,t}$ data for a single strip on the body. Noise is associated with error in the selection of the segment end points in the manual digitisation process.	80
Figure 3.15. UUS kinematic data determined from manual digitisation of an elite female athlete performing UUS.....	81
Figure 3.16. Freestyle flutter kick kinematics	81
Figure 3.17: Human Energy System diagram.....	83
Figure 4.1. Tow system design.	88
Figure 4.2. Tow system.	89
Figure 4.3. Moving camera system.	90
Figure 4.4. Tow system setup.....	91
Figure 4.5. Voltage response to applied mass..	92

Figure 4.6, Passive tow to determine surface phase passive resistance	93
Figure 4.7, Resistance of a swimmer during a passive and active tow,.	94
Figure 4.8. Velocity profile measured during a push-off glide experiment.....	96
Figure 4.9. Speed measurement system setup.	97
Figure 4.10. Drag Shorts used to provide drag change to compare push-off glide and passive tow experiments.....	99
Figure 4.11. How a P-Value is determined from a distribution according to H_0 in a permutation significance test (Hesterberg et al., 2010).....	100
Figure 4.12. Process to generate a bootstrap distribution..	101
Figure 4.13. Process used to generate the permutation distribution from permutation samples..	101
Figure 4.14. Bootstrapped distributions for each participant displaying the resistance change from drag shorts for both methods..	104
Figure 4.15. Permutation test results comparing the data for with and without drag shorts for each participant and each method.....	106
Figure 5.1. Passive resistance for male and female participants determined from surface and underwater towing.....	112
Figure 5.2. Geometry used in Thin Ship Theory to determine the wave resistance of a swimmer.....	114
Figure 5.3. Predicted wave surface profile.....	116
Figure 5.4. Above water image of subject O during surface passive tow, identifying the wave pattern.....	116
Figure 5.5. Underwater image of subject O during a surface passive tow, identifying the wave pattern.....	116
Figure 5.6. Wave resistance coefficient determined for a range of speeds and body geometries identified in table 5.1.	117

Figure 5.7. Scale factor to adjust wave resistance due to sinkage.	118
Figure 5.8. Skin friction coefficient for a range of heights and velocities determined using the ITTC 1957 correlation line (Clements, 1959).	119
Figure 5.9. Viscous pressure resistance for males and females, surface and underwater: determined by deducting friction resistance and wave resistance from the measured total passive resistance.	120
Figure 5.10. Surface resistance prediction for male swimmer of height 1.79 m and mass 75 kg.	123
Figure 5.11. Underwater resistance prediction for a male swimmer of height 1.79 m and mass 75 kg..	123
Figure 6.1. Convergence study of time step dt , for an arms only and UUS simulation, based on the mean self-propulsion velocity.	133
Figure 6.2. Convergence study of arm strip length dr , for an arms only simulation, based on the mean self-propulsion.	133
Figure 6.3. Experimental and Simulated R-T data for Athlete O during an arms only over-speed tow at 2.02 m s^{-1}	136
Figure 6.4. Simulated R-T after filtering in comparison to the experimental R-T data.	137
Figure 6.5. Comparison of experimental and simulated $R-T$	140
Figure 6.6. Experimental and simulated R-T data for two UUS kick cycles	144
Figure 6.7. Experimental and simulated R-T data for two UUS kick cycles. The simulated thrust is determined from LAEBT using the rate of change of momentum in the wake and body reaction forces..	145
Figure 6.8. Experimental and simulated R-T of two swimmers performing flutter kick.	148
Figure 6.9. Experimental and simulated R-T of two swimmers performing flutter kick. The simulated thrust is determined from LAEBT	

using the rate of change of momentum in the wake and body reaction forces.....	149
Figure 6.10. Simulating a six beat freestyle technique using the arm and the LAEBT propulsion models compared with video data	150
Figure 6.11. Experimental and simulated R-T data of five swimmers performing freestyle during an over speed tow.....	153
Figure 6.12. Experimental and filtered simulated R-T data of five swimmers performing freestyle during an over speed tow.	154
Figure 6.13. Stroke rate and velocity data, from race analysis of athletes, in a world championship final, for all male freestyle events..	157
Figure 6.14. Stroke rate and velocity data, from race analysis of athletes, in a world championship final, for all female freestyle events.....	158
Figure 6.15. Drag chute used to apply an additional known resistance to the swimmer.....	159
Figure 6.16. Resistance coefficient of an individual athlete with and without a drag chute, determined from passive towing.....	160
Figure 6.17. Simulated stroke rate sweep and resulting V/n values for with and without the 41.4% increase in resistance.	161
Figure 6.18. Passive and active towing to determine baseline conditions during the chute testing.....	162
Figure 6.19. Simulated stroke rate and velocity for a female during 200 m freestyle race (top plot). This is compared to actual race data for same female (middle plot). To achieve the correct simulated race time, arm width is increased (bottom plot).	166
Figure 6.20. Comparison of split times from the simulated and actual race.	167
Figure 6.21. Control process used to ensure the propulsive power does not exceed the maximum available power.....	169

Figure 6.22. Simulated energy contribution from aerobic and anaerobic metabolic sources during a maximal effort swim over 600 seconds.....	170
Figure 6.23. Comparison of simulated and real race decay of stroke rate and velocity due to fatigue.	172
Figure 7.1. Male and female simulated 100 m freestyle race for a range of resistance changes..	178
Figure 7.2. From left to right, 1. Chest – Hirsute, 2. Chest – Glabrous, 3. Back – Hirsute, 4. Back – Glabrous	179
Figure 7.3. Bootstrapped distributions for Hirsute and Glabrous conditions for passive tow and push-off glide methods.	180
Figure 7.4. Permutation test results comparing the data for Hirsute and Glabrous conditions for passive tow and push-off glide methods.	181
Figure 7.5. Boot strap distributions of the resistance coefficients determined using the push-off glide experiment for male and female participants wearing various suits.....	182
Figure 7.6. Permutation distributions, comparing each suit condition tested for the male participant.....	183
Figure 7.7. Permutation distributions, comparing each suit condition tested for the female participant.....	184
Figure 7.8. Bad cap and goggle arrangement (top) compared to good cap and goggle arrangement (bottom).	185
Figure 7.9. Bootstrap mean distributions of good and bad cap and goggle arrangement (left), and permutation distribution comparing both conditions.	186
Figure 7.10. Simulated race time savings for a range of imbalance coefficients, with and without fatigue modelling.....	188
Figure 7.11. Pacing strategies used for the male and female 200 m freestyle race simulation..	189

- Figure 7.12. Simulated race time (s) and work done (KJ) for the various stroke gradients for the male (left) and female (right) swimmer. 190
- Figure 7.13. Lead swimmer (right) and drafting swimmer (left). The drafting swimmer is being towed with R-T measured and the lead swimmer is free swimming..... 191
- Figure 7.14. Bootstrapped distributions of the measured R-T for free swimming and the two drafting conditions (left). Permutation test, identifying the confidence in the measured difference between the open water condition and drafting with the head at the hips. 192

DECLARATION OF AUTHORSHIP

I, Angus Webb declare that the thesis entitled “Identifying race time benefits of best practice in freestyle swimming using simulation” and the work presented in the thesis are both my own, and have been generated by me as the result of my own original research.

I confirm that:

- this work was done wholly or mainly while in candidature for a research degree at this University;
- where any part of this thesis has previously been submitted for a degree or any other qualification at this University or any other institution, this has been clearly stated;
- where I have consulted the published work of others, this is always clearly attributed;
- where I have quoted from the work of others, the source is always given. With the exception of such quotations, this thesis is entirely my own work;
- I have acknowledged all main sources of help;
- where the thesis is based on work done by myself jointly with others, I have made clear exactly what was done by others and what I have contributed myself;
- parts of this work have been published as:
 1. Webb, A., Banks, J., Phillips, C., Hudson, D., Taunton, D., Turnock, S., 2011. Prediction of passive and active drag in swimming. *Procedia Engineering* 13, 133–140.
 2. Webb, A., Phillips, C., Hudson, D., Turnock, S., 2012. Can Lighthill’s Elongated Body Theory Predict Hydrodynamic Forces in Underwater Undulatory Swimming? *Procedia Engineering* 34, 724–729.

Signed:

Date:.....

Acknowledgements

I express sincere gratitude to my supervisors, Professor Stephen Turnock and Dr Dominic Hudson, whose encouragement, guidance and experience made the completion of this thesis possible. I am very grateful for the help of Dr Dominic Taunton, Dr Alexander Forrester and Dr James Blake, who provided robust academic expertise and support throughout my PhD. I am extremely lucky to have collaborated with Joseph Banks and Christopher Phillips, where as a team, we had lots of fun and achieved a great deal as a result of our collaboration. I look forward to continuing involvement with them through future SwimSIM activities.

The whole SwimSIM project owes thanks to Dr Scott Drawer, who had the vision to award UK Sport Innovation funding, which enabled this research to be possible.

It was a privilege to work with the immensely dedicated individuals at British Swimming: Jonty Skinner, Jodi Cossor, Clare Lobb, Andrew Logan, and the coaches, who were imperative to work in this thesis. The help from colleagues in times of need, especially George Crammond, was most fulfilling. The support of Michael Ellis was greatly appreciated and whose efforts made my life significantly easier.

I thank Lindsay Smith, my beautiful girlfriend, for her unfathomable encouragement and support throughout the whole process.

My greatest appreciation goes to my parents, Stewart and Valerie Webb, whose support and sacrifice throughout my entire education has made this thesis possible. I dedicate this work to them.

Glossary

Active – Active swimming is when a swimmer is generating propulsion.

A/D – Analogue to digital conversion

Aerobic – Energy source which uses oxygen. Low power high capacity.

Anaerobic – Energy source which does not use oxygen. high power low capacity.

CAD – Computer Aided Design

CFD – Computational Fluid Dynamics

Drag/Resistance – Both drag and resistance are treated as the same force throughout this study.

FINA - The International Swimming Federation

Intervention – A change to a swimmers technique or equipment to seek an improvement in performance.

ITTC Correlation Line – An empirical formula used to estimate skin friction resistance coefficient.

Kicking Frequency (Hz) – Kicking cycles per second. This metric adopts SI units since kicking rate is not communicated by the swimming community.

LAEBT – Large amplitude elongated body theory (Lighthill, 1971).

LED – Light emitting diode

LVDT – Linearly Varying Displacement Transducer

MAD – Measurement of Active Drag system developed by Hollander et al.(1986)

NABA – Naval architecture based approach to estimating active drag. Based on a self-propulsion experiment.

P Value – A value describing the proportion of data in a distribution. Used to communicate confidence in measured changes.

Passive – Passive swimming is when a swimmer is not generating propulsion

PI – Proportional Integral control, used to control stroke rate when modelling fatigue.

PIV – Particle Image Velocimetry

PLC – Programmable Logic Controller

Propulsion/Thrust – Both propulsion and thrust are treated as the same force throughout this study.

RPM – Revolutions per minute

R-T – Resistance minus thrust. The force measured during active towing.

Stroke Rate (cycles/min) – Number of arm cycles per minute, defining the arm stroke rate. Uses cycles/min since this is the metric used by the swimming community.

Subject lettering – All participants involved in this study and individuals whose data has been extracted from the internet have been anatomised using letter and number code. The format of these letters and numbers varies due to the different studies the data has been extracted. However, the individual's name is not crucial, it is the height, mass and gender that are important parameters considered in this study.

SwimSIM – Swimming Simulation project, to which this study is a subset.

SWUM – SWimming hUman Model (Nakashima et al., 2007).

Surge Motion – motion in the forwards and backwards direction.

UUS – Underwater undulatory swimming or dolphin kick.

VPM – Velocity perturbation method. This method is used to estimate active resistance.

Nomenclature

a – lagrangian coordinate describing distance from the caudal fin, or feet, along the spine of the body

$a(t)$ – Horizontal acceleration (ms^{-2})

C_D – Resistance coefficient. The subscript often denotes the origin of the resistance. Subscript D is total resistance.

dr – Radial strip size used to numerically model the force distribution along the arm (m)

dt – Time step (s)

$e(t)$ – PI error

E_a – Aerobic energy (J)

E_{an} – Anaerobic energy (J)

f – Frequency (Hz)

F_p – power factor

Fr – Froude number

Fr_{Body} – Reaction force from the body component of large amplitude elongated body theory

Fr_{Total} – Total reaction force from large amplitude elongated body theory

Fr_{wake} – Reaction force from the wake component of large amplitude elongated body theory

g – Acceleration due to gravity (ms^{-2})

H – Height (m)

i – Index value used to describe time stepping of simulated variables

J – Advance Ratio

L – length (m)

m – Added mass per unit length

n – Arm cycle frequency (Hz)

P_a – Aerobic power (Watts)

P_{an} – Anaerobic power (Watts)

P_{Body} – Propulsive power from the body component of large amplitude elongated body theory

P_{Total} – Total propulsive power from large amplitude elongated body theory

P_{wake} – Propulsive power from the wake component of large amplitude elongated body theory

r – Radial distance from axis of rotation of the arm (m)

R – Resistance (N). A subscript often denotes the origin of the resistance. Subscripts T, V, W and F represent total, viscous pressure, wave and friction resistance.

Re – Reynolds number

S – Area (m²)

$s(t)$ – Horizontal distance travelled (m)

St – Strouhal number

t – Time (s)

$(1-t)$ – Thrust deduction

T – Propulsion (N)

T_{Stroke} – Stroke period (s)

T_x – Swimmer propulsion (N)

(u, w) – Body axis horizontal and vertical velocity components

V – Velocity or speed (ms⁻¹)

W – Mass (kg)

W_{th} - Arm width (m)

(x, z) - Space axis coordinates representing the horizontal and vertical axis.

$\dot{\alpha}$ - Rotational arm speed ($\text{deg}\cdot\text{s}^{-1}$)

λ - Large amplitude elongated body theory kinematic phase angle (rad)

∇ - Volume (m^3)

ρ - Density ($\text{kg}\cdot\text{m}^{-3}$)

ν - Kinematic viscosity ($\text{kg}\cdot\text{s}^{-1}\cdot\text{m}^{-1}$)

1 Introduction

1.1 Background and Motivation

Elite swimming is a highly competitive sport. At London 2012 the time separating first and last place in the eight man 50 m freestyle final was 0.64s (21.98-21.34s). These margins highlight that to be successful in swimming, it is important to understand the factors that relate to performance, and how they can be changed. The complexity of the forces acting on a swimmer during a race, coupled with the physiological response of the swimmer, present a significant challenge.

Prior to the 2008 Beijing Olympics, new swimsuit developments provided a step change in performance, due to a significant reduction in swimming resistance (figure 1.1). The unnatural progression in performance caused FINA (Fédération Internationale de Natation) to ban the latest generation suits, resulting in the immediate reduction of swimming performance. With the majority of science practiced by British Swimming being physiology, these circumstances identified the importance of understanding the fluid dynamics around a swimmer, prompting a hydrodynamics research programme.

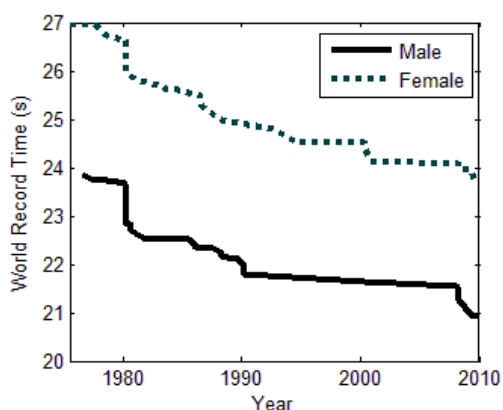


Figure 1.1. 50m Freestyle World Record Progression (Wikipedia). A 2% improvement in race time was achieved in 2008/2009 with new suit developments.

The performance convergence experienced prior to 2008 (figure 1.1), suggests that without a technological breakthrough or the arrival of genetically gifted swimmers (e.g. Michael Phelps & Ian Thorpe), finding a competitive advantage is becoming increasingly difficult. It is therefore necessary to take advantage of

Introduction

every small improvement that is practically possible. Identifying these improvements and the effect they have on performance requires the use of advanced measurement and simulation methods

The approach adopted by this thesis is based on naval architecture theory originally developed to determine ship resistance and propulsion. Measurement techniques are developed to determine the resistive and propulsive forces acting on a swimmer. These methods are used to identify how resistance can be reduced and propulsion increased, within the capabilities of a human swimmer, to increasing swimming performance. Simulation is used to understand the impact these forces have on swimming speed and race time. This also acts as a valuable tool when communicating the research to swimmers and coaches, where time to cover a set distance is the metric used by the sport of swimming.

1.2 Aims and Objectives

The aim of this thesis is to simulate the relationship between the race time achieved by a swimmer and both the resistive and propulsive forces. Using this knowledge, a further aim is to quantify real changes in swimming resistance and propulsion, and to determine the race time impacts.

1.2.1 Currently Unanswered Questions

This study will aim to provide a process in which the following questions can be addressed. To date these questions have remained un-answered in British Swimming.

1. What is the race time effect of resistance reduction? How can resistance reduction be achieved?
2. What are the race time implications of an imbalance in the propulsion from the left and right arms?
3. What is the best pacing strategy?
4. In open water swimming drafting is possible. What are the benefits in terms of work done?

1.2.2 Objectives

1. Determine a suitable architecture for a mathematical race model
2. Identify how swimming resistance, propulsion and the effects of fatigue may be modelled.
3. Construct experimental equipment to measure swimming resistance and propulsion.
4. Using experimental resistance data for a population of swimmers, supplemented by computational analysis, determine the swimming resistance components for a range of heights and weights. Use this model to predict total resistance for any height and weight, on the surface and underwater.
5. Combining the resistance and propulsion models simulate the correct swimming speed throughout a race for a range of swimmers.
6. Validate the simulation output by comparing the simulated forces and motions to real data.
7. Perform measurements of changes to swimming resistance and propulsion and use the simulation to identify the race time effects of these changes and different race strategies.

1.2.3 Limitations

To ensure that the above questions can be answered with confidence, freestyle is the only swimming stroke considered in this study. This is due to the large amount of experimental data gathered for this stroke. In addition, freestyle is performed in the most competition events. Future developments to the models generated in this study may enable the remaining strokes to be investigated.

1.3 Project SwimSIM

This study is part of a wider project, sponsored by UK Sport and working with British Swimming, with the aim to increase the race performance of podium potential swimmers. The project began in September 2009 with three PhD students, each focusing on a specific area of swimming research. In addition to this study the two other PhD projects are:

Introduction

1. Phillips, C., 2013 'Musculoskeletal Modelling of Human Swimming for Technique and Performance Evaluation'.
2. Banks, J., 2013 'Modelling the propelled resistance of a freestyle swimmer using Computational Fluid Dynamics'.

All three PhD students have collaborated to develop equipment and testing methods, to analyse the hydrodynamic performance of swimmers. The equipment developed, all being portable, includes: a tow system to measure swimming resistance over a range of speeds, a speed measurement system (measures the speed of a thin line attached to the swimmer), wave elevation measurement, and a sensor network to measure three-dimensional body kinematics. Data acquired from these three systems is synchronised with video footage of the swimmer. One minute after an acquisition, the data is presented to the test subject. This system has provided both a research tool, to support the PhD projects, and also a rich learning environment for athletes and coaches.

This system has been developed over three years in conjunction with British Swimming. A key member of project SwimSIM is Jonty Skinner, who was appointed as technical advisor to British Swimming for 2009-2012. As an ex world record holder (100 m freestyle, 1976) and a coaching specialist, his involvement has bridged the gap between the engineering data and de facto improvement of swimming technique.

In total, project SwimSIM has tested 103 participants over 1725 measurement runs. This includes 40 out of the 44 athletes in the London 2012 Olympic team. British Swimming has received a second portable towing system, designed by the SwimSIM project, to be used at Intensive Training Centres around the UK.

Not all work conducted by SwimSIM has contributed directly to the aims of this study, however, involvement with British Swimming has provided scope for the testing programme. Therefore, as a by-product, equipment, testing procedures and improved knowledge of swimming hydrodynamics has been gained.

Ethical approval has been provided by the ethics committee of the Faculty of Engineering and the Environment (Approval Number: RGO7207). This covers

the measurements conducted on swimmers, the acquisition of film and still photography, and both storage and sharing of data with British Swimming.

Beyond London 2012, project SwimSIM will receive continued support by British Swimming and UK Sport. Two new PhD students have been recruited to continue the research and provide assistance to British Swimming for the next Olympic cycle. The three initial PhD students will remain in the department in a Post-Doctoral capacity, providing assistance to the new PhD students, while continuing their individual research interests.

Introduction



Figure 1.2. Data acquisition of an athlete performing freestyle. The tow system is seen bottom left and a moving camera being pushed on the right.



Figure 1.3. Feedback of data being presented to athlete and coach by Jonty Skinner, minutes after the end of a run.

1.4 The Sport of Swimming

1.4.1 A Typical Swimming Race

Swimming at the Olympic Games is performed in a 50m long swimming pool, in individual lanes, over a range of distances and with different strokes. The swimming strokes are Freestyle, Backstroke, Butterfly, Breaststroke and Medley (all four strokes). A swimming race may be broken down into the following phases,

1. Start
2. Underwater swim (after start and each turn)
3. Surface swim
4. Turn
5. Finish,

where 2-4 is repeated depending on race distance.

For freestyle the swimmer starts out of the water on starting block roughly 0.6 m above the water surface. After a dive the swimmer can enter the water up to 3.5 meters from the start of the pool. Depending on the race distance, the number of surface and turn phases will vary. At the end of each length, a tumble turn is performed and the swimmer pushes off the wall underwater. The underwater swim phase is performed after the start and each turn. In this phase a swimmer will perform underwater undulatory swimming (UUS or dolphin kick). The underwater swim phase is limited to 15 meters; however, due to fatigue or chosen strategy, the swimmer may surface before 15 meters.

An open water event, over a distance of 10000 meters, is also performed. A strategic difference from lane swimming is the interaction between the swimmers. This can provide an advantage to swimmers who draft behind those swimming in front. There are no turns or underwater swimming; instead, swimmers swim round buoys, on an effectively oval track.

1.4.2 Swimming Equipment

The equipment used by athletes in a swimming race is governed by FINA (FINA, 2011). Three main items of equipment used by all athletes are: a suit, cap and goggles (figure 1.4). The maximum suit coverage for males is significantly less

Introduction

than for females, where in 2008 suit coverage rules were equal. This has limited the scope of suit design in males. The materials suits are made from are restricted by a maximum thickness of 0.8 mm and a minimum permeability of $80 \text{ Lm}^{-2}\text{S}^{-1}$. A complete suit must provide less than 0.5 N of buoyancy during a suit-only submersion test. Suits used in open water swimming for men and women are restricted in coverage to the neck, shoulders and ankles. All suits used in competition must be approved by FINA at the beginning of the year of competition (FINA, 2011).

Caps are defined as an independent item and cannot be attached to the suit or goggles. The shape of the cap must follow the natural form of the head. The surface should not include any artificial shaping. Goggles must also be an independent item, but no other rules apply (FINA, 2011). In open water swimming cap and goggles rules are the same.



Figure 1.4. FINA approved equipment used in competition.

1.5 Parameterisation and Constraints of Human Swimming

The parameters used to describe a swimmer are consistent throughout this study. In naval architecture, length (m) and displacement (tonnes) are two key parameters. In this study swimmer height (m) and mass (kg) are used. Height is defined as the distance between the floor and the top of a swimmers head when standing naturally. Mass is measured using standard pan scales. Figure 1.5 identifies the range of participant height and mass involved in this study. The height and mass range for analysis will therefore be 1.6-1.9 m and 40-100 kg respectively. Of the 103 participants tested by project SwimSIM, in total 22

male and 22 female participants are involved in the studies throughout this thesis.

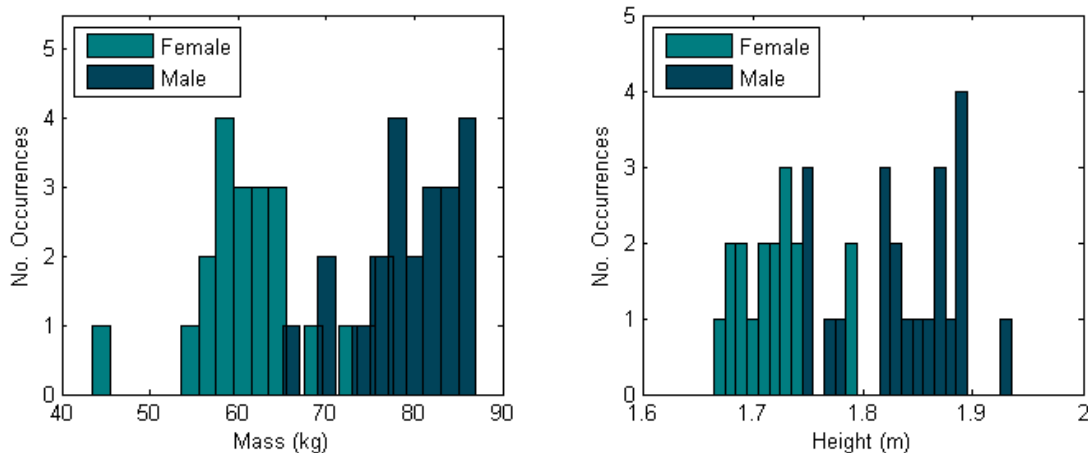


Figure 1.5. Histogram of heights and masses for participants involved in this study.

Surface area is an important parameter affecting resistance. The surface area of a human may be described as,

$$S = 0.20247H^{0.725}W^{0.425}, \quad (1.1)$$

where H is height (m) and W is mass (kg) (DuBois, 1916). This formula has been developed by measuring the dimensions of body segments, on nine participants, from which surface area is determined. It is the most commonly used formula, however has been found to be inaccurate for children (Shuter and Aslani, 2000; Verbraecken et al., 2006). Since this study mainly deals with fully grown swimmers, this inaccuracy is not considered problematic.

Body volume is determined as,

$$\nabla = \frac{W}{\rho_{Human}}, \quad (1.2)$$

where ρ_{Human} is the density of a human, taken to be 1060 kgm^{-3} and 1043 kgm^{-3} for males and females respectively (Krzywicki and Chinn, 1966; M. L. Pollock et al., 1975).

The slenderness ratio is a non-dimensional value used to describe the shape of a swimmer. Slenderness is defined as,

Introduction

$$\text{slenderness} = \frac{H}{\sqrt[3]{1}} \quad (1.3)$$

Other anthropometric information such as limb length can be determined from published data (figure 1.6). However this data is not gender specific.

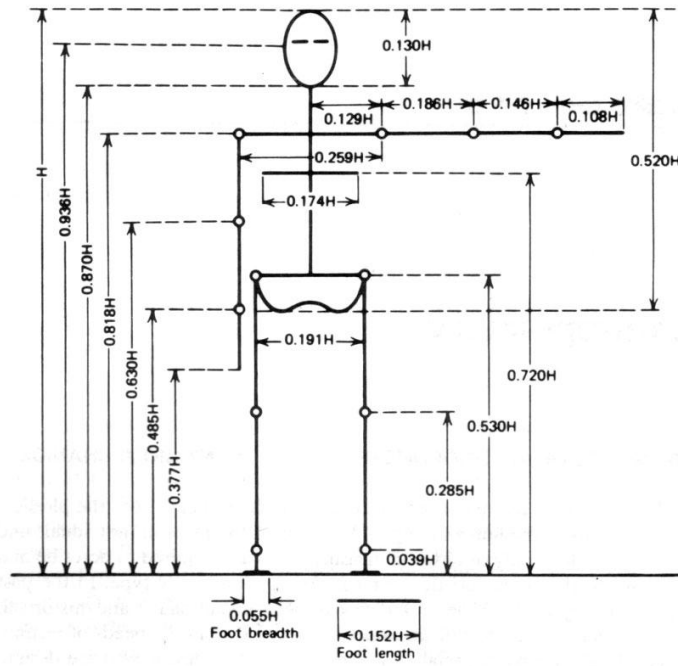


Figure 1.6. Anthropometric data related to height (Winter, 1979).

By considering swimming speeds achieved during a race, the maximum swimming speed on the surface is 2.6 m s^{-1} , experienced during a male 50 m freestyle sprint. Therefore the analysis of surface swimming will be performed for a speed range of $0\text{--}3 \text{ m s}^{-1}$. Maximum underwater speeds are greater, due to the speeds achieved after a dive and push-off. Lyttle (1999) found the maximum push-off speed after a tumble turn to be 3.1 m s^{-1} . However, maximum entry speeds after a dive are as great as 5 m s^{-1} (Cossor and Mason, 2001), therefore the speed range assumed for underwater swimming is $0\text{--}5 \text{ m s}^{-1}$.

When discussing directions and planes of motion the following terms in figure 1.7 will be used.

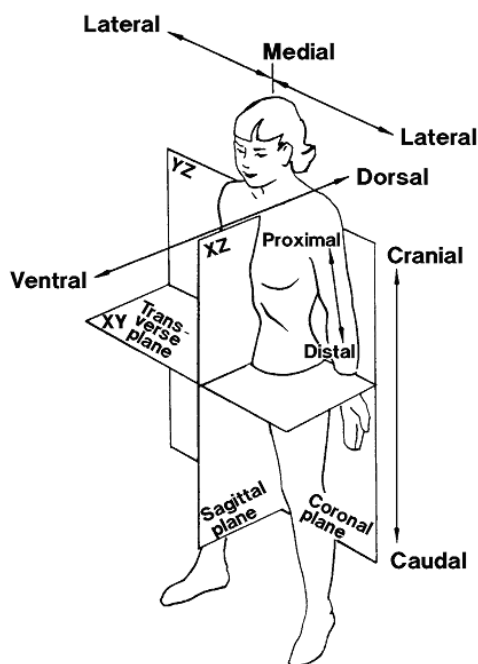


Figure 1.7. Human planes and directions of movement (NASA, 1978).

1.6 Current Publications

Two pieces of work from this study have been published, and a third is to be submitted to a journal in the sports science and engineering field. The first publication was the investigation of swimming active resistance using a naval architecture based approach, where current methods appear to produce variable results. This new method is necessary in the development of the resistance models in Chapter 5. The second publication looks into the use of Large Amplitude Elongated Body Theory (Lighthill, 1971) as a method to predict swimming propulsion from underwater undulatory swimming. This paper outlines the required procedure to determine human swimming propulsion from this theory as conducted in Chapter 3. In addition, it describes the approach used to compare the theoretical results with experimental results, as performed in Chapter 6 of this thesis. The third paper looks into the repeatability and confidence in swimming resistance measurements, using two different measurement approaches. The procedures used in Chapter 7, to determine changes in swimming resistance, are based on the outcomes of this paper.

Introduction

1. Webb, A., Banks, J., Phillips, C., Hudson, D., Taunton, D., Turnock, S., 2011. Prediction of passive and active drag in swimming. *Procedia Engineering* 13, 133–140.
2. Webb, A., Phillips, C., Hudson, D., Turnock, S., 2012. Can Lighthill's Elongated Body Theory Predict Hydrodynamic Forces in Underwater Undulatory Swimming? *Procedia Engineering* 34, 724–729.
3. Webb, A., Turnock, S.R., Hudson, D.A., Forrester, A.J., Taunton, D., 2013. Repeatable techniques for assessing changes in passive swimming resistance. To be submitted to a journal in the sports science and engineering field.

1.7 Structure of Thesis

Utilising methods existing in engineering and naval architecture, this study aims to develop a mathematical model to simulate a swimmer in a race. This will enable the effect of many input parameters which define the swimmer, their equipment and their technique to be understood in the context of race time.

In Chapter 2 a review of naval architecture theory identifies the origin of resistance for a body moving on the free surface and how total resistance is contributed to by individual components. Measurement methods for total resistance and the individual components are detailed.

A review of swimming research identifies the methods used to determine the total resistance of a swimmer and attempts to determine the resistance components of a swimmer. Some initial data are presented. The difficulty of decoupling resistive and propulsive forces is identified. A review of swimming propulsion determines the various methods a swimmer uses to produce thrust throughout a race. Methods of modelling these propulsive forces are detailed.

Simulation methods used in sport to optimise equipment design and athlete technique are investigated. A swimming force model called SWUM (Nakashima et al., 2007) is identified which can determine swimming speed and body segment forces for a self-propelled swimmer. Inaccuracies in the predicted swimming speed suggest that this approach is not appropriate for a race

simulation. No published race time models exist for swimming, and therefore the need to construct a bespoke race time model is identified. A process for validation and verification of a mathematical model is also outlined.

Chapter 3 details the construction of a swimming race simulation. The algorithm used to model a swimming race is explained, identifying the phases which will and will not be physically modelled. The time stepping model and equation of motion used to simulate the motion of a swimmer are described. The requirement to understand the resistance of a swimmer in the various phases of a swimming race is identified. A resistance model which can predict the resistance of any swimmer over a range of swimming speeds is proposed, identifying the need for an independent experimental and computational study. In addition, the propulsion models and their theory, used to simulate the propulsion produced by the arms and the legs, are described.

Chapter 4 details the development of experimental procedures for measurement of swimming resistance and propulsion. This includes the construction of both a tow system and a speed measurement system. The calibration process and protocols to ensure accurate measurements are described. These methods enable both the acquisition of data necessary to develop the resistance and propulsion models, and the capability to measure specific changes to an athlete's resistance and propulsion.

Chapter 5 details the experimental, theoretical and computational study conducted to develop a resistance model. The model can predict surface and underwater swimming resistance, for both males and females, for a range of heights and masses. A novel approach to the prediction of active resistance is detailed and compared to a conventional method.

Chapter 6 covers the setup and validation of the various models, comparing the simulated output with experimental data. The process required to simulate the correct propulsion and swimming speed, to accurately model race time, is detailed. The outputs of the race simulation are compared to race data supplied by British Swimming.

In Chapter 7, using the testing methods and the race simulation, the key questions of this study are investigated.

Introduction

1. A range of resistance changes are simulated and the race time change presented. Specific reductions in swimming resistance are measured experimentally, and the potential race time improvements identified.
2. A range of imbalance severities are simulated and the potential race time improvements identified.
3. Utilising the fatigue model, different pacing strategies are investigated. An optimum pacing strategy is identified based on fastest race time.
4. The effect of drafting is quantified experimentally by towing an athlete behind a lead swimmer. Using the race simulation, a 10000 m race is simulated and the energy differences between drafting and swimming in clear water quantified.

2 Literature Review

2.1 Introduction

In order to perform a review of the swimming resistance literature, it is necessary to consider hydrodynamic resistance theory. Therefore, an overview of resistance theory, as published by Molland et al. (2011), is performed in Section 2.2. This theory provides the necessary understanding of: how resistance components combine to produce the total resistance; the individual components when on the surface and underwater; and the relevant swimmer parameters which affect each component of resistance. The swimming literature is then reviewed in Section 2.3. This outlines the methods and results from various studies, quantifying the individual components and total swimming resistance. Swimming propulsion is reviewed in Section 2.4. This sets out the approach this thesis will use to model the propulsion from the arms and the legs.

The effects of fatigue are a significant contributor to race time (Maglischo, 2002). To improve the fidelity of a race simulation, the maximum propulsive power that can be produced by a swimmer, and the effects of fatigue throughout a race, must be included. Section 2.5 outlines bioenergetics theory, which describes the sources of energy to perform exercise, and how they deplete causing fatigue. Previous studies, investigating maximum power and energy capacity, for a range of male and female athletes, provide the necessary data to construct a fatigue model.

Current simulation techniques are reviewed in Section 2.6. This outlines the use of simulation as a predictive tool in performance sport. A current swimming force model SWUM is reviewed, identifying its shortcomings in accurately modelling swimming speed and inability to model a swimming race. This identifies the need for a new simulation approach. In addition, a procedure for validation and verification of a simulation is proposed.

2.2 Hydrodynamic Resistance Theory

The total hydrodynamic resistance of an object moving, with constant velocity, on the free surface is the contribution of individual components: Friction, Viscous Pressure and Wave (Molland et al., 2011). Figure 2.1 describes how these components combine.

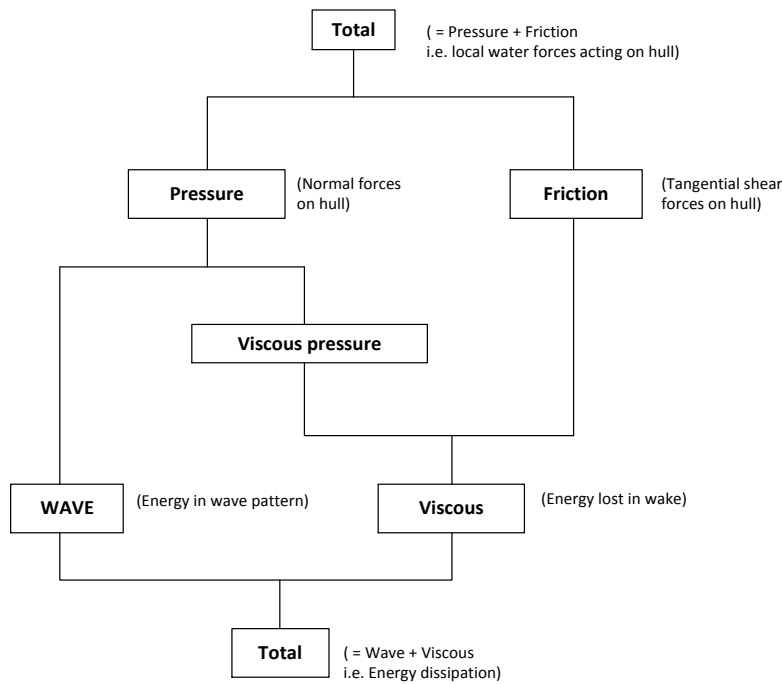


Figure 2.1. Resistance component breakdown of body moving at a constant speed on the free surface (Molland et al., 2011).

The total resistance is therefore expressed as,

$$R_T = R_F + R_V + R_W. \quad (2.1)$$

Because the individual resistance components scale independently, total resistance does not scale with respect to a single parameter. It is therefore necessary to know the contribution from the individual resistance components, to enable scaling of total resistance, for different sizes and shapes of swimmers.

Resistance data is commonly presented in a coefficient (non-dimensional) form. This enables the resistance of an object to be described without the influence of speed, fluid density, or scale. A resistance coefficient is defined as

$$C_D = \frac{R}{1/2 \rho S V^2}, \quad (2.2)$$

where R is the resistance, ρ is the fluid density, S is a representative area and V is speed. The area chosen depends on the origin of the resistance. For friction resistance, the wetted area is used, since the total shear force on a body is directly proportional to the surface area it is acting upon. For pressure resistance, projected area used, since the resistance from a pressure is due to it acting over the area normal to the flow. If a coefficient of total resistance is being calculated, where more than one resistance component is present, the area influencing the dominant component is used.

2.2.1 Wave Resistance

When a body moves through the water, pressure variations occur due to acceleration of the fluid over curvature of the body. These pressure variations cause a disturbance to the free surface in the form of waves, which travel with the body as it moves. Wave resistance occurs as a result of the energy that is dissipated from this pressure field into the wave system.

These waves may be expressed mathematically in the form of a Kelvin wave system, comprised of transverse and divergent waves created by a travelling pressure point. The wave system generated by a geometric shape, such as a ship or a swimmer moving on the free surface, will be governed by high and low pressure along the body. This can be considered as a series of moving pressure points. Figure 2.2 displays an example of a kelvin wave system generated for a three dimensional body moving on the free surface.

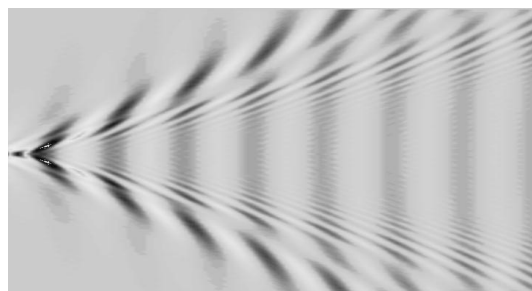


Figure 2.2. Numerically predicted Kelvin Wave System using Thin Ship Theory. With waves being generated at various points along the body, interference of these waves will occur. The phasing of these waves relative to each other changes as the speed of the body changes, and therefore at certain speeds wave interaction will cause constructive or destructive interference. As a result

Literature Review

of this interference the wave resistance of the body oscillates across a range of speeds, causing ‘humps and hollows’ in the resistance curve.

When describing a ships speed in terms of its wave system, Froude number is used,

$$Fr = \frac{V}{\sqrt{gL}}, \quad (2.3)$$

where V is ship speed, g is acceleration due to gravity and L is the wetted length of the ship.

The Froude number identifies the number of waves being generated along the length of a ship. A significant increase in wave resistance is encountered when constructive interference of the bow and the stern waves occurs. This happens at the Froude number range of 0.35 – 0.5 for displacement ships (Tupper and Rawson, 2001). For a swimmer of height 1.95 m and velocity of 2.22 m s⁻¹ (Cesar Cielo Filho 2011 World Championships 50 m Freestyle Final – World Record Swim) gives a Froude number of 0.51. This suggests that swimmers are operating at maximum wave resistance coefficient.

A physical measurement of wave resistance may be performed if wave elevation is known (Gadd and Hogben, 1965; Insel et al., 1994; Newman, 1977). The wave resistance is expressed as,

$$R_W = \frac{1}{4} \rho g b \left\{ (\xi_0^2 + \eta_0^2) + \sum_{n=1}^{\infty} (\xi_n^2 + \eta_n^2) \left[1 - \frac{1}{2} \cos^2 \theta_n \right] \right\}, \quad (2.4)$$

where coefficients ξ_n and η_n can be found from wave pattern elevation measurements.

Wave pattern elevation measurements are performed using one of two methods: a transverse cut or longitudinal cut. A transverse cut involves elevation measurements taken for at least two positions behind the body, moving with the body. Longitudinal cuts are made parallel to the centreline of the body from a stationary position, while the body moves past the wave probes. In the context of measuring wave elevation in a swimming pool, a transverse cut is not practical therefore a longitudinal cut is the favourable technique. The wave elevation for a longitudinal cut is expressed as

$$\zeta = \sum_{n=0}^{\infty} [\xi_n \cos(x\gamma_n \cos \theta_n) + \eta_n \sin(x\gamma_n \cos \theta_n)] \cos\left(\frac{2\pi ny}{b}\right). \quad (2.5)$$

Using the theory of a Kelvin wave system, a method of predicting the wave system of ship, known as ‘Thin Ship Theory,’ was introduced by Michell, 1898 and developed by Insel, 1990. It is assumed the ship hull or swimmer is slender i.e. have a high length to breadth ratio. A wave field may be modelled using the velocity potential of a source located within a domain. To model the wave field of a specific geometry, an assembly of sources and sinks are distributed along a vertical longitudinal plane. To represent the shape of the geometry the individual source strengths are adjusted depending on the form of the geometry at that point. A relationship to determine the source strengths from a geometry divided into panels, is represented as,

$$\sigma = \frac{U_x dx}{2\pi dy} \times A_{Projected}, \quad (2.6)$$

where U_x is the local panel velocity, $\frac{dx}{dy}$ is the local body slope and $A_{Projected}$ is the projected area of the panel in the swimming direction.

The wave system generated by Thin Ship Theory is described using the Eggers series, and the wave resistance of the geometry is determined.

Thin Ship Theory, makes the following assumptions;

1. Potential Flow
2. Surface tension neglected
3. Wave height is small compared to wave length
4. Zero sinkage and trim
5. Geometry advances at a constant velocity

For wave resistance prediction of a swimmer, assumptions 1 to 3 are satisfactory since the fluid conditions experienced by a swimmer are the same as for a model in a towing tank. However the assumption of zero sinkage and trim may be violated during active swimming, which may affect the estimation of wave resistance. The assumption of constant velocity may not apply for free swimming, however, if the swimmer is towed the advance velocity will be

Literature Review

constant. Changes to the swimmer geometry from movement of the limbs may result in the actual wave resistance differing to that predicted by Thin Ship Theory for a fixed geometry.

Wave resistance predictions made using Thin Ship Theory for a swimmer, should be validated from experimental data to ensure that any violation of the above assumptions does not significantly affect the wave field prediction.

2.2.2 Skin Friction Resistance

Skin friction resistance arises from shear stress between the fluid and the surface of the body, resulting in the formation of a boundary layer. The thickness of the boundary layer relates to the magnitude of the shear stress, and is governed by local Reynolds number,

$$Re = \frac{Vl}{\nu} \quad (2.7)$$

where V is velocity, l is the wetted length and ν is the kinematic viscosity of the fluid. At a Reynolds number of roughly 5×10^5 the boundary layer flow transitions from laminar to turbulent. A turbulent boundary layer is thicker than a laminar boundary layer and therefore has greater shear stress (Hoerner, 1965).

The summation of the shear stress over the surface area of the body amounts to the total skin friction. Direct measurement of skin friction involves either measuring the velocity profile in the boundary layer or the shear stress on the surface of the body. This requires devices sufficiently small to prevent disturbance to the fluid flow. These methods are generally difficult and impractical, and are only used for specific fluid shear analysis such as identifying transition from laminar to turbulent flow (Molland et al., 2011).

Another method is to predict skin friction drag based on data from flat plate friction tests. These tests measure the resistance of a flat plate at a range of Reynolds numbers. Skin friction data from these tests is used to approximate the skin friction of a ship. A common method used in naval architecture is the 'ITTC model-ship correlation line' (Clements, 1959). This provides a skin friction coefficient based on a Reynolds number,

$$C_f = \frac{0.075}{(\log(Re) - 2)^2} \quad (2.8)$$

This 'ITTC model-ship correlation line' is used to correlate the skin friction coefficient experienced by a model with that of a ship at a much higher Reynolds number. It also incorporates the effect of form, differentiating it from other flat plat friction lines. This approximation assumes the flow is turbulent.

For laminar flow a similar skin friction formula exists called the Blasius friction line (Blasius, 1908; Dhawan and Engineer, 1953),

$$C_f = \frac{0.664}{\sqrt{Re}} \quad (2.9)$$

Assuming a Reynolds number transition of 5×10^5 (Hoerner, 1965) and a swimmer travelling at 1.8 m s^{-1} , transition will occur at 0.28 m from the leading edge. Therefore assuming the boundary layer remains laminar the Blasius friction line would be required to predict the skin friction coefficient in the head and neck region of a swimmer.

Both the Blasius and ITTC model-ship correlation lines may be used to predict the frictional resistance coefficient of a swimmer. However, since these are approximations it may be better to use a skin friction value determined from a more direct source such as computational fluid dynamics (Date and Turnock, 2000) and use the formulae to predict how this value will vary with Reynolds number (Swimming speed and swimmer height).

The dimensional skin friction resistance is determined from

$$R_f = \frac{1}{2} \rho V^2 S C_f \quad (2.10)$$

where ρ is the density of the fluid, V is velocity and S is the wetted surface area of the swimmer.

Literature Review

2.2.3 Viscous Pressure Resistance

Pressure drag arises from a distribution of forces normal to the body surface (Hoerner, 1965). For non-streamlined bodies separation occurs due to an adverse pressure gradient along steep re-entrant angles on the body (figure 2.3).

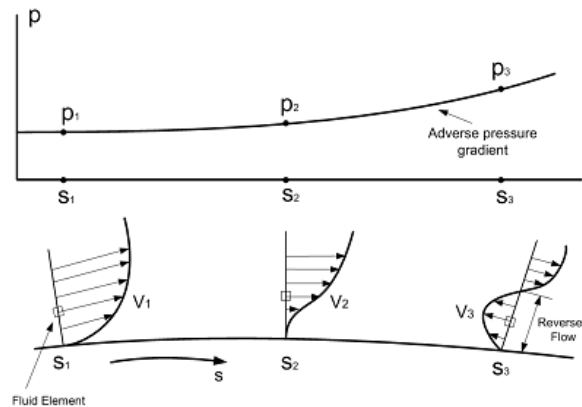


Figure 2.3. Boundary layer separation due to adverse pressure gradient (Anderson, 1985).

The drag associated with this separation contributes to viscous pressure drag. When a body is on the surface, total pressure drag is composed of wave drag and viscous pressure drag. If a body is completely submerged, such that wave drag is zero, total pressure resistance is equal to viscous pressure resistance. Viscous pressure drag is a function of the projected area of the body (Hoerner, 1965).

Measurement of total viscous resistance may be conducted by a wake traverse. A wake traverse measures the total head loss in the wake due to the body upstream (Molland et al., 2011). However a major disadvantage of performing a wake traverse is the experimental time required. This is an unpractical approach to estimating the viscous pressure resistance of a human swimmer. This may explain why no previous research of a wake traverse on a human swimmer exists. A potential solution may be to perform a wake traverse on a human mannequin in a tow tank or wind tunnel. Computational fluid dynamics may also provide an insight into the viscous pressure drag of a swimmer, in a similar manner to its current use in naval architecture (Molland et al., 2011).

Using equation 2.1, it is possible to determine any component of resistance if total resistance is known along with the two other components. This is

performed for residuary resistance in the Froude scaling method (Molland et al., 2011). Towing tank tests are performed to determine total drag, frictional drag is estimated from the ITTC model-ship correlation line, and the deficit is the residuary resistance (primarily wave resistance for slender bodies).

As estimation of viscous pressure resistance may be made based on data published for basic shapes in a range of flow conditions. Hoerner, 1965 published drag coefficient data for elliptical sections with a range of aspect ratios for supercritical and subcritical Reynolds numbers, figure 2.4. If a swimmer torso is regarded as an elliptical section the pressure drag at supercritical Reynolds number may be determined. For a swimmer with torso length of 0.6m and chest depth of 0.25m, giving a length/depth ratio of 2, the drag coefficient in turbulent flow is in the region of 0.2. However it can be seen in figure 2.4, that for low aspect ratio ellipses the drag coefficient is very sensitive to small changes in aspect ratio.

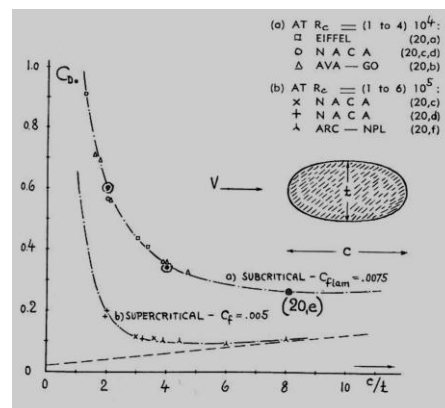


Figure 2.4. Viscous pressure drag for elliptical sections of varying aspect ratio (Hoerner, 1965)

Literature Review

2.2.4 Added Mass

Added mass is an unsteady resistance component, which arises from acceleration of a volume of surrounding fluid. The volume of fluid that is subject to acceleration is dependent on the shape of the body. This volume of fluid is treated as an added mass to the object, therefore providing an additional force when the body accelerates. Through experimentation, added mass coefficients have been determined for a range of shapes. For a two dimensional cylinder, heaving in water of a finite depth, an added mass coefficient of 1.5 has been estimated (Bai, 1977).

2.3 Resistance of a Human Swimmer

2.3.1 Passive Resistance

Passive resistance is the total resistance of a swimmer, when not producing any propulsion, for example during the glide phase after push-off or dive. This condition is the most simple to analyse as the swimmer is in a static position. Passive resistance is generally measured by towing or in a circulating water channel (Kolmogorov and Duplishcheva, 1992; Lyttle and Elliott, 1998; Mason et al., 2007; Takagi, 1998; Vennell et al., 2006). However, computational fluid dynamics is bringing more insight to the problem with its ability to separate the components of resistance (Bixler et al., 2007; Marinho, 2009; Silva and Rouboa, 2008; Zaïdi et al., 2008). The tow systems used to measure swimming resistance, consist of a rotating winch to pull the swimmer at a set velocity and the force is measured using either dynamometry built into the tow cable or the structure of the winch itself. In a circulating water channel the dynamometry is suspended above the moving water and the swimmer is attached to the dynamometry (Naemi et al., 2009). Passive resistance can therefore be measured on the surface or underwater and in both the streamlined or arms by side position.

Kolmogorov and Duplishcheva, (1992) published a large dataset of passive resistance measured by towing swimmers in the 'front gliding position'. It is not known whether this was on the surface or underwater, however it is assumed to be on the surface since these measurements were compared with active drag measurements made on the surface. This dataset, presented in figure 2.5, provides a useful benchmark for other passive resistance measurements. There is a wide spread to the data with a clear trend of increasing passive resistance with velocity. When presented as C_D against $\text{Length}/\text{volume}^{1/3}$ the data becomes more spread out, although displays a trend of less resistance as the body becomes more slender.

Literature Review

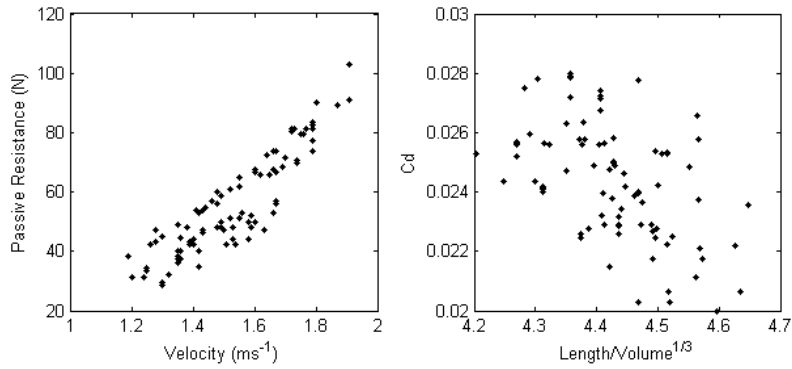


Figure 2.5. Compiled passive tow data (Kolmogorov and Duplishcheva, 1992)

Mason et al., (2010) performed a passive drag study to determine an appropriate fitting procedure for passive drag data (figure 2.6). This process was performed for a large number of athletes, however height and mass data were not published.

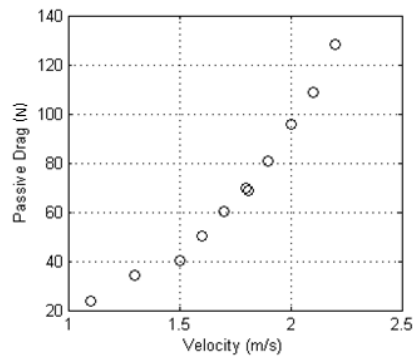


Figure 2.6. Passive drag data figure taken from Mason et al. (2010).

Takagi, (1998) performed passive drag measurements using tethered swimmers in a circulating water channel for a range of speeds (figure 2.7). Resistance was measured using a suspended dynamometry system above the water which the swimmer was attached to with a harness. Swimmer angle of attack was also measured and defined as the angle between the free surface and a line between the shoulders and hips. Little variation in angle of attack for the four tested swimmers was found which may explain the very repeatable results between the swimmers.

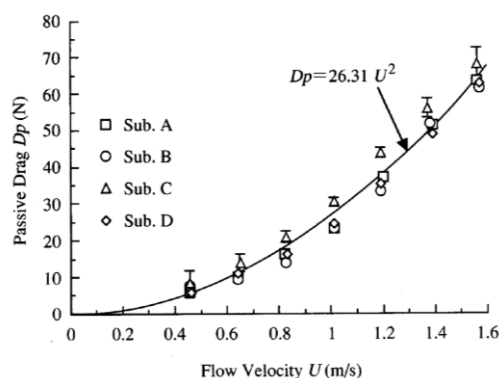


Figure 2.7. Passive drag data (Takagi, 1998).

Comparing the drag data from the three independent studies, drag at 1.5 m s^{-1} for Kolmogorov, Mason and Takagi is roughly 55 N, 40N and 60N respectively. These results are similar, however differences are likely due to the range of swimmers tested. The data presented by Kolmogorov and Duplishcheva, (1992), identifies that when a large number of swimmers are tested the variation in the data can become large (roughly $\pm 10 \text{ N @ } 1.5 \text{ m s}^{-1}$).

Computational fluid dynamics has been used to determine the passive drag of a male swimmer (Bixler et al., 2007), and validated by testing a mannequin of the geometry in a circulating water channel (Table 2.1). It is reported that the CFD prediction is 18% lower than experimental data from passive testing of the real swimmer (similar to the values presented above). The effect of angle of attack is also investigated with CFD and found that a +3 and -4.5 degree angle of attack results in an increase of 2.3% and 2.4% in passive drag respectively.

Table 2.1. Passive Drag determined from CFD (Bixler et al., 2007).

Velocity (ms^{-1})	Passive Resistance (N)	Coefficient
1.50	31.58	0.302
1.75	42.74	0.300
2.00	55.57	0.298
2.25	70.08	0.297

Marinho, (2009), used CFD to determine the passive resistance of a fully submerged geometry in two conditions: arms in the streamlined position and arms by side. A 72% increase in passive resistance is found with arms by side. However it has been reported that passive towing underwater has found that arms by side produces an additional 21.5% passive resistance (NECHITA, 2009). The difference between these two findings is large, however the

Literature Review

geometry used in the CFD study did not accurately represent the human form. This may identify the importance of geometry accuracy when using CFD to determine passive resistance.

No passive resistance measurements appear to have been performed on the surface with arms by side.

2.3.2 Resistance Components in swimming

Swimming during a race is performed at a range of depths. This causes an interesting problem in terms of quantifying the wave resistance of a swimmer. Vennell et al. (2006) performed drag measurements of a human mannequin at a range of depths. The mannequin was towed using a winch system with a dynamometer measuring resistance. It was found that drag on the surface was 2.4 times the drag when fully submerged, due the presence of a wave system on the free surface. On the surface wave resistance was found to be 50-60% of total resistance at 1.7 m s^{-1} . Wave drag was found to be less than 5% of total resistance at depths greater than 0.7m (2.8 chest depths) and sharply increased towards the surface. Figure 2.8 displays the absolute drag values and non-dimensional drag, based on frontal area, for the towed mannequin at various depths and speeds.

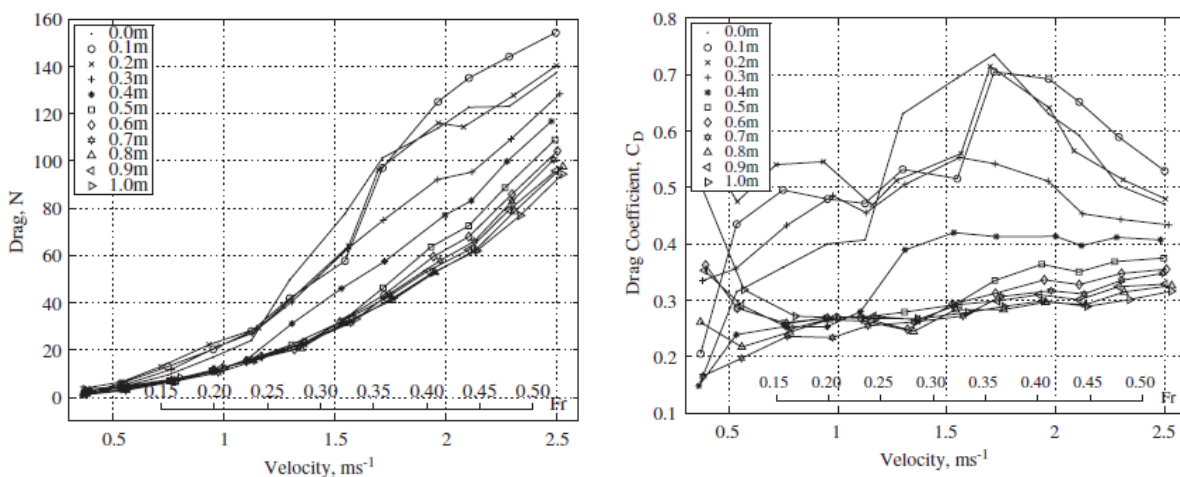


Figure 2.8. Drag results for a mannequin towed at a range of depths and speeds (Vennell et al., 2006).

Lytle and Elliott (1998) performed a similar study however towed forty male swimmers in the streamlined prone position. Towing was performed for a range of speeds on the surface and 0.2, 0.4 and 0.6 m below the surface.

Results from this study are tabulated. This study has not displayed the magnitude of resistance reduction report by Vennell et al (2006). At 1.6 m s^{-1} the resistance reduction at 0.6m is 14% unlike the ~54% presented by Vennell et al (2006) for a similar condition. However the uncertainty in these measurements is quite large and if the extremes of the of the variations are taken, the drag reduction at 1.6 m s^{-1} could be as great as 51%, bringing it much closer to the findings of Vennell et al (2006).

Table 2.2. Drag results presented for 40 male swimmers in the prone position at a range of depths and speeds (Lyttle and Elliott, 1998).

Velocity	Surface	0.2 m Deep	0.4 m Deep	0.6 m Deep
1.6 m s^{-1}	$67.5 \pm 12.0 \text{ N}$	61.1 ± 10.2	$59.2 \pm 10.3 \text{ N}$	$58.1 \pm 9.3 \text{ N}$
1.9 m s^{-1}	$93.2 \pm 12.1 \text{ N}$	$86.6 \pm 10.2 \text{ N}$	$83.2 \pm 10.7 \text{ N}$	$80.4 \pm 10.0 \text{ N}$
2.2 m s^{-1}	$135.4 \pm 14.6 \text{ N}$	$121.8 \pm 14.2 \text{ N}$	$114.8 \pm 13.0 \text{ N}$	$109.4 \pm 11.1 \text{ N}$
2.5 m s^{-1}	$175.3 \pm 17.3 \text{ N}$	$153.1 \pm 16.8 \text{ N}$	$144.2 \pm 15.6 \text{ N}$	$140.5 \pm 14.4 \text{ N}$
2.8 m s^{-1}	$211.0 \pm 23.1 \text{ N}$	$182.9 \pm 19.1 \text{ N}$	$173.0 \pm 17.0 \text{ N}$	$169.7 \pm 16.1 \text{ N}$
3.1 m s^{-1}	$247.0 \pm 25.6 \text{ N}$	$216.0 \pm 20.7 \text{ N}$	$205.6 \pm 21.0 \text{ N}$	$204.1 \pm 19.2 \text{ N}$

Toussaint (2002) attempted to estimate wave resistance from measurement of the other resistance components. Wave resistance was assumed to be negligible at speeds less than 1.6 m s^{-1} and therefore the speed dependency of friction and pressure resistance was assessed below 1.6 m s^{-1} . At a mean speed of 1.89 m s^{-1} the total resistance, minus the predicted pressure and friction resistance, resulted in a wave resistance contribution of 12.1%. When comparing this study with Lyttle and Elliott (1998) and Vennell et al. (2006) the assumption of negligible wave resistance at speeds below 1.6 m s^{-1} would appear incorrect as both studies have presented an influence of wave resistance at this speed. The assumption used by Toussaint (2002) would suggest that the wave resistance predicted will be less than is actually experienced since some wave resistance would have been present at speeds below 1.6 m s^{-1} .

Towing at a range of depths measuring total resistance to determine wave resistance (Lyttle and Elliott, 1998; Vennell et al., 2006) assumes that the absolute change in resistance is due only to wave resistance. It is likely that skin friction and viscous pressure drag will also vary from on to below the surface, due to the change in projected and wetted surface area. This may result in an under prediction of wave resistance using the variable depth tow

Literature Review

method, as viscous pressure and skin friction would increase as the body becomes more immersed. Taunton et al. (2012) has conducted a preliminary study, measuring the wave resistance of a swimmer during a surface passive tow, with arms by side. This was performed using longitudinal wave elevation measurements and the Eggers formula. The measured wave resistance is compared to a prediction of the same condition and swimmer geometry using Thin Ship Theory. The total resistance measured using an instrumented winch tow system was found to be 116.9 ± 10.4 N for female of height 1.71 m and mass 63 kg, towed on the surface at 1.86 m s^{-1} . The wave resistance measured from wave elevation measurements is 30.35 ± 3.8 N and the prediction from Thin Ship Theory for the same condition is 31.86 N, accounting for about 25% of total resistance.

Taunton et al. (2012) also investigated the effect of glide depth using Thin Ship Theory. Figure 2.9 compares the Thin Ship Theory prediction with the data produced by Vennell et al. (2006). This identifies a large resistance hump predicted by Thin Ship Theory not present in the data presented by Vennell et al. (2006). A potential reason for this is the reference point used to define the depth of the swimmer. The sensitivity of variations in depth on the surface is presented in figure 2.10 identifying the importance of body depth when comparing surface resistance data. However, only the trends in these datasets can be compared, since the drag values have not been normalised and the geometries are a different shape and size.

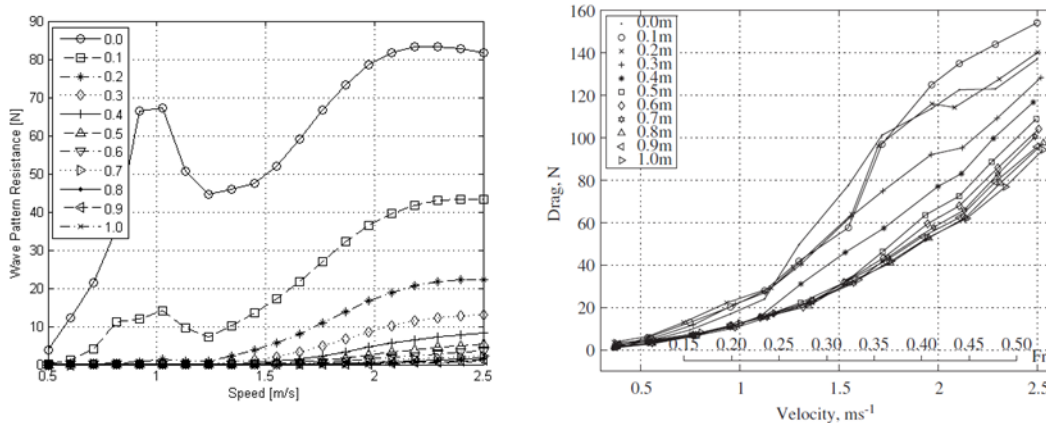


Figure 2.9. Effect of sinkage on the wave pattern resistance speed relationship (Taunton et al., 2012).

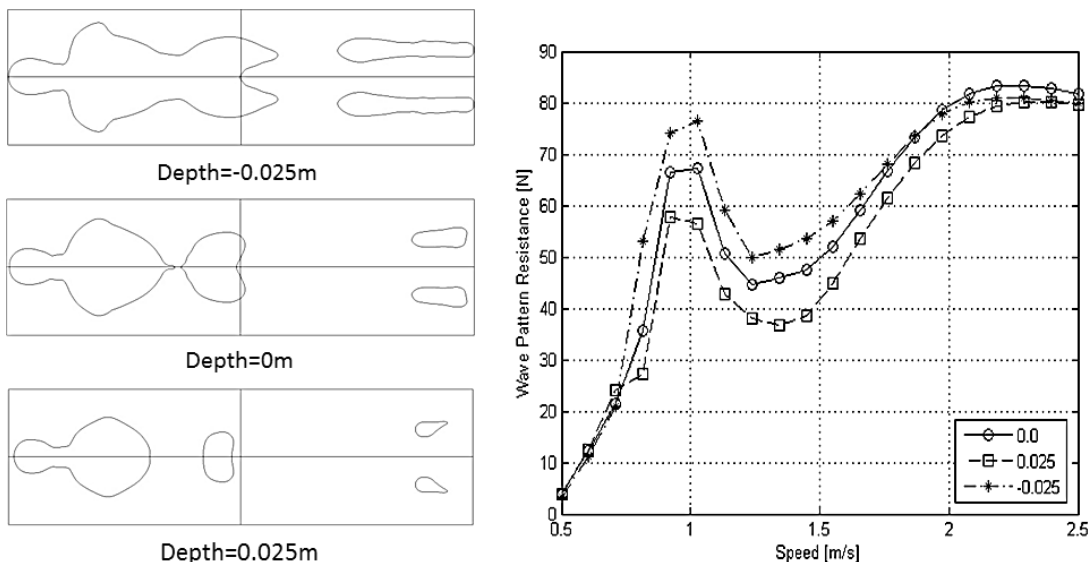


Figure 2.10. Effect of surface penetration on wave resistance (Taunton et al., 2012).

Comparison of the drag decay predicted by Thin Ship Theory is made with Lytle and Elliott (1998) and Vennell et al. (2006). The Thin Ship Theory predicts a similar trend to Vennell et al. (2006), however both differ from Lytle and Elliott (1998). It is suggested that this may be due to the definition of swimmer immersion where Lytle and Elliott (1998) use distance from the mid-line of the frontal plane, except on the surface, where it was defined as the point at which the dorsum of the swimmers back was on the surface. Vennell et al. (2006) defined depth as the distance from the swimmers hands. Depth in the Thin Ship Theory study was defined from the dorsum of the swimmers back.

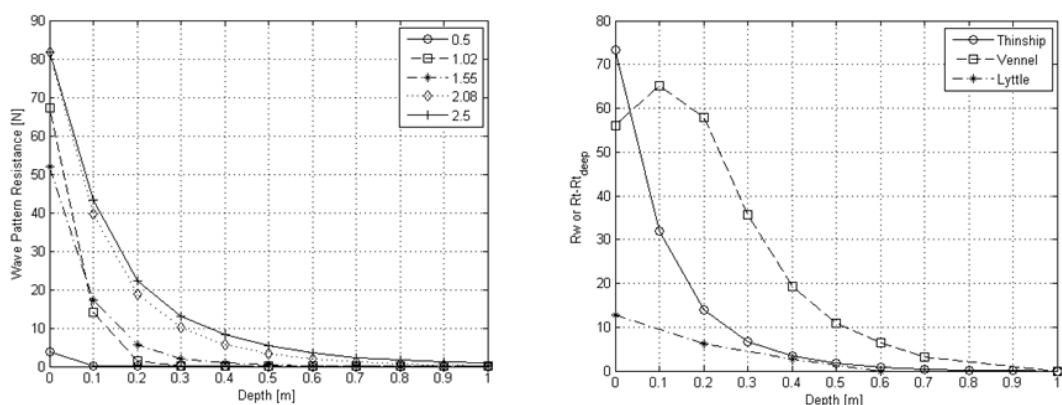


Figure 2.11. Wave resistance decay with sinkage (Taunton et al., 2012).

Skin friction resistance has been studied as a component of resistance that can potentially be reduced. Polidori et al. (2006) investigated the effect of adjusting

Literature Review

the thermal gradient between the swimmer and the pool water as a method of reducing the shear stress in the boundary layer and hence skin friction resistance. It was found that a change in pool temperature from 20 to 30 degrees Celsius provided a reduction in skin friction of 5.3% and 1.5% for laminar and turbulent flow respectively. Additionally, skin friction was quantified by integrating the shear over the surface area of the body for laminar and turbulent boundary layers. The skin friction resistance was determined as 20 & 22 N at 2.8 m s^{-1} for fully submerged female and male swimmers respectively. Using the fluid properties ($\rho=996.68 \text{ kgm}^{-3}$, $\nu=0.865 \times 10^{-6} \text{ m}^2\text{s}^{-1}$) and the surface area of the swimmers (female: 1.78 m^2 , male: 2.04 m^2) reported, skin friction resistance coefficients (C_f) of 0.002876 and 0.00276 can be determined for females and males respectively. Comparison with that predicted by ITTC (equation 2.8), for the same swimming speed and lengths (streamlined prone) of swimmers (Female: 2.2 m, Male: 2.5 m), yields C_f values of 0.003330 and 0.003279, for females and males respectively. The values predicted by ITTC are 11% higher than those determined by Polidori et al. (2006). The higher predicted skin friction by the ITTC approach, may be due to the incorporation of form effects in the ITTC correlation line, which are not accounted for in the estimation by Polidori et al. (2006). In addition the ITTC approach assumes only turbulent flow, where in fact transition occurs at 0.16 m from the leading edge. It is not possible to correct for this as the surface area in this region is not known.

Reduction of skin friction resistance has also been attempted using suits. Toussaint et al. (2002) investigated the effect of a Fast-skin™ body suit, in comparison to a conventional suit, using active drag swimming tests of 6 male and 7 female swimmers. A statistically non-significant result ($p=0.31$) of 2% drag reduction was reported.

Unlike friction and wave, pressure resistance has not been extensively quantified in the literature. This may be due to experimental difficulty. In an attempt to measure wave resistance, Toussaint, (2002) measured pressure resistance at low speeds ($<1.6 \text{ m s}^{-1}$) and found an average velocity squared relationship of $24.125 \text{ kg} \cdot \text{m}^{-1}$ (relating pressure drag to velocity squared) for 8 swimmers. However this relationship assumes wave drag is negligible at speeds less than 1.6 m s^{-1} and therefore may over predict pressure drag if some wave resistance is present.

Computational fluid dynamics has been used to determine the contribution of the resistance components. Bixler et al. (2007) determined the passive drag of a swimmer and found a skin friction contribution of 26% and a pressure contribution of 74% (figure 2.12). Marinho, (2009) performed a similar study and found a skin friction contribution of 8% and pressure drag contribution of 92%.

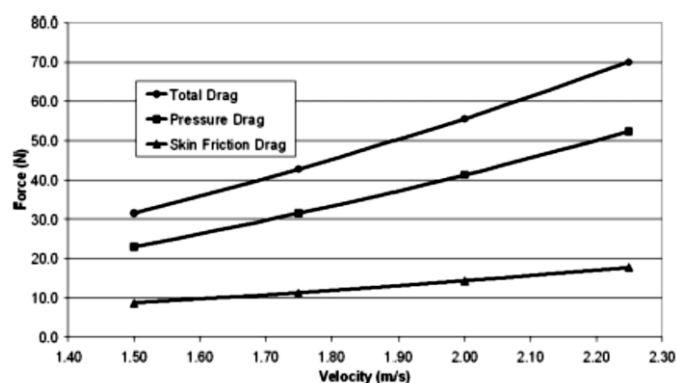


Figure 2.12. CFD study of a submerged swimmer in the prone streamlined position, displaying the components of resistance (Bixler et al., 2007).

2.3.3 Active Resistance

Active resistance is the resistance experienced by the swimmer during active swimming. This can also be considered the same as the amount of thrust needed to swim at a certain speed. Active resistance is different to passive resistance due to the dynamic motion of the body during active swimming, and the interaction effects between the propulsion, produced by both the arms and legs, and the non-propulsive body. Due to the non-continuous thrust delivered by a swimmer, active drag can be considered as either a time varying value or an average value over a stroke cycle. Direct measurement of active resistance on a human is extremely difficult, because no method has yet been devised to separate the resistive and propulsive forces. Therefore, the only methods that can ever fully resolve the origin of resistance and propulsion are those that analyse the flow around the swimmer, such as particle image velocimetry (PIV) or computational fluid dynamics. PIV has had limited use in swimming (Hochstein et al., 2009; Matsuuchi et al., 2009), and these studies have focused on specific areas of flow on the hands and feet. Therefore, unless the whole swimmer is analysed, PIV cannot provide the total thrust (or resistance) produced by the swimmer. The reason for such limited use of PIV is likely due

Literature Review

to the impractical nature this experimental method (calibrated cameras looking through windows in the side of a flume, specifically treated water containing particles, limitations of viewing the whole body and large quantities of data). Additionally, CFD has been used to attempt to model the entire flow situation (Keys et al., 2010), however no validated cases have been published. This suggests that the current CFD fidelity is not yet sufficient.

The most common methods of estimating active resistance have been to experimentally measure the forces produced by a swimmer. The velocity perturbation method (VPM) (Kolmogorov and Duplishcheva, 1992; Mason and Formosa, 2009; Toussaint et al., 2004) requires a swimmer to be tested at two different velocities, a free swim velocity and a perturbed velocity. The perturbed velocity is achieved by exerting an additional known resistance to the swimmer. The original method (Kolmogorov and Duplishcheva, 1992) requires the swimmer to tow an object of known resistance, resulting in a decrease in velocity. In an alternative approach (Mason et al., 2007) the active swimmer is towed at an increased speed with the residual resistance measured using a dynamometer. It is assumed the swimmer produces equal power for the free swim and the swim at the perturbed velocity. To ensure equal effort for both conditions, the swimmer is tested at maximal effort, with enough recovery time between tests to ensure no fatigue. Active resistance is expressed as,

$$R_{Freeswim} = \frac{R_{Towline} V_{Perturbed} V_{Freeswim}^2}{V_{Perturbed}^3 - V_{Freeswim}^3}, \quad (2.11)$$

where $R_{Freeswim}$ is active resistance at free swim speed, $R_{Towline}$ is the resistance required to perturb the swimming speed, $V_{Perturbed}$ is the perturbed swimming speed and $V_{Freeswim}$ is free swimming speed. To deduce the above relationship for active resistance, it is assumed that the swimmer drag coefficient and wetted area are the same for both free swimming and perturbed swimming speeds, and that the resistance is proportional to velocity squared.

An alternative to the velocity perturbation method is a system developed by Hollander et al. (1986) called the Measurement of Active Drag (MAD) System. The MAD system is a series of rigid push pads submerged beneath the free surface, connected to a dynamometer, which a swimmer uses to propel against

during arms only freestyle. The mean force recorded is assumed equal to the mean active drag (or mean thrust) at the equivalent swimming velocity. The limitations of the MAD system are: it can only measure arms-only freestyle where in reality the legs contribute to the total thrust, the hand is not in contact with the pad for the full stroke cycle, the arm does not slip in the water and therefore the time varying swimming speed is not likely to be accurate.

A comparison of the active resistance predicted with the VPM and the MAD system was performed for a group of six elite swimmers (Toussaint et al., 2004). The VPM and MAD systems predicted average active resistance values of 53.2 N and 66.9 N respectively at 1.64 m s⁻¹. It was concluded that both methods measure the same phenomenon, but the assumption of equal power (or effort) was violated in the velocity perturbation method.

Mason and Formosa (2009) compared a tethered swimming force, produced by a stationary swimmer performing maximal effort freestyle with active resistance measured using the VPM. It was found that stationary tethered swimming was not an acceptable alternative to the VPM for predicting active resistance.

Takagi (1998) attempted to measure active resistance in a circulating water channel combining both passive resistance measurements and residual thrust measurements. The active resistance is assumed to be the passive resistance, at the free swimming speed, plus kinetic resistance derived from residual thrust measurements,

$$T_r = T_0 - Da = T_0 - (Dp + Dk), \quad (2.12)$$

$$Dk = T_0 - T_r - Dp, \quad (2.13)$$

where T_r is the residual thrust at free swim velocity, T_0 is the thrust produced by the swimmer with zero advance velocity, Da is active resistance, Dp is the passive resistance at free swim velocity and Dk is kinetic resistance. This appears to be a sensible method, as the majority of active resistance is comprised of passive resistance, and therefore any error caused by the measurement of kinetic resistance will have a small effect on the total error of the active drag prediction.

Literature Review

In naval architecture, the self-propulsion experiment is used to determine the required thrust to propel a hull at a specific speed (Molland et al., 2011). Interaction effects, due to increased local flow velocity over the hull from the propeller, cause the hull to have increased resistance. This experiment determines a thrust deduction ($1-t$) as a result of this interaction, so that the thrust can be appropriately increased to achieve the correct self-propulsion speed. Thrust deduction is determined as

$$t = \frac{(T - R)}{T}, \quad (2.14)$$

where T is the thrust produced by the propeller and R is the naked hull resistance.

To conduct a self-propulsion test, a model fitted with a propeller and motor is towed from a dynamometer at a fixed velocity. The propeller n is set and the tow force measured is $R-T$. The thrust produced by the propeller is also measured. The propeller n is varied until $R-T$ is zero, this is called the self-propulsion point. Using the known resistance of the hull at the tow velocity and the thrust required to achieve self-propulsion, t is determined.

2.4 Propulsion of a Human Swimmer

2.4.1 Overview of Propulsion

Propulsion in a freestyle swimming race originates from: arm and leg propulsion, while swimming on the surface; and leg propulsion from undulation of the whole body, while swimming underwater. This section will categorise these propulsive forces as *arm propulsion* and *leg propulsion*, combining propulsion produced by the legs on the surface and underwater.

2.4.2 Arm Propulsion

In freestyle, arm propulsion provides the majority of total propulsion while swimming on the surface. A study comparing the contribution of arms and legs to swimming velocity on eight male subjects, found that arm propulsion provides 90% of maximal swimming velocity (Deschodt et al., 1999).

The fluid dynamic forces generated by the arm as it moves through the water may be considered as lift, drag and added mass (Childress, 1981). These forces are governed by the shape of the arm and its motion, in three dimensions, as it moves through the water. Considering the arm as a foil, the shape will affect the contribution of lift, drag and added mass (Hoerner, 1965). Therefore, the propulsion generated by the hand, forearm and upper arm is likely to be different due to both differences in shape and motion through the water. However, studies to determine the propulsive force produced by the arms differ in approach: some studies treat the arm as individual elements and others treat the whole arm as a single element.

Berger et al. (1995) measured the lift and drag forces acting on a hand and forearm model in a towing tank. The model was rotated about the vertical axis, the sagittal axis and the longitudinal axis of the forearm. A maximum lift coefficient of 0.4 and corresponding drag coefficient of 0.2 was measured at a forearm rotation of 30 degrees. The hand was compared to a 'Joukowski' cambered foil. Lift and drag coefficients for the hand alone were measured for a range of angles of attack. A maximum lift coefficient of 1.2 and a corresponding drag coefficient of 0.6 was measured at 30 degrees angle of attack.

Gardano and Dabnichki, (2006) performed a similar study on a prosthetic arm, in a wind tunnel at various angles of attack. For a straight arm, a maximum lift

Literature Review

coefficient of 0.9 was found for 30 degrees angle of attack, and a maximum drag coefficient of 1.2 was found for a 60 degree angle of attack. A maximum lift coefficient of 0.9 and drag coefficient of 1.3 was found for a 20 degree arm bend, at 40 degrees and 100 degrees angle of attack respectively.

Gourgoulis et al., (2008) estimated the hand force during front crawl using lift and drag coefficients, published by Arellano (1999), and velocities determined from digitised video of the hand motion. A maximum hand force of 13.91N was determined for the push phase of the stroke, comprising 7.87N drag and 8.82N lift. The hand velocity during the push phase was 2.37 m s^{-1} with a pitch angle of 35.66 degrees and a sweepback angle of 250.36 degrees. BERGER, (1999) used a similar methodology to determine arm propulsion and compared values determined from the same swimmer using the MAD system. The two methods estimated propulsion within 5% of each other.

Toussaint et al. (2002) questioned the validity of performing quasi-steady analysis, to determine arm propulsive forces, and performed flow visualisation and pressure measurements on a swimmers arm during active swimming. Flow during the in-sweep and out-sweep of the arm pull was found to be highly unsteady. A pressure gradient with radial flow along the arm was observed during the out-sweep. It is suggested that these flow phenomena are significant and not captured in quasi-steady analysis.

Following the analysis of Toussaint et al. (2002), Lauder and Dabnichki, (2005) performed a comparison between the results obtained from quasi-steady analysis and unsteady analysis of arm propulsion. A full scale mechanical arm was constructed that could be rotated to achieve a realistic rotational velocity profile. The arm was tested in a towing tank, at fixed speeds and angles of rotation, and a quasi-steady analysis performed. The arm was also tested dynamically, where the arm was actively rotated through the water, while being towed, and shoulder torque measured. Comparison of results from the two methods identified the quasi-steady approach does not capture the full detail of the force generated by a swimmers arm. Sidelnik and Young, (2006) performed towing experiments on an oscillating hand and found that hand acceleration contributed up to 8N of stroke force for a total stroke force of 30N, identifying an added mass component of 1.364.

Computational fluid dynamics has been used to gain further insight into arm propulsion. Bixler and Riewald, (2002) performed a basic study in steady flow conditions, to validate the use of CFD, to determine arm forces at various angles of attack. Comparable lift and drag forces with that found by Berger et al. (1995) were determined. Rouboa et al., (2006) used CFD to investigate the effect of hand and forearm acceleration on arm propulsion. A steady flow Cd of 1.16 was determined for the hand and forearm. Under acceleration conditions the propulsive force was found to be 22.5% higher than the force produced under steady conditions (55.4 N versus 44.4 N).

Minetti et al., (2009) investigated the effect of finger spread using CFD and found that a finger spacing of 12 degrees increased the hand drag coefficient by 8.8%. Sidelnik and Young, (2006) found a similar value of 10 degrees from towing tank experiments of a hand and arm geometry.

Akis, (2004) developed a three dimensional, three segment mathematical arm model to simulate arm propulsion. The upper arm and fore arm are considered as cylinders and the hand is considered as an elliptical plate. Only drag based propulsion is modelled. A kinetic model using the propulsion determined from the arm model and a simplistic velocity squared resistance relationship, is used to determine swimming velocity. The propulsion produced by the arm model compares well to experimental thrust of a tethered swimmer at a range of stroke rates. Additionally, by adjusting the resistance coefficient the relationship between stroke rate and free swimming speed from kinetic model can be matched to experimental data.

These studies identify that the arm propulsion may be modelled if the relevant force coefficients, motion and geometry are known. Using the coefficients quoted, a drag only arm propulsion model for this thesis is proposed. Using arm motion data acquired from video footage the correct time varying arm speed can be achieved. Further complexity could be achieved by incorporating a lift component; however, the arm dimensions can be artificially scaled to ensure the correct propulsive force, as achieved by (Akis, 2004).

Literature Review

2.4.3 Leg Propulsion

In a freestyle swimming race, leg propulsion is used in two manners: freestyle flutter kick (on the surface accompanying freestyle arms) and underwater undulatory swimming (UUS) (after starts and turns, also known as dolphin kick). Both methods of leg propulsion use an undulatory motion, however flutter kick is performed from the hip down, with legs moving alternatively and UUS performed from the trunk down with the legs together. This propulsion method is comparable to the propulsion used by fish (Fish, 1994). The undulatory motion produced by the swimmer is a wave like motion that propagates towards the feet increasing in amplitude. In fish this motion is symmetrical and continuously grows in amplitude towards the tail (Fish, 1993), whereas in humans, the asymmetry in the musculoskeletal makeup prevents both symmetry and continuous growth of motion.

Based on propulsive kinematics, fish may be separated into four categories (Vogel, 1940): Anguilliform, Sub-carangiform, Carangiform, Thunniform. Anguilliform encompasses eel like fish, where there is a small caudal fin and a relatively large amplitude wave running along the body. The motion wavelength is less than a body length, allowing multiple waves along the body at one time. The amplitude of the wave remains relatively large towards the anterior. With progression through the categories towards Thunniform, the wavelength becomes longer, amplitude becomes smaller and the decay of the amplitude towards the anterior becomes greater (Vogel, 1940).

The progression from Anguilliform to Thunniform is generally associated with swimming speed, however Lighthill (1969) found that the fastest marine animals have adopted Carangiform motion. Different modes of propulsion exist in Anguilliform to Thunniform, with a combination being used in the intermediate categories. Propulsion in Anguilliform is mainly generated by added mass through displacement of the surrounding fluid. A wave travelling through the body from anterior to posterior displaces fluid backwards, generating forward propulsion (Lighthill, 1971). In Thunniform, where little wave motion exists, propulsion is created by vortex shedding from the caudal fin, causing a change in momentum in the wake (Lighthill, 1969). This momentum change arises from a jet, producing thrust, and two alternating pairs of vortices (Triantafyllou, 1993; Triantafyllou et al., 1991; Weihs, 2006).

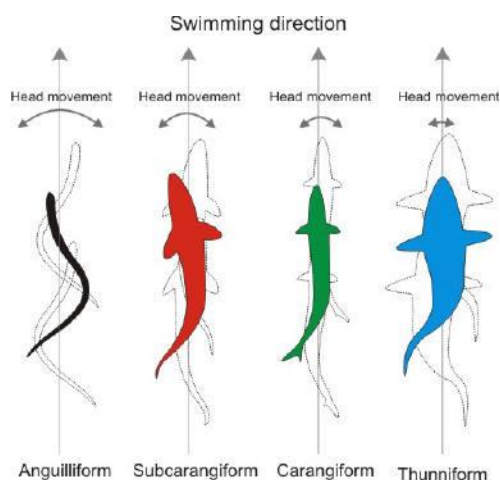


Figure 2.13. Categories of fish kinematics (Hoar and Randall, 1978).

Von Loebbecke et al. (2009) made a comparison of human UUS stroke kinematics, in 22 swimmers, to that of cetaceans. It was found that humans have a similar kick amplitude, however a greater kick frequency for equivalent speeds. Strouhal number was used to non-dimensionalise and compare kinematics,

$$St = \frac{fL}{V}, \quad (2.15)$$

where f is the kicking frequency, V is the forward velocity and L is either kick amplitude, for ratio of tip speed to forward speed or body length, for number of kicks per body length travelled. Humans required five kicks per body length travelled, whereas cetaceans required 1.3, identifying the underperformance of humans. Von Loebbecke et al. (2009) identified the Strouhal number for human UUS was above the optimum required for oscillatory swimming. This may be explained by the kinematics and anthropometrics of human UUS, where humans generally perform Carangiform motion, however do not possess the large caudal fin of cetaceans to impart momentum into the wake.

Lighthill (1971) proposed large-amplitude elongated-body theory, a mathematical method to determine the energy cost of locomotion and the forces acting between fish and the water. This theory differed from a previous attempt (Lighthill, 1960), where only small amplitudes of motion relative to the fish length could be modelled. Large-amplitude elongated-body theory is valid for arbitrary large amplitudes of motion, making it more applicable for the motion of human undulatory swimming (flutter kick & UUS). However, the

Literature Review

appropriate application of large-amplitude elongated-body theory is for fish with slender caudal fins which use carangiform propulsion.

This theory is based on the assumption that reactive forces due to acceleration of the surrounding fluid dominate propulsion for carangiform motion. The reason for this domination is the high acceleration caused by the flick of the posterior portion of the fish.

The formulation of this theory is based on the following three principles,

1. The fluid momentum near the fish is perpendicular to the fish body longitudinal axis and is expressed as the component of added mass m per unit length of the fish, multiplied by velocity w .
2. Total thrust acting on the fish is the rate of change of momentum within the volume of fluid surrounding the fish bound by a perpendicular plane Π intersecting the tip of the caudal fin, figure 2.15.
3. When balancing the momentum it is necessary to account for momentum transfer across Π through convection and also from the resultant $1/2 mw^2$ of the pressures generated within Π .

To describe the motion of the fish, a lagrangian coordinate a is used to define the distance along the spine from the posterior end of the fish, and space axis position coordinates (x,z) are used to define the position of point a at time t . Therefore the position of the fish at point a and time t would be $z(a,t)$ and $x(a,t)$ (figure 2.14).

The spinal column is assumed to be inextensible therefore,

$$\left(\frac{\partial x}{\partial a}\right)^2 + \left(\frac{\partial z}{\partial a}\right)^2 = 1. \quad (2.16)$$

The horizontal velocity vector $\left(\frac{\partial x}{\partial t}, \frac{\partial z}{\partial t}\right)$ has the component u tangentially to the spine and w perpendicular to the spine as seen in figure 2.14 and expressed by

$$u = \frac{\partial x}{\partial t} \frac{\partial x}{\partial a} + \frac{\partial z}{\partial t} \frac{\partial z}{\partial a}, \quad (2.17)$$

$$w = \frac{\partial z}{\partial t} \frac{\partial x}{\partial a} - \frac{\partial x}{\partial t} \frac{\partial z}{\partial a}. \quad (2.18)$$

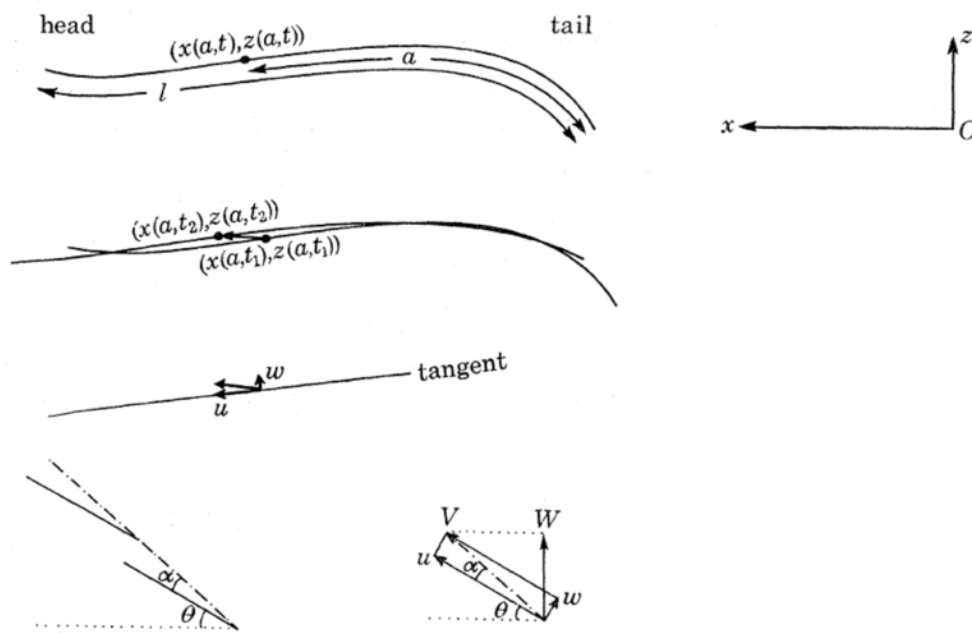


Figure 2.14. Axis System and velocity calculation for Large amplitude elongated body theory (Lighthill, 1971).

The momentum per unit length of the fish is expressed by the vector,

$$mw \left(\frac{-\partial z}{\partial a}, \frac{\partial x}{\partial a} \right), \quad (2.19)$$

where m is the added mass per unit length of the fish. The added mass is determined for an ellipse as,

$$m = \frac{1}{4} \pi \rho s^2, \quad (2.20)$$

where ρ is the water density and s is the local cross-section depth.

In order to calculate the thrust produced by the fish motion, it is necessary to imagine a volume V surrounding the fish, excluding the wake, and bounded by the plane Π intersecting the tip of the caudal fin (figure 2.15).

Literature Review

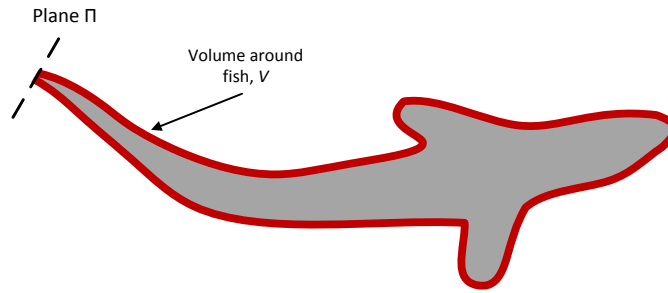


Figure 2.15. Rate of change of momentum is calculated in volume surrounding fish bounded by plane Π (Lighthill, 1971).

The momentum in V may be written as the integral of equation 2.19 (momentum per unit length) from 0 to l with respect to a , and its rate of change is determined at the sum of the following three parts.

1. Rate of change due to convection out of V across plane Π .
2. Rate of change of pressure force acting on plane Π .
3. Minus the reactive force (P, Q) acting on the fish

The rate of change of momentum in V is therefore expressed as,

$$\frac{d}{dt} \int_0^l mw \left(-\frac{\partial z}{\partial a}, \frac{\partial x}{\partial a} \right) da = \left[-umw \left(-\frac{\partial z}{\partial a}, \frac{\partial x}{\partial a} \right) + \frac{1}{2}mw^2 \left(\frac{\partial x}{\partial a}, \frac{\partial z}{\partial a} \right) \right]_{a=0} - (P, Q), \quad (2.21)$$

where the terms on the right hand side appear in the order as written in the above three points.

Through manipulation of the terms in the square bracket using equations 2.16, 2.17 and 2.18, the propulsion P and side-force Q experienced by the fish may be written as

$$(P, Q) = \left[mw \left(\frac{\partial z}{\partial t}, -\frac{\partial x}{\partial t} \right) - \frac{1}{2}mw^2 \left(\frac{\partial x}{\partial a}, \frac{\partial z}{\partial a} \right) \right]_{a=0} - \frac{d}{dt} \int_0^l mw \left(-\frac{\partial z}{\partial a}, \frac{\partial x}{\partial a} \right) da. \quad (2.22)$$

Lighthill (1971) used this theory to determine the mean thrust produced by a fish, swimming at a constant mean velocity, from experimental data of its motion. Motion was gathered using pictures taken vertically above the fish at 16 frames per swimming cycle, from which $\frac{\partial x}{\partial a}, \frac{\partial z}{\partial a}, \frac{\partial x}{\partial t}$ & $\frac{\partial z}{\partial t}$ along the body could be determined. The mean propulsion, determined from equation 2.22, was compared to the mean resistance of a similar fish determined from previous towing experiments. The mean resistance is cross checked with estimates for

similar shapes at similar Reynolds numbers (Hoerner, 1965). The propulsion predicted is found to be less than the resistance of the fish. Possible sources of error are in the estimation of the resistance, however the most obvious being the neglect of a resistive component in the thrust prediction. The resistive component accounts for lift over the caudal fin, producing propulsion. This is less of a concern in human swimming, where the feet do not represent a good lifting surface and therefore the lift component, at the feet, is likely to be small. Therefore, it is proposed that this theory may be used to model propulsive forces produced by underwater undulatory swimming and freestyle flutter kick.

Bertetto et al. (2001) compared the predicted thrust from Lighthill's large amplitude elongated body theory (LAEBT), and numerical calculations of instantaneous aerofoil kinematics and dynamics, with experimental data from a robotic fish. Comparison of the analytical results with experimental data showed that LAEBT accurately approximated the experimental thrust. The numerical approach fell short in fully quantifying the thrust, however provided a good qualitative picture. Additionally, Yu and Yi (2009) compared the velocity predicted by a kinetic model using LAEBT to define thrust with a self-propelled robotic fish. It is found that the relationship between swimming velocity, oscillation frequency and amplitude for the prediction was the same as achieved with the robotic fish.

Computational fluid dynamics has been used to analyse the propulsion generated in underwater undulatory swimming. Liu (1999) conducted time accurate CFD analysis of a tadpole and compared it to Lighthill's LAEBT. Better understanding of the contribution to propulsion from the jet and vortex flow is achieved. Von Loebbecke et al. (2009) performed fully unsteady CFD on human swimming geometries performing UUS. Laser scan geometries were morphed using video footage of the swimming technique to animate the stages throughout a UUS stroke cycle. Analysis of the vorticity and fluid velocity in the wake identifies a three dimensional vortex ring as a result of a jet flowing from the feet. A two dimensional slice through the vortex ring compares well with two dimensional experimental data. It is also reported that the majority of propulsion is produced by the feet and that the down-kick (while swimming on the front) produces a much larger thrust than the up-kick. Using this method, Von Loebbecke et al. (2009b) determines the propulsive efficiency of five

Literature Review

Olympic level swimmers and compares it to that of a cetacean. Propulsive efficiency is defined as the propulsive work done in the direction of swimming divided by the total work done. The human swimmers are found to have a propulsive efficiency ranging from 11 to 29% and the cetacean 56%.

2.5 Swimming Fatigue

2.5.1 Race Analysis

To understand how fatigue affects the performance of a swimmer, race data supplied by British Swimming has been analysed (figure 2.16). In sprint events, a swimmer performs a maximum effort and fatigue dictates the resultant propulsive power. In longer distance events, tactics are more dominant and swimmers chose to limit their propulsive power to conserve energy. This identifies that to accurately simulate how a race is swum, a race needs to be modelled both tactically and physiologically.

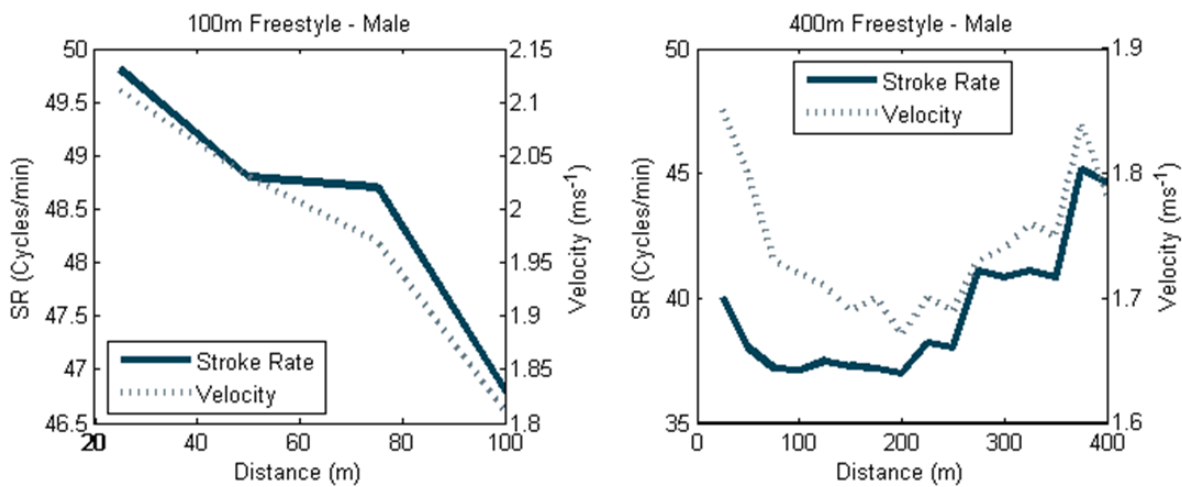


Figure 2.16. Race strategy for sprint and long distance male freestyle events. Fatigue is dominant in the 100m event, while race tactics appear dominant in 400m event.

2.5.2 Bioenergetics Theory

To model the fatigue of a swimmer during a race, the energy sources of the human metabolic system need to be considered. This section presents bioenergetics theory as published by Hoffman (2002). These sources of energy need to be analysed with respect to energy capacity, rate of exploitation and rate of recovery. With this information, in conjunction with the work being

done by the propulsion models, the power available to the swimmer may be modelled.

Three sources of energy for muscle contraction exist in the human body. All three systems operate differently, with independent energy supply attributes for various intensities and durations of exercise. Two of these processes are anaerobic, meaning they operate without the presence of oxygen, called the *phosphagen energy system* (ATP-PC) and the *glycolytic energy system*. The third system is an aerobic process called the *oxidative energy system* and utilises a supply of oxygen and removal of carbon dioxide by the cardiovascular process and breathing.

Energy in the muscle may be generalised as: the production of adenosine triphosphate (ATP), which is then broken down to adenosine diphosphate (ADP) and Pi with the release of a large amount of energy.

The ATP-PC system utilises stored ATP-PC in the muscle which is readily available for immediate use. This provides the largest power source of all three systems, and therefore is used for high intensity exercise. However, the supply energy from the ATP-PC system is exhausted within 30 seconds. Recovery of ATP-PC is initially rapid, with 50% replenishment in 20-30s however full replenishment may take up to 20mins. Although, most of the replenishment is achieved in about 3 minutes.

The Glycolytic energy system undergoes an extra phase, stored ATP is not utilised, but is produced through the breakdown of glucose into pyruvic acid. Glucose can be present in the muscle, blood or generated through breakdown of glycogen from the liver. The glycolytic energy system can produce more energy than the ATP-PC system, however due to its added complexity this energy process cannot produce as much ATP per unit time (peak power). Since this process operates without the presence of oxygen a bi-product, pyruvic and lactic acid, builds up in muscle tissue, hindering the glycolytic energy process. Therefore, this process is only sustainable for a short period of time. This process is the primary source of energy for high intensity exercise lasting 1-3 minutes.

The Oxidative system utilises an oxygen supply, stored fats and carbohydrates in the production of ATP. Due to their abundance, the oxidative system can

Literature Review

provide energy for prolonged periods of time, however cannot provide enough ATP per unit time for high intensity exercise. The oxidative system is therefore the primary source of energy for long duration aerobic events. Due to the presence of oxygen, pyruvic acid is also converted back into ATP plus CO₂ and H₂O. This enhances the energy production of the oxidative energy system, albeit at a low production rate relative to the anaerobic processes.

All energy systems operate at all times, but exercise intensity dictates the contribution from each source. The more intense the exercise, the greater the energy production from anaerobic processes; as intensity decreases and duration increases, energy production will be primarily aerobic. Table 3.1 summarises the energy systems in terms of their capacity, power output and fuels used.

Table 2.3. Summary of Metabolic Energy Systems used to create muscle contraction (Hoffman, 2002)

System	Power (rate of ATP production)	Capacity (total ability to produce ATP)	Fuels Used
Phosphagen system (Anaerobic)	Very High	Very Low	Stored ATP
Glycolytic system (Anaerobic)	High	Low	Blood glucose Muscle & liver glycogen
Aerobic system	Low	Very High	Blood glucose Muscle & liver glycogen Adipose & intramuscular fat

2.5.3 Exhaustion Studies

Bioenergetics theory provides an overview of the energy production. However, to model the energy supply from each system it is necessary to know maximum power output, energy capacity and recovery rate.

By measuring total and aerobic work over 30 seconds, during exercise on a cycle ergometer, Hill & Smith (1993) identified an anaerobic capacity of 158 J Kg⁻¹ and 242 J Kg⁻¹, for women and men respectively. Total work was measured through the cranks on the ergometer and aerobic power was measured through breath-by-breath \dot{V}_{O_2} and converted into Watts using the conversion factor 20.92 KJ l O₂⁻¹ and gross muscle efficiency of 22%. Peak power was

measured to occur in the first 5 seconds of the test and was found to be 10.2 W Kg⁻¹ and 13.3 W Kg⁻¹ for women and men respectively. Since this test cannot separate the power contribution from the ATP-PC and Glycolytic energy systems, it is therefore necessary to treat anaerobic power as one source.

Maximum aerobic power measured from VO₂ max tests, on a cycle ergometer and treadmill, has found an average of 2.52 L min⁻¹ and 3.4 L min⁻¹ for women and men respectively (Patton et al., 1982). This identifies a maximum aerobic power of 193.3 W and 276.2 W for women and men respectively. To scale aerobic power with athlete size Hill & Smith (1993) assumed a linear relationship with body mass. Therefore, with an average body mass of 62.6 kg and 80.3 kg for the 24 females and 27 males tested by SwimSIM, an anaerobic power relationship of 3.1 W Kg⁻¹ and 3.4 W Kg⁻¹ for women and men respectively is assumed. With indoor swimming events lasting no longer than 9 minutes, aerobic capacity is assumed infinite.

Maximal effort exercise of 75 seconds derives approximately equal output from aerobic and anaerobic energy systems (Baker et al., 2010). Pripstein et al. (1999) studied the energy contribution for 16 elite female rowers performing 2 km ergometer rowing race. An average maximum VO₂ consumption of 3.55 Lmin⁻¹ was found and the average anaerobic power contribution to 7 minute race was 12.3%.

2.6 Simulation

Analysis in sport can be defined in three components: qualitative, quantitative and predictive (Lees, 2002). Mathematical modelling or simulation falls under the predictive component. The aim of simulation (in sport) is to predict performance based on information that has been supplied. The success (or fidelity) of a simulation is governed by the mathematical architecture adopted and the input parameters used. The more complex the mathematical architecture, the more detailed the input parameters become.

An advantage of using simulation is the ability to systematically adjust the input information to answer hypothetical questions, whereas qualitative and quantitative analysis can only comment on performance that has been achieved in reality (Lees, 2002).

Brannigan and Adali (1981) constructed a mathematical model of a tennis racket hitting a ball. The model was validated with known experimental results. The simulation provided insight into quantifying the forces and moments transferred to the athlete's hand, to enable greater understanding to the causes of injuries, such as tennis elbow. Additionally, a parametric study of the racket dimensions was performed, with relation to overall performance, allowing optimal design of racket to be determined. Sprigings and Neal (2000) developed a model of a three segment arm swinging a golf club. Parameters were adjusted to achieve maximum club head velocity, identifying the importance of achieving a high wrist torque.

Hatze (1981) developed a 17 segment humanoid model, with the ability to control the relative segment motion from 46 modelled muscles. This basic musculoskeletal model was combined with external constraints allowing locomotion (running and jumping) and trajectory to be modelled. Analysis of long jump take off parameters allowed optimisation of technique to be performed.

2.6.1 Swimmer Force Model

Nakashima et al. (2007) developed a full body human swimming model (Name: SWUM) considering rigid body dynamics and unsteady fluid forces. The scope of the simulation is to model the fluid forces exerted over the whole body and the resultant motion of the centre of gravity for any swimming stroke. Five degrees of freedom equations of motion, for the body centre of gravity, are defined (sway ignored). The body is modelled as 21 rigid elements. To achieve the shape of the human body, the elements have varying degrees of taper and ellipse. Fluid forces acting on the segments are buoyancy, inertial, normal and tangential forces (figure 2.17), dictated by the segment position, velocity and acceleration.

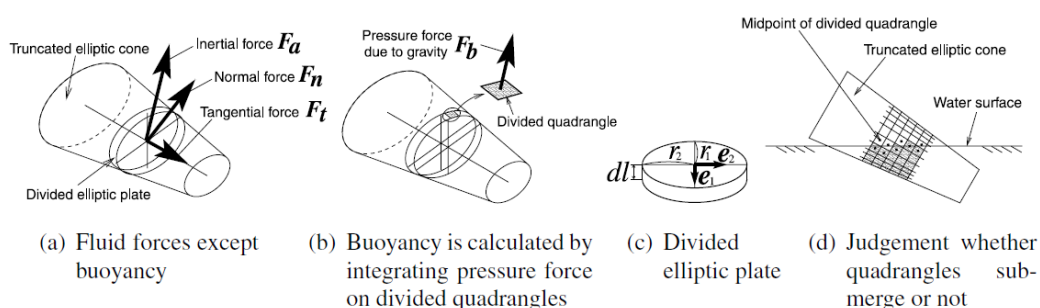


Figure 2.17. Fluid forces acting on each segment in SWUM (Nakashima et al., 2007).

Buoyancy is determined theoretically, with inertial, normal and tangential force coefficients determined experimentally. A three segment experimental model, proportioned to be the average size and shape of the body segments, was tested to determine the coefficients for all segments on the body. The model was oscillated in water, measuring torque and rotation angle. This provided the added mass coefficient and the drag coefficient normal to the segment. The forces on the torso, head and neck were assumed to be relatively small, and therefore inaccuracy in these segments, due to differences in shape from the tested model, was acceptable. Replicating the experiment in a simulation, based on the same segment dimensions and motion, provided forces within an error of 10%, when compared to the experimental data.

Tangential drag acting on a segment is reported to mainly represent the passive resistance of the swimmer, while normal and inertial forces contribute to the propulsive forces. To determine a segment tangential drag coefficient, a total passive resistance coefficient of 0.03, from literature, was assumed. A

Literature Review

representative simulation was performed, at a constant velocity, and the tangential drag coefficient adjusted until the total drag coefficient (including normal drag on all segments) was equal to 0.03.

To model the body forces while swimming, motion is defined through joint angles. Three dimensional joint angles are determined from digitised video footage, gathered from two camera planes.

The resulting self-propulsion speed of a six beat freestyle simulation is 7.5% slower than the actual swimming speed. This error is likely due to the oversimplification of the total resistance of the swimmer. Assuming the passive resistance is mainly comprised of tangential and normal segment forces, ignores the dominant surface and underwater components: wave resistance and viscous pressure resistance.

More recent developments to the SWUM model have been made to perform multi object simulation, such as the simulation of a mono-fin attached to the swimmer and the release of a water polo ball after a throwing motion (Nakashima et al., 2010).

Based on a review of the literature, no swimmer force models have been used to simulate a swimming race. This therefore highlights the need to develop a model which can accurately simulate the swimming speed of a swimmer throughout the various phases of a swimming race.

2.6.2 Modelling and Simulation – Validation and Verification

Sargent (2005) discussed methods for model verification and validation. It is reported that no universal tests exist to determine the ‘correctness’ of a model, due to the specific application of mathematical models. Therefore the following practical approaches are recommended,

- Animation to allow comparison with reality
- Comparison to other models
- Event validity – event of occurrences in comparison to reality
- Extreme condition tests – extreme circumstances should not lead to unrealistic output
- Face validity – asking individuals knowledgeable about the system if the model outputs are reasonable

2.7 Summary

The hydrodynamic resistance of a body moving at a constant velocity on the free surface is comprised of *Friction*, *Viscous Pressure* and *Wave* resistance. The total resistance is the sum of these three components.

Froude number is used to describe ship speed in terms of its wave system. Maximum wave resistance occurs at Froude numbers 0.35-0.5. Sprint swimmers have a Froude number of 0.51, identifying the importance of wave resistance. Measurement of wave resistance can be performed with wave elevation measurements or predicted analytically using Thin Ship Theory

Skin Friction resistance arises from shear stress between the fluid and the moving body. Skin friction resistance is dependent on Reynolds number. Empirical relationships can be used to predict the skin friction at a range of Reynolds numbers.

Viscous pressure resistance is due to development of the boundary layer and separation, caused by an adverse pressure gradient due to harsh re-entrant angles along the body. Measurement of viscous pressure resistance is difficult and is usually determined by measuring total resistance and deducting friction and wave resistance.

Swimming passive resistance is the resistance of a swimmer when not producing propulsion (gliding). Passive resistance is measured either by towing or in a circulating water channel using dynamometry to measure force. Passive resistance has been reported in many different studies. Where data is presented in the same units, the results appear to be similar (40-60 N @ 1.5 m s⁻¹, underwater streamlined).

Measurement of the resistance components in swimming identify varied results, mainly due to differences in the conditions tested. Wave resistance is found to range from 14-60%. However, differences in the surface penetration are found to significantly affect the results. Comparison of a skin friction resistance prediction, using the ITTC empirical formula, is found to compare well with directly modelled friction on a swimmer. Skin friction and viscous pressure resistance are found to contribute 8-26% and 74-92% to total underwater resistance respectively.

Active resistance is the dynamic resistance experienced by the swimmer during active swimming. It is not possible to measure active resistance directly and therefore various techniques have been developed to predict it. Comparison of active resistance values, determined for the same swimmers, using two different methods, find a significant difference between the values. The velocity perturbation method and the measurement of active drag system predict active resistance values of 53.2 N and 66.9 N respectively at 1.64 m s^{-1} . The difference between active and passive resistance is considered similar to the thrust deduction concept in naval architecture theory.

Swimming propulsion is considered as arm propulsion and leg propulsion. In freestyle swimming, arm and leg propulsion are used on the surface and underwater undulatory swimming is used after the starts and turns. Arm propulsion is considered as lift and drag generated by the arm motion, and a large body of literature reports measured force coefficients for a swimmers arm. It is proposed that the arm propulsion can be modelled assuming drag only propulsion using the drag coefficients reported and time accurate arm motion from video data. The correct arm propulsion can be achieved by scaling the arm geometry as performed by (Akis, 2004). Leg propulsion is considered similar to fish propulsion in both freestyle flutter kick and UUS. Using large amplitude elongated body theory (LAEBT) developed by Lighthill (1971) it is possible to predict the propulsion generated by a known motion. Comparison of the predicted thrust with both computation and robotic studies, identify similar results. It is therefore proposed LAEBT can be used to model the propulsive forces of freestyle flutter kick and underwater undulatory swimming.

Fatigue is identified as an important contributor to race time, and therefore must be modelled to ensure accurate race time simulation. Fatigue occurs due to depletion of the available energy and power to the muscles. Bioenergetics theory identifies the various sources of energy for exercise, and how they deplete during fatigue. Exhaustion studies identify the energy capacity and maximum available power per unit body mass, for males and females, for anaerobic and aerobic energy sources.

Analysis techniques for sport have been defined as qualitative, quantitative and predictive, with mathematical modelling and simulation being a predictive

Literature Review

method. Simulation has been used for many applications in other sports, however a model developed by Nakashima et al. (2007) is the most relevant to this study. SWUM, a full body fluid force model, predicts the free swimming speed and segment forces of a 21 segment human, performing any movement in the water. Although complexity is achieved through modelling the forces on each body segment, free swimming speed is under predicted by 7.5%. This error is likely to be due to neglecting the influence of individual resistance components.

No published swimmer force models have been used to simulate a swimming race. This identifies the need to develop a model which can simulate the swimming speed of any swimmer throughout the various phases of a freestyle race. Such a model can therefore be used to predict race time.

Validation and verification methods for simulations identify the importance of testing a model appropriately, to ensure confidence in the output. A range of test methods are detailed. White-box validation ensures the individual components correctly model the problem and black-box validation ensures the whole model simulates the real world situation. Therefore, to ensure simulation validity in this study, both white box and black box validation will be performed.

3 Race Simulation

3.1 Introduction

In this chapter a simulation is designed so that the race time implications of selecting different equipment, changing technique or race strategy can be determined. No previous studies, investigating the resistance and propulsion of swimmers, have attempted to model the swimming speed or work done by a swimmer throughout a race. This chapter describes the process to model the resistive and propulsive forces acting on a swimmer in each phase of a swimming race, enabling the swimming speed (in each phase) to be simulated and race time predicted. The forces acting on a swimmer are modelled individually with separate resistance and propulsion models, feeding into an equation of motion, which outputs the swimmer motion throughout a race.

Since the swimming resistance literature lacks the relevant information to create a robust resistance model, the need to conduct a resistance study is identified. This will enable the resistance of a population of male and female swimmers, on the surface and underwater, to be modelled. The implementation of a resistance model within the race simulation is described in section 3.6; however the process to generate the resistance model is detailed in Chapters 4 and 5.

The arm propulsion model is based on a single rotating element producing drag. Section 3.7 describes the theory used to model the force along the arm, the method used to acquire the input motion and the numerical implementation of the arm motion for a range of stroke rates. A common technique trait, identified during the SwimSIM testing program, is an imbalance in propulsion from between the two arms. In most cases, this due to one arm rotating more slowly, during the *in water* phase of the arm rotation. To understand the race time implications of an imbalance, it is necessary to simulate this technique trait. To achieve this, a modification to the implemented arm motion is made.

Large amplitude elongated body theory (Lighthill, 1971), described in Chapter 2, is used to model the propulsion generated during freestyle flutter kick and underwater undulatory swimming. Section 3.8 describes the numerical

Race Simulation

implementation of this theory, the acquisition of kinematic data, and how LAEBT is used to simulate the propulsion for both UUS and freestyle flutter kick.

Combining the simulated work done by the propulsion models with bioenergetics theory and experimental data from exhaustion tests, the fatigue of a swimmer may be modelled. This ensures the simulated propulsive power remains within human capabilities and can provide a better insight into race strategy. In section 3.9 the fatigue model is described. The depletion of anaerobic energy, as work is done by the propulsion models, is modelled based on a battery. Limiting stroke rate with a PI controller, to ensure propulsive power does not exceed the available power, simulates the effect of fatigue as the available power depletes.

3.2 Model Requirements and Aims

The aim of the race simulation is to simulate the swimming speed, work done and fatigue, throughout a male and female freestyle race, for a range of heights, masses and race strategies. This will enable the key questions of this study to be addressed.

It is important to note that this study does not attempt to model or capture the full physics of the flow around a swimmer. This would require lengthy, complex experimentation and substantial computational resource. Instead, basic models, supplemented with experimental data, will be used to predict the resistance and propulsion of a swimmer in the various phases of a swimming race. In addition, experimental data will be used to ensure the relationship between swimming speed, resistance, propulsion and fatigue are captured.

3.3 Modelling a swimming race

To accurately simulate total race time, it is necessary to capture time spent in each phase of a race. This ensures that any change in swimming speed, modelled in a particular phase, has the correct relative influence on total race time.

The proportion of race time spent in each phase varies across events (figure 3.1). However, for all events, little time is spent in both the *dry start* and the *turn rotation* portions of the race. The *dry start* phase is where the swimmer executes a push-off from the block, travels through the air, before entering the water. The *turn rotation* phase is where the swimmer rotates during the change of swimming direction, in a turn. The key questions of this study relate to surface and underwater swimming. Therefore, to prevent unnecessary complexity in the simulation, the physics of the start and turn are not modelled. Instead, the effect of the start and turn are simulated at the appropriate stage of the race, by adjusting swimming speed, distance swum and race time to account for these phases. A dive entry and push-off turn speed of 4 m s^{-1} and 3 m s^{-1} respectively are assumed for all swimmers (Cossor and Mason, 2001; Mason and Cossor, 2001). The distance achieved after a dive and time taken to perform a turn are assumed fixed at 3.5 m and 1.36 s. These values have been determined from race data supplied by British Swimming.

For surface and underwater phases, the resistance and propulsion of the swimmer are modelled independently. When swimming on the surface, propulsion is produced from the arms and legs, and the total resistance of the swimmer includes wave making resistance. When swimming underwater, propulsion is produced from the legs only, and the total resistance of the swimmer does not include wave making resistance. These differences influence both the swimming speed and work done by the swimmer; therefore, it is important the phases are modelled independently, to accurately simulate race time and fatigue.

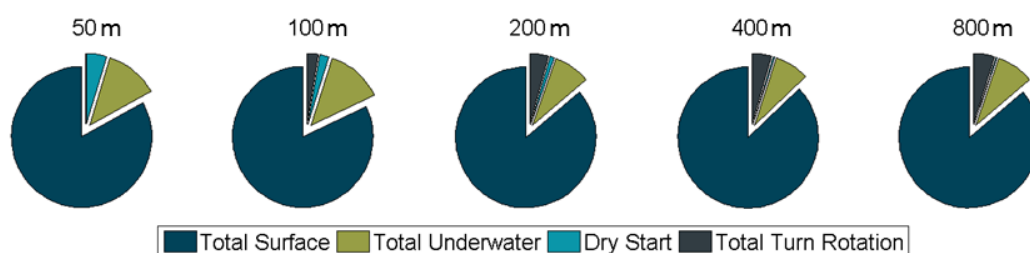


Figure 3.1. Male freestyle race phase contributions. Race distance is displayed above each pie chart.

The race phase algorithm is displayed in figure 3.2. This logic is accessed continuously throughout a race simulation.

Race Simulation

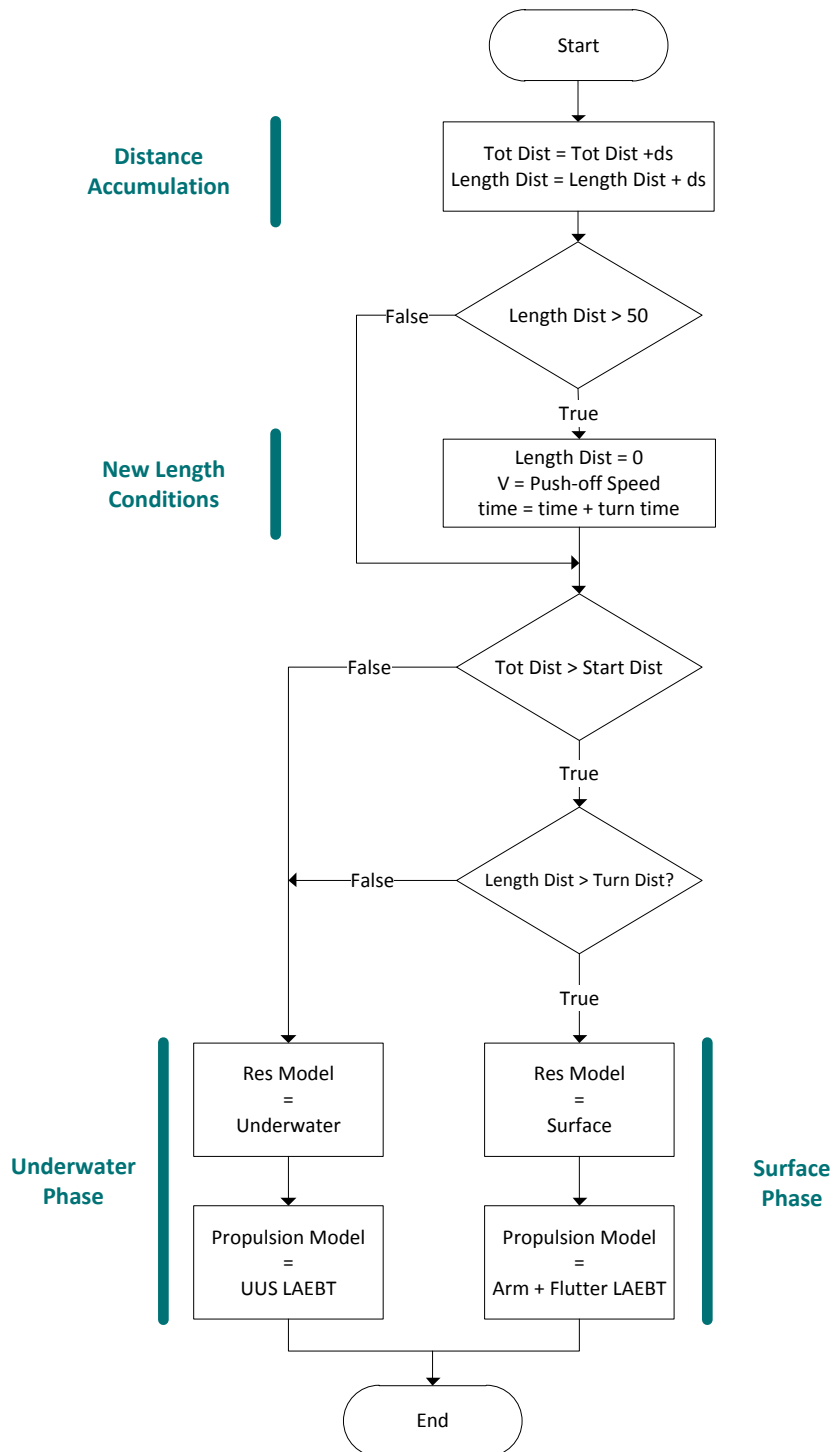


Figure 3.2. Race Phase Algorithm. The total race distance swum and distance with each length is accumulated. If the end of a length is reached (length Dist > 50), new length conditions are assigned, which resets the length distance to zero, accounts for the time taken to turn, and increases the speed of the swimmer, simulating a push-off. The resistance and propulsion models, which dictate the forces in the equation of motion, are switched on/off depending on the position of the swimmer within each length and within the race. This simulates the different resistive and propulsive forces and the work done by the swimmer in the underwater and surface phases.

3.4 Modelling Motion

To model motion, it is necessary simulate the progression of the swimmer through time and space. To numerically model the mechanics of a system in time, time stepping is required. A time stepping model operates in a loop, where all calculations are performed for small increments of time. Equations of motion, through time stepping, provide the motion of an object, depending on the net forces it is subject to. An object in space has six degrees of freedom and experiences forces and moments in those directions. To model the motion of a swimmer, it is necessary to determine these force and moments. However, when passive and active resistance measurements are performed, the force measured is assumed a result of the tow velocity, which is a motion in surge (forward/aft motion). These measurements are likely to include forces influenced by motion in other degrees of freedom; however, due to the complexity of capturing these motions, the measured force is treated as a result of surge motion only. Therefore, due to this limitation, the swimmer is assumed to only experience motion in surge. Although, limiting motion to surge only may lead to inaccuracies in the origin of the resistive force, this provides the relevant information to model the progression of a swimmer through a race.

3.4.1 Time Step Model

This study uses a first order finite backwards differencing Euler approach. A fixed time step of size dt is used to calculate the state of the system at $t+dt$. An index value i is used to describe the progression of time for each time dependant variable in the model. At the end of each loop the index value is increased and the elapsed time is accumulated,

$$i = i + 1, \quad (3.1)$$

$$t(i + 1) = t(i) + dt, \quad (3.2)$$

where t is the elapsed time at each time step.

A first order approach has been adopted due to the simplicity of implementation for both the equations of motion and modelling the generation of forces in the propulsion models. To ensure the numerical error is minimised

Race Simulation

an appropriate time step is determined. The time step needs to be sufficiently small to ensure that the physics being described by the various models is fully captured. This is achieved by performing a convergence test: the time step dt is systematically reduced until the solutions from each model converge to constant values. The results from the convergence test for each propulsion model are detailed in Chapter 6.

3.4.2 Motion in Surge

The acceleration in surge is a result of the net force acting on the swimmer,

$$a(i + 1) = \frac{T_x(i + 1) - \frac{R(i + 1)}{(1 - t)}}{m + m_{added}} \quad (3.3)$$

where T_x is the resolved thrust in the X - direction (direction of swimming), R is the resistance of the swimmer, m is the mass of the swimmer and m_{added} is the added mass of the swimmer. The resistance and propulsion are determined by individual models, specific to the race phase.

Velocity and distance are determined as

$$V(i + 1) = a(i + 1) \times dt + V(i) \quad (3.4)$$

$$dS(i + 1) = V(i + 1)dt. \quad (3.5)$$

Progression through the race is determined by,

$$S(i + 1) = S(i) + dS, \quad (3.6)$$

where S is the accumulated distance swum throughout the race and dS is the distance swum during a time step. When the distance swum reaches the race distance, the model is stopped. The swimmer is treated as a point mass which is assumed to cover the full distance of the race. The distance covered by the point mass is assumed to be not affected by the dimensions of the swimmer.

3.5 Computational Approach

Figure 3.3 identifies the computational process used to simulate a swimming race. The process is split into four stages. The *Input* stage provides the parameters specific to each condition (swimmer and race), and defines the number of conditions being modelled. The *Swimmer + Race Definition* stage sets up the various models with the relevant parameters defined in the *Input* stage. The *Time Domain Race Modelling* stage steps the model through time, calculating the swimmer motion based on race phase, resistance and propulsion. At the end of a simulated race, the *Output stage* provides data that has been accumulated in an output file for post processing.

In the *swimmer parameters* all the information necessary to define the swimmer and the race is provided. Height, mass and gender define the dimensions of the swimmer. The race distance is defined here. The swimming strategy is defined by stroke rates throughout the race and distances swum underwater. Parameters describing the technique of the swimmer and adjustments to the resistance and propulsion models are defined in the *swimmer parameters*. Multiple conditions can be defined and run as a batch. The *model input parameters* are a series of tasks to provide information and initial conditions to the forthcoming models. The height, mass and gender information in the swimmer parameters is used to determine the dimensions of the arms and legs, and scale the kinematics for the propulsion models. This process uses the anthropometric data described in figure 1.6. In addition, height, mass and gender are used by the *resistance model*, to generate a surface and underwater resistance curve for the swimmer. The *race phase definition* provides the *phase model* (figure 3.2) with the distances swum underwater after the start and turns. In the *R&P calculation*, the resistive and propulsive values for the current time step are calculated, before being fed into the *kinetic model*, which contains equations 3.3 to 3.6, to calculate the swimmer motion. During the surface phase, when both the arm and leg propulsion models are in operation, the total propulsion is the sum of the outputs from each model. The *time step model* increments time and the index value i . This process is repeated until the race distance is covered.

This model is constructed using the numerical computing tool Matlab™. The final version of code for the race simulation is provided in Appendix 1.

Race Simulation

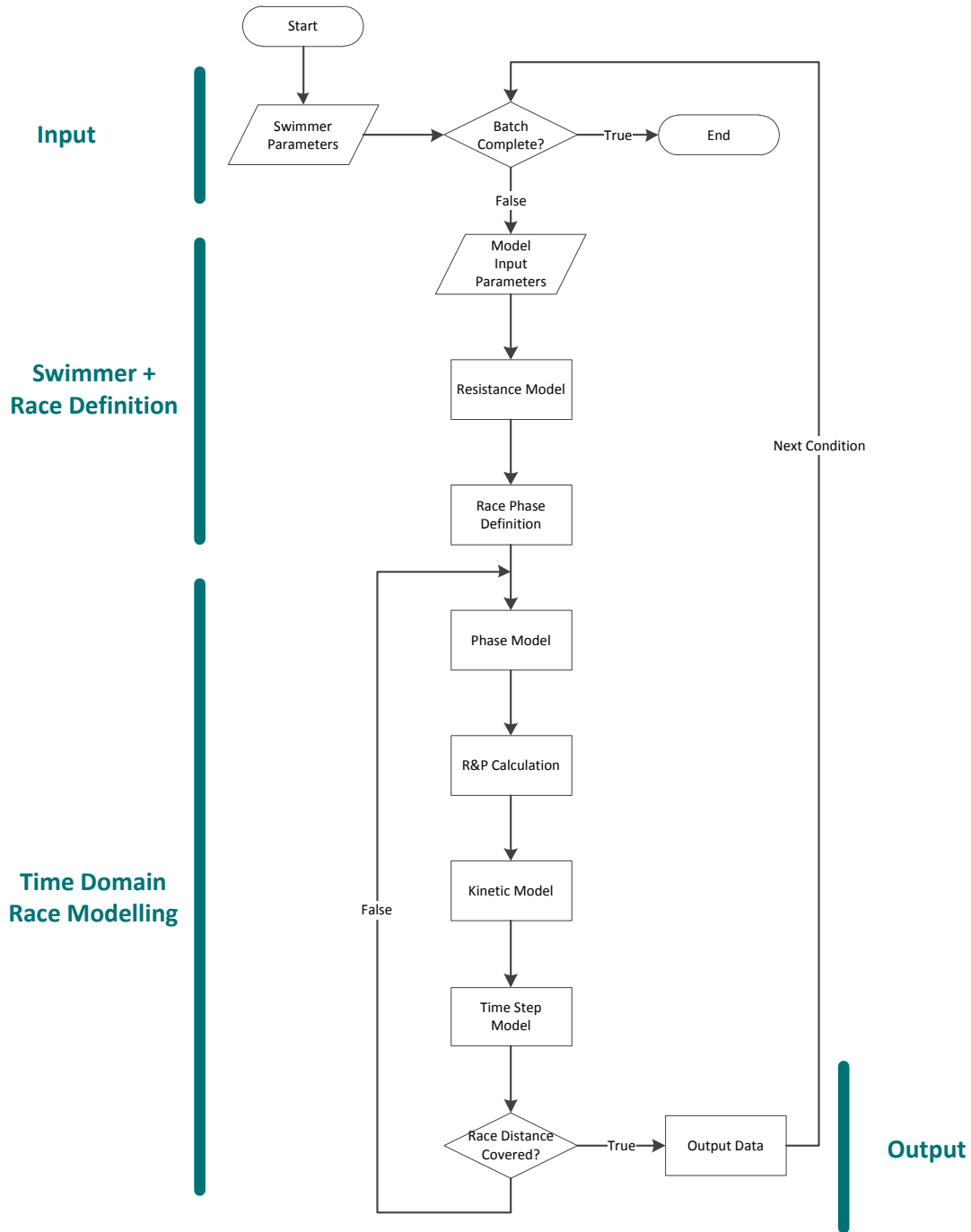


Figure 3.3. Race Simulation Process.

3.6 Resistance Model

The role of the resistance model is to provide the resistance of a swimmer for each phase in a race. Therefore the resistance needs to be known during surface and underwater swimming for any height, mass and gender. This data is stored in the model and using height, mass and gender, a surface and underwater resistance curve, for the appropriate range of speeds, is generated. During the *R&P calculation*, the appropriate resistance curve is interpolated with respect to speed, using a spline interpolation. This provides equation 3.3 with a resistance value $R(i + 1)$ for $t(i)$, based on $V(i)$.

Based on published swimming resistance studies, it is not currently possible to accurately predict surface and underwater swimming resistance, over a range of speeds for a specific height, mass and gender. Therefore, this study aims to combine empirical, computational and experimental methods to determine the resistance components for the population of swimmers tested by SwimSIM. This requires the development of bespoke experimental equipment, detailed in Chapter 4, and the subsequent generation of a resistance model is reported in Chapter 5.

3.7 Arm Propulsion

The aim of the arm propulsion model is to simulate the arm propulsion and propulsive power for a range of stroke rates. In addition, the effect of swimming technique, such as arm speed through the water or imbalance, is to be modelled. This will enable the impact of changes to these technique characteristics to be quantified.

3.7.1 Model

The arm is represented as a single element, with motion on a single plane, following a circular pattern. Figure 3.4 displays how the arm model is represented.

Race Simulation

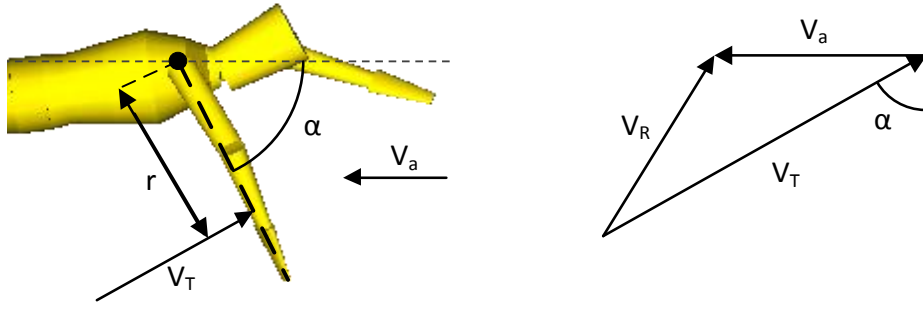


Figure 3.4. Arm free body diagram. The fluid velocity experienced by the arm is vector addition of the arm tangential velocity and the swimmer advance velocity. The yellow graphic on the left is taken from a figure published by Nakashima (2007) and has subsequently been annotated.

The resultant local velocity along the arm V_R is determined by vector addition of the local tangential velocity V_T generated by the arm rotation and the advance velocity of the swimmer V_a . The local tangential velocity of the arm V_T is determined as,

$$V_T = \dot{\alpha}r, \quad (3.7)$$

where $\dot{\alpha}$ is the rotational velocity of the arm in radians per second and r is the radius at points along the arm from the axis of rotation.

Assuming the axis of rotation to be the origin $[0 \ 0]$, any point along the arm is represented by the vector $[r \cos \alpha \ r \sin \alpha]$. Therefore, the unit vector of the tangential velocity V_T is perpendicular to the arm vector and is determined as,

$$\widehat{V}_T = \frac{[-r \sin \alpha \ r \cos \alpha]}{|[-r \sin \alpha \ r \cos \alpha]|}. \quad (3.8)$$

The unit vector representing the direction of the advance velocity is simply $[-1 \ 0]$, since the direction of motion is purely horizontal. Therefore, the resultant velocity acting on the arm is,

$$V_R = \dot{\alpha}r\widehat{V}_T + V_A[-1 \ 0]. \quad (3.9)$$

To determine the thrust and torque generated by the arm, it is necessary to determine the relevant components of velocity. For thrust, the component of V_R acting in the horizontal direction is required, and for torque, the component of V_R tangential to the arm is required. These components are determined by

taking the dot product of V_R with the relevant unit vector ($Thrust: [-1 \ 0]$, $Torque: \widehat{V}_T$).

The thrust generated by the arms is determined by the integral,

$$Thrust = \int_0^l \frac{1}{2} \rho (V_R \cdot [-1 \ 0])^2 Wth(r) C_d(r) dr, \quad (3.10)$$

where l is the length of the arm, ρ is the density of the fluid, $Wth(r)$ is the width along the length of the arm and $C_d(r)$ is the drag coefficient along the length of the arm. A C_d value of 1.3 is assumed for the arm (Berger et al., 1995; Gardano and Dabnichki, 2006).

The torque about the shoulder ($[0 \ 0]$) is determined by taking moments along the arm in the following integral,

$$Torque = \int_0^l \frac{1}{2} \rho (V_R \cdot \widehat{V}_T)^2 Wth(r) C_d(r) r dr, \quad (3.11)$$

where inertial forces, due to unsteady arm motion acting on the local fluid and arm mass, are ignored.

Arm power is determined from the torque exerted on the arms and the rotational speed of the arms and therefore is determined as,

$$Power = Torque \times \dot{\alpha}. \quad (3.12)$$

This model makes the assumption that the forces experienced by the arm may be modelled quasi-statically. Toussaint et al. (2002) found through flow visualisation, that a pressure gradient along the arm, only seen during active tests, causes significant radial flow towards the hand. This caused a greater pressure difference over the hand and increased the fluid dynamic load. It is concluded that the effect of axial flow, potentially increasing propulsion generated by the hand, needs further investigation. If axial flow causes significant unsteady forces, it may be possible to account for this using an added mass coefficient multiplied by the local tangential arm acceleration.

Race Simulation

3.7.2 Input Motion

The rotational velocity of the arm is dictated by both the technique and strokerate adopted by the swimmer. The strokerate quantifies the period of one full arm rotation; however, it is necessary to determine the instantaneous rotational velocity of the arm throughout a stroke cycle, to ensure V_T at any point in time is modelled. This is achieved by analysing video data. Figure 3.5 displays the manual digitisation process, where the angle of the arm is determined throughout the *in water* phase of the stroke. For every frame of video, the angle between the hand and the shoulder, relative to a horizontal reference (tiles on the wall) is determined. For the latter portion of the *in water* phase the arm bends, therefore the angle captured by this process does not represent the angle of the actual arm segments; however, provides a representative motion if the arm were a single segment.



Figure 3.5. Generating two dimensional arm motion data from manual digitisation of video data footage.

This process produces a dataset of arm angle against frame number, for the *in water* phase only. A fixed frame rate of 50 frames per second was used. To determine the arm motion in the *out of water* phase, a cubic spline fit has been used across two *in water* phase datasets (figure 3.6). This fit is then cropped to one stroke cycle producing the arm angle data against frame number for a single stroke cycle. It is important to determine an accurate *out of water phase* time as this dictates the relative time spent in the *in water* and *out of water* phases for any given stroke rate. This ensures the arm velocity, in both the *in water* and *out of water* phases, can be correctly scaled according to stroke rate.

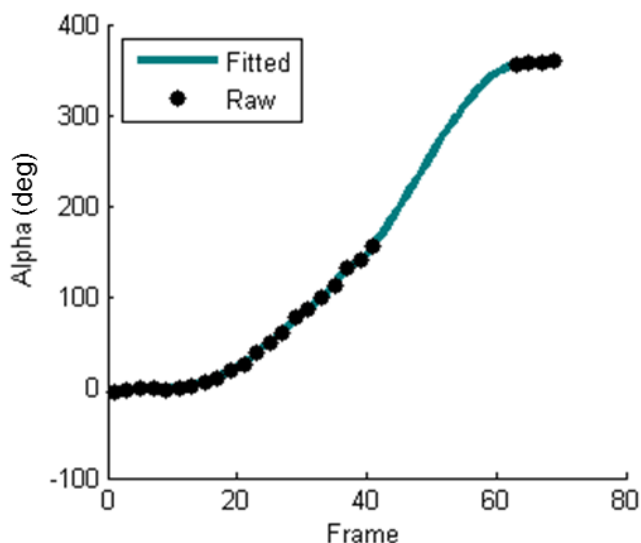


Figure 3.6. Fitting process to determine the arm motion in the *out of water* phase which is not captured by video data.

This process was conducted for five elite athletes performing their regular freestyle stroke technique, and one non-elite athlete performing straight arm freestyle and a catch-up technique (catch-up: where only one arm rotates at any given time, the stationary arm points forward until the moving arm completes the cycle). This enabled the influence of different techniques on instantaneous arm rotational velocity to be determined. Figure 3.7 displays the rate of change of α , determined from the delta α between each frame, against arm angle for each athlete tested. Common between all athletes is a low rate at the beginning of the arm cycle, followed by a peak at about 90 degrees, and then a significant increase in velocity during the *out of water* phase. Plotting delta α values against frame number allows the effect of instantaneous arm velocity to be observed against time. This data can be scaled to a different stroke rate, by scaling the time data it is plotted against.

Race Simulation

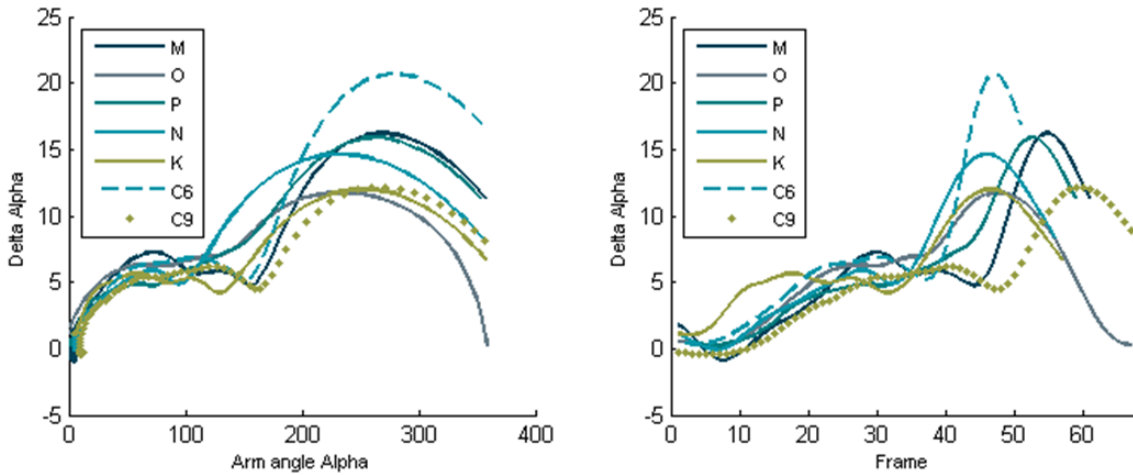


Figure 3.7. Rate of change of arm angle throughout a stroke cycle for five elite athletes performing regular freestyle technique (solid lines) and a non-elite athlete performing straight arm freestyle (dotted line) and catch-up freestyle (dashed line). Delta Alpha (degrees) is the rate of change of Alpha, with respect to the x-axis variable in both the left and right plot.

To minimise the amount of input data required, a generic arm motion to simulate all swimmers is used. The motion data in figure 3.7 (left plot) for athlete C9 is roughly the mean of the data for all other swimmers, during the *in water* phase ($\alpha < 180$). This data is for a straight arm freestyle technique and therefore the digitisation process will have been more effective in capturing the instantaneous velocity of the entire arm. In addition, a straight arm freestyle technique will be more representative of a single element arm model. Therefore, this motion scaled to the appropriate stroke rate will be used to model the arm motion for any swimmer. However, if a higher level of accuracy in the arm motion data is required, specific swimmer data can be used.

3.7.3 Numerical Implementation

To implement the above physics numerically, the arm is divided into an array of discrete strips with thickness dr and a distance r from the shoulder. For each strip along the arm the calculations in equations 3.7 to 3.9 are performed and the integration in equations 3.10 and 3.11 is performed using trapezoidal rule.

To implement the arm motion for athlete C9 in figure 3.7, the data is stored in a lookup table. The strokerate dictates the time for one cycle and a time vector (equation 3.13) defines the arm angle against time throughout a stroke cycle.

$$\frac{T_{stroke\ Period}}{No.\ Arm\ Angles} : \frac{T_{stroke\ Period}}{No.\ Arm\ Angles} : T_{stroke\ Period} \quad (3.13)$$

where the left most and right most terms are the start and end points of the time vector and the centre term is the time increment of the values between start and end. $T_{stroke\ Period}$ is the period of time to complete one stroke cycle and $No.\ Arm\ Angles$ is the number of angle data points. This provides a series of uniform time values, governed by stroke rate, to match the angle values.

At each time step a stroke time point is calculated

$$T_{stroke}(i + 1) = T_{stroke}(i) + dt. \quad (3.14)$$

$\alpha(i + 1)$ is determined from spline interpolation of the arm angle data and the time vector, with $T_{stroke}(i + 1)$ as the interpolant. At the end of the stroke cycle $T_{stroke}(i + 1)$ is reset to zero and the process is repeated for each cycle.

This process is identified in figure 3.8 (green), displaying $\alpha(i + 1)$ calculated in the interpolation process. A dot product calculation is used to back calculate the angle between the arm and the horizontal as a check that the appropriate angle has been achieved. Since the dot product calculates angles both clockwise and anticlockwise, the calculated angle is always between 0 and π . The defined angle is between 0 and 2π , measured anticlockwise from the horizontal. However, this confirms the defined angle is actually being implemented.

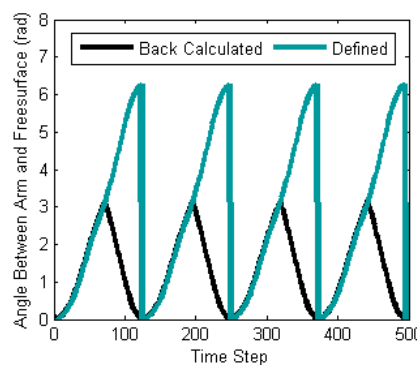


Figure 3.8, Defined arm angle, from interpolation of the arm angle data, and back calculated arm angle; confirming the correct implementation of arm angle.

$\dot{\alpha}$ is determined by first order numerical differentiation as follows,

Race Simulation

$$\dot{\alpha} = \frac{\alpha_{i+1} - \alpha_i}{dt}, \quad (3.15)$$

where α_i and α_{i-1} are the arm angles of the current and previous time steps.

Since the thrust and torque calculations are performed for all angles of α , it is necessary to implement a fluid phase change, to simulate the arm leaving the water. Therefore, when $\pi < \alpha < 2\pi$ (arm is out of the water), the density ρ is set to zero.

To model both arms the above procedure is duplicated, with the initial angle between the arms separated by π radians. The total thrust produced by the arm model is the sum of the thrust produced by each arm at each time step.

3.7.4 Stroke Imbalance

The most common attribute of freestyle, identified from athlete testing, is a thrust imbalance between left and right arm strokes. To simulate this imbalance, the rotational speed of one arm is reduced relative to the other. This needs to be achieved without causing a systematic phase change between the two arm strokes. Therefore, the rotational speed of the arm is reduced during the *in water* phase and sped up during the *out of water* phase to ensure the total cycle time is unchanged.

To implement this, the time vector for the slow arm needs to be split into a separate time vector for the *in water* and *out of water* phases. The *in water* time vector achieves the correct rotational arm velocity to model the forces and the *out of water* time vector speeds the arm up to ensure the total rotational time remains the same. The imbalance of the swimmer is defined with a coefficient C_{imb} describing the proportional *in water* arm speed deficit from left to right.

The time vector for the *in water* phase is described using the imbalance coefficient,

$$\frac{T_{stroke\ Period} C_{imb}}{No.\ Arm\ Angles} : \frac{T_{stroke\ Period} C_{imb}}{No.\ Arm\ Angles} : T_{stroke\ Period\ IN} \quad (3.16)$$

where $T_{stroke\ Period\ IN}$ is the stroke period of the *in water* phase.

The out of water time vector must speed the arm up relatively so that the total stroke time remains the same from left to right, preventing a phase change.

$$T_{stroke\ Period\ IN} + \frac{T_{stroke\ Period} - T_{stroke\ Period\ IN}}{No.\ Arm\ Angles\ OUT} : \frac{T_{stroke\ Period} - T_{stroke\ Period\ IN}}{No.\ Arm\ Angles\ OUT} : T_{stroke\ Period} \quad (3.17)$$

where *No. Arm Angles OUT* is the number of data points in the *out of water* phase and $\frac{T_{stroke\ Period} - T_{stroke\ Period\ IN}}{No.\ Arm\ Angles\ OUT}$ is the time increment for time vector in the *out of water* phase.

Figure 3.9 displays how this is achieved. In both the *No-Imbalance* and *Imbalance* case the red arm rotates at the same speed. In the *Imbalance case*, the green arm rotates slower during the *in water* phase and faster during the *out of water* phase. By adjusting the imbalance coefficient C_{imb} , different severities of imbalance can be investigated.

Race Simulation

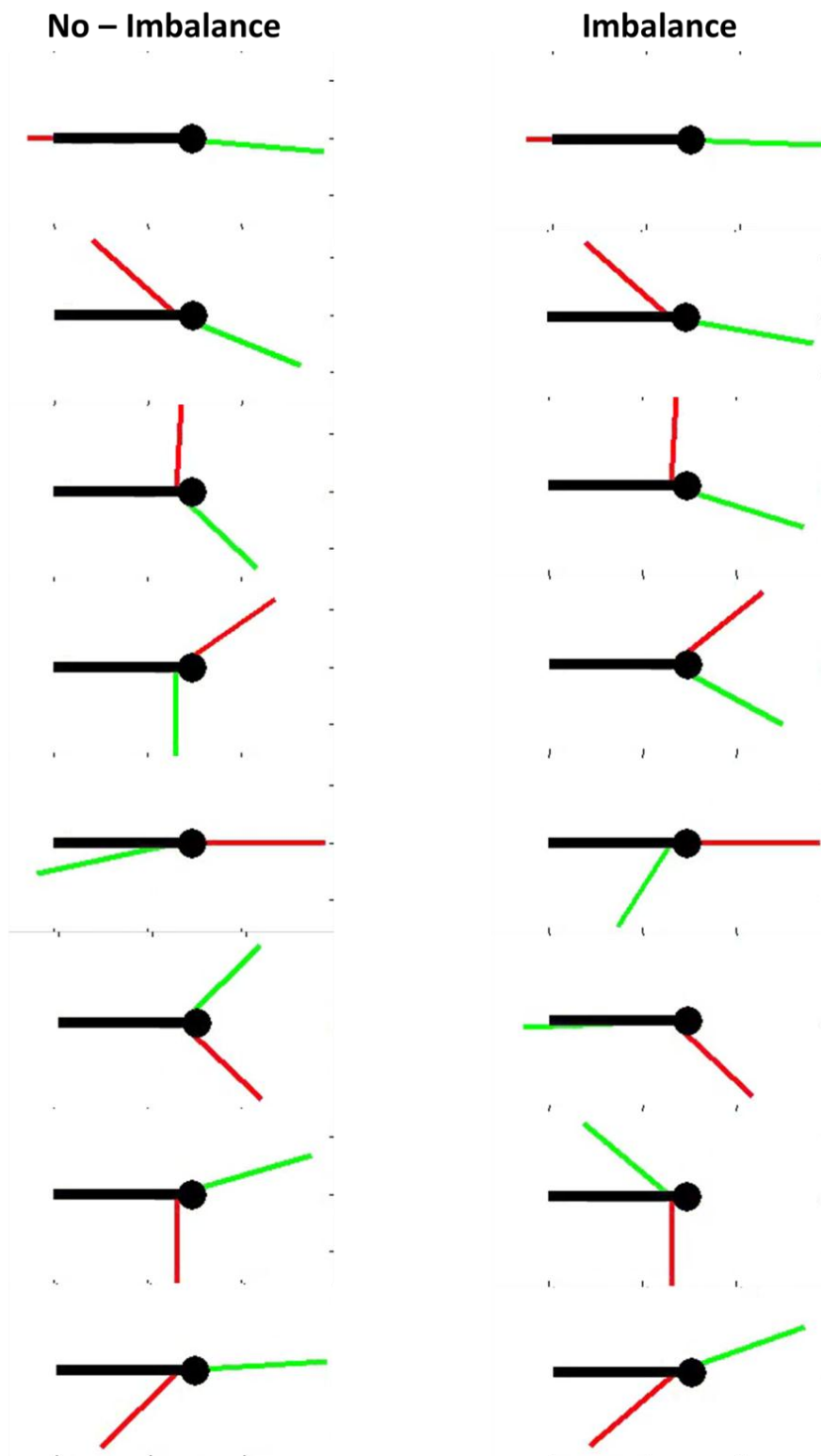


Figure 3.9. Arm motion graphics display how an imbalance is modelled without changing the stroke rate. In both cases the red arm rotates at the same speed.

3.8 Implementation of Large Amplitude Elongated Body Theory

The propulsion produced during underwater undulatory swimming (UUS) and freestyle flutter kick is to be modelled using Large Amplitude Elongated Body Theory (Lighthill, 1971) outlined in Chapter 2. The assumption that propulsion is generated from reactive forces due to acceleration of the surrounding fluid remains the same for both UUS and flutter kick, however the definition of the geometry and the input motion will differ. Equation 3.18 describes the propulsion produced from arbitrarily large motion.

$$P = \left[mw \left(\frac{\partial z}{\partial t} \right) - \frac{1}{2} mw^2 \left(\frac{\partial x}{\partial a} \right) \right]_{a=0} - \frac{d}{dt} \int_0^l mw \left(-\frac{\partial z}{\partial a} \right) da. \quad (3.18)$$

This propulsion prediction may be split into two components,

1. Rate of change of momentum in the wake (calculated at the tips of the toes, $a=0$). This component provides the total mean thrust experienced by the swimmer.
2. Minus the rate of change of momentum around the body i.e. a reaction force due to the acceleration of the fluid around the body. This component provides zero mean thrust over a stroke cycle, therefore only contributes to the time varying thrust.

3.8.1 Numerical Interpretation of LAEBT

The axis system described by Lighthill (1971) has the fish swimming from right to left. In this study, positive swimming velocity is assumed from left to right, therefore the original axis system defined by Lighthill (1971) is horizontally reversed. Positive is defined from left to right and bottom to top. This applies to momentum, acceleration and reaction force when resolved into the global axis system.

Although equations 2.17 to 2.20, describing the motion and added mass of the body, are defined continuously, it is necessary to apply these numerically to discrete strips along the body. The swimmer is assumed infinitely thin, in the ventral/dorsal direction. Figure 3.10 outlines how the motion of a strip, with

Race Simulation

length da and width S (into the page), may be defined. The vertical and horizontal velocity is defined as $\frac{\partial x}{\partial t}$ and $\frac{\partial z}{\partial t}$ respectively. The orientation of the strip is defined as $\frac{\partial x}{\partial a}$ and $\frac{\partial z}{\partial a}$ (figure 3.11). Equations 2.17 and 2.18 are used to determine the body axis velocities w and u . This process is conducted for every strip along the body.

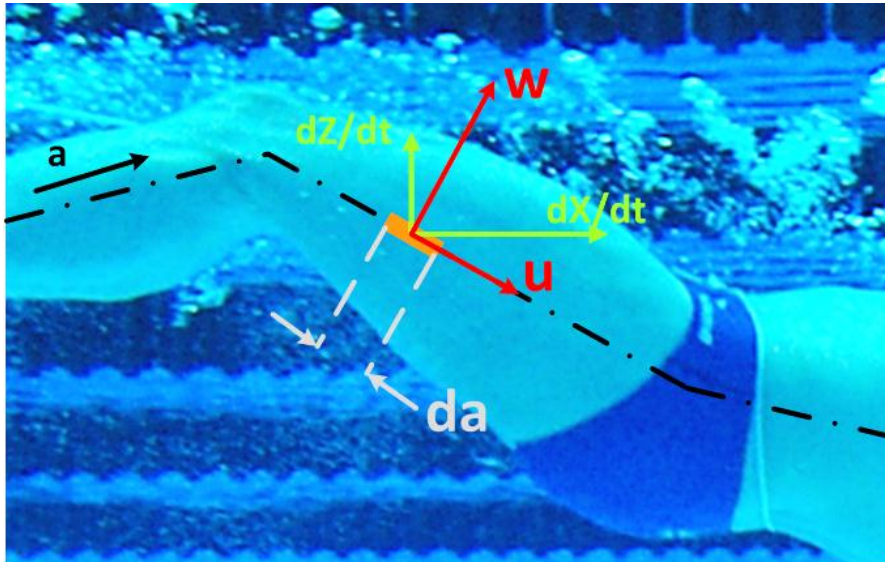


Figure 3.10. Motion and orientation of an infinitely thin strip of length da and width S , extending laterally through the swimmer (into the page), used to describe the motion of a swimmer during UUS

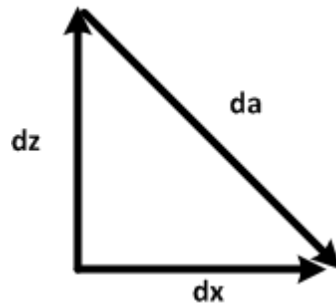


Figure 3.11. Definition of strip orientation

Numerical differentiation is performed for $\frac{\partial x}{\partial t}$ and $\frac{\partial z}{\partial t}$ between two time steps, using a single step finite backwards differencing method for all values of a . Vertical strip velocity is determined as

$$\frac{d}{dt}z(a_n, t_i) = \frac{z(a_n, t_i) - z(a_n, t_{i-1})}{dt}. \quad (3.19)$$

The kinematic data $x(a, t)$ and $z(a, t)$ is defined with a global axis system moving at the same speed as the swimmer. Therefore, it is necessary to apply the forward speed of the swimmer to the horizontal velocity of a strip. The horizontal strip velocity is therefore determined as

$$\frac{d}{dt}x(a_n, t_i) = \frac{x(a_n, t_i) - x(a_n, t_{i-1})}{dt} + V_i \quad (3.20)$$

where V_i is the horizontal speed of the swimmer.

For strip orientation, differentiation with respect to a is performed at each time step. For example

$$\frac{d}{da}z(a_n, t_i) = \frac{z(a_n, t_i) - z(a_{n-1}, t_i)}{da}. \quad (3.21)$$

Equation 3.22 describes the reaction force from the rate of change of momentum in the wake. The velocities and body orientation are defined at $a=0$, therefore values determined for the first strip, at the tips of the toes, are used.

$$Fr_{wake} = \left[mw \left(\frac{\partial z}{\partial t} \right) - \frac{1}{2} mw^2 \left(\frac{\partial x}{\partial a} \right) \right]_{a=0} \quad (3.22)$$

Equation 3.23 describes the reaction force due to rate of change of momentum along the body. Trapezoidal rule is used to integrate the momentum per unit length, $mw \left(-\frac{\partial z}{\partial a} \right)$, at each strip along the body. For periodic swimming movements, producing a mean motion in the x -direction, Lighthill (1971) notes that there is no contribution to the mean thrust from the reaction force along the body (equation 3.23). This component therefore allows a time accurate thrust prediction, however, will have zero mean thrust.

$$Fr_{body} = -\frac{d}{dt} \int_0^l mw \left(-\frac{\partial z}{\partial a} \right) da. \quad (3.23)$$

The total reaction force at any point in time is

$$Fr_{total} = Fr_{wake} + Fr_{body}. \quad (3.24)$$

Race Simulation

The hydrodynamic power required to perform UUS is determined from the local reaction force multiplied by the local velocity. The hydrodynamic power required to generate the rate of change of momentum in the wake is determined from

$$P_{wake} = \left[mw^2 \left(\frac{\partial z}{\partial t} \right) - \frac{1}{2} mw^3 \right]_{a=0}. \quad (3.25)$$

This expression has been determined from multiplying the unresolved components in equation 3.22 by w . The component $\frac{\partial x}{\partial a}$ is not taken, as it is the total power that is required and not the horizontal component. The hydrodynamic power due to the rate of change of momentum along the body is determined from

$$P_{body} = \int_0^l w \cdot \frac{d}{dt} mw da \quad (3.26)$$

where $\frac{d}{dt} mw$ is the perpendicular reaction force per unit length in each strip along the body. Therefore, total power is

$$P_{total} = P_{wake} + P_{body}. \quad (3.27)$$

3.8.2 Capturing the motion of the body

When viewing a swimmer in the sagittal plane, it is assumed to consist of the following seven rigid segments. This is a similar approach to that adopted by Nakashima (2009), however the torso is treated as one segment:

(1) Foot, (2) Shank, (3) Thigh, (4) Torso, (5) Upper Arm, (6) Lower Arm, (7) Hand

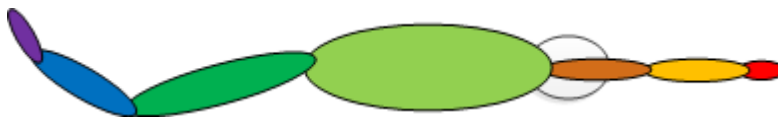


Figure 3.12. Body segments in the sagittal plane

The motion of the segments for specific UUS or flutter kick technique is determined from manual digitisation of underwater video footage of a swimmer. For UUS all seven segments are considered, whereas for flutter kick,

only the foot, shank and thigh are considered. Figure 3.13 displays the manual digitisation process where, for each frame, the segment end points are defined. Pixel location is calibrated from the known lengths of the segments. This process is repeated for every video frame throughout a kick cycle. A frame rate of 25 frames per second was used. As described above, LAEBT is performed numerically on strips along the body, therefore each segment is subdivided into strips. The individual strip position $x(a, t)$ and $z(a, t)$ is defined by the motion of the segment and determined from linear interpolation of the segment end points.

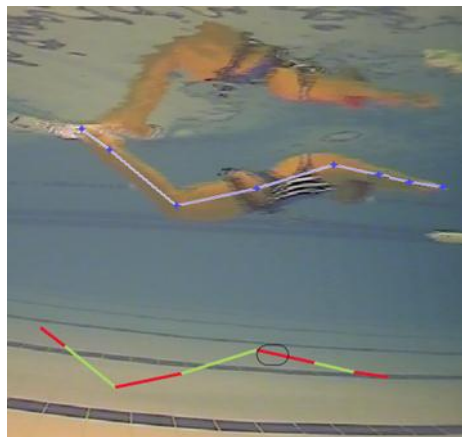


Figure 3.13. Manual Digitisation to determine body segment motion during UUS.

If motion capture is performed with a stationary camera or the speed of the moving camera does not exactly match the speed of the swimmer, the swimmer will drift across the field of view between frames. Therefore, the $x(a, t)$ data will include this drift. To eliminate this, the velocity at the hands is assumed to be equal to the speed of the swimmer and therefore any drift in the $x(a, t)$ data at hands is subtracted from the $x(a, t)$ for the rest of the body. For flutter kick, the $x(a, t)$ and $z(a, t)$ at the hips is subtracted from the rest of the data to eliminate camera drift and any hip roll.

In the manual digitisation process there is error associated with the selection of the segment end points. This produces a noise in the motion of the segment through time. Therefore, the motion data has been filtered to smooth this noise. Figure 3.14 displays example data of raw and filtered $x(a, t)$ motion for a single strip. A second order low-pass Butterworth filter with a cut-off frequency of 2 Hz has been used.

Race Simulation

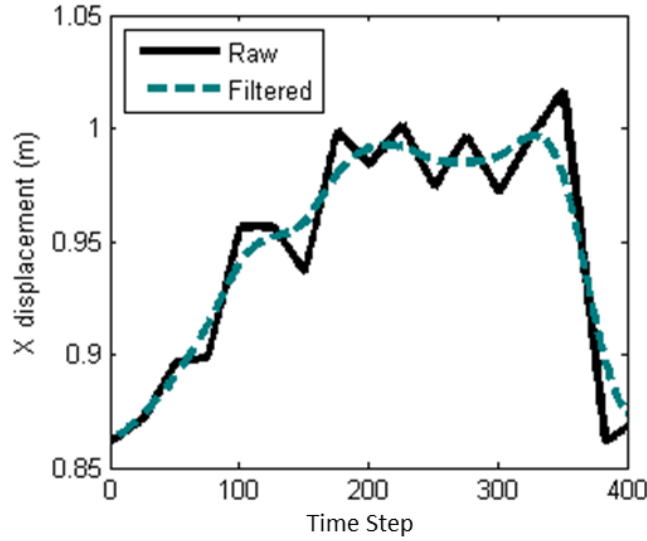


Figure 3.14. Raw and filtered $x(a, t)$ data for a single strip on the body. Noise is associated with error in the selection of the segment end points in the manual digitisation process.

To allow kinematic data to be used for other kicking frequencies the progression of a single stroke cycle through **time** is replaced with **phase**. Values of 0 to 2π described the progression of a kick from the beginning to the end of the cycle. This kinematic data, along with a phase vector is stored in a lookup table. To simulate the motion in time, a phase value is determined at each time step and used as an interpolant to determine the $x(a, t)$ and $z(a, t)$ for every strip along the body, at a specific point in the stroke cycle. The phase value λ , at each time step, is determined as

$$\lambda(i + 1) = \lambda(i) + freq \times 2\pi \times dt \quad (3.28)$$

where $\lambda(i)$ is the phase value at the previous time step, $freq$ is the kicking frequency in Hz and dt is the time step in seconds.

To model the propulsion for a generic swimmer performing UUS, kinematic data has been acquired for a single female elite athlete (Height: 1.71 m, Mass: 60.5 kg) performing UUS during a tow experiment (figure 3.15). It is assumed that this data can be used to generate the motion for any swimmer, based on their height and kicking frequency. This is achieved by scaling the original $x(a, t)$ and $z(a, t)$ data for swimmer height and Strouhal number (equation 2.15). Scaling the data with height ensures the amplitude of the kicking is proportional to the size of the swimmer. A fixed Strouhal number enables a

kicking frequency to be defined and the amplitude of the kick adjusted accordingly. This approach is beneficial when the kicking amplitude is not known but the frequency is. The original kinematic data was acquired from UUS performed at a Strouhal number of 0.39 (frequency: 1.7 Hz, Amplitude: 0.46 m, Swimming Speed: 2 m s⁻¹), therefore kicking amplitude for other frequencies will be determined assuming a Strouhal number of 0.39 at a swimming speed of 2 m s⁻¹. This Strouhal number is similar to that found in other human UUS studies (Von Loebbecke, Mittal, Fish, et al., 2009a). If the propulsion of a specific UUS technique is required, individual swimmer $x(a, t)$ and $z(a, t)$ data determined from manual digitisation is necessary.

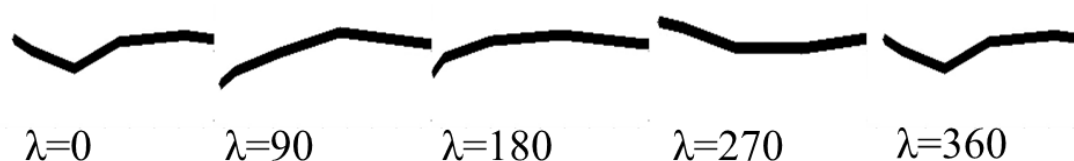


Figure 3.15. UUS kinematic data determined from manual digitisation of an elite female athlete performing UUS.

For freestyle flutter kick, a similar process has been conducted: the kinematic motion has been acquired for an individual athlete, to represent generic technique, from which the thrust for any other athlete performing freestyle flutter kick can be determined. The motion of one leg has been determined and is assumed the same as the other. As with freestyle arms, the motion of each leg is out of phase by π radians. Figure 3.16 displays how freestyle flutter motion is implemented for each leg.



Figure 3.16. Freestyle flutter kick kinematics

Combining the numerical approach for LAEBT and the kinematic data for UUS and freestyle flutter kick, the leg propulsion during surface and underwater phases in freestyle race may be modelled.

3.9 Modelling Fatigue

Using the experimental data for aerobic and anaerobic energy, identified in literature, a basic fatigue model can be constructed. The fatigue model must perform three functions:

- Calculate the energy and power being consumed by the propulsion models
- Calculate the physiological energy and power available based on bioenergetics theory
- Limit the propulsive power consumed by the propulsion models when the energy consumption approaches the energy available.

Propulsive power is accumulated each time step, to determine work done. Propulsive power is dependent on effort and race phase (underwater or surface swimming). Stroke rate is assumed to be the only parameter controlled by effort. In reality other factors, such as technique (Maglischo, 2002), will change with effort, however during a simulation, technique cannot be changed or controlled.

Figure 3.17 displays how the aerobic and anaerobic energy systems are modelled as two sources, and how they interact to provide available energy and power. Since aerobic capacity is assumed infinite, aerobic power is not subject to fatigue and therefore remains constant. Maximum anaerobic power is initially equal to peak power, determined from the experimental data, but reduces proportionally as stored anaerobic energy is depleted. Anaerobic energy is initially equal to the anaerobic capacity, determined from experimental data; however is depleted as work is done by the propulsion models.

To model the interaction of the aerobic and anaerobic systems, the anaerobic system is treated as battery with aerobic power coming in and total power, consisting of aerobic and anaerobic power, going out. If the total power is greater than the aerobic power, the stored anaerobic energy will deplete, reducing the available anaerobic power, causing fatigue. If the total power is less than the aerobic power, the anaerobic energy will replenish, increasing the available anaerobic power.

Anaerobic energy cannot become negative or be greater than anaerobic capacity. When anaerobic energy becomes zero, anaerobic power becomes

zero and the maximum available power is equal to the aerobic power. When $E_{an} = E_{an\ capacity}$ the model has fully recovered.

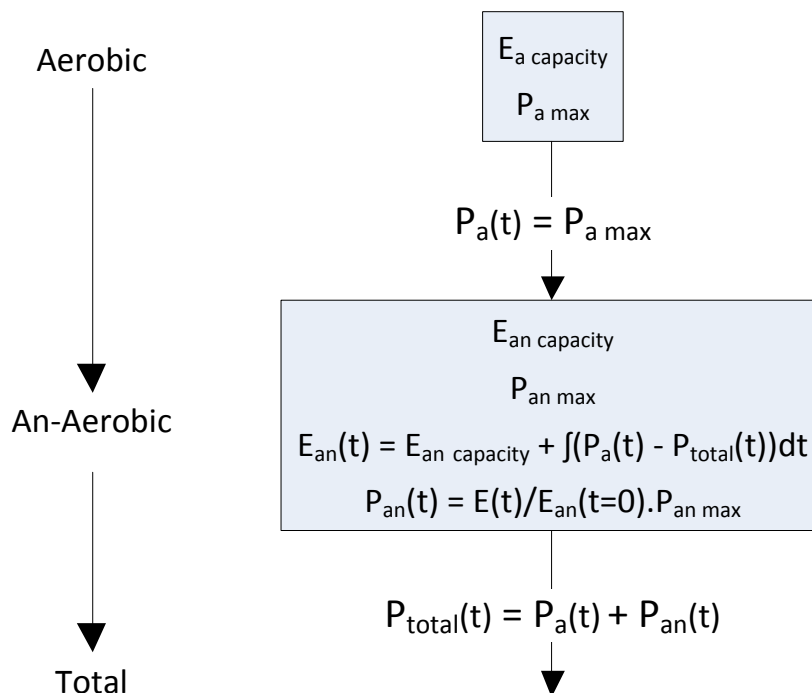


Figure 3.17: Human Energy System diagram, where E is energy, P is power and subscripts a and an identify aerobic and anaerobic respectively.

It is not possible for the propulsive power to be greater than the total available power. To ensure this condition remains true, it is necessary to control the swimming effort. This has been achieved using a proportional and integral control algorithm, controlling stroke rate (Doyle et al., 2009). Equations 3.29 to 3.31 display the methodology used to control stroke rate.

$$e(t) = (P_{propulsive} - P_{available} \cdot F_T)^{1/3} \quad (3.29)$$

$$PI = K_p e(t) + K_I \int_0^t e(t) dt \quad (3.30)$$

$$F_p = 1 - \frac{PI}{Strokerate} \quad (3.31)$$

It is assumed that $P_{propulsive} \propto Strokerate^3$. For arm propulsion, stroke rate dictates the rotational velocity and hence tangential flow velocity over the arm. The arm force is proportional to tangential velocity squared, therefore arm power is power is proportional to tangential velocity cubed. For leg propulsion,

Race Simulation

stroke rate dictates the perpendicular velocity of the strips along the body and power is proportional to strip velocity cubed. The error $e(t)$, the difference between the propulsive power ($P_{propulsive}$) and the available power ($P_{available}$), is raised to the power of $1/3$, and therefore becomes proportional to the error in stroke rate. PI is the sum of the proportional and integral terms. K_p and K_I are the proportional and integral gain values, which weight the influence of stroke rate control to either the instantaneous proportional error or the cumulative integral error. These values are adjusted (using a trial and error approach) to ensure the control model has a quick response, with minimum overshoot, and low steady state error. F_p is the power factor used to scale stroke rate.

With this control method, stroke rate will be reduced or increased when propulsive power is greater than or less than the available power. To ensure the fatigue model only reduces effort, the error is treated as zero when propulsive power is less than available power. This allows low stroke rates, or energy conservation tactics, to be specified without intervention from the control algorithm.

3.10 Summary

The architecture and computational approach for a model to simulate the swimming velocity throughout a race, and predict race time, has been outlined. Modelling each phase ensures the correct resistance, propulsion and therefore swimming speed and work done throughout a race is simulated. The simulation includes the effects of swimmer height, mass, gender, and race tactics.

A 1st order, one degree of freedom equation of motion uses the net force from the resistance and propulsion models and the mass of the swimmer to determine the acceleration of the swimmer, at each time step. This acceleration is used to determine the velocity and distance swum at each time step.

The requirement to construct a resistance model, to provide the equation of motion with a resistance value at each time step, is outlined. It is necessary to know the surface and underwater resistance for a swimmer of any height, mass and gender. This will allow the resistance of any swimmer to be modelled throughout a swimming race. The following chapters will detail the

development of the equipment and methods in order to obtain the necessary information to generate a resistance model.

Arm propulsion is modelled as the drag force produced by a single segment rotating with two dimensional motion. Propulsion is taken as the horizontal component of the total tangential force along the arm. Arm power is determined from torque and rotational speed. The arm speed through the water is determined from digitisation of video of swimmers performing freestyle. This data is scaled to simulate a range of stroke rates. An imbalance in propulsion, between the left and right arms, can be simulated by reducing the speed of one arm relative to the other, during the *in-water* phase.

Freestyle flutter kick and UUS propulsion is modelled using large amplitude elongated body theory. This theory derives propulsion from rate of change of momentum along the body and in the wake, based on kinematics of segments along the body. Kinematic data is determined from digitisation of video for swimmers performing UUS and flutter kick. This data is scaled for swimmers of different heights. Kicking amplitude is scaled, assuming a constant Strouhal number, for different kicking frequencies.

To model the effects of fatigue throughout a swimming race, bioenergetics theory and data from exhaustion studies are used. A battery model including aerobic and anaerobic energy is simulated, which depletes as work is done by the propulsion models. The maximum available power is assumed to be linearly proportional to the stored energy, which therefore reduces as the energy depletes. To model the effects of fatigue, a control algorithm reduces stroke rate to ensure the propulsive power does not exceed the available power.

This chapter provides the architecture of a freestyle race simulation. However it is necessary to include a resistance model, before the simulation can be used to address the key questions of this study.

4 Methods of measuring Resistance and Propulsion

4.1 Introduction

It is necessary to measure swimming resistance and propulsion for the following purposes,

- Quantify surface and underwater swimming resistance for a range of heights, masses and genders
- Validate resistive and propulsive forces occurring in a simulation
- Quantify the resistive and propulsive impact of changes to swimming equipment or technique.

This chapter describes the experimental equipment and procedures used to quantify swimming resistance and propulsion. Two experimental setups are used: a tow system, which tows a swimmer at a set speed, measuring force, and a speed system which attaches to a swimmer and measures swimming speed. Both systems are synchronised with video acquired from a moving camera system, allowing the swimming technique to be related to the measured data. The tow system provides all of the experimental capability for this study, however at the cost of a complex and time consuming experimental procedure. Therefore, it is proposed to utilise a simpler speed measurement system to determine glide resistance from the deceleration after a push-off.

A study to investigate the accuracy of both the passive tow experiment and push-off glide experiment is conducted. The added resistance caused by wearing drag shorts is investigated on three males and three females and the results from both methods compared.

Due to limited access to elite athletes, time constraints and participant fatigue, tests are often limited to a small sample size. To better understand the confidence in the resistance measurements of different conditions, statistical techniques bootstrapping and permutation are utilised.

4.2 Tow System

4.2.1 Design

A bespoke tow system was designed to the following specifications.

- Tow a swimmer at a constant speed on the surface or underwater
- Measure the resistive force applied by the subject
- Be portable
- Quick to set up and take down
- Fix to the start block mountings on poolside
- Operate in both 25m & 50m swimming pools
- Tow speeds up to 3 m s^{-1}
- Low voltage
- Have enough power to achieve tow speeds for all subjects

Figure 4.1 displays the tow system CAD model. The tow lever extends into the pool to tow at various depths.

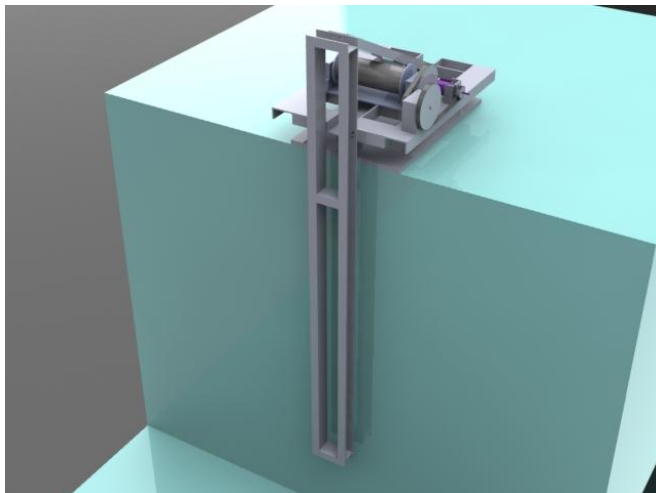


Figure 4.1. Tow system design.

The towing mechanism of the tow system consists of the following components;

1. Power Supply
2. Motor Controller
3. Motor
4. Gearbox
5. Bearings
6. Winch Drum

Electrical safety standards, provided by British Swimming, restrict the voltage within the area directly surrounding the pool to 50 Volts DC. Therefore, a 48V 2500 watt DC brushless motor is used to drive the tow system. Two mains powered 48V 1600 watt DC power supplies provide the power to the motor. To reduce the maximum motor speed (7150 RPM) to an appropriate drum speed, a synchronous belt and pulley system is used. This gearbox system has a reasonably high efficiency of about 0.95 per pulley (Information provided by manufacturer). A four pulley system results in an efficiency of 0.81. A programmable logic controller (PLC) is used to provide the motor controller with the signal to set the tow speed. A PLC provides a user friendly interface and allows repeatable tow speeds to be set.

The horizontal tow force exerted on the swimmer is measured using three force transducers mounted between the tow system and the ground (Figure 4.2). A force transducer is a metal geometry shaped to shear in one direction, providing a linear displacement to force response. The displacement is measured using a linearly varying displacement transducer (LVDT). The LVDTs are energised using an amplifier, which outputs an analogue voltage proportional to the displacement of the LVDT. Providing the force applied to the force block is within its linear range, the analogue output has a linear response to the applied force.



Figure 4.2. Tow system fitted on poolside, displaying the force transducers mounted between the tow system and ground (Left). A close up view of a force transducer, displaying the LVDT used to measure the linear displacement of the force block (Right).

To accurately measure the tow speed, the rotational velocity of the winch drum is measured using a rotary encoder. The rotary encoder outputs a voltage linearly proportional to drum velocity. The conversion of voltage to drum

Methods of Measuring Resistance and Propulsion

speed, with units $\{(m/s)/volt\}$, is determined from a lab calibration and assumed to remain constant.

A moving camera system, providing underwater footage adjacent to the swimmer (figure 4.3), is pushed along poolside to follow the test subject. A frame rate of 50 frames per second is used.



Figure 4.3. Moving camera system.

The analogue outputs from the LVDT amplifier and the rotary encoder are input into a 16-bit analogue to digital (A/D) converter. An acquisition sample rate of 250 Hz is used to ensure the dynamic force, caused by the swimming motion and unsteady flow around the swimmer, is fully captured. In addition, this can allow filtering up to 125 Hz without aliasing based on the Nyquist frequency (Eyer and Bartholdi, 1999). The video footage and data from the A/D are fed into a data acquisition laptop. Bespoke software is used to convert the voltage data to the relevant units determined from the calibration processes. The software also synchronises the video footage with the data from the A/D. A synchronisation check is performed using a flashing LED in front of the camera and acquiring the voltage to the LED with the A/D. Therefore the maximum synchronisation error is ± 1 frame.

The experimental setup is displayed in figure 4.4.

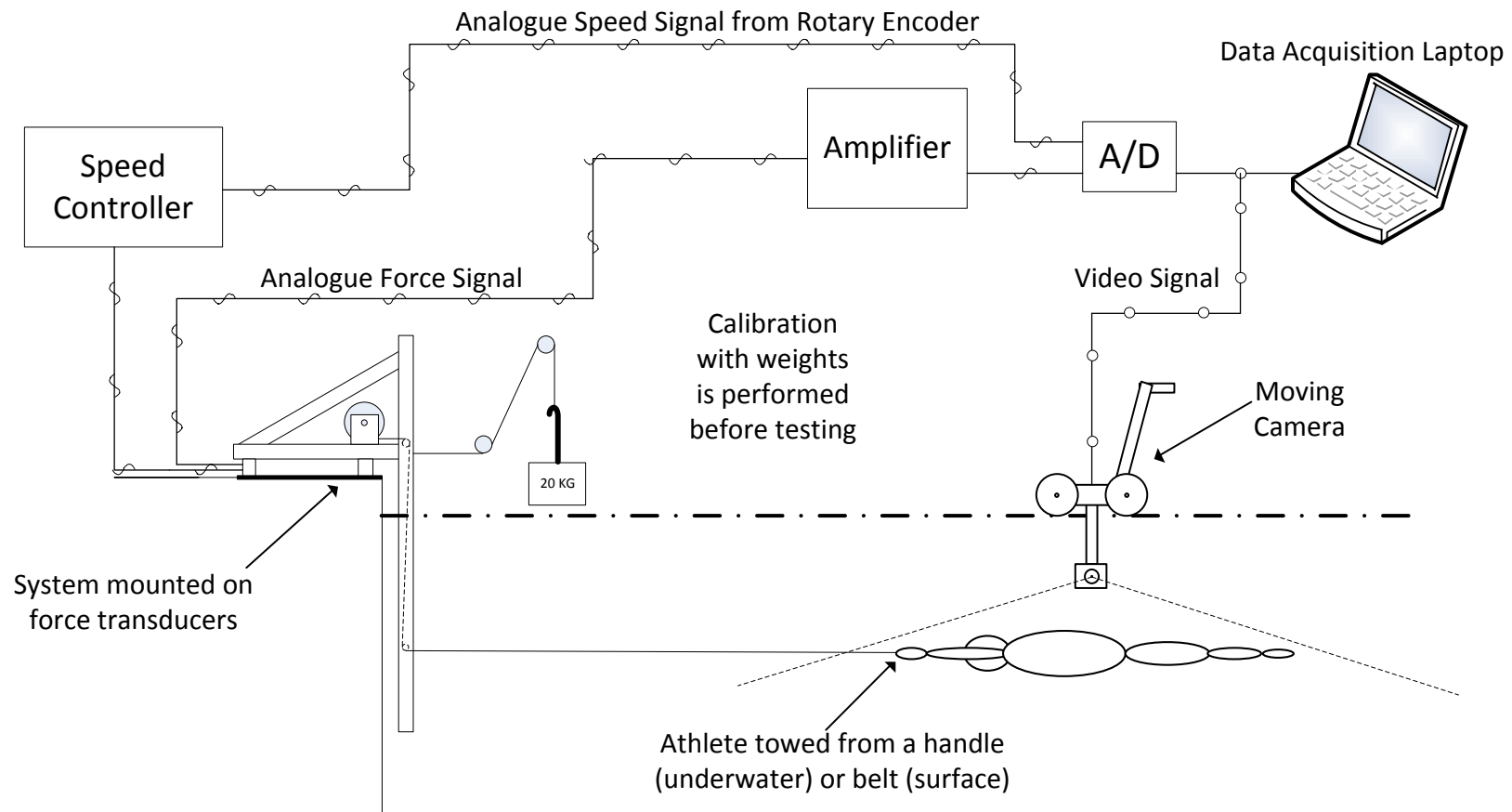


Figure 4.4. Tow system setup, displaying the mechanical and electrical components used to measure the drag of a swimmer.

4.2.2 Calibration

Calibration of the tow system is performed by applying a known load to the tow system and measuring the voltage response. This determines the conversion factor, with units Newtons/Volt, which converts the voltage measurements into force. It is necessary to calibrate the system after installation on poolside and at appropriate time intervals thereafter. This ensures any temperature change over time, which would change the response of the system, is accounted for.

It is assumed the system responds linearly and therefore only one calibration load is required. A linearity study has been conducted (figure 4.5), which confirms this.

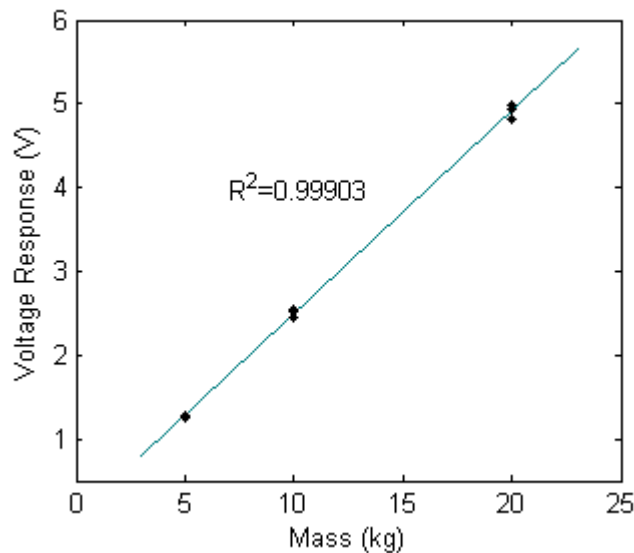


Figure 4.5. Voltage response to applied mass. Two, three and four data points were acquired for 5, 10 and 20 kg masses respectively.

4.2.3 Tow Procedure

The tow procedure is dictated by whether active or passive resistance measurements are being made. The passive resistance of a swimmer is of interest both on the surface and underwater. When swimming underwater, after the starts and turns, a streamlined position is adopted with arms in front. To measure the passive resistance for this condition, a swimmer is towed at a specific depth underwater, in the streamlined position holding a handle. When a swimmer is swimming on the surface, the arms and legs are moving, generating propulsion. To understand the drag of the swimmer on the surface,

only the drag of the non-propulsive body is required. However, it is not possible to measure the drag of a swimmer without the presence of the arms and legs. It is therefore important that the influence of the arms and the legs be minimised. To represent the non-propulsive body shape, the swimmer is towed on the surface from a strap around the torso with arms by the side (figure 4.6). Varying the strap position and tow depth identified that towing from the surface, with the strap around the upper torso, provided a body attitude similar to free swimming. This ensures the measured passive drag and contribution from the individual components is as close as possible to that experienced during free swimming. When measuring resistance during active swimming, the same tow arrangement is used. For every tow, swimmers fully inhale and hold their breath for the entirety of the tow. This helps to improve the repeatability of swimmer attitude over a number of tows.

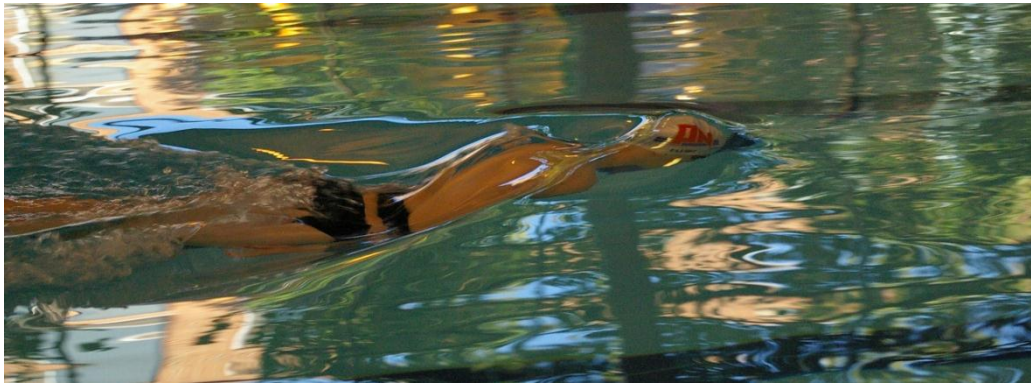


Figure 4.6, Passive tow to determine surface phase passive resistance

Before every measurement, an acquisition with no load on the tow system is performed to provide a datum. This datum is subtracted from the subsequent measurement data providing the correct absolute force measurement. When the tow is started the swimmer is accelerated up to tow speed, while adopting the desired tow position (passive) and/or stroke characteristics (active). The acceleration phase produces a large force at the beginning of a tow (figure 4.7). For mean passive resistance measurements, the averaging period is during the constant speed phase and when the swimmer is in the appropriate position (figure 4.7, left). During an active tow, the measured force is the resistance minus the thrust (R-T). For mean R-T, the averaging period is taken over an integer number of stroke cycles after the acceleration phase (figure 4.7, right).

Methods of Measuring Resistance and Propulsion

Resistance measurements for active swimming can be used to determine active resistance or characterise a swimmers stroke. This information is useful for both a coaching tool, in terms of stroke technique and also understanding the relationship between passive resistance and active resistance.

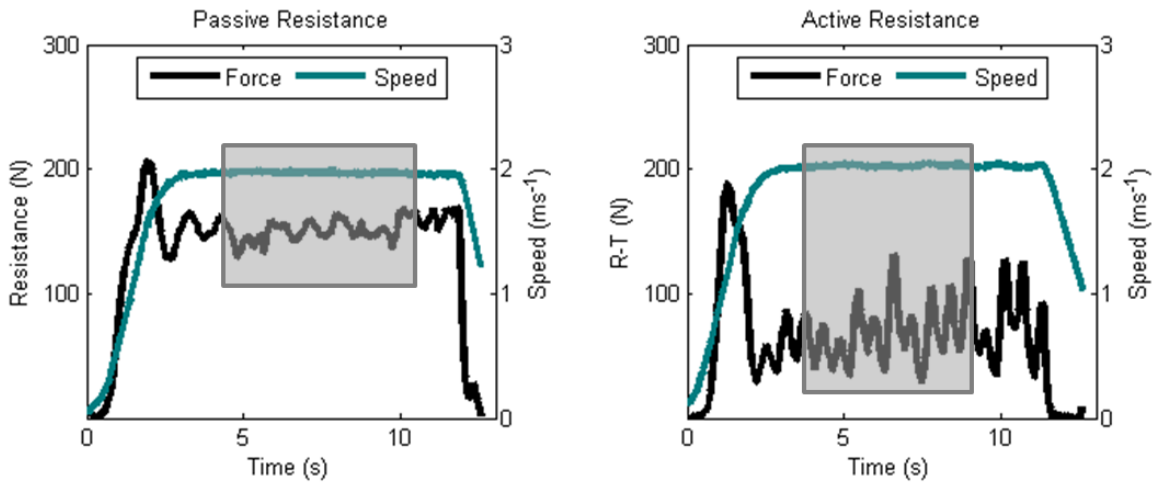


Figure 4.7, Resistance of a swimmer during a passive (left) and active (right) tow, with acceleration peak, constant velocity region and averaging period displayed by the grey box. Both tows are performed at the same speed for the same athlete.

4.3 Predicting Resistance from Deceleration Measurements

The deceleration during a push-off glide is affected by a swimmers passive resistance. Therefore, it is proposed that by measuring this deceleration, swimming passive resistance may be determined. A similar method has been developed to determine resistance for autonomous underwater vehicles, in the open sea, by measuring rate of vertical ascent (Babb, 1994). The proposed alternative method to measuring passive resistance is by the means of a push-off glide experiment, measuring velocity, from which a passive resistance coefficient is derived.

Assume a point mass experiencing the following forces,

$$R \longleftarrow \bullet \longrightarrow (M + m) \frac{dV}{dt} \quad (4.1)$$

where R is the velocity dependent resistance of the swimmer and the term on the right hand side is the inertial force of the swimmer and the surrounding water. M represents the mass of the swimmer and m is the added mass from the surrounding fluid (assumed 20% of body mass), with $\frac{dV}{dt}$ the rate of change of velocity at any point in time. Therefore, the equation of motion for the swimmer is expressed as,

$$R(V) - (M + m) \frac{dV}{dt} = 0. \quad (4.2)$$

If the resistance coefficient C_D is assumed constant over the velocity range evaluated in the glide test, the equation for a drag coefficient (equation 2.2) can be substituted into equation 4.2 to give

$$C_D = \frac{(M + m) \frac{dV}{dt}}{\frac{1}{2} \rho V^2 S}. \quad (4.3)$$

It is worth noting that although the frictional resistance coefficient of the swimmer will increase as they slow down, the fractional change in viscous form resistance will be small between the start and finish speeds of the recording period. For a typical push-off velocity range of 2.5 – 1.5 m s⁻¹, this provides a change in skin friction coefficient of 3.4 × 10⁻⁴; this is not considered to significantly affect the predicted drag coefficient.

4.3.1 System Design and Measurement Procedure

A speed measurement system has been developed based on the above approach. The system, shown schematically in figure 4.9, operates by fastening a 0.4mm Dyneema™ line to the swimmer, which is led back to a rotary encoder, used to measure the line velocity. Two pulleys fixed to a frame allow the line to be pulled out at various depths underwater. The line is attached to a thin, tight fitting waist belt worn by the swimmer. The rotary encoder and data acquisition system are identical to that described for the tow system. The swimmer initiates a push-off and the velocity trace is recorded at 250 Hz.

Figure 4.8 displays a velocity profile measured during a push-off glide experiment. It contains a steep increase in velocity during the push-off, a peak

Methods of Measuring Resistance and Propulsion

where the feet leave the wall and a deceleration region where the swimmer is gliding through the water. The data during the deceleration period is selected to perform the analysis. Second order central difference numerical differentiation is performed to determine rate of change of velocity for each point in time. The mean resistance coefficient throughout the deceleration period is determined from Equation 4.3.

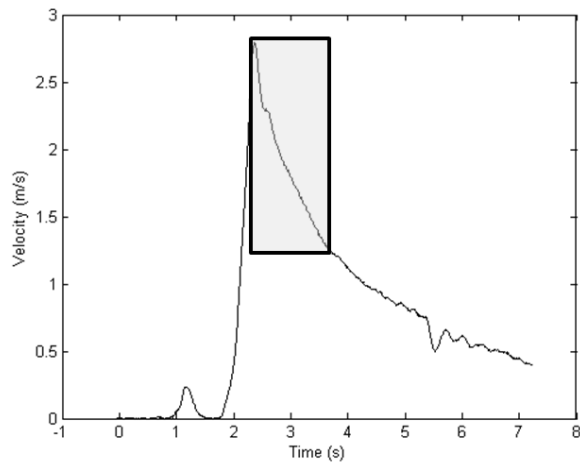


Figure 4.8. Velocity profile measured during a push-off glide experiment. Deceleration is determined by performing numerical differentiation of the data in the grey window.

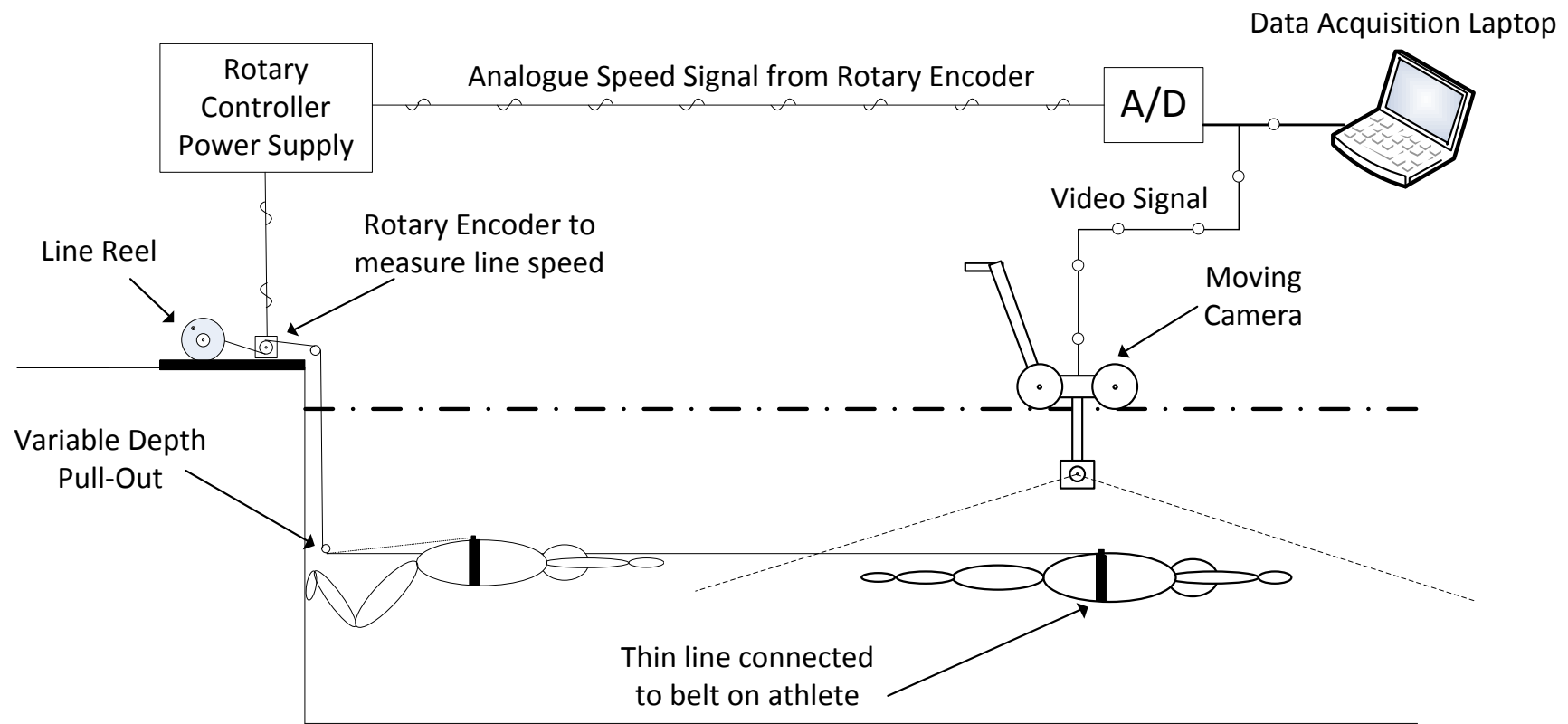


Figure 4.9. Speed measurement system setup, displaying the mechanical and electrical components.

4.4 Measuring changes in Resistance

It is known that selecting alternative equipment (suits, hats, goggles) or changing body posture can reduce swimming resistance with the potential to reduce race time. What is more challenging is accurately quantifying these resistance changes.

4.4.1 Drag Shorts Repeatability Study

It is proposed that a specific form of resistance change can be used to compare the measurement accuracy of the passive tow experiment and the push-off glide experiment. The drag increase from wearing drag shorts (figure 4.10) is quantified using both methods on six participants and the accuracy of each method compared. For a single participant, tests with and without drag shorts were alternated to ensure that any progressive technique change would not create a bias to either condition.

Three male and three female non-elite swimmers participated in the drag shorts study which was conducted over three sessions. The height and mass of all the swimmers was recorded on the day of testing. Passive tow experiments were conducted at a tow speed of 1.5 m s^{-1} over a distance of 25 m with a constant depth of 2m in lane 2. The water temperature was assumed constant at 27 degrees (FINA, 2012).



Figure 4.10. Drag Shorts used to provide drag change to compare push-off glide and passive tow experiments.

4.4.2 Statistical Analysis of Measurements

To understand the quality of the data gathered and to quantify the significance of the measured difference between conditions, statistical techniques are adopted. If a limited number of repeat experiments are conducted, a bootstrapping method can be used to enhance the normal distribution of measurements taken. In addition a permutation significance test can be used to determine the probability of the observed differences between the conditions (Hesterberg et al., 2010).

The bootstrap method allows a normal distribution, emulating a large sample size, to be determined from a small sample. Where the original sample may have been skewed due to changes in a participant's technique, affecting drag, the random resampling process can help alleviate these effects. A bootstrap distribution is generated by resampling the original data **with** replacement at random. Figure 4.12 displays an example of the bootstrap method. Generally, 10000 bootstrap resamples are used.

A significance test allows the difference between two measured conditions to be either attributed to chance, or an effect that is actually present in reality. The permutation significance test is used to quantify the probability of the observed drag change based on the variability of the data. To conduct a permutation test a null-hypothesis is assumed, e.g. the drag measurements

Methods of Measuring Resistance and Propulsion

from both conditions are the same condition. A probability distribution is generated for all the possible mean differences in the measured drag values, with the most probable being zero according to the null-hypothesis. Therefore the probability of the actual observed drag change is the proportion of the data (p-value) outside this region on the distribution (figure 4.11). Large drag changes are therefore less probable on the distribution, disproving the null hypothesis and confirming the observed drag change is in fact another condition. The more variability in the data and therefore the wider the distribution, the larger the drag change required to disprove the null hypothesis. P-values less than 0.05 (2σ) are assumed significant. The observed statistic, in the case of this study, is a measured resistance difference between two conditions. Figure 4.13 displays how this process is computed, where each are chosen at random **without** replacement to generate two permutation samples from which the difference is determined. For all analysis 10000 samples are used to generate a permutation distribution centred at zero.

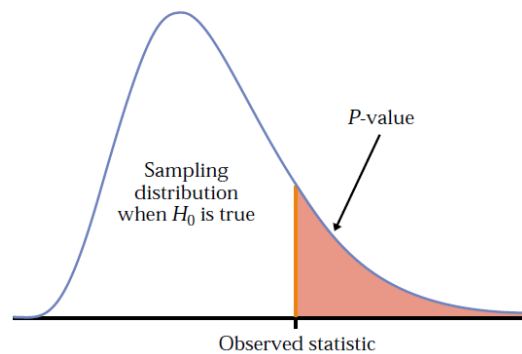


Figure 4.11. How a P-Value is determined from a distribution according to H_0 in a permutation significance test (Hesterberg et al., 2010).

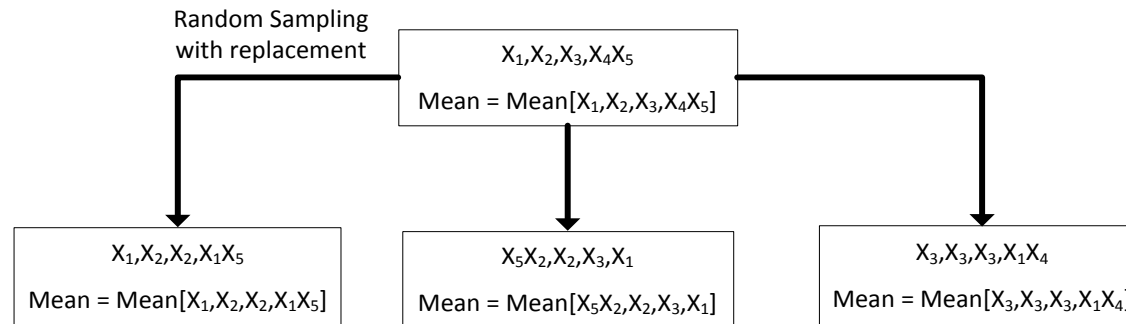


Figure 4.12. Process to generate a bootstrap distribution. Random sampling **with** replacement of the original data is used to generate a bootstrap sample.

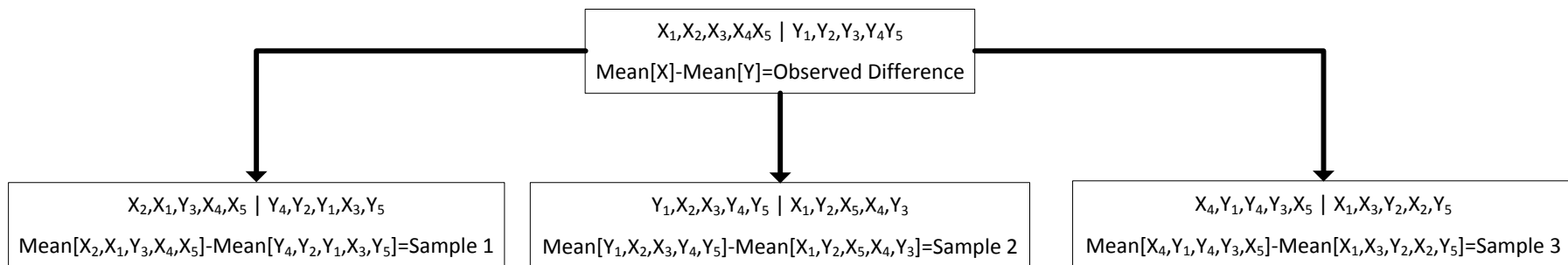


Figure 4.13. Process used to generate the permutation distribution from permutation samples. Random sampling **without** replacement of the original data is used to generate a permutation sample.

4.4.3 Drag Shorts Study Results

The average time per run for the passive tow and the push-off glide experiments was 1m 51s and 1m 24s per run respectively.

Tables 4.1 and 4.2 display the mean resistance coefficients for both conditions determined from the passive tow and push-off glide experiments. When comparing the drag change measured using the two different experiments for each participant, it can be seen that they match within a few percentage points. Although, in certain cases there is a difference between measured changes from the tow and push-off glide experiments. A t-test finds this difference is non-significant ($p=0.58$), identifying that both methods, on the whole, have quantified the same drag change.

Table 4.1. Mean resistance coefficient data determined for male participants, with and without drag shorts for both push-off glide and passive tow experiments. The height (m) and mass (kg) for each participant is also displayed.

Participant	Male 1, H=1.75, W=81				Male 2, H=1.93, W=83.5				Male 3, H=1.88, W=77			
Method	Tow		Push-off		Tow		Push-off		Tow		Push-off	
	Coef	Stdev	Coef	Stdev	Coef	Stdev	Coef	Stdev	Coef	Stdev	Coef	Stdev
With	0.034	0.0012	0.025	0.0022	0.032	0.0011	0.029	0.0016	0.024	0.0016	0.024	0.0008
Without	0.032	0.0005	0.024	0.0014	0.032	0.0028	0.029	0.0020	0.024	0.0019	0.023	0.0013
% Change	4.79		5.35		-0.61		1.43		1.50		1.92	
Diff	0.56				2.04				0.42			

Table 4.2. Mean resistance coefficient data determined for female participants, with and without drag shorts for both push-off glide and passive tow experiments. The height (m) and mass (kg) for each participant is also displayed.

Participant	Female 1, H=1.68, W=57				Female 2, H=1.68, W=52				Female 3, H=1.57, W=50			
Method	Tow		Push-off		Tow		Push-off		Tow		Push-off	
	Coef	Stdev	Coef	Stdev	Coef	Stdev	Coef	Stdev	Coef	Stdev	Coef	Stdev
With	0.043	0.0029	0.027	0.0017	0.033	0.0009	0.025	0.0009	0.032	0.0008	0.031	0.0033
Without	0.040	0.0011	0.025	0.0045	0.029	0.0006	0.023	0.0006	0.026	0.0021	0.024	0.0017
% Change	6.99		10.62		10.66		5.85		18.62		21.12	
Diff	3.63				4.81				2.49			

Figure 4.14 displays the bootstrapped distributions of the data. As displayed in tables 4.1 and 4.2, these distributions identify more clearly that the outputs

from both experimental methods reflect the increase in drag associated with wearing drag shorts.

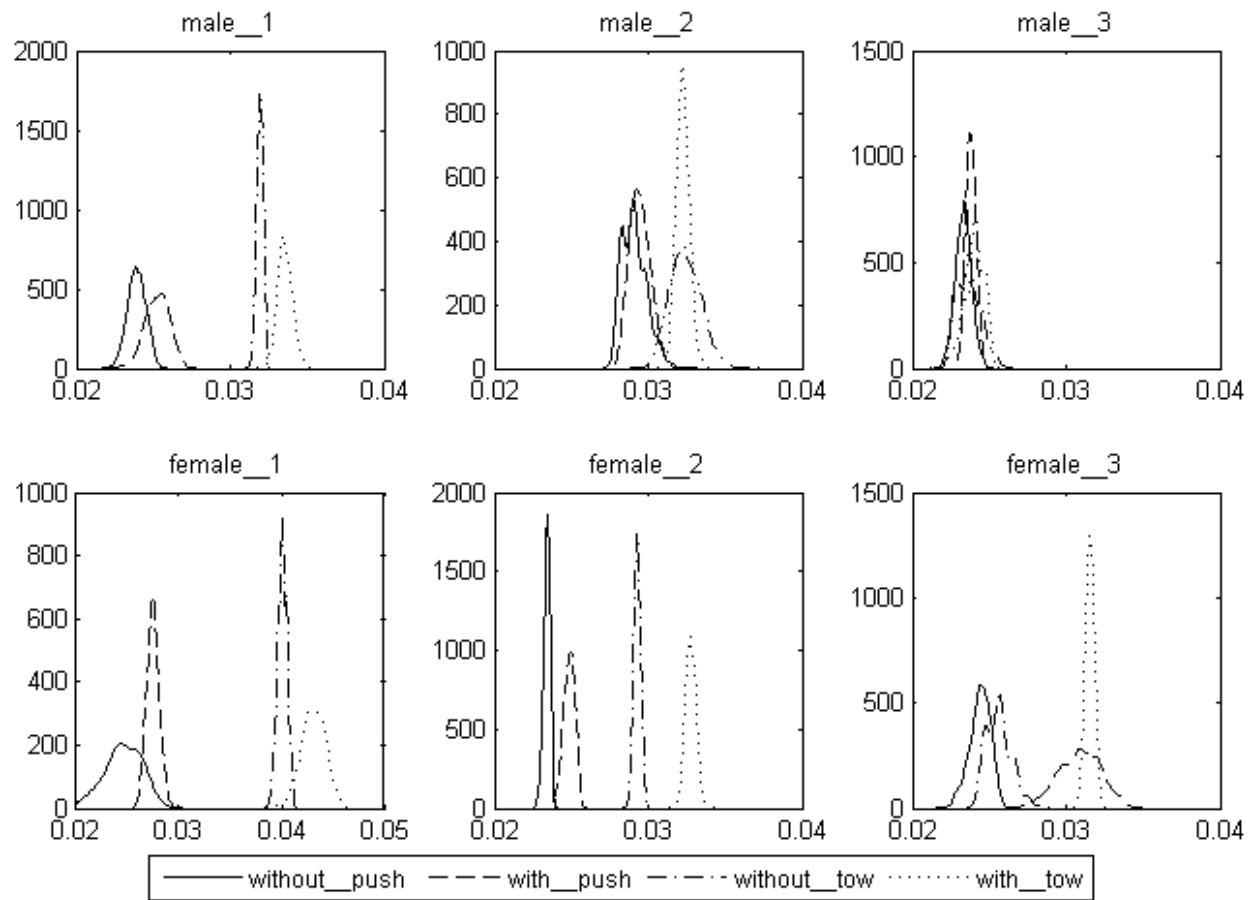


Figure 4.14. Bootstrapped distributions for each participant displaying the resistance change from drag shorts for both methods. On the x-axis is resistance coefficient and y-axis is probability density.

Although both methods predict similar relative changes in drag, in some instances the absolute drag coefficient measured is quite different. For all participants the drag coefficient measured by the tow experiment is greater than that measured by the push-off glide experiment. A potential reason for this is that during the tow experiment, directional instability of the swimmer sometimes occurs. Therefore any angle of attack the swimmer may adopt during a tow will increase measured drag. Directional instability may be dependent both on the shape of the swimmer and skill required to keep the body traveling straight. Any self-alignment actions taken by the swimmer will also increase drag. These factors may explain the consistent higher drag coefficient measured by the tow experiment. For the push-off glide experiment an added mass, m , was assumed proportional to body mass. However this may not fully capture variations in body shape and could explain why the differences between the measured drag coefficients differ for each participant.

Figure 4.15 displays the output from the permutation tests, identifying the confidence in the measured drag change for both methods. On each plot the black line represents the probability of differences between the conditions, assuming the null hypothesis (conditions are the same). The circle marker on the x-axis identifies the observed difference. Comparing the p-values for male and female, the female data shows greater confidence. This is because the drag shorts provided a greater relative drag increase for females. The fit of the drag shorts varied depending on body size and therefore the larger the participant, the tighter the fit and the less absolute drag increase that was observed.

For the female data, both methods demonstrated sufficient confidence to quantify the difference between conditions. There is greater confidence in the tow experiment observation, however its longer measurement period with typically 1750 samples per run versus 375 for the push-off glide experiment, will provide a more statistically significant result. For the male data, where the drag difference between conditions is small, both methods produce similar predictions; however, they are unable to provide significant confidence. To achieve greater confidence more repeat tests would be necessary.

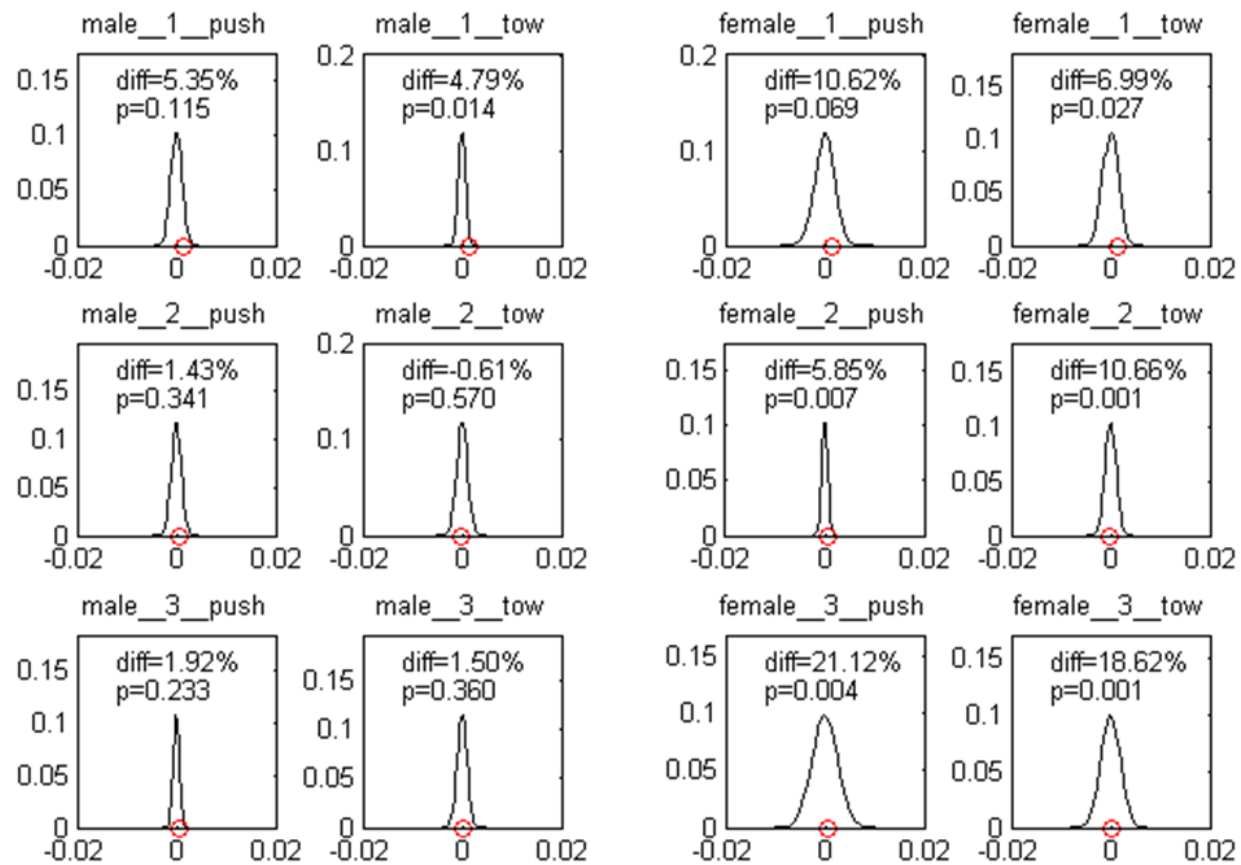


Figure 4.15. Permutation test results comparing the data for with and without drag shorts for each participant and each method. A plot displays the probability of a range of drag changes according to the null hypothesis that the conditions (with, without) are the same. The circle marker identifies the observed change in drag and the percentage difference and probability are quantified above.

4.5 Summary

Two methods of measuring swimming resistance have been detailed: the passive tow experiment and the push-off glide experiment.

The passive tow experiment consists of a low voltage portable tow system, which can tow a swimmer on or below the surface, at a constant speed, and measure resistance. Passive swimming resistance is measured when the swimmer is in a static position, either on the surface or underwater, with the aim to quantify resistance of the non-propulsive body. When on the surface the swimmer is towed using a strap around the torso, with arms by side, and when underwater the swimmer is towed from a handle with arms in front. A study has been performed to ensure the tow arrangement enables the swimmer to adopt a natural swimming position, during a passive tow. During an active tow the swimmer is generating propulsion and therefore resistance minus thrust (R-T) is measured. Active towing can be used to determine active resistance or provide insight into the propulsive characteristics of a swimmers stroke.

An alternative form of resistance measurement is the push-off glide experiment, where the resistance of the swimmer is derived from the rate of deceleration. This experiment provides a simpler less time consuming approach to measure changes in resistance, however is limited to measurement of gliding resistance.

The accuracy of the passive tow and push-off glide experiments, in measuring changes in swimming resistance, is assessed. The added resistance from wearing drag shorts is quantified using both methods, in a six participant study. Both methods demonstrate sufficient precision to identify the drag change associated with drag shorts with five repeat tests. However, the passive tow experiment provides a greater level of confidence.

Statistical methods, bootstrapping and permutation are utilised to gain better insight into the confidence of measured differences in resistance.

5 Swimming Resistance Model

5.1 Introduction

In order to accurately model the speed of a swimmer throughout a race, it is necessary to understand the resistive forces experienced. After the start and every turn a swimmer is fully submerged before coming to the surface to swim the remainder of a length. Therefore, it is necessary to model the resistance of a swimmer underwater, as the swimmer approaches the surface and on the surface.

In this chapter swimming resistance will be studied with the aim to create a resistance model to predict the resistance of any swimmer in any phase of a swimming race. This requires the investigation of how resistance varies over a range of body sizes, shapes and swimming speeds. Due to the nature of hydrodynamic resistance, these parameters influence each component of resistance differently. Therefore, it is necessary to investigate both total swimming resistance and the individual resistance components: wave, skin friction and viscous pressure.

Total passive resistance is determined through passive tow testing a population of male and female swimmers, on the surface and underwater. Wave resistance is investigated using Thin Ship Theory for a range of heights, masses and Froude numbers. Additionally the effect of sinkage identified by Taunton et al. (2013) is used to model the effect of a swimmer approaching the surface. Skin friction resistance is determined from the ITTC correlation line. Viscous pressure resistance is determined as the difference between total passive resistance and skin friction plus wave resistance.

All resistance data are presented in coefficient form (equation 2.2), based on surface area (equation 1.1). Wave resistance is affected by slenderness and Froude number and therefore is presented as a surface plot against these parameters. Skin friction is affected by Reynolds number and therefore is presented as a surface plot against height and speed. The viscous pressure resistance coefficient is assumed constant for all speeds and is affected only by slenderness. Therefore, viscous pressure resistance is presented against slenderness for males and females, on the surface and underwater. These data

Swimming Resistance Model

are presented in the form that they are stored in the resistance model. This enables total resistance to be determined for any height, weight and gender, over a range of speeds, by combining the contribution from each component (equation 2.1).

The resistance of a swimmer during active swimming is greater than the passive resistance for the same speed, due to the dynamic motion of the swimmer and interaction effects between the arms and the body. To understand the thrust and propulsive power required to achieve a certain swimming speed, it is important to model the active resistance. Therefore, active resistance is quantified for a single participant using both the velocity perturbation method and a naval architecture based approach, and their accuracies compared.

5.2 Total Passive Resistance

Through the SwimSIM testing program, passive resistance has been measured for many participants to determine optimum body shape, position and equipment. This provides a range of passive resistance values for each participant. The aim of this section is to determine how the measured passive resistance varies over the range of heights and masses tested. Swimmers were tested on the surface with arms by side, towing from a belt worn round the chest, and underwater in a streamlined glide position, towing from a handle.

5.2.1 Results

The results from passive resistance testing are displayed in figure 5.1. 13 males and 6 females were tested on the surface, and 7 males and 5 females were tested underwater. Resistance coefficient (equation 2.2), deduced from surface area (equation 1.1), is plotted against slenderness ratio (equation 1.3) to identify the effect of body shape. Body shape primarily affects viscous pressure and wave resistance, as this influences the size of the separated region behind the swimmer and acceleration of fluid around the body. The effect of body shape on skin friction resistance is likely to be small, as it is governed by Reynolds number and therefore height is more significant than body shape. The original data, detailing the height, weight, gender and tow speed is tabulated in Appendix 2.

Most swimmers were tested multiple times. The vertical distribution of data for a single slenderness value identifies the variation in measured resistance for a single swimmer. It is apparent that the effect of body shape, on total resistance coefficient, is small in comparison to the variability of a single swimmer. For male swimmers there is a slight trend of decreasing resistance (surface and underwater) for increased slenderness, which is expected (Hoerner, 1965; Molland et al., 2011). For females, the trends are the opposite, but also very slight.

Variation of resistance for a single swimmer will be due to experimental uncertainty, or testing a different condition. Equipment has an effect on resistance; however, it was not practical to ensure all swimmers were wearing the same equipment and that individual swimmers wore the same equipment on different testing dates. Future investigation of body shape for a population of swimmers should ensure equipment is consistent. Repeatability of body position will affect the variability of resistance for a single swimmer. When comparing different swimmers, differences in the body positions must be considered. Conditions where extreme body positions were investigated have been removed from this dataset. Swimmer pitch, and factors affecting projected area (e.g. head and feet angles), will influence the measured resistance. A resistance coefficient calculated using wetted area will not remove these effects. When on the surface, the area of free surface being penetrated significantly affects the wave resistance (figure 2.10) (Taunton et al., 2013). Therefore variations in swimmer sinkage, which are not accounted for, may also affect the resistance coefficient.

For the underwater passive tow experiment, tow depth was kept consistent. However, swimmers tended to adopt different natural tow depths due to technique differences when starting a tow. If swimmers became too close to the bottom or the free-surface, a bottom effect (reducing resistance) or wave resistance (increasing resistance) may have been experienced; these tests were ignored and repeated. The front gliding data published by Kolmogorov and Duplishcheva (1992), presented figure 2.5, has a passive resistance coefficient range of 0.02 – 0.03, for the population of elite swimmers tested. In this study the underwater passive resistance coefficient range is 0.03 – 0.04. These higher resistance values may be due to testing non-elite swimmers.

Swimming Resistance Model

Effort was made to ensure each swimmer was towed consistently and the body shape, head position and leg positions were representative of their natural swimming technique. However, this has not prevented a significant variability in the data for a single swimmer.

To conclude, the effect of swimmer slenderness on passive resistance has been identified, however this is insignificant in comparison to variability of resistance for a single swimmer. It is necessary to incorporate projected area and area of the free surface penetrated, to collapse the resistance data more effectively. This would allow the effect of slenderness on total passive resistance to be more effectively identified.

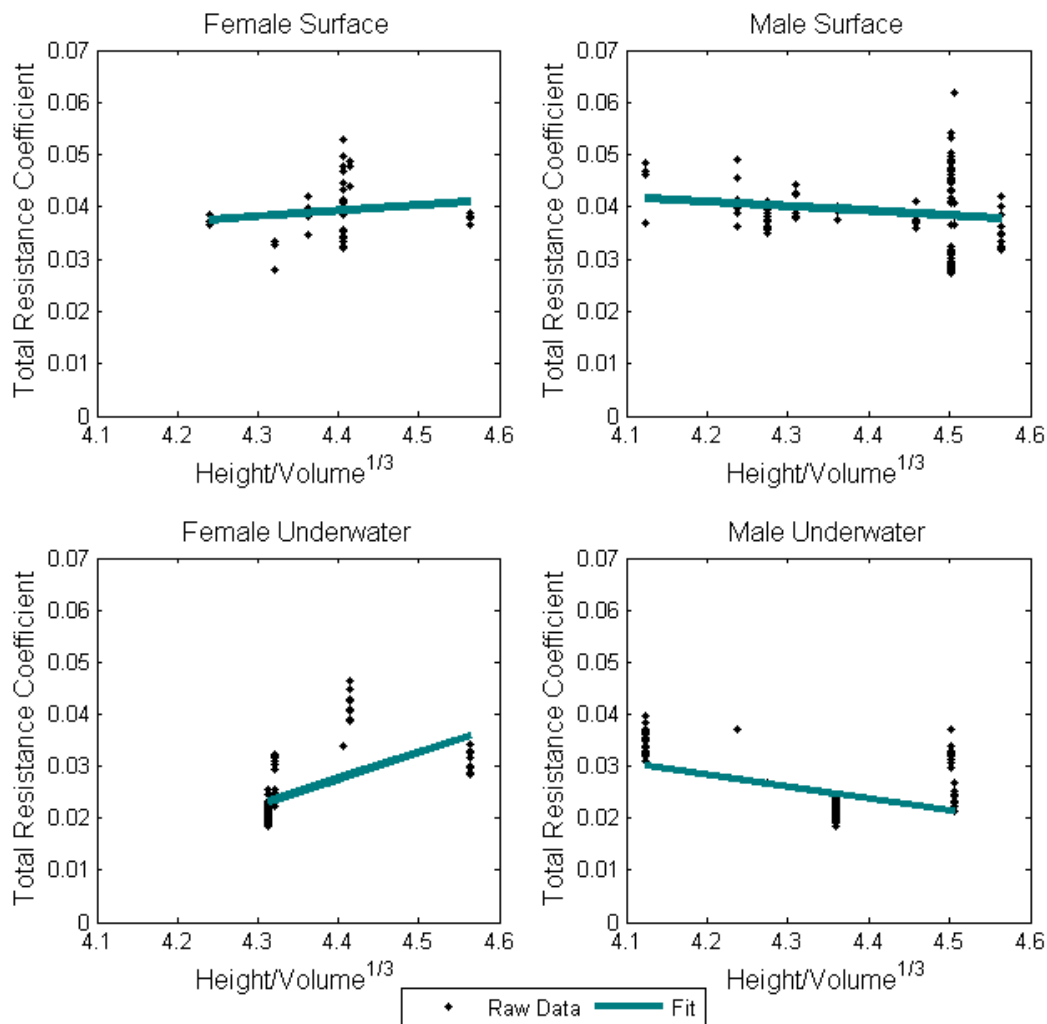


Figure 5.1. Passive resistance for male and female participants determined from surface and underwater towing.

5.3 Wave Resistance

The wave resistance of a swimmer may be determined experimentally from wave elevation experiments or computationally using Thin Ship Theory and CFD. A study to predict the wave resistance of a swimmer geometry using Thin Ship Theory has been performed and validated using wave elevation measurements (Taunton et al., 2013). This section therefore aims to use Thin Ship Theory to determine the passive wave resistance for a range of swimmer heights, masses and Froude numbers.

5.3.1 Thin Ship Theory for Swimmer Wave Resistance

An explanation of Thin Ship Theory can be found in section 2.2.1. The following information is required to use Thin Ship Theory to determine wave resistance: swimmer geometry, domain definition, geometry sinkage and trim, and advance speed.

In order to determine wave resistance for a range of heights and masses, a number of geometries were analysed. The geometry (figure 5.2) originates from a laser scan of an athlete in a prone position, who was not a swimmer, however, represents well the position adopted by a swimmer during a surface passive tow. To achieve range of slenderness values required for the resistance model, the height, depth and breadth of the laser scanned geometry are scaled. The length of the geometry is scaled to achieve the correct height and the breadth and depth are scaled to achieve the correct volume using the following relationship,

$$Scale\ Factor = \sqrt{\frac{\nabla_{desired}}{\nabla_{original}}}. \quad (5.1)$$

A square root rather than a cubic root is used because length is pre-scaled and then remains fixed.

Swimming Resistance Model

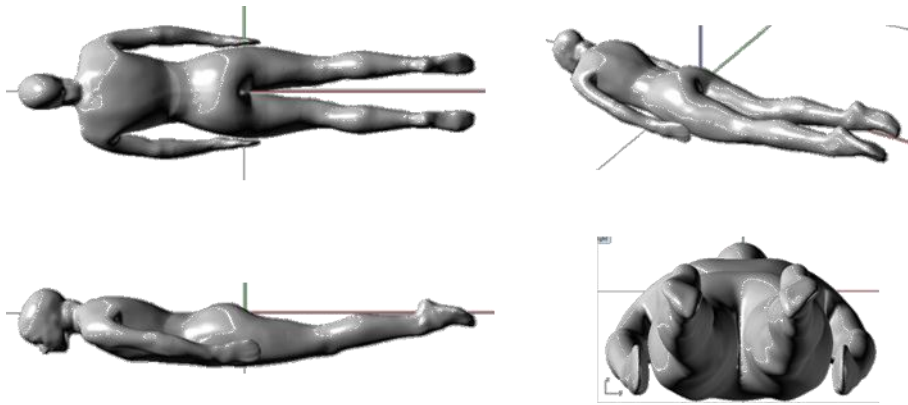


Figure 5.2. Geometry used in Thin Ship Theory to determine the wave resistance of a swimmer. The geometry was scaled to investigate a range of heights and masses.

Table 5.1 displays the geometry dimensions used which covers the range of swimmer slenderness tested by SwimSIM. The surface area is determined using equation 1.1.

Table 5.1. Geometry dimensions used to determine wave resistance from Thin Ship Theory.

Geometry	Length (m)	Breadth (m)	Draught (m)	Surface Area (m ²)	Mass (kg)	L/Volume ^{1/3}
A	1.60	0.66	0.270	2.02	100	3.51
B	1.64	0.64	0.258	2.00	94	3.68
C	1.68	0.61	0.247	1.98	88	3.85
D	1.72	0.58	0.235	1.95	82	4.04
E	1.76	0.55	0.224	1.92	76	4.24
F	1.80	0.55	0.224	1.89	70	4.45
G	1.84	0.49	0.201	1.84	64	4.69
H	1.88	0.47	0.189	1.80	58	4.95
I	1.92	0.44	0.177	1.74	52	5.24
J	1.96	0.41	0.165	1.68	46	5.58
K	2.00	0.38	0.152	1.61	40	5.96

Taunton et al. (2013) identified the importance of ensuring the correct domain depth. A domain depth less than 2 m was found to provide some blockage which increased the predicted resistance of the swimmer. The minimum depth

of an Olympic pool is 2 m and the lane width is always 2.5 m (FINA, 2012). Therefore a domain size of 2 m deep, 2.5 m wide and 50 m long was used.

The attitude of the geometry is as displayed in figure 5.2. Sinkage of the geometry is fixed with the lower back touching the free surface and trim is zero degrees from the lower back to the top of the head.

The advance speeds modelled are 1-3 m s⁻¹. Thin Ship Theory tends to over predict wave resistance at low speeds (Insel et al., 1994) due to the assumption of an inviscid fluid. Therefore, advance speeds less than 1 m s⁻¹ have been ignored and wave resistance coefficients, for speeds less than 1 m s⁻¹, will be assumed the same as 1 m s⁻¹. Since geometries have different lengths, the resulting Froude number range for the tested speeds will vary for each geometry. Therefore, all wave resistance results are interpolated and presented for a fixed swimmer height based Froude number (equation 2.3) range.

The wave resistance values predicted are presented in coefficient format determined from equation 2.2, using surface area (equation 1.1), and a pool water density of 1000 kgm⁻³.

5.3.2 Results

An example wave surface profile, predicted by Thin Ship Theory, is displayed in figure 5.3. The predicted wave height is roughly 0.4 m. When compared to real wave profiles for a similar body size and tow speed (figures 5.4 and 5.5), the Thin Ship Theory predicted wave height would appear to be larger. This may result in an over prediction of wave resistance. The main wave from the head appears to match well with the real scenario. However, where wave breaking occurs in reality, Thin Ship theory does not capture this. Wave breaking is then treated as part of viscous resistance (Molland et al., 2011) and since wave breaking cannot be modelled, this will result in a proportionally larger wave resistance coefficient.

Swimming Resistance Model

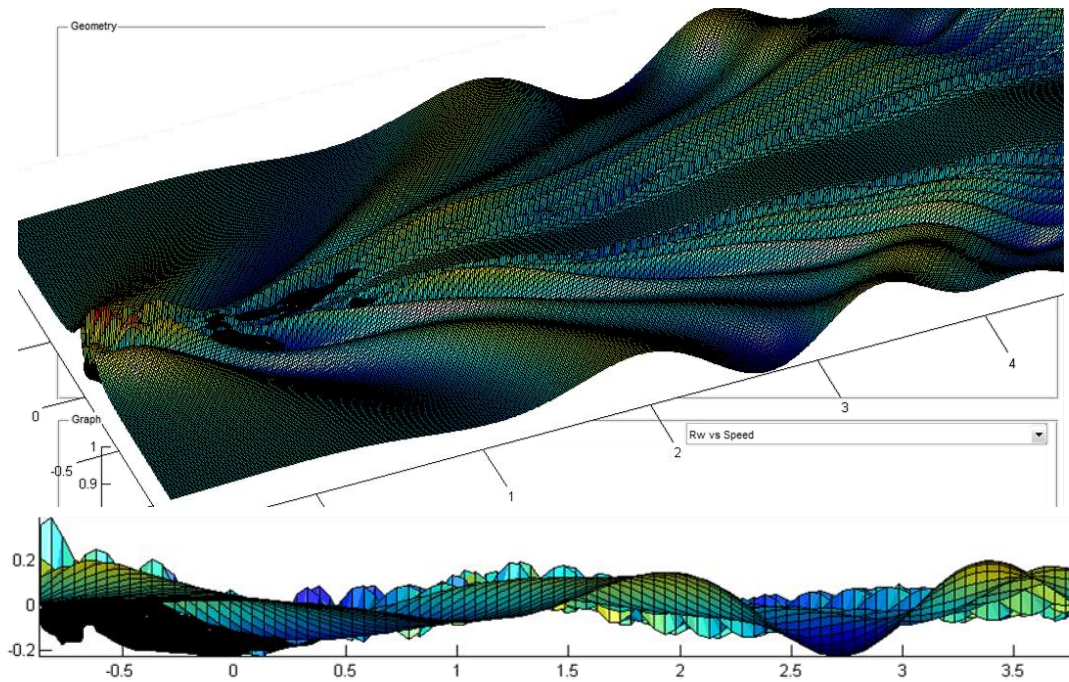


Figure 5.3. Predicted wave surface profile for geometry E at 1.8 m s^{-1} in 2 m deep, 2.5 m wide lane.



Figure 5.4. Above water image of subject O during surface passive tow, identifying the wave pattern.



Figure 5.5. Underwater image of subject O during a surface passive tow, identifying the wave pattern.

The predicted wave resistance for the geometries in Table 5.1 are displayed in figure 5.6 and tabulated in Appendix 3. The effect of Froude number and slenderness are apparent. The predicted wave resistance coefficients for Froude numbers less than 0.3 is large; however, the dimensional wave

resistance will be small at these speeds. A wave resistance hump is evident at a Froude number of 0.45, with wave resistance coefficient decreasing steadily as speed increases. Due to the complex curvature along a human body, the wave interference will differ to that of ship. This may explain the large wave resistance coefficient at low Froude numbers and the less prominent resistance hump, which on a ship, is usually due to constructive interference of the bow and the stern waves. This is less apparent in figures 5.3, 5.4 and 5.5. The effect of slenderness causes a clear increase in wave resistance with a decrease in slenderness ($L/\text{volume}^{1/3}$).

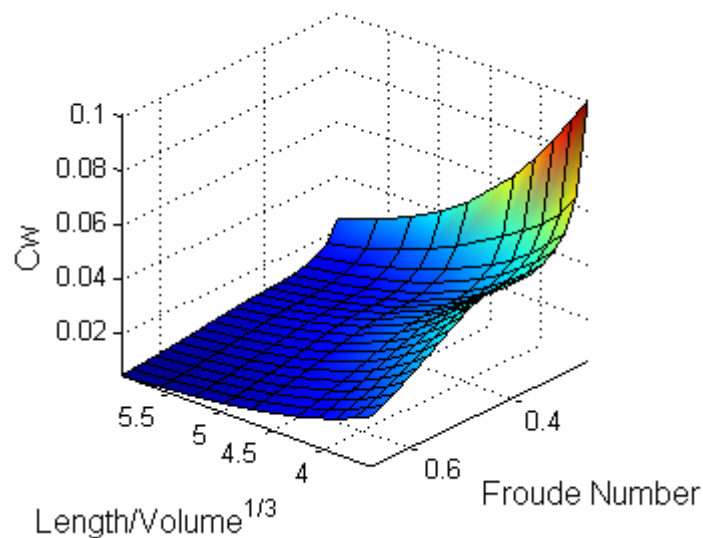


Figure 5.6. Wave resistance coefficient determined for a range of speeds and body geometries identified in table 5.1.

5.3.3 Submersion Model

To account for the effects sinkage on wave resistance, the relationship determined by Taunton et al. (2013) will be used (figure 2.11). A wave resistance scale factor allows the data in figure 5.6 to be determined for a sinkage of up to 1 m. Figure 5.7 identifies this scale factor for a range of sinkage values.

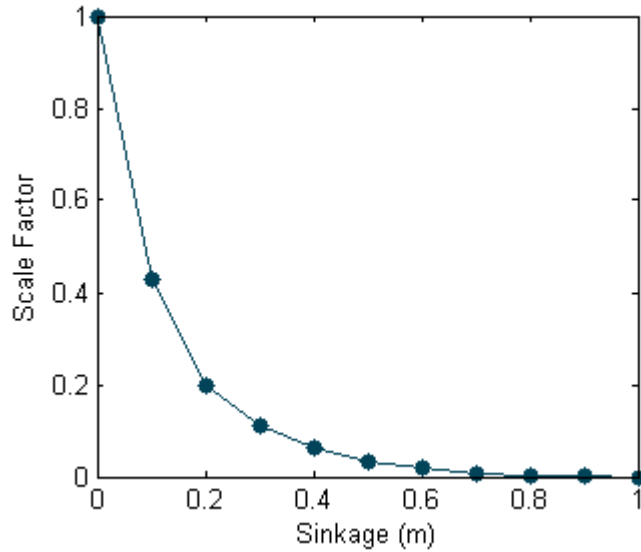


Figure 5.7. Scale factor to adjust wave resistance due to sinkage.

5.4 Skin Friction Resistance

The skin friction resistance coefficient is determined using the ITTC 1957 correlation line (Clements, 1959) for a range of heights and velocities (figure 5.8). Skin friction coefficient increases as Reynolds number decreases. Therefore, as height and velocity decrease the skin friction coefficient increases. The skin friction coefficient is plotted against height and velocity separately, to identify how it may vary across a population of swimmers. The skin friction resistance coefficient, for a fixed height and speed, is assumed the same for both surface and underwater swimming. In reality having the arms stretched out in front during underwater swimming, will increase the effective length of the swimmer, increasing Reynolds number, and therefore reducing skin friction resistance coefficient. In addition, the surface area of the swimmer is assumed the same for both surface and underwater swimming. In reality, when swimming on the surface, not all area is wet and therefore will not be subject to skin friction resistance. A future improvement to the skin friction resistance model would be to account for the increased length, when swimming underwater, and to reduced wetted area used in equation 2.2, when swimming on the surface.

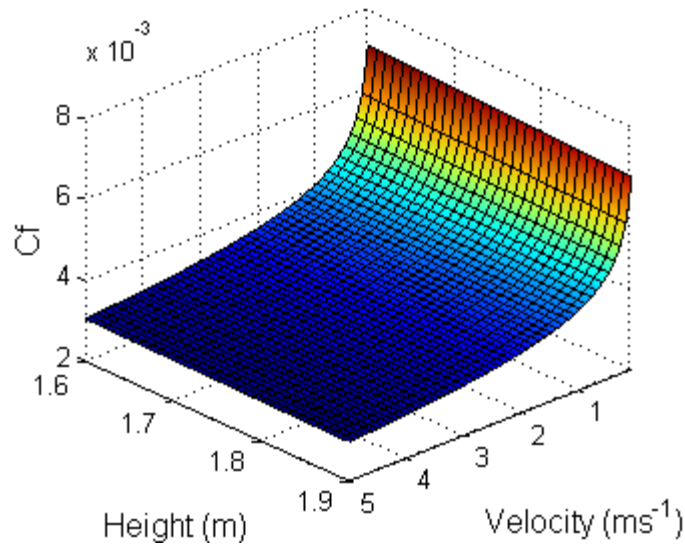


Figure 5.8. Skin friction coefficient for a range of heights and velocities determined using the ITTC 1957 correlation line (Clements, 1959).

5.5 Viscous Pressure Resistance

If total, wave and friction resistance are known, viscous pressure resistance can be determined from equation 2.1. The data determined from the passive tow experiments provide the total resistance. For each participant tested in the passive tow study, the relevant wave and skin friction resistance coefficients, according to height, mass and tow speed were determined. These values were subtracted from the total to determine the viscous pressure resistance coefficients.

Viscous pressure resistance is presented in figure 5.9. Since the friction and wave resistance values are determined theoretically, the variability measured in the passive tow experiment is passed onto the viscous pressure resistance. If variability in the passive resistance tests were due to changes in projected area, it is likely that this variation in viscous pressure resistance is correct. However if the variation occurred due to changes in the penetrated free surface, the variability is more likely to be a wave resistance effect.

The viscous pressure resistance coefficient, for any slenderness, is determined from a linear fit through the dataset. For the surface condition, the range of potential viscous pressure values is small (Female: 0.009-0.012, Male: 0.014-0.01). In the submerged condition, the range of potential viscous pressure values is larger (Female: 0.0195-0.032, Male: 0.0275-0.019). Reasons why the

Swimming Resistance Model

absolute values in submerged condition are larger than the surface condition, may be due to when the body is on the surface the projected area is less, since not all of the body is submerged. However, the wetted area used to non-dimensionalise the resistance values is the same. Additionally, if Thin Ship Theory is over predicting wave resistance, the proportion of viscous pressure resistance determined on the surface will be smaller than in reality.

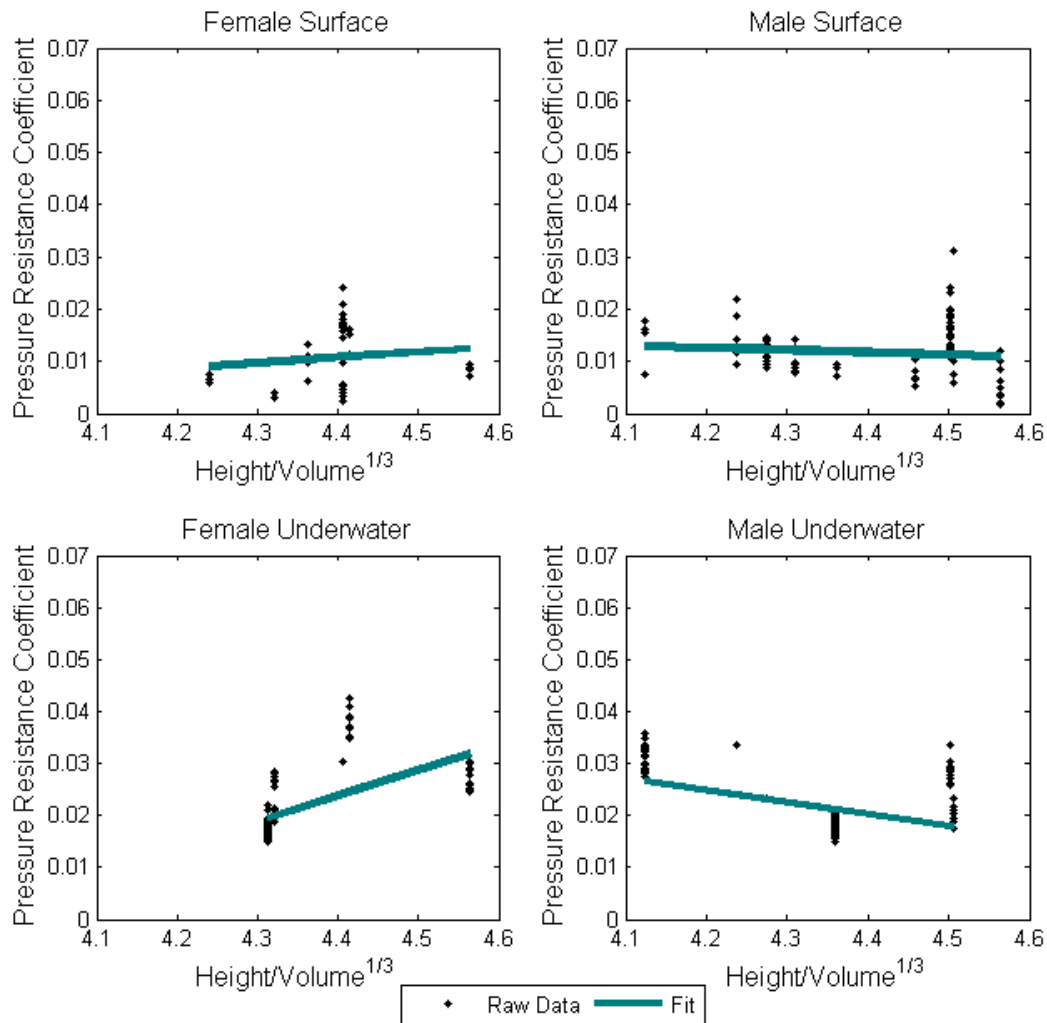


Figure 5.9. Viscous pressure resistance for males and females, surface and underwater: determined by deducting friction resistance and wave resistance from the measured total passive resistance.

5.6 Passive Resistance Prediction

Using the data presented for wave, skin friction and viscous pressure resistance, total resistance, across the range of swimming speeds, can be predicted for any height and mass (within the range of swimmers analysed). Figures 5.10 and 5.11 display a surface and underwater resistance prediction for a male swimmer: height 1.79 m, mass 75 kg and slenderness of 4.33. These parameters are about the middle of the range for the male resistance model. For the surface condition the contribution of wave, viscous pressure and skin friction components are 60%, 31% and 9% respectively at 2 m s^{-1} . This wave resistance contribution is similar to that found by Vennell et al. (2006), however is larger than the prediction by Taunton et al. (2013). For the underwater condition the contribution of viscous pressure and skin friction components are 85% and 15% respectively at 2 m s^{-1} . Polidori et al. (2006) determined a skin friction resistance of 22N at 2.8 m s^{-1} for a fully submerged swimmer of height 1.73 m and mass 66 kg. Interrogating the resistance model for the same height, mass and velocity, produces a skin friction value of 23.3 N, identifying that the ITTC approach is satisfactory.

5.6.1 Resistance Uncertainty

The uncertainties in the resistance predictions are displayed by the error bars in figures 5.10 and 5.11. These uncertainties have been determined from the experimental errors in viscous pressure resistance only. The errors in the prediction of skin friction and wave resistance are not influenced by experimental uncertainty and therefore are assumed small.

The error in the total passive resistance data consists of uncertainty due to bias (the accuracy of the experimental equipment) and precision (the variability of the measured data) (Stern et al., 1999). Combining individual components of uncertainty is determined by adding together the square of the components and taking the square root. The bias uncertainty consists of the following components, which combine to produce a total bias uncertainty of 1.07%.

- Assumed calibration weight uncertainty: 1%
- Assumed tow system misalignment uncertainty of ± 5 degrees: 0.4%
- A/D manufacturer stated digital linearity uncertainty: 0.02%
- A/D manufacturer stated conversion process uncertainty: 0.07%

Swimming Resistance Model

The precision uncertainty was determined using the method reported by Stern et al. (1999). The standard deviation of the viscous pressure resistance data (figure 5.9), is assumed to be the deviation from the fit, for each condition. This was performed by subtracting the fit from the raw data, leaving the data without any relationship to slenderness from which the standard deviation could be determined. This provided a precision uncertainty of 22%, 32%, 36% and 36% for female surface, male surface, female underwater and male underwater conditions respectively. These were combined with the bias uncertainty of 1.07% to provide the total uncertainty for the viscous pressure estimation of 22%, 32%, 37% and 36% for female surface, male surface, female underwater and male underwater conditions respectively. It is clear that the dominant source of error comes from the variability across multiple data points and not from error in the experimental equipment. Therefore, improved accuracy could be achieved from methods which improve swimmer repeatability across runs.

5.6.2 Comparison with experimental data

An independent resistance study over a range of speeds has been conducted for a swimmer of height 1.79 m and mass 75 kg. Passive towing was performed on the surface and underwater. The experimental data is overlaid in figures 5.10 and 5.11. For the surface condition, the predicted resistance matches closely with the independent experimental measurements. For the submerged condition, the predicted resistance is on average 23% less than the experimental data; however, is within the error in the resistance prediction. This identifies the poor quality of the male underwater viscous pressure resistance data, the main contributor of total underwater resistance. No data points exist for the Height/Volume^{1/3} region of 4.33, and therefore the resistance prediction relies on the fit, describing the relationship between viscous pressure resistance and slenderness. However, due to the lack of data, it is not possible to confirm the accuracy of this relationship. To reduce the uncertainty in predicted viscous pressure resistance, a larger sample size is required and greater number of slenderness values needs to be examined. For the surface resistance prediction, a larger number of slenderness values have been tested, which may contribute to the greater accuracy of the total surface resistance prediction.

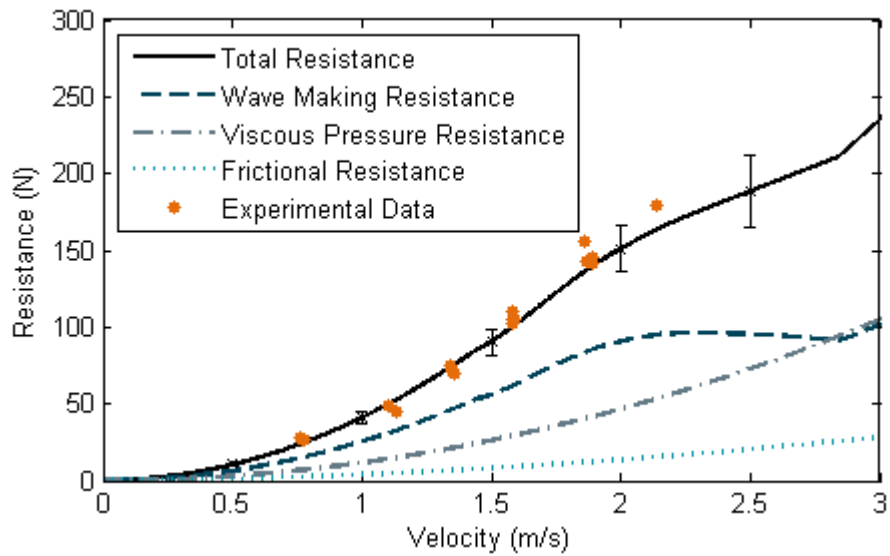


Figure 5.10. Surface resistance prediction for male swimmer of height 1.79 m and mass 75 kg. Error bars display the error in the total resistance prediction, based on the experimental uncertainty in viscous pressure resistance data.

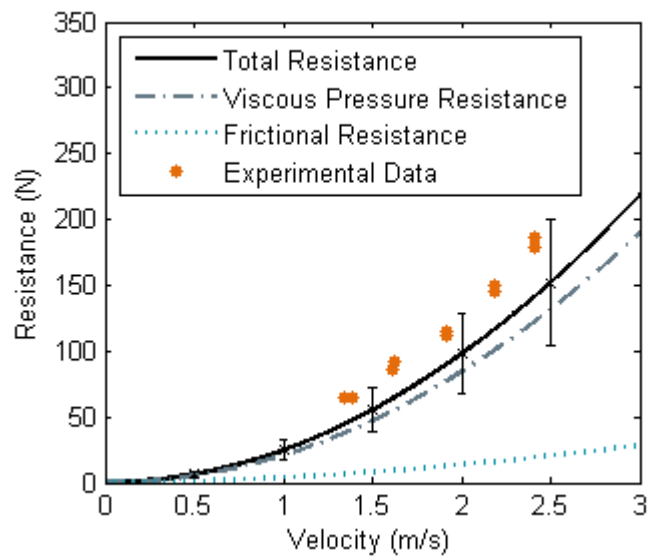


Figure 5.11. Underwater resistance prediction for a male swimmer of height 1.79 m and mass 75 kg. Error bars display the error in the total resistance prediction, based on the experimental uncertainty in viscous pressure resistance data.

5.7 Active Resistance Model

Active resistance is the resistance experienced by a swimmer during self-propulsion. Active resistance is greater than passive resistance due to the dynamic motion of the body and interaction effects between the arms and the body. As mentioned in section 2.3.3, active resistance may be determined using the velocity perturbation method (VPM). The theory of the VPM enables active resistance to be determined by testing a swimmer at two different speeds tests, due to a known change in total resistance, with the assumption of an equal swimming effort. An alternative method is a naval architecture based approach (NABA), which uses the theory of the self-propulsion experiment. This method differs from the VPM such that the passive resistance needs to be measured or predicted in addition to performing active tests. It is proposed that the measurement of passive resistance is less subject to error as it does not require the assumption of equal effort, and contributes to the majority of active resistance magnitude. The active tests therefore quantify the remaining resistance making up the total active resistance. These active tests are subject to the assumption of equal propulsion, between free swimming and towed conditions, containing uncertainty similar to the VPM. However, this uncertainty only affects a small proportion of the total active resistance prediction.

This section aims to quantify active resistance using both the VPM and the NABA. The sources of error in each method will be identified, to determine which approach provides the most robust prediction. The tests are performed on one non-elite participant.

Due to the lengthy experimental process required for both methods, the ratio between active and passive resistance, determined in this study, will be used to determine active resistance from future passive resistance measurements.

5.7.1 Velocity Perturbation Method

The resistance of a swimmer during free swimming and towed conditions is described in equations 5.2 and 5.3 respectively. This assumes that the drag coefficient, surface area and water density remain constant for both conditions

$$R_{Free} = \frac{1}{2} \rho S C_D V_{Free}^2 \quad (5.2)$$

$$R_{Perturbed} = \frac{1}{2} \rho S C_D V_{Perturbed}^2 - (R - T) \quad (5.3)$$

The velocity perturbation method makes the assumption that the effective power (resistance multiplied by velocity) is the same during free swim and towed conditions, if a swimmer performs a maximum effort (equation 5.4).

$$R_{Free} V_{Free} = R_{Perturbed} V_{Perturbed} \quad (5.4)$$

Substituting equation equations 5.2 and 5.3, the following expression is derived.

$$\frac{1}{2} \rho S C_D V_{Free}^3 = \frac{1}{2} \rho S C_D V_{Perturbed}^3 - (R - T) V_{Perturbed} \quad (5.5)$$

Solving equation 5.5 for C_D and substituting into equation 5.2, enables the active resistance to be determined from two swimming speeds and a measured change, assuming the effective power remains the same (equation 5.6 & 2.11).

$$R_{Free} = \frac{(R - T) V_{Perturbed} V_{Freeswim}^2}{V_{Perturbed}^3 - V_{Freeswim}^3}, \quad (5.6)$$

5.7.2 Naval Architecture Based Approach to Predict Active Drag

The naval architecture based approach (NABA) assumes that the arms act as a propeller and the body as a hull. It is necessary to know the passive resistance of the body for the free swimming and towed speeds. This can either be determined from a passive resistance experiment, or predicted from the passive resistance model.

Unlike a self-propulsion experiment, the self-propulsion velocity of a swimmer is already known. However, the thrust is not known and cannot be measured at the free swim velocity. Therefore, it is necessary to test the swimmer at a different velocity and measure the tow force, $R-T$. This measured force will include the difference between the passive resistance at free swim speed and tow speed, plus the added resistance effects of active swimming.

Swimming Resistance Model

During free swimming, the average active resistance and thrust throughout a stroke cycle are equal. Therefore assuming the propulsion remains the same when towed, only the resistance is increase. Therefore, the active resistance may be expressed as,

$$R_A = (R_{A\ towed} - T_{Freeswim}) - \Delta R_{Correction} + R_{P\ Freeswim}, \quad (5.7)$$

where $\Delta R_{Correction}$ is the difference between the passive resistance at the free swimming and towed speeds. This value may be generated from interpolating passive resistance data or predicted. This approach avoids the assumption of scaling resistance proportional to velocity squared. $(R_{A\ towed} - T_{Freeswim})$ is the average measured tow force over a whole number of stroke cycles. The subscripts A and P in equation 5.7 denote active and passive. It is assumed that the absolute difference between active and passive resistance is the same for the free swimming and towed speeds. The error as result of this assumption is likely to be small; however, this identifies the importance of towing as close to the free swim speed as possible.

To ensure the propulsion does not change between the free swim condition and the towed conditions, it is necessary to maintain a constant advance or tip speed ratio,

$$J = \frac{V}{nL_{Arm}}, \quad (5.8)$$

where V is the swimming or tow speed, n is the arm rotational frequency and L_{Arm} is the arm length. Therefore, when increasing the speed, the swimming stroke rate needs to be increased accordingly. It is assumed the stroke is a perfect six beat front crawl and by adjusting the arm stroke rate, the leg stroke rate follows. In this study, a range of tow speeds, faster than free swim velocity, are investigated.

The thrust deduction may be determined by

$$(1 - t) = \frac{R_{Passive}}{R_{Active}}, \quad (5.9)$$

which describes the additional resistance of the body during active swimming. It may also be used as a value to describe the effectiveness of a stroke.

5.7.3 Results

Comparing the active drag predictions from the NABA and the VPM in Table 5.2, both methods predict similar active resistance values, with the standard deviation of the NABA less than the VPM. The standard deviation is determined over the number of runs completed for each tow speed.

The largest standard deviation is experienced for the 5% over speed test. This may be due to the standard deviation in J , which is greater than for other speeds. This perhaps identifies the importance of stroke rate accuracy when predicting active resistance.

There appears to be an increasing trend in the NABA prediction of active drag with tow velocity. This trend may be due to an error in the stroke rate, where changing the required stroke rate may have only resulted in the out of water phase being adjusted with the arm velocity through the water remaining the same. This will result in less thrust being generated as tow speed is increased. This may also be due to the assumption of an equal absolute difference in passive and active resistance between the towed and free swimming velocities.

Discrepancy in the J values (NABA) or effort (VPM) between the towed and free swim tests, will add error to the predicted active drag. By comparing the VPM and NABA (equations 5.6 and 5.7), the sensitivity to error in $R-T$ is greater for the VPM, since active resistance is directly proportional to $R-T$, whereas with the NABA, $R-T$ is a small contribution to the total value calculated. This may explain the larger standard deviation experienced in the VPM predictions. Error may be reduced by ensuring the swimmer is appropriately acclimatised under testing conditions before $R-T$ measurements are made.

Thrust deduction values of 0.78 and 0.79 were determined for the NABA and VPM respectively. To determine mean active resistance from arbitrary passive resistance measurements, mean passive resistance can be divided by thrust deduction. A value of 0.8 will therefore be assumed for this study. The thrust deduction value determined in this study is for a single participant. To gain an accurate relationship between passive resistance and active resistance for a population of swimmers, this study would need to be extended to a large number of participants.

Swimming Resistance Model

Table 5.2. Passive and Active drag prediction results using the NABA and VPM.

Test Condition	No. Runs	Speed (m/s)	Passive R (N)	Resistance Correction (N)	R-T (N)	Active Drag NABA (N)	(1-t) NABA	Active Drag VPM (N)	(1-t) VPM	J
Free Swim	2	1.53 ± 0.03	104.05	-	-	-	-	-	-	2.85 ± 0.06
5% Over speed	6	1.69 ± 0.028	119.30	15.25	41.97 ± 4.13	130.78 ± 2.96	0.80	131.95 ± 15.22	0.79	2.98 ± 0.11
10% Over speed	4	1.73 ± 0.017	124.25	20.19	49.18 ± 1.79	133.04 ± 1.49	0.78	126.66 ± 7.64	0.82	2.98 ± 0.07
15% Over speed	2	1.74 ± 0.002	125.99	21.93	55.75 ± 1.91	137.87 ± 2.28	0.75	135.44 ± 6.03	0.77	3.18 ± 0.03
Mean						133.90	0.78	131.35	0.79	
Standard Deviation						3.62	0.021	4.42	0.03	

5.8 Added Mass

An external force is applied to the swimmer by a surrounding mass of fluid, when it is accelerated. The mass of this accelerating fluid is known as added mass. The added mass is dependent on the shape of the moving object. Numerous experiments have been conducted to quantify the added mass for a range of shapes (Hoerner, 1965). Based on this data, the added mass of a human body is assumed to be 20% of body mass.

An improvement to this estimation would be to determine the added mass from analysis of the acceleration force, produced during a passive tow. The difference between the measured force and resistance of the swimmer over the acceleration period, divided by the acceleration, should provide the added mass. This method would require the tow to be at a constant rate of acceleration and the swimmer to hold a fixed position.

5.9 Summary

The resistance of swimmers on the surface and underwater has been investigated. Passive resistance measurements have enabled the total resistance to be determined for males and females, on the surface and underwater, for a range of heights and masses. A wave resistance study using Thin Ship Theory has been conducted for a range body geometries and Froude numbers. Comparison of the wave elevation predicted using Thin Ship Theory with real data, suggests that Thin Ship Theory may over predict wave resistance. Using the ITTC 1957 correlation line, skin friction resistance for the full swimming Reynolds number range is determined. Viscous pressure resistance is determined as the difference between the passive resistance, and wave and skin friction resistance. With each component of resistance known for any height, mass and swimming speed, the total resistance for any swimmer on the surface and underwater can be predicted.

The resistance prediction compares well to literature. Contributions from wave, viscous pressure and skin friction resistance are 60%, 31% and 9% respectively at 2 m s^{-1} for a swimmer of height 1.79 m and mass 75 kg. An independent study measuring the surface and underwater resistance of a male participant, whose data has not contributed to the resistance model, found the surface

Swimming Resistance Model

resistance prediction was very close; however, the underwater resistance prediction was 20% less than measured, but followed a similar trend. This error is likely due to the lack of total underwater resistance data for a range of heights and masses, which results in an error in the predicted underwater viscous pressure component.

Active resistance is investigated, comparing the velocity perturbation method (VPM) with a naval architecture based approach (NABA) in single participant study. It is found that an active drag prediction using the NABA is less influenced by error in the swimmer stroke rate or effort, which is a major downfall of the VPM (Toussaint et al., 2004). A thrust deduction value of 0.8 is determined, which is proposed can convert passive drag measurements to mean active drag. However to improve the accuracy of this measurement, a larger population of swimmers needs to be tested

Swimmer added mass is assumed 20% of body mass determined from literature. However, it is proposed the added mass could be determined from measurement of total force minus the instantaneous resistance during the acceleration phase of a tow.

The information determined in this chapter allows the resistance of a swimmer to be modelled in any phase of a swimming race. Combining this with the propulsion from the various models enables the motion of the swimmer during freestyle, on the surface, and underwater undulatory swimming to be simulated.

6 Simulation Setup and Validation

6.1 Introduction

To enable the key questions of this study to be addressed, this chapter aims to validate the race simulation as outlined in Chapter 3. With the resistance model, described in Chapter 5, combined with the propulsion models, it is now possible to simulate the free swimming velocity of a swimmer, throughout the various phases of a race.

Before a simulation can be performed it is necessary to ensure the time step dt and numerical strip dimensions, dr (arm propulsion) and da (LAEBT), are sufficiently small to capture the detail being modelled. A convergence study is therefore performed before the validation process is conducted.

A validation process identified by Sargent (2005) and Robinson (1997b) is adopted. Comparison with real world data is achieved by simulating a towed scenario to produce simulated R-T data. This data is compared to experimentally generated data, for equivalent real life scenarios, to assess the validity of the individual models. White box validation is performed by comparing experimental R-T data of arms only, legs only, full stroke freestyle and underwater undulatory swimming, with the equivalent simulated output. This process is performed for a number of athlete heights, masses and genders. This enables the appropriate model parameters to be determined, to simulate the correct R-T for a population of swimmers

Black box validation is performed by comparing the simulated freestyle swimming speed, for a range of stroke rates, heights, masses and genders. To ensure the simulated speed responds accurately to changes in resistance, comparison with experimental data, for a change in swimming speed from a known change in total resistance, is made. Further validation is performed by simulating a freestyle race and comparing the velocity throughout the race with race data supplied by British Swimming. The process to ensure accurate split times and total race times is outlined.

By enabling the fatigue model, detailed in Chapter 3, the decay in stroke rate and swimming speed, as a result of fatigue, is simulated. The energy capacity

Simulation Setup and Validation

and maximum power parameters are adjusted by comparing the simulated decay in swimming velocity, in a 50m sprint, with real race data. Modelling fatigue improves the fidelity of the race simulation as it ensures the propulsive power of the swimmer remains within human capabilities. This improves the swimming speed response to changes in resistance and allows the effect of race tactics to be investigated.

A table detailing the tested athletes and protocols used to gather the validation data can be found in Appendix 4.

6.2 Simulation Convergence

Before accurate simulation of swimming speed can be carried out, it is necessary to ensure an appropriate time step dt and strip lengths dr and da are determined. This ensures the individual models capture the appropriate detail, and therefore allows the validation process to proceed, to assess whether the models fundamentally simulate the real life scenario.

6.2.1 Time Step Convergence

To ensure an appropriate time step is implemented, for both the arm propulsion and the large amplitude elongated body theory models, a convergence study has been conducted. This has been achieved by systematically adjusting dt , for an arms only and UUS simulation, until the self-propulsion velocity converges (figure 6.1). An appropriate time step of 0.01 s has been identified for both models, which will be used for all simulations.

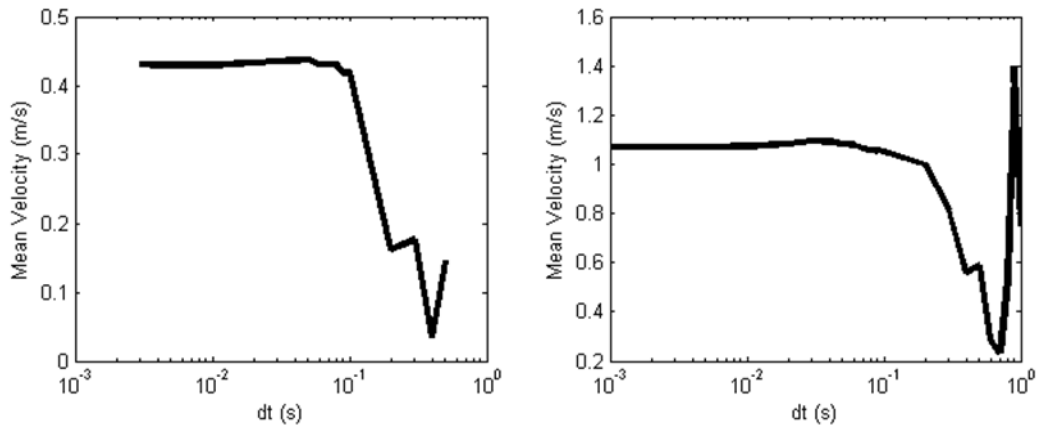


Figure 6.1. Convergence study of time step dt , for an arms only and UUS simulation, based on the mean self-propulsion velocity.

6.2.2 Strip Length Convergence

Similar to the time step, the strip length for the arm propulsion model was systematically adjusted, for an arms only simulation, until the self-propulsion velocity converged (figure 6.2). An appropriate arm strip length of 0.01 m was identified and will be used for all simulations. A strip length convergence study was not conducted for LAEBT, however a strip size of 0.01 m has been assumed to be sufficiently small.

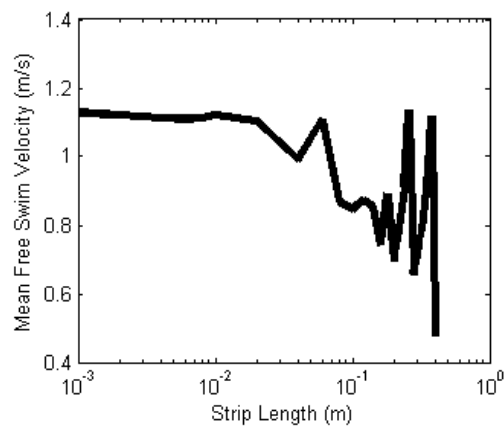


Figure 6.2. Convergence study of arm strip length dr , for an arms only simulation, based on the mean self-propulsion.

6.3 Simulating a tow

In order to compare the simulated forces from the propulsion models with experimental data, it is necessary to simulate a tow. During a towed situation,

Simulation Setup and Validation

the swimmer is being towed faster than they can swim. This is the same as prescribing a minimum velocity – the tow velocity. To simulate a tow the following restriction to the simulated velocity is prescribed,

$$\begin{aligned} \text{IF } V(i + 1) < V_{Tow} \\ V(i + 1) &= V_{Tow}, \end{aligned} \quad (6.1)$$

where V_{Tow} is the tow velocity. As would be experienced in a real tow situation, if the tow velocity is not fast enough, self-propulsion velocity will be faster than the tow velocity.

The force measured during a tow is $R-T$. Therefore, the simulated tow force is determined as

$$\text{Tow Force} = \frac{R(i + 1)}{(1 - t)} - T_x(i + 1), \quad (6.2)$$

where $(1 - t)$ is the thrust deduction used to convert a passive resistance value to active resistance and T_x is the total simulated thrust from the propulsion models.

6.4 Comparison of Simulated and Experimental R-T

It is necessary to consider the differences between the experimental and simulated R-T data, to identify the limitations of making a comparison between the two. The simulated R-T is in the purest form: all simulated propulsive forces are subtracted from the resistive forces. With a tow experiment, this cannot be fully captured, since dampening will occur within the swimmers body, attachment to the swimmer and within the experimental equipment. For example, 10 N of thrust generated at a high rate (or impulse) on the hand of a swimmer, during an over speed tow, has to react through the arm, along the torso, through the flesh, into the neoprene strap around the waist, along 5-25 m of thin tow line before it measured at the tow system. An example of this can be seen in figure 4.7, where both a passive tow and arms only tow, performed at the same speed, are displayed. During the active case, at no point does the R-T return to the mean passive resistance, between arm strokes. This suggests that either the propulsive force from the arms never approaches zero (It is expected that arm propulsion approaches zero between arm pulls) or

attenuation of the measured R-T is occurring. Although effort has been made to minimise this attenuation, it is inevitable that smoothing of the force signal will occur. This smoothing should not affect the mean measured R-T, however the measured time varying R-T will be different to the true R-T occurring on the body of the swimmer.

To allow comparison of the simulated and experimental R-T, it is necessary to apply smoothing to the simulated data. This is achieved using a low pass Butterworth filter. Selecting an appropriate low pass frequency has been determined by comparing simulated and experimental R-T data. Figure 6.3 displays experimental data of an arms only tow for athlete O. The tow is performed at a constant 2.02 m s^{-1} , and observations of the experimental tow speed identify it remains within 0.02 m s^{-1} of the mean tow speed. This scenario has been simulated to provide R-T. The inputs to the simulation are height, mass, stroke rate and tow speed. Sources of error in the simulation could be in either the resistive or propulsive forces. The simulated resistance, determined from the resistance model is 147.57 N at 2.02 m s^{-1} . Eight runs of passive resistance measurements have been performed for athlete O at 1.84 m s^{-1} , providing a mean resistance of $127.6 \pm 7.24 \text{ N}$. Scaling this resistance value to 2.02 m s^{-1} assuming a V^2 relationship provides a passive resistance of 153.79 N . This is close to the simulated resistance; therefore, it is assumed the simulated resistance is correct. A thrust deduction of 0.8 is assumed for simulations of all active swimming. The simulated R-T data includes this thrust deduction, thus increasing the passive resistance by 25% to represent active resistance. Comparing the experimental and simulated R-T, the simulated data varies significantly more than the experimental, however the mean values are similar (Mean Exp R-T: 98.97 N , Mean Sim R-T: 104.4 N). This identifies the smoothing process that occurs during an experimental measurement. To achieve similar magnitudes of variation, a low pass frequency of 4.7 Hz has been determined (Figure 6.4). This does not affect the forces modelled within the simulation, but allows the comparison with experimental data. A stroke rate of 49.2 cycles/min , which provides two propulsive phases, equates to a propulsion frequency of 1.64 Hz . To ensure aliasing does not occur, it is necessary to filter at a frequency no less than two times the stroke frequency (Proakis and Ingle, 2011), therefore 3.28 Hz . For arms only freestyle a filter frequency of 4.7 Hz is therefore sufficient to ensure aliasing should not occur.

Simulation Setup and Validation

For full stroke freestyle, the frequency of the leg kick needs to be considered. Assuming a six beat leg kick, a stroke rate of 49.2 cycles/min would produce a kicking frequency of 4.92 Hz, therefore a filter frequency can be no less than 9.84 Hz. Considering a very high stroke rate, performed in a 50 m freestyle race, of 61.2 (Cesar Cielo Filho 2011 World Championships 50 m Freestyle Final – world record, Data Source: British Swimming), this would require a minimum low pass frequency of 12.24 Hz.

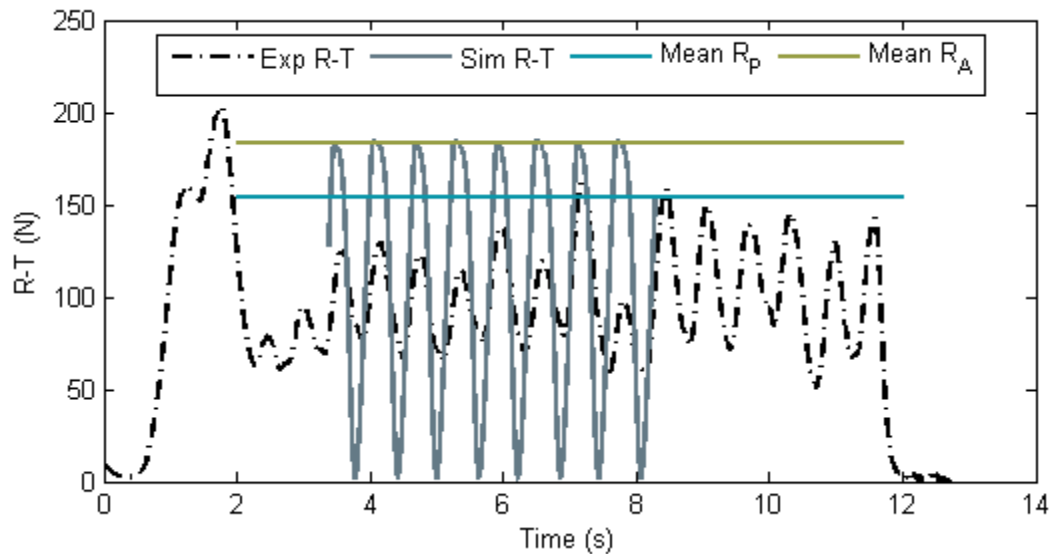


Figure 6.3. Experimental and Simulated R-T data for Athlete O (Height: 1.75 m, Mass: 71 kg) during an arms only over-speed tow at 2.02 m s^{-1} . Stroke rate was 49.2 cycles/min. The passive resistance at the tow speed, determined from experimental measurements, is 153.8 N. The simulated passive resistance is 147.6 N. The simulated mean active resistance, determined from a thrust deduction of 0.8 is 184.5 N.

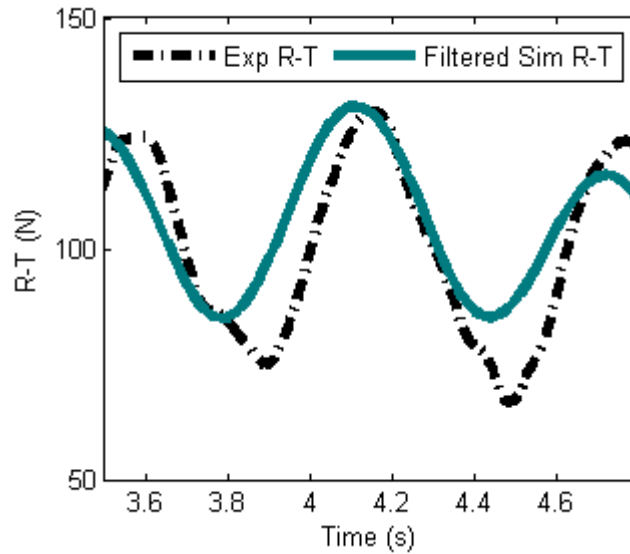


Figure 6.4. Simulated R-T after filtering in comparison to the experimental R-T data.

6.5 Arm Model Setup and Validation

To identify the accuracy of the arm model, five athletes were towed performing arms only freestyle and $R-T$ was measured. A simulation was performed to recreate the towed scenario for each athlete. Figure 6.5 displays a comparison between the measured and simulated $R-T$ for the five athletes over one stroke cycle (left arm and right arm propulsive phases). The same arm motion, as described in section 3.7.2, was simulated for each athlete. All simulated data is filtered with a low pass frequency of 4.7 Hz.

By comparing the mean experimental and simulated R-T data, the arm dimensions are adjusted to achieve the correct propulsion. The arm width used in the simulation is assumed to be linearly proportional to height. A relationship has been determined for a single participant with arm width of 0.12 m and a height of 1.79 m.

$$W_{th} = 0.067H \quad (6.3)$$

To achieve the correct propulsion for the five athletes simulated, an arm length relationship has been developed for males and females,

$$L_{arm\ male} = 0.1H + 0.67 \quad (6.4)$$

Simulation Setup and Validation

$$L_{arm\ female} = 0.18H + 0.45 \quad (6.5)$$

In general the variation of $R-T$ for all athletes is captured by the simulation. For athlete O, the experimental and simulated $R-T$ data are very similar. For athlete P11, simulating an imbalance provides a closer match to the experimental $R-T$. For the remaining athletes, the variation in the data is less sinusoidal, which suggests that the interaction between resistance and propulsion is more complex.

It is not possible to distinguish between resistance and propulsion from $R-T$ measurements. The specific motion of the body (causing resistance) or arms (generating propulsion) will both have an effect on the measured $R-T$. The dynamic motion of the body and its interaction with the arms is accounted for using a thrust deduction value, determined from the active resistance study. Therefore, the active resistance of the swimmer is modelled **on average** and does not vary with time throughout a stroke. As a result, the simulated time varying $R-T$ may be less accurate for athletes who have complex body motions, but on average will be similar to the experimental measurement. In addition, the actual propulsive forces achieved by the swimmer will be due to a complex three dimensional motion of their arm causing lift and drag forces. The simulated propulsion is based on drag only, generated from a generic two dimensional motion. However, since the arm length has been scaled to achieve the correct mean propulsion, the magnitudes of the experimental and simulated $R-T$ are similar. An improvement to this approach would be to use swimmer specific arm motion data. Additionally, a limitation of the two dimensional drag only approach, is that three dimensional arm motion, producing lift and drag forces, may have different time varying propulsion.

To achieve time accurate $R-T$, the requirement to more specifically model both the motion of the body and the arms is evident. To improve the arm propulsion model, the number of elements used to simulate the arm could be increased to three and a three dimensional motion prescribed to include a lift component. Akis (2004) proposed a three element arm model with motion in three dimensions, however did not include a lift component. Therefore, incorporating it with a lift calculation and using lift coefficient data described in Chapter 2, a more time accurate propulsion may be achieved. A disadvantage of modelling the motions of the arms and body more accurately,

would be the complex and time consuming three dimensional motion analyses required to generate the input data. With the correct mean simulated $R-T$, the correct mean swimming speed will be achieved. Therefore, the time inaccuracies will have a small effect on the modelled velocity variation throughout a stroke cycle.

The energy consumed by the arm propulsion is determined from the arm power. Therefore, it is important that the time varying arm power is accurate. Arm power (equation 3.12) is governed by torque, which is governed by the tangential force on the arm. Therefore the accuracy of the simulated arm power will relate to the accuracy of the simulated propulsion. With $R-T$ measurements containing the superposition of resistance and propulsion, it is difficult to prove this. However, for athletes O, P and M, the simulated $R-T$ is similar, suggesting that the simulated propulsion is similar to the real propulsion. Since the observed arm motion (from video) of athletes K and N was similar to O, P and M, it is assumed the difference in experimental $R-T$ was due to time varying resistance, and therefore the propulsive power of these swimmers is likely to be similar, and captured by the simulation.

Simulation Setup and Validation

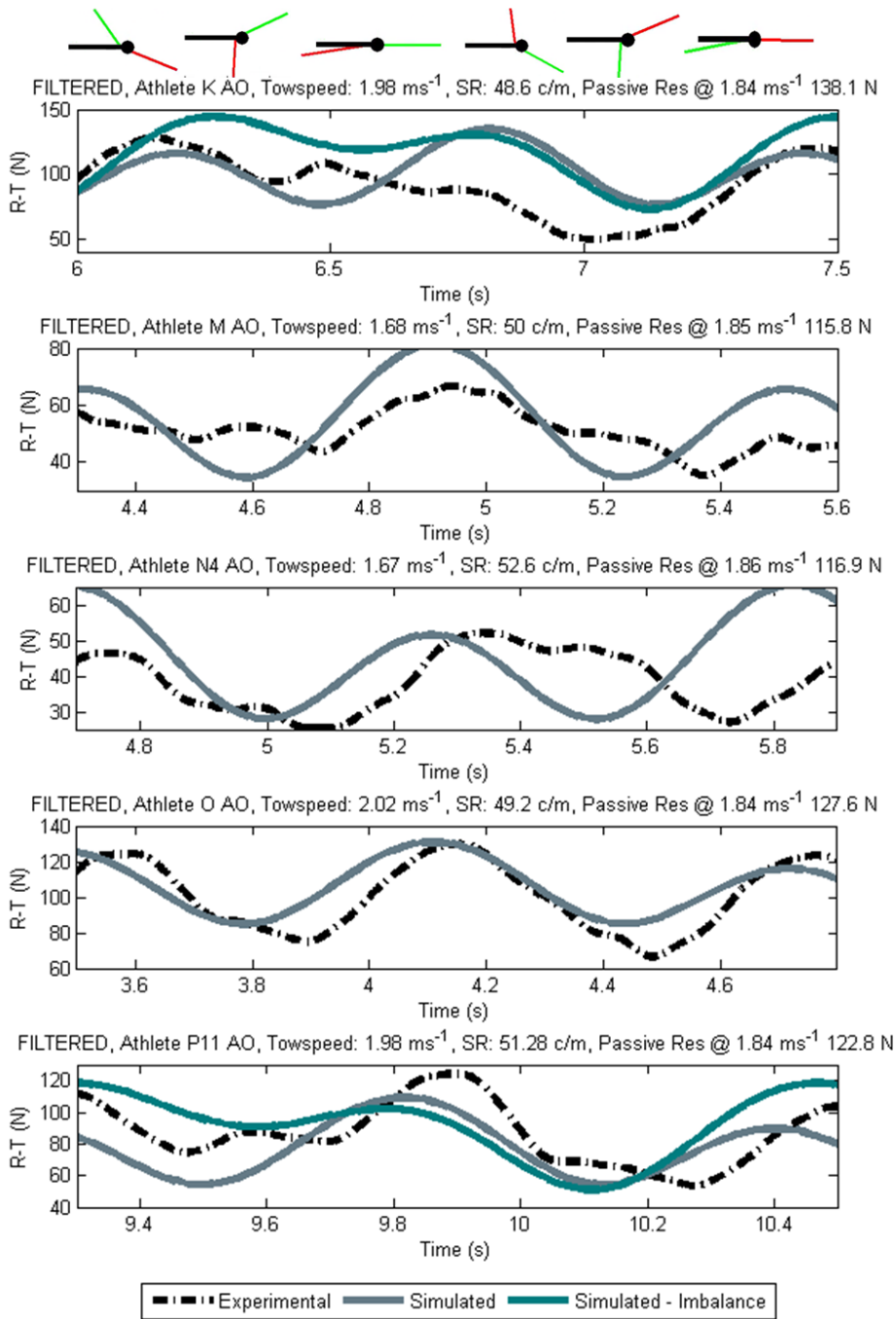


Figure 6.5. Comparison of experimental and simulated $R-T$ for five athletes. Where necessary an imbalance has been applied to achieve a more accurate simulated $R-T$. The parameters specified in the simulation for each athlete are height, mass, gender, stroke rate, tow speed and imbalance coefficient.

6.6 LAEBT Setup and Validation

6.6.1 Underwater Undulatory Swimming

As a validation for the LAEBT thrust prediction, a male and a female swimmer were towed underwater performing UUS at two kicking frequencies and $R-T$ was measured. The tow speed for all cases was 2.2 m s^{-1} . The female swimmer (Athlete G, Height: 1.71 m, Mass: 60.5 kg) performed UUS at 1.69 Hz and 2.01 Hz. The male swimmer (Athlete F, Height: 1.82 m, Mass: 84 kg) performed UUS at 1.28 Hz and 1.9 Hz. Kicking frequencies were determined by analysing video data of the experimental runs. A simulation was performed to recreate these towed scenarios. Figures 6.6 and 6.7 display the experimental and simulated $R-T$ values. The kinematic data used for all UUS simulations is the motion performed by Athlete G for a kicking frequency of 2.01 Hz. By comparing the mean experimental and simulated $R-T$ data, for Athlete G at a kicking frequency of 2.01 Hz, the cross sectional width of the swimmer S is adjusted to achieve the correct propulsion. This process provided an S value of 0.23 m. Thereafter S is scaled linearly for other heights. Considering the correct mean thrust is generated by the wake component of LAEBT (at the feet), an S value similar to the dimensions of the feet would be expected. According to Winter (1979), the width of the feet can be determined as $0.055H$, where H is height. This provides a foot width of 0.094 m and therefore a total width (both feet) of 0.19 m, which is similar to the estimated S value. For other kicking frequencies, kicking amplitude is scaled by Strouhal number, as described in section 3.8.2.

In Figure 6.6 the simulated $R-T$ only contains propulsion from rate of change of momentum in the wake. This will have the same **mean** value as the total propulsion predicted by LAEBT. However, the time variation of the simulated $R-T$ will be different because the reactive forces along the body are not included (Lighthill, 1971). Comparing the mean experimental and simulated $R-T$ values, all simulated cases are within 12% of the experimental data.

In addition to the active testing, a single underwater passive resistance measurement was made for both athletes F and G. The experimental and simulated resistance values for Athlete F are 184.19 N and 137.95 N respectively. The experimental and simulated resistance values for Athlete G

Simulation Setup and Validation

are 143.56 N and 119.6 N respectively. The simulation under predicts the passive resistance by 25 % and 17 % for athlete F and G respectively. Although similar experimental and simulated R-T values have been achieved, if resistance is under predicted, the appropriated S may also be under predicted. The thrust deduction value of 0.8 is used to convert all passive resistance into active resistance, when simulating swimming. However this value has been determined from experimental measurements of freestyle. When simulating UUS, this thrust deduction value may not appropriately represent the active resistance. In UUS, there may be less added resistance due to interaction between the propulsor and the body; where in freestyle high local velocity generated by the arms increases the local resistance of the body (Banks, 2013). The added resistance due to the dynamic movement of the body is likely to be less than in freestyle, since the upper portion of the body remains in a streamlined position. However, during certain phases of UUS, the legs present a large projected area. Improved accuracy in the thrust deduction value, used to simulate UUS, could be achieved by conducting the VPM or NABA for active resistance on UUS, as described in section 5.7.

Error in the propulsive forces could be due to over-simplification of LAEBT. Lighthill (1971) discusses that the neglect of a resistive component in the theory may result in under-prediction of the thrust. Reactive forces along the body are proportional to local acceleration and oscillation between fixed limits results in zero mean thrust. However, with a resistive component, force along the body would be proportional to local velocity, and therefore may provide net thrust.

Although the S value was determined so that the correct mean R-T value was achieved in the initial case, the subsequent change in kicking frequency for the same athlete (Athlete G) and Athlete F has resulted in an error in the mean thrust prediction. Error in the resistive or propulsive forces will therefore have artificially been eliminated in the first case (due to the manual adjustment of S), but are apparent in the other cases. Error may also be due to the scaling of the kicking amplitude and the S value. It was assumed that all athletes kick at the same Strouhal number, and therefore kicking amplitude is scaled relative to kicking frequency. This assumption may be invalid, however it is necessary to predict kicking amplitude when it is not known. A relationship has been found between kicking frequency and amplitude (Von Loebbecke, Mittal, Fish,

et al., 2009a), however wide scatter in the data from which the relationship was determined means not all kicking occurred at the same Strouhal number. In addition the scaling relationship between S and height may have an error, however Winter (1979), reports that foot width is proportional to height.

The clear difference between the time variation of the experimental and simulated data is the number of thrust producing phases in a kicking cycle. The experimental data has one thrust producing phase per cycle, experienced during the down kick. The simulated data has two phases, one on the up kick and one on the down kick. Two propulsive phases would be expected for a symmetrical body producing symmetrical motion, however in reality, losses are occurring due to either reduction in thrust or added resistance during the up kick. When the body reaction forces are included, the LAEBT thrust prediction (figure 6.7) does not result in a time varying signal similar to the experimental data. However, it produces a more significant single thrust and single drag phase per cycle. With the inclusion of a resistive component, proportional to velocity and using a drag coefficient, this may provide the thrust prediction with the missing component, and provide an R-T signal more similar to the experimental measurement.

Simulation Setup and Validation

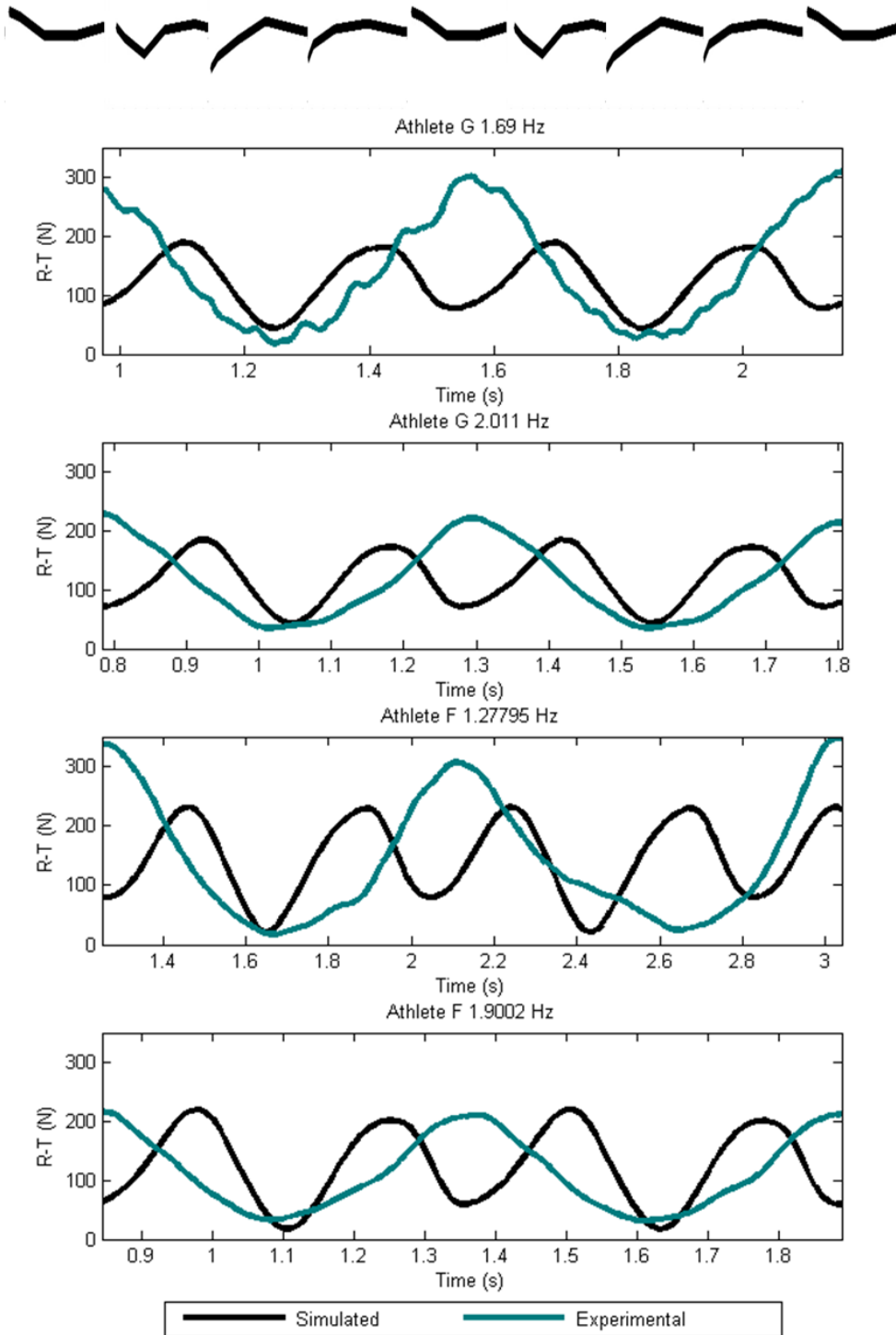


Figure 6.6. Experimental and simulated R-T data for two kick cycles by two swimmers performing UUS at a high and a low kicking frequency. The simulated thrust is determined from LAEBT using the rate of change of momentum in the wake component only. Two kick cycles are presented.

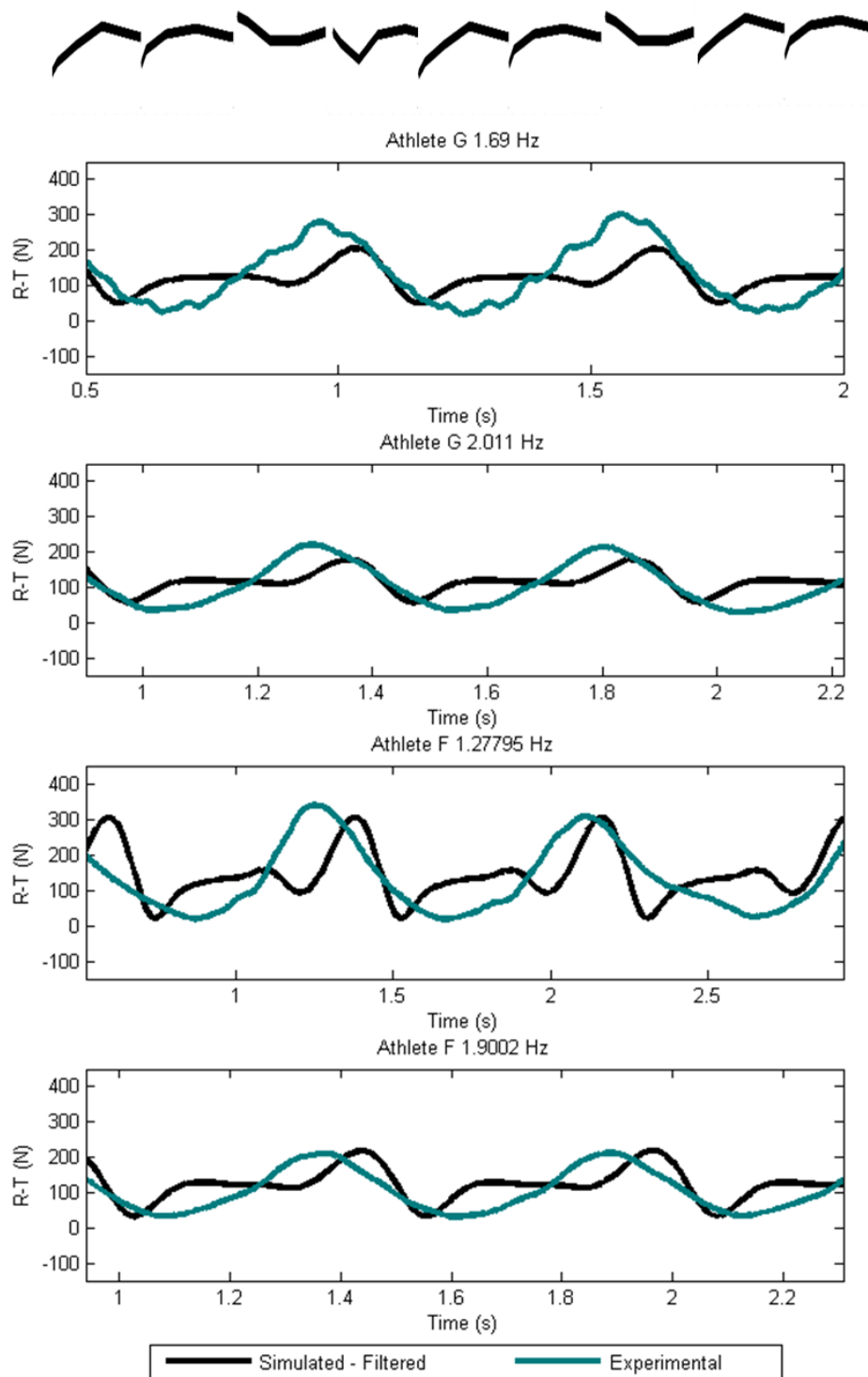


Figure 6.7. Experimental and simulated R-T data for two kick cycle by two swimmers performing UUS at a high and a low kicking frequency. The simulated thrust is determined from LAEBT using the rate of change of momentum in the wake and body reaction forces. Two kick cycles are presented.

Simulation Setup and Validation

6.6.2 Freestyle Flutter Kick

The process applied to UUS has also been conducted for flutter kick. Over speed tows were performed at 1.99 m s^{-1} and 1.94 m s^{-1} for athlete O and P respectively, both with a kicking frequency of 2.5 Hz. The tow speeds were similar to their freestyle self-propelled speeds, the condition in which flutter kick is performed. Figures 6.8 and 6.9 display experimental and simulated R-T data, with and without body reaction forces respectively. The simulated data has been compared to two runs of the same condition for each athlete, therefore the simulated data is the same, but the experimental data is a repeat measurement. Like with UUS, the S value has been adjusted to achieve the correct $R-T$, when compared to experimental data. It would be expected that a flutter kick S value, for a single leg, is similar to half the S value for UUS, since in UUS both legs are modelled as a single segment. However, an S value for flutter kick of three quarters the dimension used in UUS has been determined. This supports the argument that the S value determined for UUS is may be too small, due to the under prediction of underwater resistance.

The thrust deduction value of 0.8 is also assumed for flutter kick. Observation of the video footage identifies upper body movement, which will contribute to increased resistance, above the passive resistance. However the absence of the arm propulsion may suggest the thrust deduction results in an over prediction of the active resistance. To determine an accurate thrust deduction for flutter kick R-T simulations, it would be necessary to perform active resistance testing of flutter kick.

The mean experimental and simulated R-T values are within 9 %. Without body reaction forces (figure 6.8), the magnitude of the simulated oscillations are significantly greater than the experimental. In reality, thrust only occurs from the down kick of each leg. In the simulation, thrust occurs during the up and down kick, with thrust from down kick of one leg undergoing superposition with thrust from the up kick of the other leg. This effect increases the amplitude of the simulated R-T oscillations.

When body reaction forces are included and a 12 Hz low pass filter is applied, the simulated R-T data becomes more similar to experimental data (figure 6.9). The superposition process that causes the large magnitudes is alleviated by the body reaction forces, and the filtering provides a smoother signal over the

stroke cycle. However, as with UUS, it is likely a resistive component included in LAEBT would improve the thrust prediction, producing a signal more similar to the measured R-T. For athlete O, the experimental oscillations are smaller than for athlete P. Observation of the video footage, identifies both athletes have different kicking techniques. The feet of Athlete O break the surface more severely, therefore spending less time in the water generating propulsion. This may suggest the larger oscillations in the experimental R-T data for athlete P (figure 6.9).

Simulation Setup and Validation

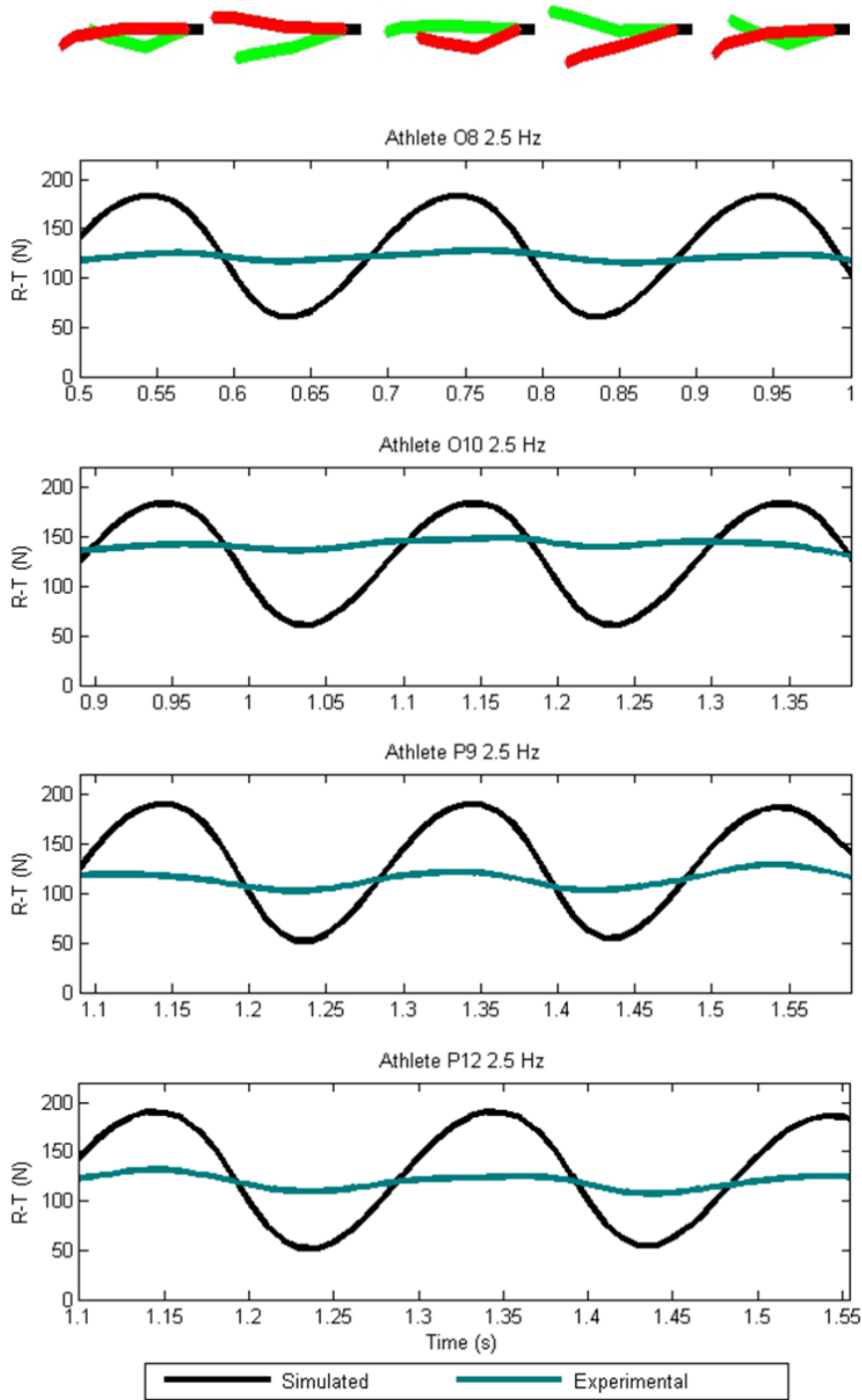


Figure 6.8. Experimental and simulated R-T of two swimmers performing flutter kick at 2.5 Hz. The simulated thrust is determined from LAEBT using the rate of change of momentum in the wake only. One kick cycle for each leg is presented.

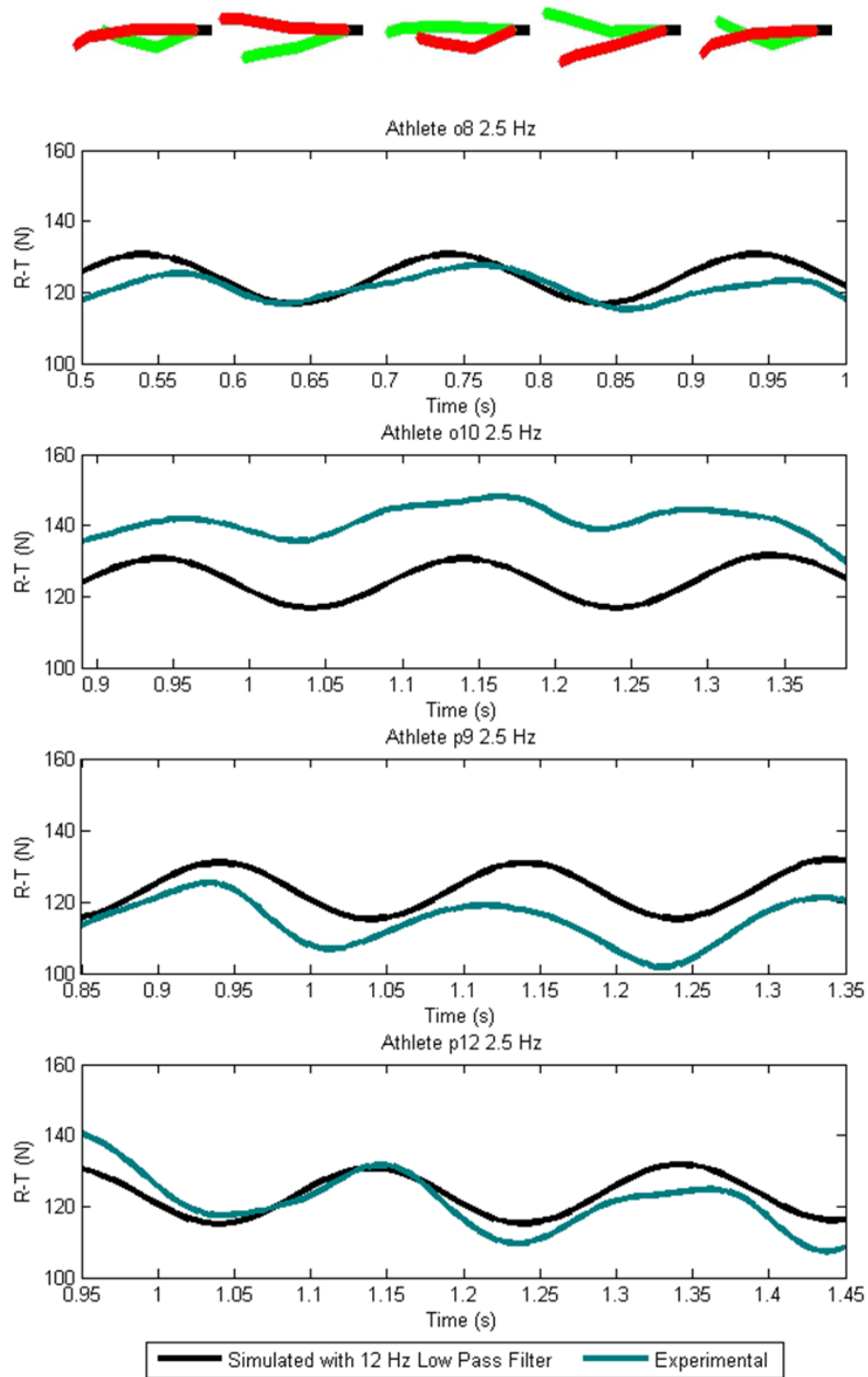


Figure 6.9. Experimental and simulated R-T of two swimmers performing flutter kick at 2.5 Hz. The simulated thrust is determined from LAEBT using the rate of change of momentum in the wake and body reaction forces. One kick cycle for each leg is presented.

6.7 Stroke Reconstruction

Using the arm and the leg kick propulsion models, full stroke freestyle swimming can be simulated. It is important to achieve the correct timing of the arm and the leg stroke to ensure the propulsion is modelled accurately. This includes the number of leg kicks to one arm cycle and the phasing between the arms and the legs. Figure 6.10 illustrates a typical six beat freestyle technique, where there are three leg kicks for every one arm cycle (per arm and leg). The phasing of the leg kick has been adjusted to match athlete O, whose technique is very repeatable, and will be assumed sufficient for all other athletes. Most athletes have a phasing error between arm strokes and leg kicks, which varies across stroke cycles.

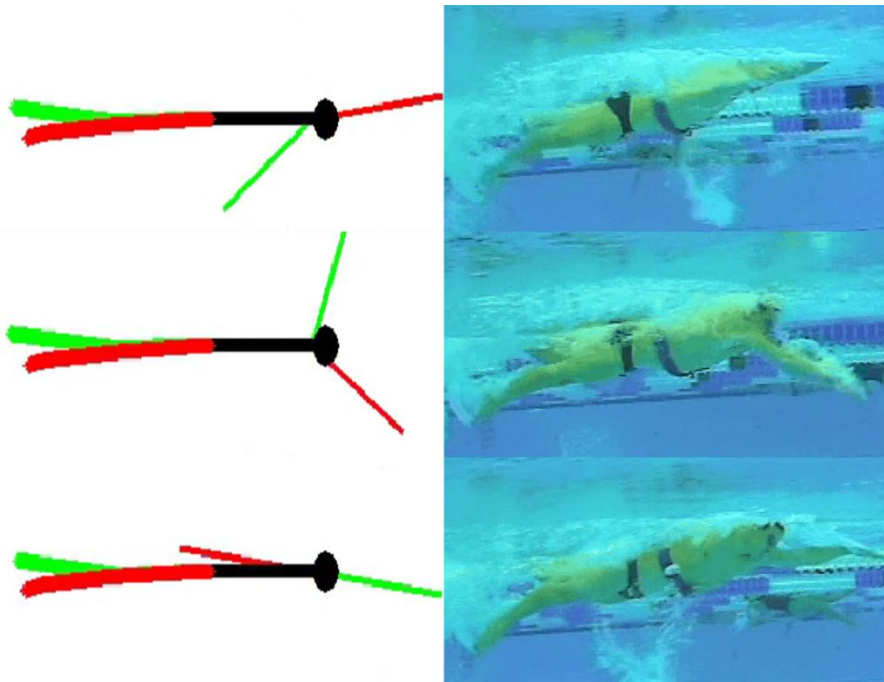


Figure 6.10. Simulating a six beat freestyle technique using the arm and the LAEBT propulsion models compared with video data of Athlete O.

Over speed tows were performed for five athletes performing freestyle. These tows were simulated using the propulsion models as defined in the previous section, without any alterations to the arm or leg dimensions. Figures 6.11 and 6.12 compare the unfiltered and filtered simulated data with the experimental data. Table 6.1 compares differences in the mean simulated and experimental R-T values. These differences are also identified as a percentage of the active swimming resistance to quantify the accuracy of the simulation. The difference

between the simulated and experimental R-T values are less than 5% of the total active resistance at the tow speed. Where an imbalance has been simulated, to achieve a more representative time varying R-T, this has shifted the mean R-T, increasing the error. To achieve increased accuracy while modelling an imbalance, a more swimmer specific arm and leg dimensions would be required to reduce the overall error.

Table 6.1. Comparison of experimental and simulated mean R-T data for freestyle over speed tows. $\Delta(R-T)$ as a percentage of active resistance R_A is determined to quantify the accuracy of the simulation.

Swimmer	Exp R-T	Sim R-T	$\Delta(R-T)$	Sim R-T Imbalance	$\Delta(R-T)$ Imbalance	R_A	%Diff	%Diff Imbalance
K3	53.0	59.3	6.2	71.0	17.9	205.7	3.0	8.7
M3	28.3	10.0	-18.3			128.0	-4.3	
N3	36.2	40.0	3.7			144.0	2.6	
O6	63.6	59.0	-4.6			185.6	-2.5	
P5	41.0	18.1	-22.9	23.7	-17.2	186.3	-2.3	-9.3

In the unfiltered data (figure 6.11), the low and high frequency contributions from the arm and the leg models are clear. However the magnitude of the variation is much greater than the experimental data. In order to reduce the overall magnitude, similar to the experimental data, a low pass frequency of 4.7 Hz, as used for the arms only case, is required (figure 6.12). However, this removes the leg contribution from the simulated signal, which occurs at a higher frequency. When observing the experimental data in figure 6.12, a faint leg kick contribution can be seen. Therefore, the natural smoothing process that occurs during over speed towing is allowing some high frequency components to reach the dynamometer. Another effect that may be reducing the magnitude of the variation in the experimental R-T data, but allowing some high frequency signals to pass, may be the effect of body roll. As the swimmer performs freestyle arm motion, they roll. Observation of the video data, for all athletes tested, identifies the point of towing moves during the body roll. If this movement is sufficient, in the direction of the tow, it will affect the resistance measurement. The timing of this movement will therefore be important; affecting how the measured R-T differs from the actual R-T occurring on the body of the swimmer. This effect may also be athlete specific,

Simulation Setup and Validation

due to differences in swimming technique. This may suggest why the simulated R-T signal matches some athletes better than others. For example, the experimental R-T for athlete k, does not display two clear propulsive phases unlike most of the other athletes. This may be an attribute of asymmetric body roll, causing one of the propulsive phases to be missed in the R-T measurement. However, this phenomenon will not affect mean R-T, and it is important the correct mean R-T is achieved before the time varying R-T can be considered.

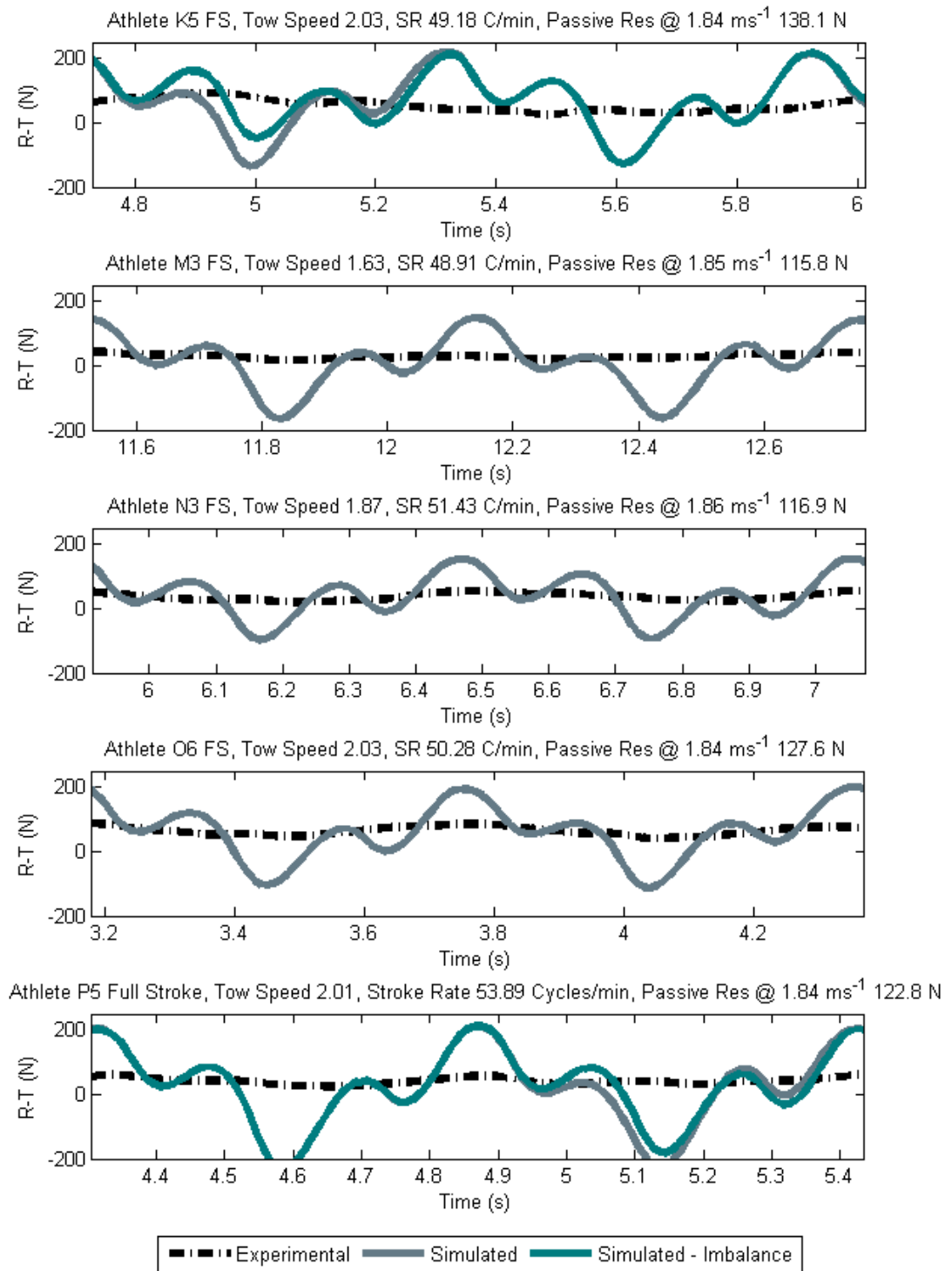


Figure 6.11. Experimental and simulated R-T data of five swimmers performing freestyle during an over speed tow. Thrust contributions are from the arm model and the leg kick model using LAEBT.

Simulation Setup and Validation

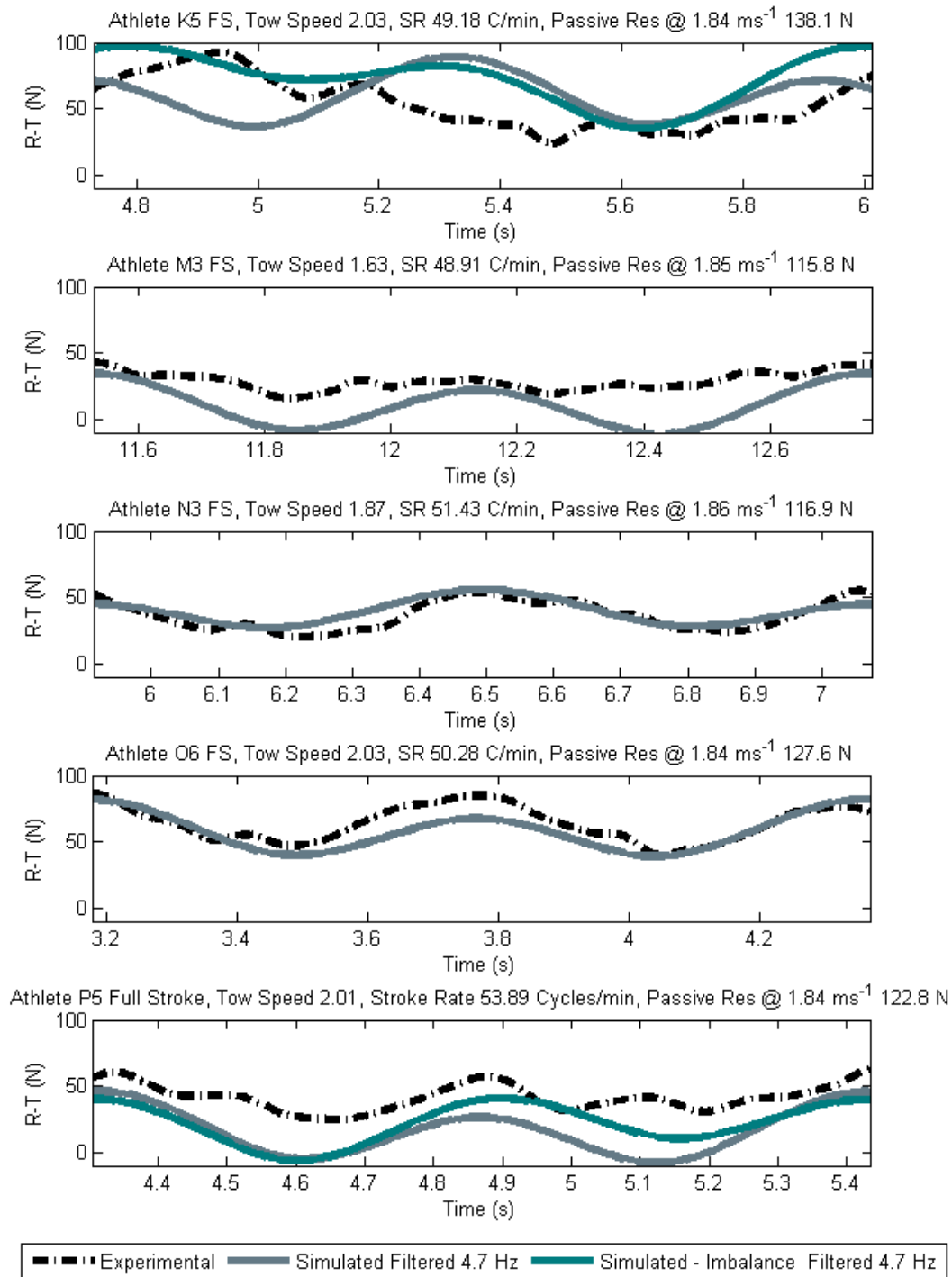


Figure 6.12. Experimental and filtered simulated R-T data of five swimmers performing freestyle during an over speed tow. Thrust contributions are from the arm model and the leg kick model using LAEBT.

6.8 Free swim Speed

To ensure the simulator achieves the correct swimming speed for a range of swimmers and stroke rates, its output has been compared to race data supplied by British Swimming. This race data is for arbitrary male and female world championship finalists (not included in the previous model setups in sections 6.5 to 6.7), and has been analysed to determine stroke rate and corresponding velocity. A self-propelled simulation for the same height, mass and stroke rate data has been performed. The relationship between stroke rate and mean swimming velocity for the real race data and simulation is compared for males and females in figures 6.13 and 6.14 respectively.

Looking at the real race data, there is a general trend of increased velocity with increased stroke rate. However, in certain cases swimmers achieve similar speeds with different stroke rates. This is likely due to variations in technique such as the arm velocity through the water, arm orientation affecting the lift and drag, and leg kick frequency. In the simulation, these parameters do not change with stroke rate, and therefore there is a defined trend of increased swimming speed with increased stroke rate. In addition, the error in swimming speed is least for stroke rates around 50 cycles/min. This is roughly the stroke rate performed by the athletes used to set up the propulsion models. This suggests, at the higher and lower stroke rates technique change may occur, and the accuracy of the simulation becomes less.

In general, the simulated speeds are less than the real race speeds for a given stroke rate, for both males and females. A reason for this may be due to the quality of the swimmers used in R-T validation cases for the propulsion models. Out of the five athletes used to validate the full stroke simulated R-T data (figure 6.12), only Athlete N reached a world championship final. Therefore, the propulsive force for a given stroke rate will be less than is achieved for the worlds very best swimmers. In addition, these real race velocities are achieved when the athletes are fully prepared and rested. The validation R-T data was taken while swimmers were in training and may have been influenced by fatigue associated from a swimmer being half way through a training cycle. Although in training an athlete can replicate a race stroke rate, it is plausible that they self-regulate their arm motion to achieve the correct stroke rate without producing race levels of propulsion. Without performing

Simulation Setup and Validation

detailed analysis of the arm motion for every experimental run, it is not possible to determine if this is occurring.

It is necessary to model the correct swimming speeds so that the correct simulated race time is achieved. This allows the effect of an intervention on race time to be determined more accurately. However, small error in race time is acceptable since this will have a small impact on a relative race time change.

If the simulated race time is significantly different to the real race time for a given athlete, it may be necessary to change the parameters in the propulsion models to achieve the correct swimming speeds. A factor can be applied to the arm width and S value to change both arm and leg propulsion respectively. This is similar to the original process of setting up the propulsion models to achieve the correct R-T. This process will achieve the correct swimming speed for a given stroke rate, however will not affect the relationship between stroke rate and swimming speed. Therefore, athletes who have variations in technique across a range of stroke rates will be less accurately modelled.

The most consistent swimmer analysed is athlete F2, whose stroke rate and speed relationship is consistent across the range of stroke rates performed. The simulated swimming speed for this athlete is less than the real swimming speed, however the trend of the data are similar. This identifies, that the simulation is accurate for athletes with consistent technique.

Simulation Setup and Validation

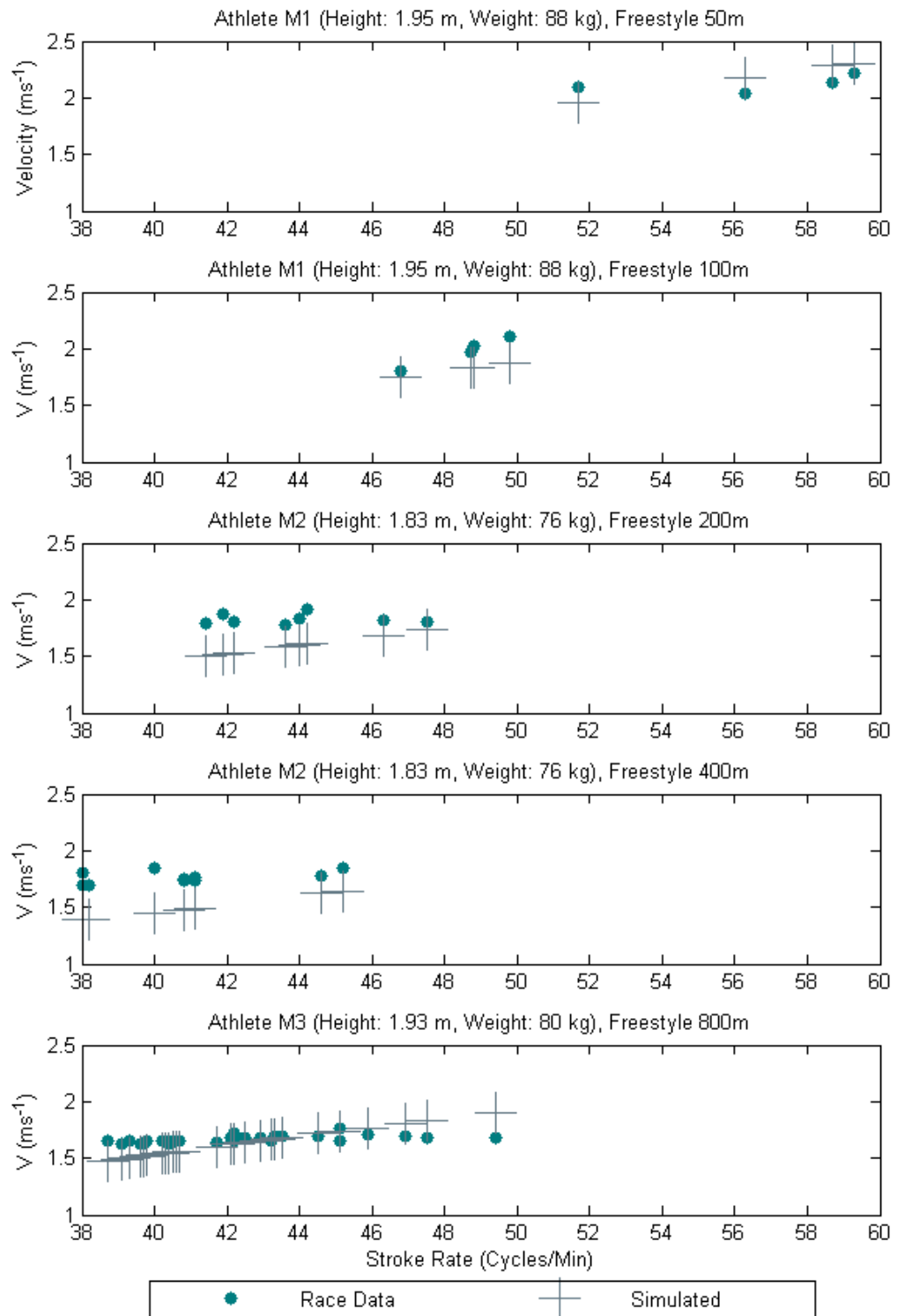


Figure 6.13. Stroke rate and velocity data, from race analysis of athletes, in a world championship final, for all male freestyle events. A simulation has been performed for the same height, mass, gender and stroke rate. The resulting velocity is displayed.

Simulation Setup and Validation

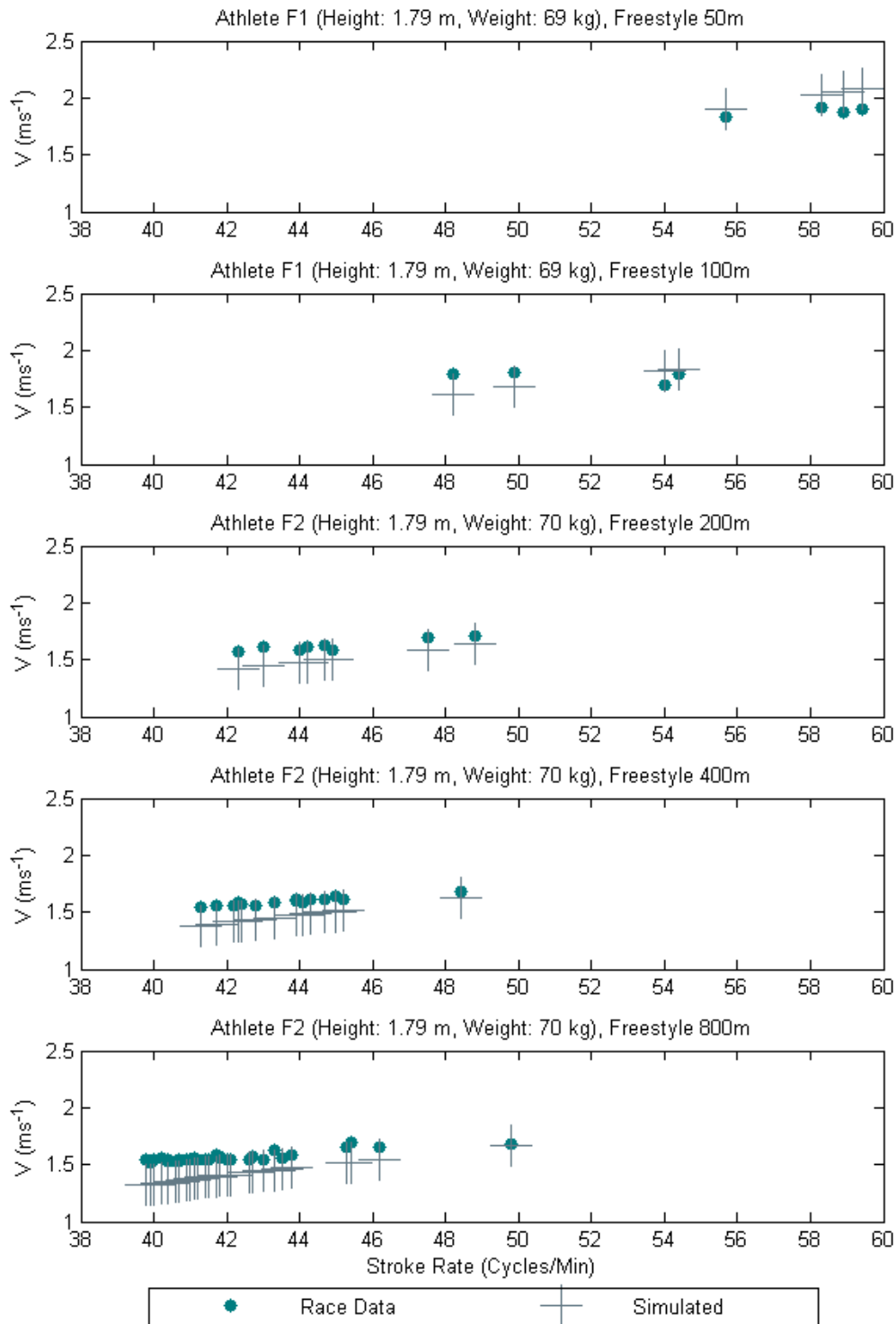


Figure 6.14. Stroke rate and velocity data, from race analysis of athletes, in a world championship final, for all female freestyle events. A simulation has been performed for the same height, mass, gender and stroke rate. The resulting velocity is displayed.

6.9 Effect of a resistance augment on speed

It is necessary for the simulator to answer questions on the effect of changes to swimmer resistance and how this impacts swimming speed and race time. An experimental study has been performed where a known change in total resistance and the resulting change in swimming speed have been measured. This was performed on an individual male athlete (Height: 1.88 m, Mass: 90 kg), who specialises in freestyle sprint events (50 m & 100 m).

The total resistance of a swimmer was measured, by passive towing, with and without a small chute attached (figure 6.15) at a speed of 1.52 m s^{-1} and 1.56 m s^{-1} respectively. The reduction in tow speed was a result of the significant increase in resistance due to chute. A resistance coefficient (equation 2.2) is determined to allow the resistance measured at these two speeds to be compared. It is assumed this marginal change in tow speed will not change the change the flow regime around the swimmer or chute. Figure 6.16 displays the bootstrap distributions of the two conditions measured. The bootstrapping process is detailed in section 4.4.2. The mean added resistance from the chute is 41.4%.

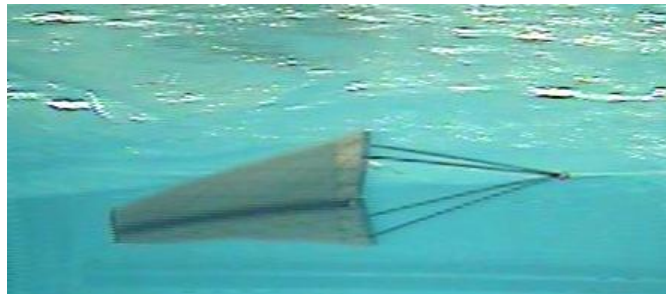


Figure 6.15. Drag chute used to apply an additional known resistance to the swimmer.

Simulation Setup and Validation

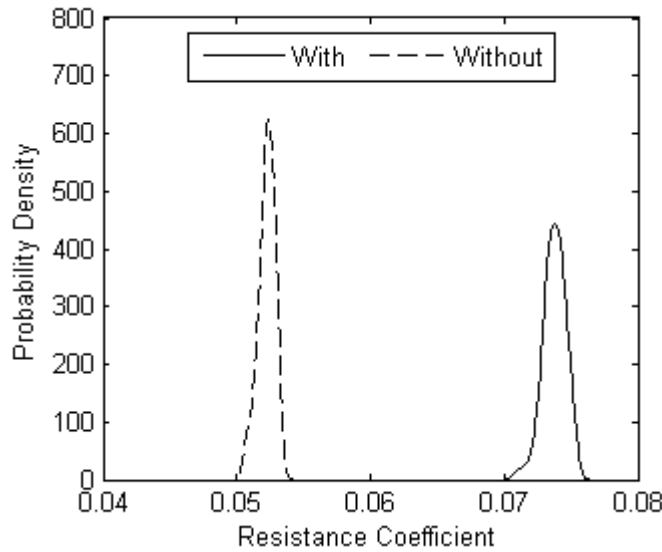


Figure 6.16. Resistance coefficient of an individual athlete with and without a drag chute, determined from passive towing.

Free swim tests were performed, at maximum effort, over a distance of 15 m, without and with the chute, measuring time to complete the distance. Time was measured independently, by three individuals, using a stopwatch. Stroke rate was not measured. Table 6.2 displays the results. A 21% reduction in free swim speed was measured with the chute.

Table 6.2. Results of a timed free swim test at maximum effort with and without the chute.

	Without Chute	With Chute
Distance (m)	15	15
Time 1 (s)	7.58	9.64
Time 2 (s)	7.6	9.75
Time 3(s)	7.8	-
Average Time (s)	7.66	9.695
Speed (ms^{-1})	1.958	1.547

A simulation was performed for the same height and mass. The results are displayed in table 6.3. Stroke rate was not known, therefore was adjusted until the correct free swim speed ($\sim 1.96 \text{ m s}^{-1}$) was achieved. This provided the baseline simulation case. For the same stroke rate, a 1.414 factor was applied to the total resistance to simulate the increase in resistance caused by the

chute. This resulted in a free swim speed reduction of 12%, significantly less than was measured experimentally. However, it is assumed that if both free swim tests, with and without the chute, were performed at maximum effort, the mean propulsive power in both tests is the same. If the same stroke rate is used when the resistance factor is applied, the resulting propulsive power increases as a result of the decrease in swimming speed and the higher fluid force experienced by the propulsion models. To ensure the same propulsive power after the 41.4% increase in resistance, the stroke rate is reduced. This resulted in a free swim speed reduction of 15%, still less than measured experimentally. Another approach is to assume the same advance ratio J (equation 5.8). Therefore the stroke rate needs to be adjusted relative to the free swim speed. Figure 6.17 displays the results of a stroke rate sweep with and without the 41.4% increase in resistance. It is evident that the same V/n values cannot be achieved with and without the 41.4% increase in resistance within the range of stroke rates a swimmer would perform.

Table 6.3. Simulated free swim velocity with and without a 41.4% increase in total resistance.

Condition	SR (C/min)	V (ms^{-1})	% Change	V/n	P (Watts)
Without Chute	55	1.963		0.000595	1461.9
With Chute, 1.414*R	55	1.722	12.28	0.000522	1600.4
With Chute Same P, 1.414*R	53.2	1.663	15.28	0.000521	1427.8

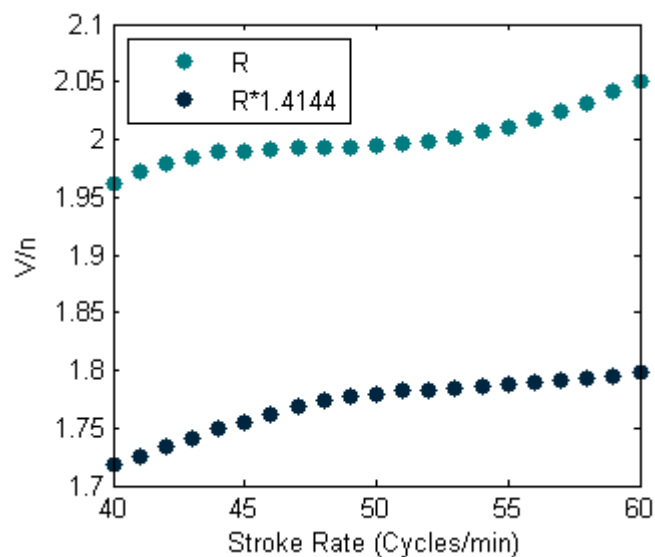


Figure 6.17. Simulated stroke rate sweep and resulting V/n values for with and without the 41.4% increase in resistance.

Simulation Setup and Validation

The passive resistance measurements, performed at 1.52 m s^{-2} without the chute, were used to check the simulated resistance. The experimental and simulated passive resistance was found to be 130.10 N and 107.1 N respectively; an under prediction by the simulation of 18%. Observing the video footage from the five runs in the experiment, the athlete has a similar attitude for both active and passive tows (figure 6.18), suggesting the passive tow attitude is satisfactory and represents the natural free swimming attitude. A potential reason for the under prediction of passive resistance, may be because the height and mass are near and beyond the limits of the dataset used to generate the resistance model. This may result in inaccuracy in the resistance prediction, since few resistance measurements were conducted for athletes of these dimensions, when generating the resistance models. The athlete's slenderness however, 4.28, is within the limits of the dataset. A potential error will be in the prediction of surface area (DuBois and DuBois, 1916), however the height and mass limits of this estimation are not known.

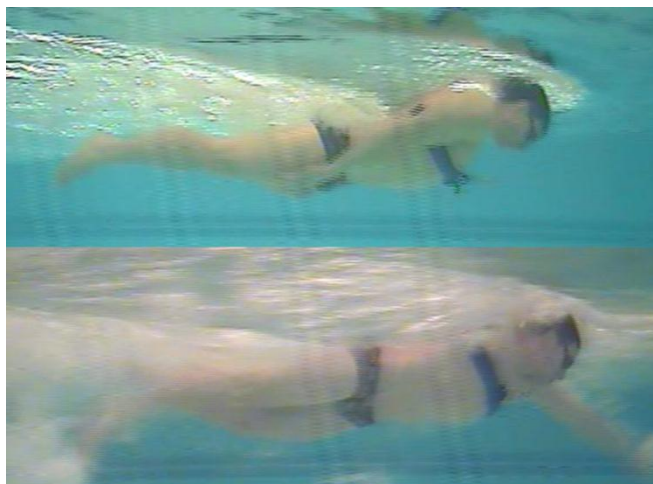


Figure 6.18. Passive and active towing to determine baseline conditions during the chute testing. Comparison of the two images identifies the change in attitude between passive and active towing.

To ensure this resistance deficit wasn't responsible for the under prediction in the reduction of swimming speed, the simulation was rerun with an increased passive resistance. To increase the simulated resistance, to that measured in testing, a factor of 1.21 was applied. The results are displayed in table 6.4. The simulated reduction in swimming speed is marginally greater, with a greater simulated passive resistance, however remains 5% less than was experienced in reality.

Table 6.4. Simulated free swim velocity, with increased simulated resistance, with and without a 41.4% increase in total resistance.

Condition	SR (C/min)	V (ms ⁻¹)	% Change	V/n	P (Watts)
Without Chute, 1.21*R	58.44	1.956		0.000558	1814
With Chute, 1.21*1.414*R	58.44	1.706	12.71	0.000487	1979.7
With Chute Same P, 1.21*1.414*R	56.5	1.647	15.71	0.000486	1799.1

It is important to note that only one test was performed and larger sample size would be desirable, in both the number of tests per athlete and the number of athletes with different heights and masses. This would improve confidence in the experimental results. The athlete performed the maximal effort free swim without the chute before performing the free swim with the chute. It is assumed that there is no fatigue between tests, however some fatigue may have occurred, resulting in the “with chute” condition being too slow. In addition, the higher hydrodynamic load on the arms, when swimming with the chute, may have changed the technique of the swimmer resulting in a further loss of propulsion. Although a maximum effort swim is assumed to produce the same propulsive power, albeit at different torques and rotational speeds (in the arms), the muscle response might be limited by maximum force as well as power. This may result in less propulsive power due to the load in the arms. Perrine and Edgerton (1978) determined the force velocity relationship for fifteen subjects performing maximal dynamic knee extensions. It was found at the lower test velocities deviation of up to 15% occurred in the force-velocity relationship. This is a similar situation to swimming with the chute and therefore the simulation may benefit from an empirical model defining the torque and rotational speed relationship of the arms to ensure unrealistic performances cannot be modelled.

The additional drag added by the chute is large. The potential changes in resistance that can be achieved by elite swimmers, through choice of equipment and technique change, will be significantly less than experienced by the chute. This study identifies the accuracy of the simulator at predicting changes in swimming speed from changes in resistance. Simulating a 41.4% increase in resistance has resulted in an under prediction of a change in swimming speed of 0.1 m s⁻¹. A more realistic change in resistance will have a significantly smaller absolute error. This therefore serves as useful tool in

Simulation Setup and Validation

understanding the impact of changes to swimming resistance on free swimming speed and potentially race time.

6.10 Race Reconstruction

To assess the race time impact of changes to any of the simulated parameters, it is necessary to simulate the correct total race time and time spent in each phase. Using the race phase algorithm a swimming race may be modelled. The inputs required to model a race are listed.

1. Height
2. Mass
3. Gender
4. Race Distance
5. Stroke Rate for each length
6. Dive Distance
7. Entry Speed
8. Start underwater distance
9. Start underwater kicking frequency
10. Time spent stationary during a turn
11. Turn push-off speed
12. Turn underwater distance

Height, mass, gender and stroke are required by the resistance and propulsion models, which are used to calculate swimming speed during each phase. Entry speed and turn speed dictate the initial speed at the start of the race and the beginning of each length, providing the speed influence of a push-off and dive. The dive distance is the initial distance which the accumulated distance is added to. This captures the distance achieved by a dive, but the dive is not modelled. The start and underwater distance dictate when race phase changes from underwater to surface, after the start and turns. The time spent stationary during a turn, is the time it takes for a swimmer to perform a tumble turn, before pushing off. This time is added to the time vector at the beginning of each length, capturing the effect of a tumble turn on race time, without modelling the mechanics of the movement.

With the above information, a 200 m race for a female (Athlete F2, height: 1.794 m, Mass: 74 kg) has been simulated and compared to real race data (figure 6.19). The top plot displays the output of the simulation where a race time of 131.03 s has been achieved. The start and turns can be seen in the velocity plot as a large spike in velocity, as a result of the dive and push-offs.

The high frequency oscillations in the velocity data are the velocity variations throughout each stroke cycle. The underwater phase, where UUS is performed, can be seen after start and turns. A fixed stroke rate was defined for each length of the race and was determined from real data for same athlete in the same event. The resultant mean velocity from the change in stroke rate between each length is visible.

Race data is displayed in the middle plot. A data point for stroke rate and velocity is displayed for each 25 m portion of the 200 m race. The race time achieved in reality was 119.4 s, 11.63 s faster than the simulated race. This is due to the simulated free swimming speed for a given stroke rate being too slow, as displayed for the same athlete (F2) in figure 6.19. The reasons for not achieving the correct free swimming speed are discussed in section 6.8. To achieve the correct swimming speed, the arm width is increased, increasing the arm propulsion for a given stroke rate. The bottom plot displays the simulated output with an increased arm width. A simulated race time of 119.54 s is achieved. Comparing this to the real race data, the velocity variation throughout the race is similar.

Simulation Setup and Validation

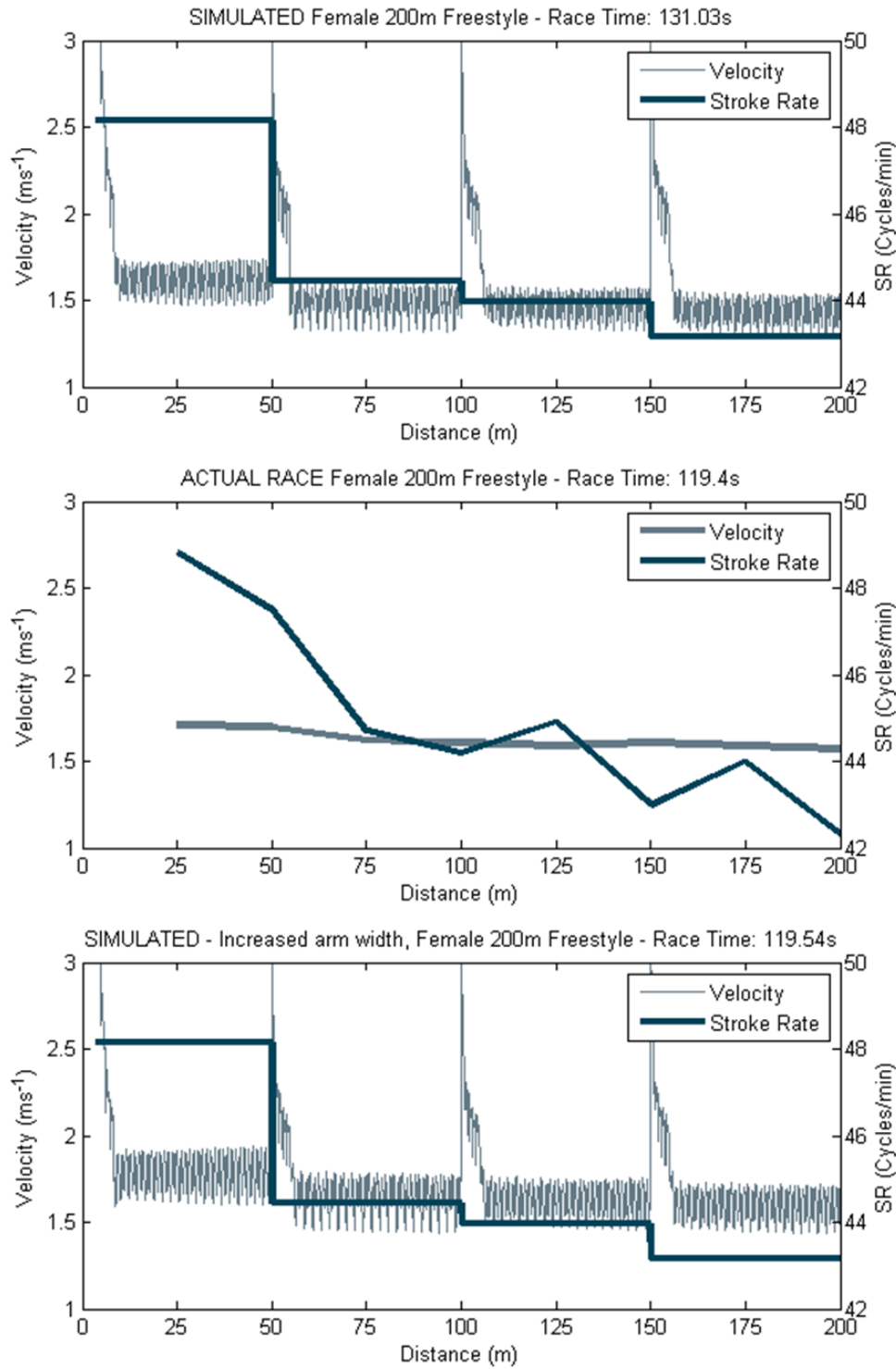


Figure 6.19. Simulated stroke rate and velocity for a female (height: 1.794 m, Mass: 74 kg) during 200 m freestyle race (top plot). This is compared to actual race data for same female (middle plot). To achieve the correct simulated race time, arm width is increased (bottom plot).

The simulated split times are compared to the actual race split times in figure 6.20. The simulated and actual total race times are the same due to the arm width being adjust to achieve the correct race time. In the former part of the race the simulation is faster than reality, where stroke rates are high, and in the latter part of the race, slower than reality, where stroke rates are low. However, these speed deficits are no greater than 4.7% and are likely to be an attribute of simulating a single technique, where in reality a swimmer may adjust technique for different stroke rates.

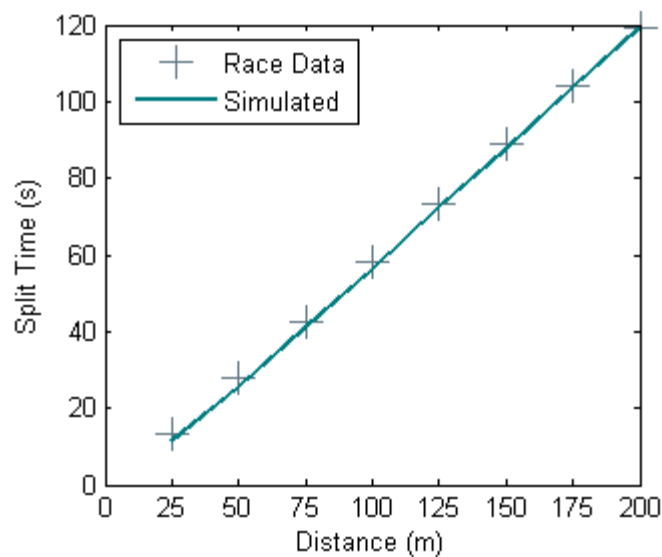


Figure 6.20. Comparison of split times from the simulated and actual race.

6.11 Simulation Uncertainty

It is important to understand the uncertainty in the simulated output to appreciate the limitations and accuracy of this approach. The uncertainty in the simulated race time arises from uncertainty in the output of the equation of motion (equation 3.3). The inputs to the equation of motion are: resistance, propulsion, mass and added mass. It is assumed that there is no error in mass and added mass. The uncertainty in the resistance model has been quantified in section 5.6.1. Therefore the remaining uncertainty is the uncertainty in the simulation propulsion. This uncertainty is a conceptual uncertainty as a result of the simulation not fully capturing actual physics of swimming propulsion. This uncertainty can only be quantified by comparing the simulated response to a real response. In section 6.9 the simulated change in swimming speed, from an increase in resistance, was 5% less than a real measured change in

Simulation Setup and Validation

swimming speed. Therefore, this may be considered the conceptual uncertainty of the simulation.

The uncertainty in the resistance prediction was determined as an uncertainty in the viscous pressure component and quantified as 22%, 32%, 37% and 36% for female surface, male surface, female underwater and male underwater conditions respectively. Simulating these changes in viscous pressure resistance, for a male (Height: 1.95 m, Mass: 88 kg) and female (Height: 1.79 m, Mass: 69 kg) 100 m freestyle race, provided a maximum race time change of 8.5%. Therefore, it is assumed that the resistance uncertainty contributes to a maximum race time uncertainty of $\pm 8.5\%$.

Combining the conceptual uncertainty of 5% and the race time uncertainty due resistance provides a total simulation uncertainty of 10%. Therefore, all quoted race times are subject to this uncertainty.

6.12 Energy Model

As identified in section 6.9, a race can be simulated tactically by specifying different stroke rates for different portions of the race. In this section a fatigue model is included to limit the stroke rate if the propulsive power is more than the simulated available power.

This process is displayed in figure 6.21, where the fatigue during a male (height: 1.95 m, mass: 88 kg) 50 m sprint race is simulated. This model is based on the peak power and anaerobic capacity presented by Hill and Smith (1993). The power factor F_p has been scaled 1000 times to be displayed on the same axis as power. In the first 4 seconds underwater undulatory swimming is being simulated, which has a low propulsive power and therefore the power factor remains equal to 1. When the surface swimming phase is initiated, the propulsive power required to perform the initial stroke rate of 61 cycles/min is larger than the available power producing an overshoot. The power factor therefore reduces and the stroke rate is reduced, bringing the propulsive power down to the same as the maximum available power. As the stored anaerobic energy depletes over the duration of the race, the maximum available power continues to reduce, thus reducing the power factor, stroke rate and swimming velocity of the swimmer.

This identifies that the fatigue model can effectively reduce stroke rate when the propulsive power is too high. However, the initial stroke rate of 61 cycles/min, achieved in reality, required a propulsive power greater than was available, and therefore the fatigue model over-limited the stroke rate. To ensure that this stroke rate can be simulated in the former portion of the race, it was found that the maximum anaerobic power needed to be increased by 9%. In addition, comparison of the simulated and real, velocity and stroke rate decay over the 50 race, identified that the simulated decay was too severe. To achieve the correct rate of decay, the anaerobic capacity was increased by 430%.

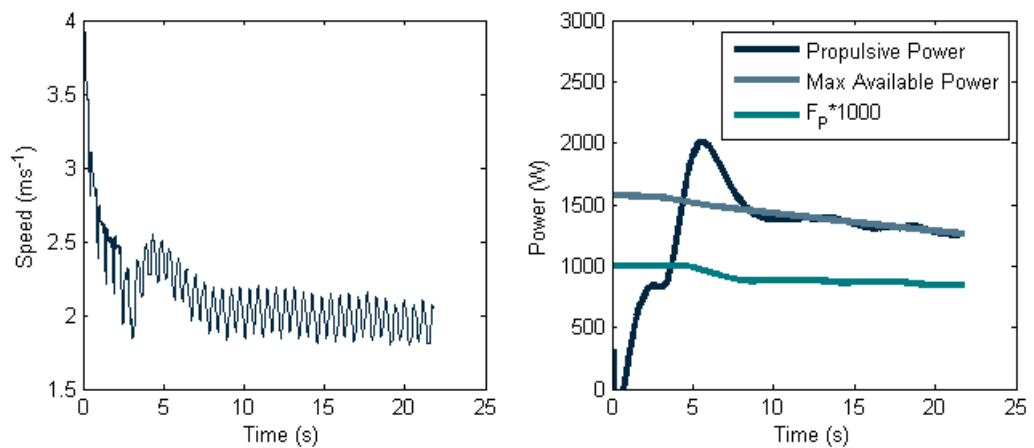


Figure 6.21. Control process used to ensure the propulsive power does not exceed the maximum available power. The power factor F_p used to control stroke rate is displayed and reduces as the maximum available power reduces.

Figure 6.22 displays the contribution from the aerobic and anaerobic energy sources for a maximal effort swim. The point of equal contribution from aerobic and anaerobic sources is 324 seconds. This differs greatly from the 75 seconds stated by Baker et al (2010). If the 430% increase in anaerobic capacity, required to match the race data, is removed, the point of equal contribution becomes 75 seconds.

Simulation Setup and Validation

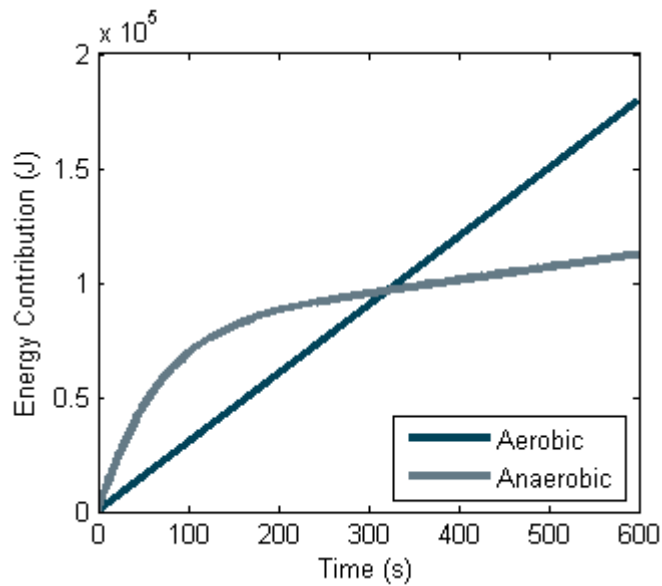


Figure 6.22. Simulated energy contribution from aerobic and anaerobic metabolic sources during a maximal effort swim over 600 seconds.

The data presented by Hill and Smith (1993) and Baker et al (2010) both used non-elite athletes performing power tests on a cycle ergometer. These studies provide insight into how muscles fatigue, however cycling and swimming are different forms of exercise, utilising different muscle groups. It is likely the relative contribution of human body muscle capacity being exploited (energy/body mass) in swimming is greater than in cycling, since swimming uses arms and legs. Therefore the anaerobic capacity normalised with body mass, quoted by Hill and Smith (1993), will be less than for exercises exploiting a larger muscle mass. This might explain the requirement to significantly increase the anaerobic capacity. The difference between world class athletes and non-elite participants may also explain the discrepancies in peak power and anaerobic capacity. In addition, the arm propulsion model is a simplification of real problem, not modelling the complex arm motion or contributions from lift based propulsion. To achieve the realistic propulsive forces from drag based propulsion only, the arm parameters have been scaled. This would suggest the simulated efficiency of the arm propulsion will be less than the real efficiency, since a significant proportion of the force generated by the arm model will not contribute to propulsion. Therefore, the arm model will demand more propulsive power, than would be required in reality, causing the energy supplies to deplete more quickly.

With the modified peak power and anaerobic capacity, simulations of male and female 50 m and 100 m sprint events have been performed and compared to real race data (figure 6.23). The velocity profile of the simulated data contains the intra stroke velocity variations. The real race velocity and stroke rate data was calculated as an average over 15 m and 25 m segments for the 50 m and 100 m events respectively. The simulated decay in stroke rate caused by the reduction in maximum available power is generally greater than is experienced in a real race; however, this results in a similar velocity decay. Fatigue in reality will also cause technique change which is not modelled in the simulation, therefore to achieve the same decay in velocity, the decay in stroke rate for the same technique will be more severe.

Simulation Setup and Validation

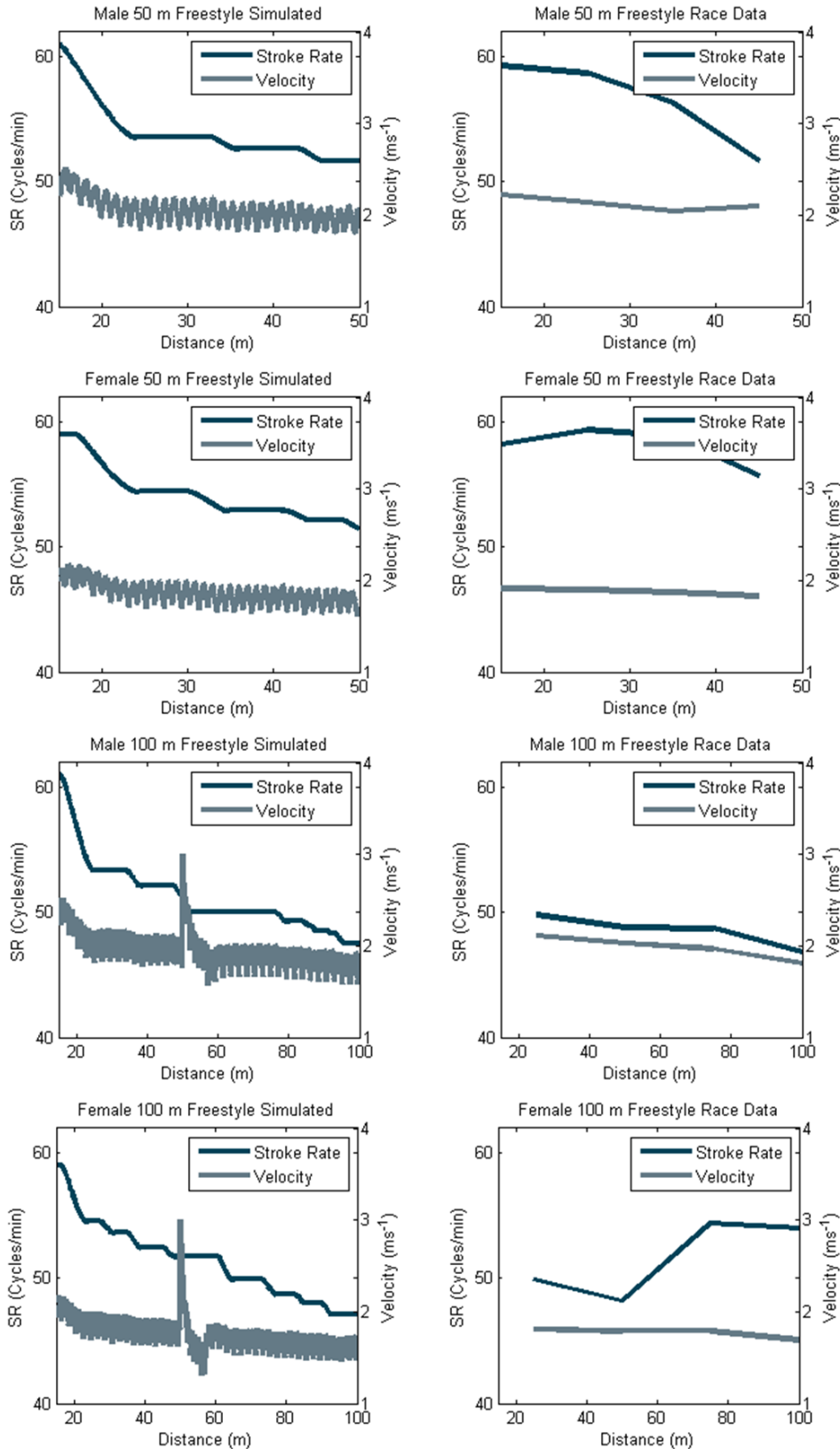


Figure 6.23. Comparison of simulated and real race decay of stroke rate and velocity due to fatigue.

Due to the inclusion of tactics in longer distance events, the fatigue of a swimmer does not appear as a decay in stroke rate and velocity. However, assuming technique does not change with stroke rate, by assessing the energy consumed over the duration of a race this model may provide insight into favourable race strategies.

6.13 Summary

Combining the propulsion models, outlined in Chapter 3, with the resistance model in Chapter 5, the motion of a swimmer can be simulated. To ensure the propulsion models numerically capture the detail of the physics they are based on, a convergence study is conducted. This determines an appropriate time step dt and strip lengths dr and da .

A validation process identified by Sargent (2005) and Robinson (1997b) is adopted to ensure simulation accuracy. The thrust produced by the propulsion models is compared to experimental data by simulating a towed scenario. It is found that to match the mean simulated and experimental R-T, the magnitude of oscillations in the simulated R-T is significantly larger than the experimental R-T. It is proposed that the measured R-T is smoothed as a result of the measurement process. Therefore, to compare simulated and experimental R-T data, the simulated data is filtered. Comparing the mean simulated R-T with experimental R-T, arm length and leg width are adjusted to achieve the correct propulsion, from the individual models, for a number of swimmers. The simulated R-T error (% of total active resistance) for the range of swimmers is less than 5%.

The simulated stroke rate and swimming speed relationship is compared to race data for a range of world championship final events. The simulated swimming speed is generally less than achieved in a race for the corresponding stroke rate; however, the error is least for stroke rates around 50 cycles/min. This is a result of setting up the propulsion models using experimental R-T data from less elite athletes during training, who only performed stroke rates close to 50 cycles/min. To achieve the correct swimming speed, the arm and leg widths are scaled.

The effect of changes to total resistance on swimming speed is investigated. The total resistance of a swimmer with and without a drag device are measured

Simulation Setup and Validation

by passive towing. A 21% reduction in swimming speed is measured, when swimming with the device. Simulating the same increase in resistance (41%), assuming constant propulsive power, provides a reduction of swimming speed of 16%. The difference between the real and simulated reduction in swimming speed is attributed to fatigue and a technique change, which is not modelled. The change in resistance provided by the drag device is significantly larger than would ever be achieved by improvements swimming equipment or body posture, therefore an error of 0.1 m s^{-1} in swimming speed is proposed to be acceptable.

Simulating the swimming velocity during each phase of a race, allows race time to be predicted. The effect of the dive and turns on speed, distance and time are incorporated without them being physically modelled. This ensures the correct split times and total race time are achieved in comparison to real race data.

An uncertainty in the simulated race time of 10% is determined. This is based on a conceptual uncertainty in the simulation of 5% and resistance model uncertainties determined in Chapter 5.

The fatigue model effectively reduces stroke rate if the propulsive power becomes greater than the available power. To ensure the maximum stroke rates achieved in a race can be simulated, the maximum aerobic power, determined from literature had to be increased by 9%. In addition, the anaerobic capacity had to be increased by 430% to simulate a decay in stroke rate and swimming speed similar to that achieved in a 50 m freestyle race.

The ability to predict race time while accurately simulating the velocity and fatigue of a swimmer throughout a race provides a tool to investigate the key questions of this study. This includes the effect of changes to resistance from swimming equipment on race time; changes to swimming technique, such as imbalance; the effect of fatigue on race time from different pacing strategies; and the energetic gain associated with drafting in open-water swimming events.

7 Simulation Case Studies

7.1 Introduction

The setup and validation of the various models in Chapter 6 has enabled the correct simulation of velocity and race time for both males and females for a range of heights and weights. A total simulated race time uncertainty of $\pm 10\%$ has been identified, which accounts for conceptual uncertainty in the simulation and uncertainty quantified for the resistance model in Chapter 5.

In this chapter, the race simulation will be used to investigate a range of potential improvements to freestyle race performance. The tow experiment and the push-off glide experiment are used to quantify real changes in resistance, achieved through changes to race equipment, swimmer physiology or drafting in open water swimming. By performing a race simulation for a range of resistance savings, the race time effect and energetic cost/saving of these measured changes can be determined. The effect of swimmer imbalance, commonly identified during the SwimSIM testing program, is investigated. A range of imbalance severities are simulated and potential race time savings identified.

For all simulations, the fatigue of the swimmer is modelled. This simulates the finite power a swimmer can produce and how it decays throughout a race. This therefore influences the swimmer response to changes in resistance and technique such as imbalance. Using the race simulation and fatigue model, various pacing strategies are investigated. This identifies favourable race strategy and the race time cost of the wrong strategy.

The ability to determine race time from interventions, which reduce resistance or increase propulsion, or identify an optimum race strategy based on available power and work done, is novel. This simulation approach will provide coaches and sports staff with quantitative evidence, allowing them to prioritise interventions in the preparation of a swimmer for a race.

7.2 Question 1: Resistance Reduction

7.2.1 Simulated Resistance Reduction

The effects of changes to swimming resistance has been simulated for a male (Height: 1.95 m, Mass: 88 kg) and female (Height: 1.79 m, Mass: 69 kg) 100 m freestyle race. The process detailed in section 6.10 was performed and using real race data the correct race times were achieved by scaling arm width. The resistance changes investigated were 1% to 10% increases and decreases in total surface and underwater resistance. Three race scenarios were investigated: Only changes to underwater resistance, only changes to surface resistance and changes to both surface and underwater resistance.

For all of the aforementioned conditions, the simulation was performed with and without fatigue modelling. In a 100 m freestyle race, the swimmer performs a maximum effort and fatigue causes decay in propulsive power. Due the constant propulsive power associated with a maximum effort, a change in swimming resistance has an effect on the resulting stroke rate, magnifying the change in swimming speed. Therefore, to ensure the effects of changes in resistance are fully captured, it is necessary to model fatigue. As stated in section 6.12 (energy model), when modelling fatigue, the control algorithm prevents the propulsive power exceeding the available power. When a race is simulated, the initial stroke rate is set and the fatigue model dictates the stroke rate for the remainder of the race. When a race is simulated without fatigue modelling, the stroke rate is set for each length and remains fixed.

Figure 7.1 displays the simulated change in race time for all conditions, with and without fatigue modelling. The total race time for the male and female is 48.01 s and 53.66 s respectively. As expected, modelling fatigue increases the change in race time for a given change in swimming resistance. Observing the magnitudes of changes in race time, a 10% change in resistance, throughout the whole race, equates to a 3 s and 3.5 s change in race time (6.2% and 6.5% of total race time) for males and females respectively. Comparing this to the speed change measured in section 6.9, where a 41.4% increase in resistance produced a 21% reduction in free swimming speed, this is similar.

It is important to note that in the female case, for zero change in resistance, when fatigue was modelled, a race time 2 s slower was simulated than when

fatigue was not modelled. The simulation not modelling fatigue was aligned to real race data; therefore, when modelling fatigue, the stroke rate was over-restricted. This is due to insufficient *maximum available power* and *anaerobic capacity*. To simulate the actual performance achieved by the swimmer, it would be necessary to increase the *maximum available power* and *anaerobic capacity*, determined in section 3.9, so that the initial stroke rate can be simulated and the decay in stroke rate and velocity match the real race data.

The data produced by this study provides insight on the effect of swimming resistance on race time; making it possible to determine the race time saving of measured improvements in resistance. This is useful information when communicating interventions to athletes and coaches and when targeting race time improvements.

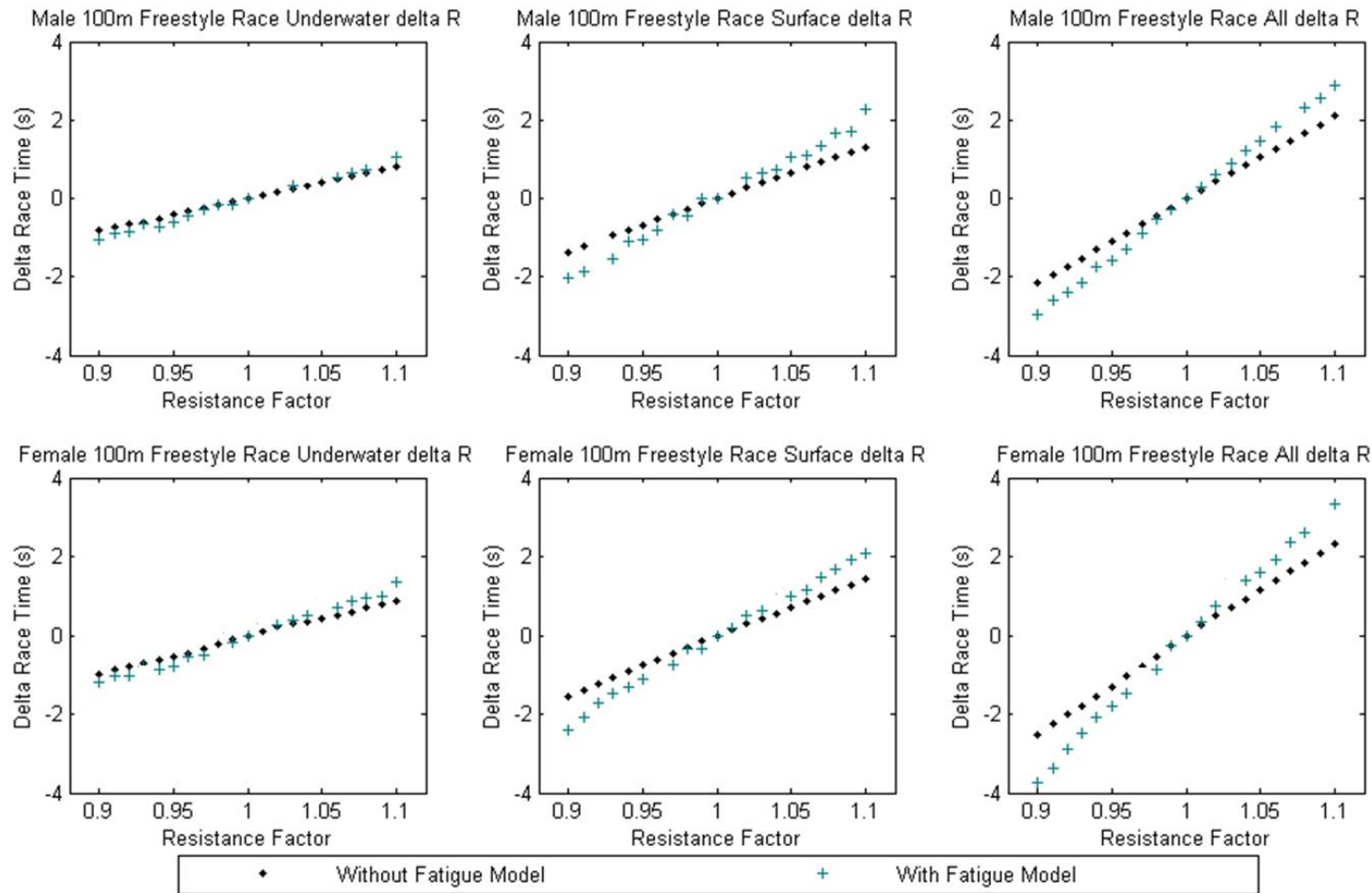


Figure 7.1. Male (Height: 1.95 m, Mass: 88 kg) and female (Height: 1.79 m, Mass: 69 kg) simulated 100 m freestyle race for a range of resistance changes. These changes have been applied to only underwater resistance (left column), only surface resistance (centre column) and both (right column). All conditions are simulated with and without fatigue modelling.

7.2.2 Hair Removal

A common approach to reducing passive resistance is to remove exposed body hair. However, no published research has quantified the actual resistance reduction achieved. Sharp et al. (1988) used blood lactate concentrations as a measure of performance over two identical swims, with and without body hair, and found a reduction of up to 28% in blood lactate in the glabrous condition. Blood lactate measurements depend on many variables specific to an athlete, and therefore can only provide an indirect approach to assessing a resistance change (Billat, 1996). This study aims to quantify the reduction in passive resistance experienced by a male swimmer, after body hair removal, using both the push-off glide and a passive tow experiments.

One male non-elite swimmer participated in a hair removal study. The study was conducted over one day with the hirsute (with hair) condition tested in the morning and glabrous (without hair) condition tested in the afternoon.

A hair length of approximately 2-3cm was present on the chest, back and arm pits, and a hair length of approximately 1.5cm on the legs and arms on the swimmer. Hair removal was performed on the chest, back, arm pits, arms and legs. The head in both conditions was shaved. Figure 7.2 displays the chest and back, before and after hair removal. The time between the testing of hirsute and glabrous conditions was approximately 4 hours. The same cap, goggles and trunks were used for both test conditions.



Figure 7.2. From left to right, 1. Chest – Hirsute, 2. Chest – Glabrous, 3. Back – Hirsute, 4. Back – Glabrous

Table 7.1 displays the resistance coefficients measured using both experimental methods for hirsute and glabrous conditions. Ten repeat tests were performed for the passive tow experiment and five for the push-off glide experiment. Both methods predicted a similar drag change of within 0.3%. The

Simulation Case Studies

passive tow experiment measured an absolute drag reduction of 13.25 N at 2.2 m s⁻¹.

Table 7.1. Mean resistance coefficient data determined for hirsute and glabrous conditions for both push-off glide and passive tow experiments

Participant	Male 4, H=1.78, W=66			
Method	Tow		Push-off	
	Coef	Stdev	Coef	Stdev
Hirsute	0.031	0.0009	0.021	0.0012
Glabrous	0.028	0.0007	0.019	0.0012
% Change	9.67		9.40	
Diff	0.27			

Figure 7.3 displays the bootstrapped mean distributions of the resistance data. As noted in table 7.1 both methods have identified a similar reduction in resistance due to hair removal. The effect of performing a greater number of repeat tests for the passive tow experiment is evident, producing sharper distributions.

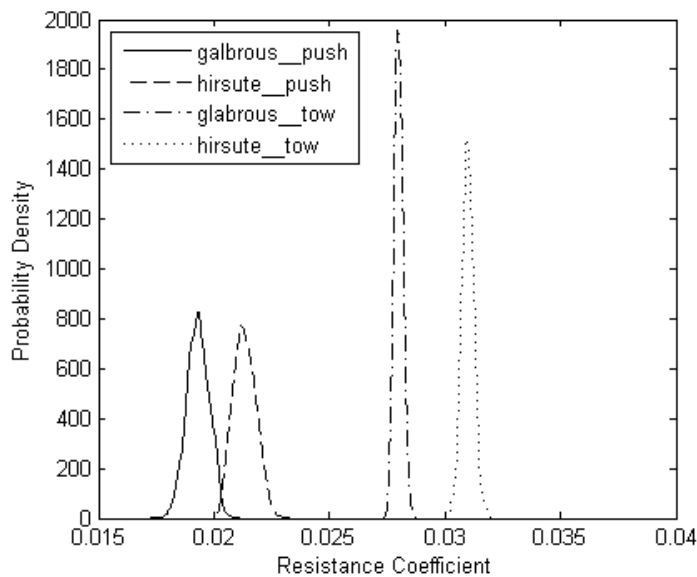


Figure 7.3. Bootstrapped distributions for Hirsute and Glabrous conditions for passive tow and push-off glide methods.

Figure 7.4 displays the results from the permutation test, comparing hirsute and glabrous conditions. For both methods, the observed differences have high confidence values, with the passive tow experiment producing a very low p-value of 1×10^{-5} evident from the sharp distributions and little overlap in figure 7.3.

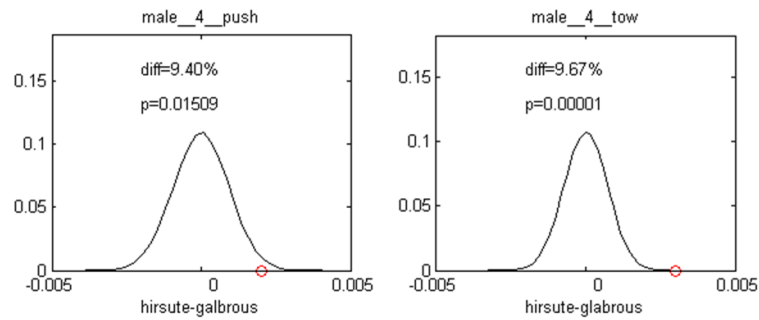


Figure 7.4. Permutation test results comparing the data for Hirsute and Glabrous conditions for passive tow and push-off glide methods.

Assuming the distributions in figure 7.3 represent the natural variation in the data, the permutation test was used to investigate the minimum resistance change that could be measured with each method, to a confidence of 95%. This was achieved by shifting the glabrous data until a p-value of 0.05 is reached. This resulted in a minimum resistance change that could be measured of 1.8% and 7% for the passive tow and push-off glide experiments respectively. To measure a resistance difference of 1.8% with the push-off glide experiment will result in a confidence of 70%.

Assuming a passive resistance change of 9.5%, this would equate to a 100 m freestyle race time difference of 2.75 s, determined from figure 7.1. If this resistance change only has an influence on the underwater resistance, a race time difference of 0.99 s would be experienced.

7.2.3 Suit Testing

A suit resistance study was performed using the push-off glide experiment on a male and female participant wearing different suits. For the male participant, four suits were tested; for the female, three suits were tested. Ten push-off measurements were made for each suit condition, in two sets of five; where between each set of five a different suit was worn. Having to remove a suit between tests, ensured it was the design of the suit that was causing the changes in resistance and not how it was being worn. The bootstrap mean distributions of the measured resistance coefficients were determined (figure 7.5). This identifies the variation in the data and the differences between the suits.

Simulation Case Studies

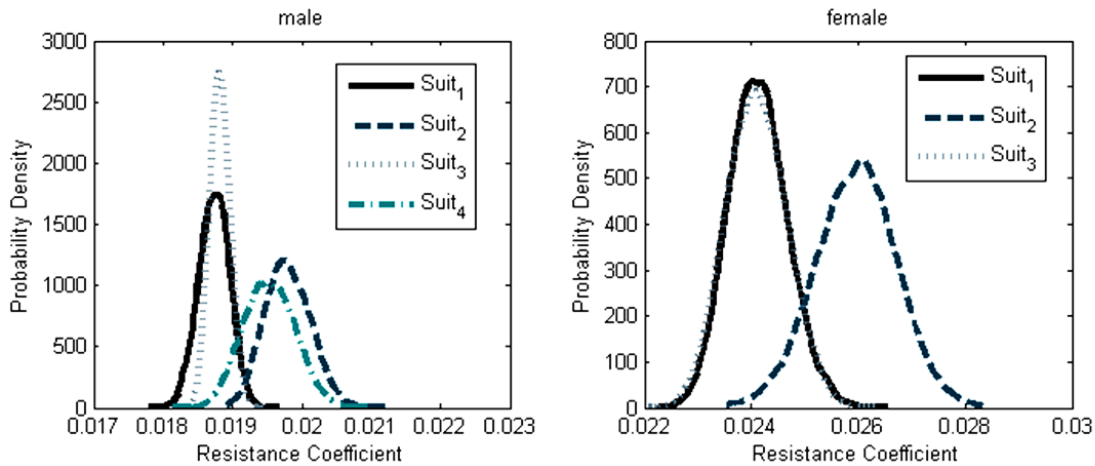


Figure 7.5. Boot strap distributions of the resistance coefficients determined using the push-off glide experiment for male and female participants wearing various suits.

To quantify the differences between each suit and determine the confidence, a permutation test was performed (figures 7.6 and 7.7). This was performed separately for the male and the female data. For the male participant, a maximum difference of 5.7% in the resistance coefficient was measured between suits one and two, with a confidence of 99%. For the female participant, a maximum difference of 7.6% in the resistance coefficient was measured between suits one and two, with a confidence of 97%.

Since the resistance measurements were only performed for an underwater case, these can only be compared to the simulation data for an underwater change in resistance. For the male data, the difference of 5.7% would have equated to a 100 m race time delta of 0.65 s. For the female data, the difference of 7.6% would have equated to a 100 m race time delta of 1.05 s. This identifies the importance of selecting the correct suit.

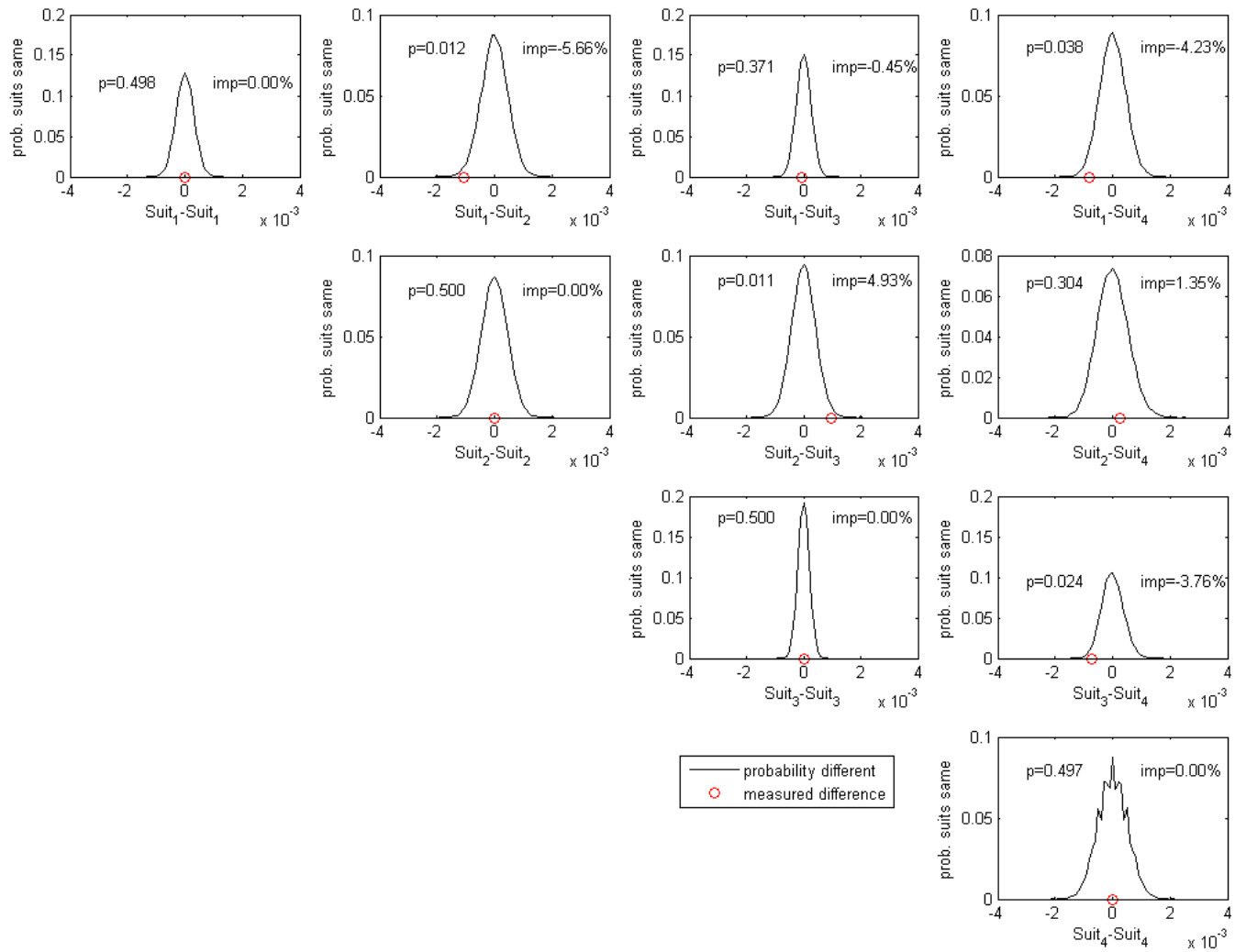


Figure 7.6. Permutation distributions, comparing each suit condition tested for the male participant.

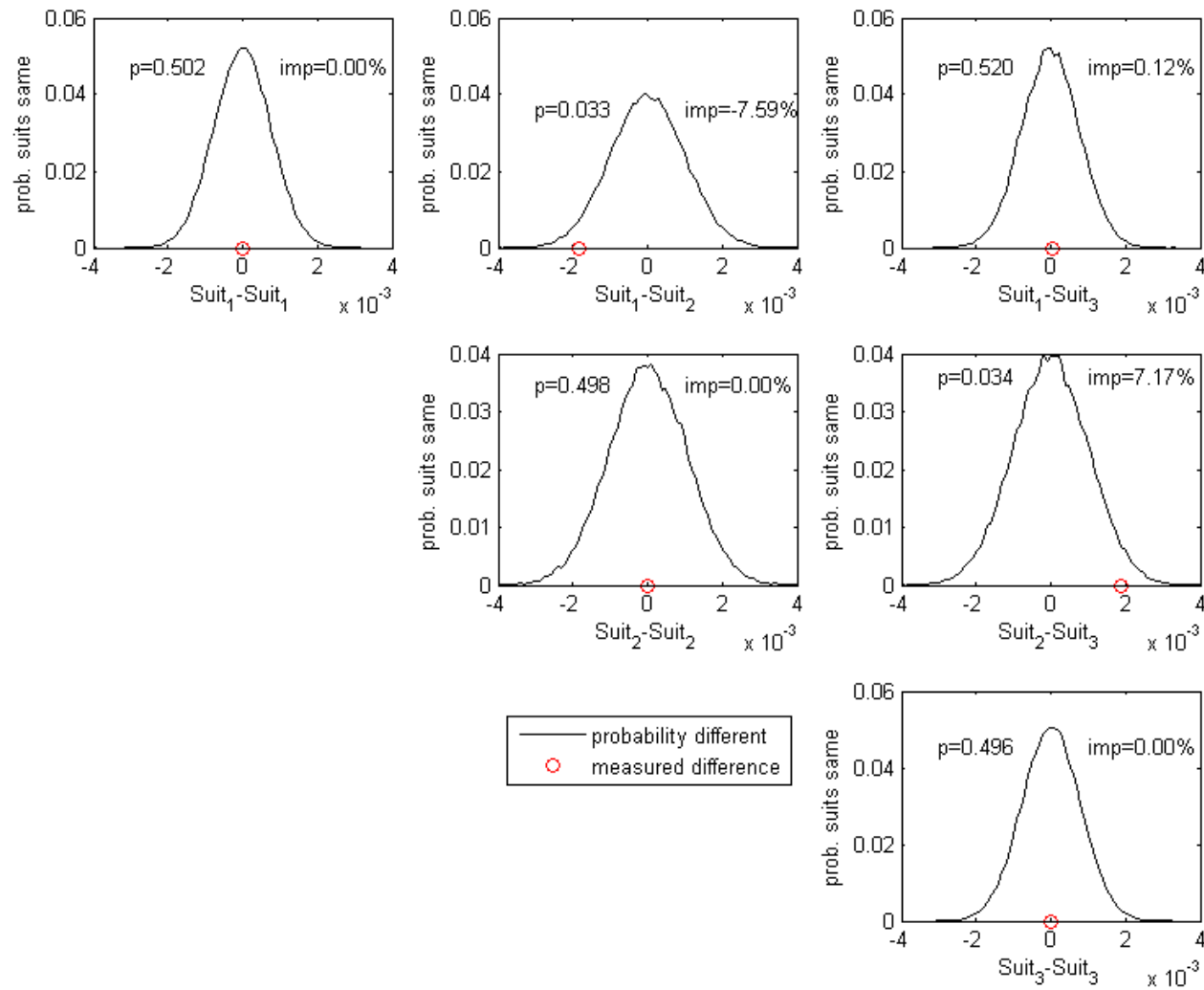


Figure 7.7. Permutation distributions, comparing each suit condition tested for the female participant.

7.2.4 Good Cap – Bad Cap

The resistance difference between wearing a wrinkly cap, with goggle straps on the outside, and a smooth cap, with goggle straps on the inside (figure 7.8), was measured with an underwater passive tow experiment. Five measurements of each condition were performed. The bootstrap mean distributions of the measured resistance coefficients were determined and a permutation test used to determine the confidence between the measured conditions (figure 7.9). A 2.1% reduction in underwater passive resistance coefficient was measured between the two conditions. However, based in the variability in the data and the small difference in resistance between the two conditions, only 89% confidence in the difference can be made. It is therefore necessary to perform more tests to improve the confidence in the measured difference. A 2.1% difference in underwater passive resistance equates to 100 m freestyle race time difference of 0.17 s and 0.27 s for males and females respectively.



Figure 7.8. Bad cap and goggle arrangement (top) compared to good cap and goggle arrangement (bottom).

Simulation Case Studies

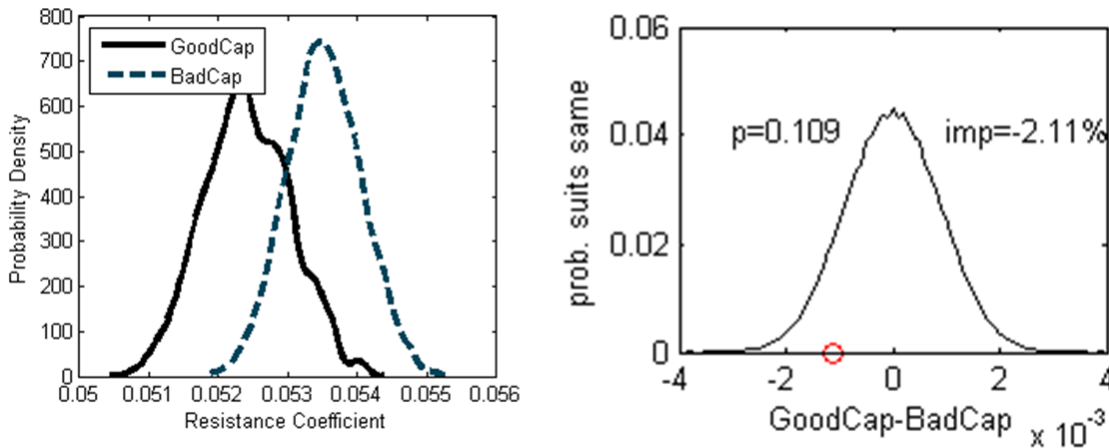


Figure 7.9. Bootstrap mean distributions of good and bad cap and goggle arrangement (left), and permutation distribution comparing both conditions.

7.3 Question 2: Technique

During a maximum effort swim, an increase in swimming speed can be gained by more efficiently converting propulsive power into effective power. This is achieved by improving technique. A common technique trait is an imbalance between the propulsion from each arm. This has been identified from active towing of elite athletes during SwimSIM testing. Examples of measured imbalances can be seen in the validation data in figure 6.5. To match the simulated R-T with the experimental data, an imbalance coefficient of 0.9 and 0.95 was used for athletes K and P respectively.

This section aims to investigate the race time impact of an imbalance in the freestyle stroke. Including the influence of fatigue ensures the propulsive gain of removing an imbalance is simply not just more propulsion to the slower arm, as this would require more propulsive power. The maximum available power, the same with and without an imbalance, is therefore more equally shared between the two arms. The propulsive gain therefore arises from a more constant delivery of propulsion from both arms rather than a more oscillatory delivery from a slow and fast arm.

7.3.1 Simulated Imbalances

The approach to simulating an imbalance is described in section 3.7.4. The effects of a range of imbalance coefficients have been simulated for a male (Height: 1.95 m, Mass: 88 kg) and female (Height: 1.79 m, Mass: 69 kg) 100 m

freestyle race (Figure 7.10). The red circles identify simulations where an error has occurred, in a single time step, when calculating propulsive power. Due to time average of the propulsive power, this has caused the fatigue model to over-limit the stroke rate for a short period causing a slow race time. However, with the remaining data the trend of imbalance, with race time saving is clear. By including the effects of fatigue, the potential race time saving – if an imbalance is removed, becomes less. This is due to more propulsive power being required when the slow arm, causing the imbalance, is sped up. Since the swimmer is producing a maximum effort, the fatigue model has to slow both arms to ensure the propulsive power does not exceed the available power. This would be expected in reality.

When modelling fatigue, the reduction in race time saving is greater for females. For both the male and female simulations, it is not possible to simulate the power achieved in a race since, based on the data determined from literature, the fatigue model over-limits the stroke rate. However, for females this power deficit is greater than for males causing the change in race time when fatigue is modelled to be greater. It is therefore necessary to determine more accurate *maximum available power* and *anaerobic capacity* for both male and female swimmers.

The imbalance coefficients of 0.9 and 0.95 determined for athletes K and P equate to a loss in 100 m freestyle race time of about 0.4 s and 0.65 s respectively. These values are based on the data in figure 7.10 and are therefore not for the exact height and mass of athletes K and P.

Examples of the simulated race output, for the male imbalances conditions, are displayed in Appendix 5.

Simulation Case Studies

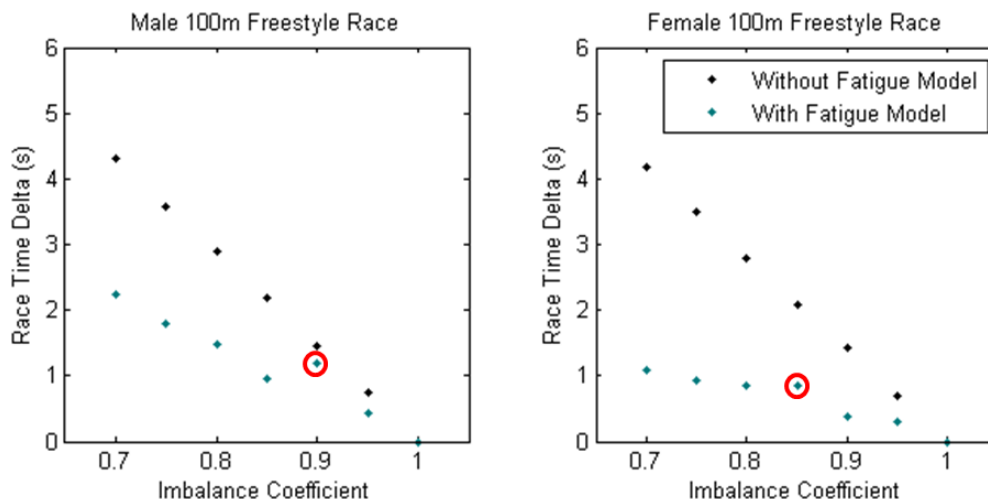


Figure 7.10. Simulated race time losses for a range of imbalance coefficients, with and without fatigue modelling. The data points circled in red are where an error in the power calculation occurred, causing the fatigue model to over-limit the stroke rate.

7.4 Question 3: Pacing strategy

It is known that a swimmer must choose how fast to swim each portion of the race, to ensure the fastest race time can be achieved (Maglischo, 2002). Assuming a fixed technique, the fastest race time is achieved when the maximum work is done while remaining within the capabilities of the swimmer. This section aims to use race simulation to investigate the effect of pacing strategy on race time.

The pacing strategy is defined as a stroke rate gradient, which describes either the decay or growth of stroke rate throughout the race. A single stroke rate is defined for each 50 m length. Figure 7.11 displays the range of input stroke rates for a 200 m race. The stroke rate gradient is determined as the absolute change in stroke rate (cycles/min) between each length. Each pacing strategy has the same average stroke rate, which was determined from race data for the male and female athletes being simulated. The stroke rates identified in figure 7.11 were simulated for a male (Height: 1.83 m, Mass: 72 kg) and female (Height: 1.79 m, Mass: 74 kg), where the average male and female stroke rates were 44 cycles/min and 45 cycles/min respectively. The resulting race times and work done for each stroke rate gradient are displayed in figure 7.12. For both male and female, optimum race times and maximum work done were

simulated for stroke rate gradients of -0.48 cycles/min/length. This gradient is identified in bold in figure 7.11.

The limitation to this approach is that pacing strategy is primarily influenced by the decay of available power. Inaccuracy in this decay relationship will result in the wrong optimum pacing strategy being identified. However, assuming the fatigue model roughly represents the decay in available power, this study has identified the optimum strategy requires a faster former portion of the race and slower latter. Analysing race data supplied by British Swimming, for all swimmers, swimming velocity decreases throughout a 200 m race. This suggests the approach used to determine the optimum pacing strategy is correct; however, improving the fidelity of the simulated decay in available power, may increase the accuracy in identifying the optimum strategy.

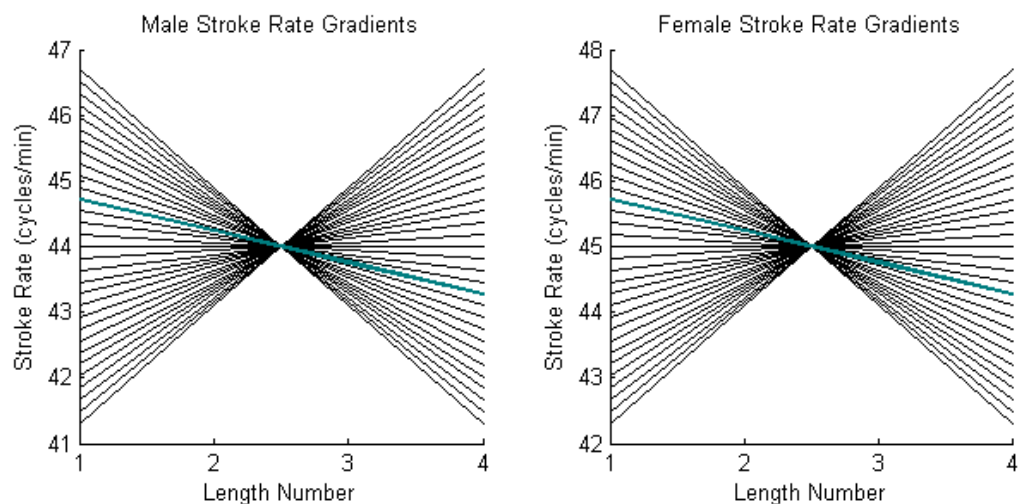


Figure 7.11. Pacing strategies used for the male and female 200 m freestyle race simulation. The line identified in bold represents the optimum pacing strategy.

Simulation Case Studies

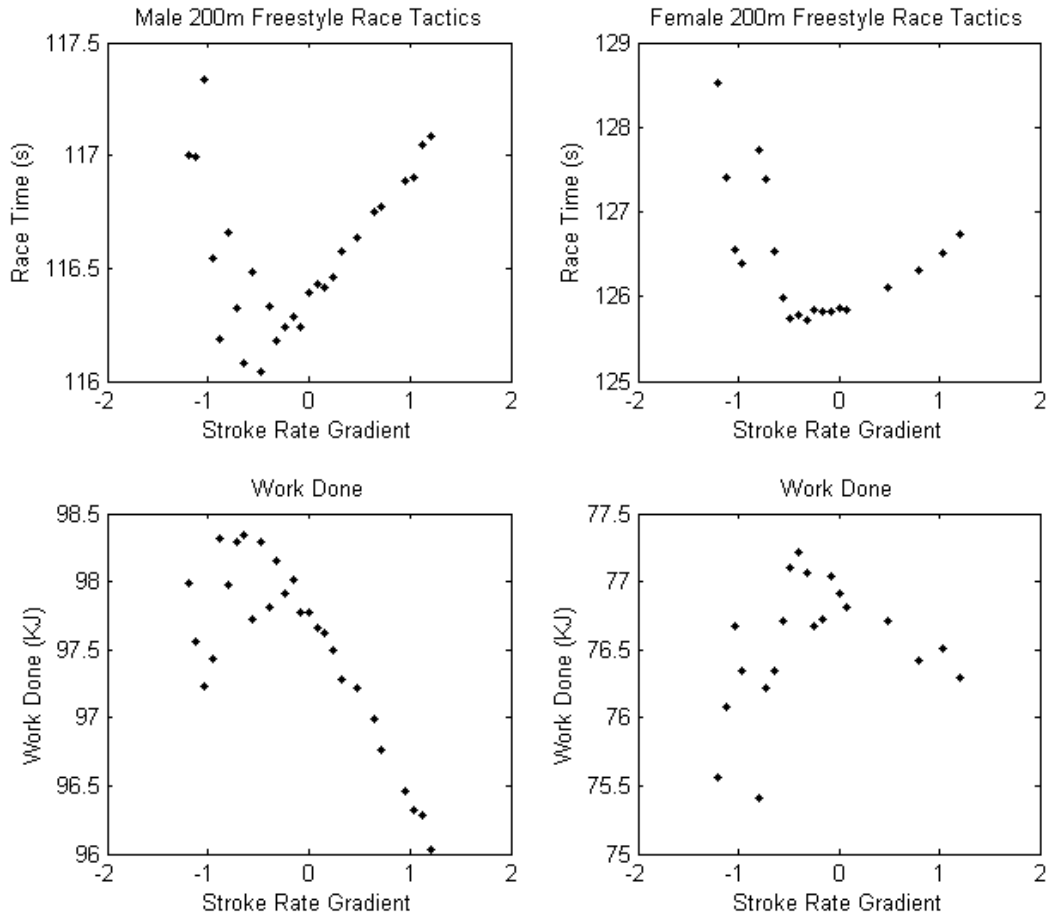


Figure 7.12. Simulated race time (s) and work done (KJ) for the various stroke gradients for the male (left) and female (right) swimmer.

7.5 Question 4: The Effect of Drafting

The potential resistance reduction benefits of swimming behind another swimmer can be utilised in an open water swimming race. This technique is known as drafting. However, the magnitude of this potential resistance reduction is unknown, and therefore many swimmers choose not to swim behind their competitors for tactical reasons. The aim of this study was to quantify the resistance reduction achieved by drafting, and perform a race simulation of a 10000 m marathon race to determine the work done benefits.

Swimming directly behind a lead swimmer takes advantage of the separated flow ahead. The local flow experienced by the drafting swimmer has a component of velocity in the direction of swimming, thus reducing resistance experienced by the drafting swimmer. Swimming with some lateral spacing

behind a lead swimmer takes advantage of the wave system ahead. This can enable destructive interference between the wave systems of both swimmers, reducing wave resistance. In addition, the orbital velocity in the wave system of the lead swimmer can reduce the local velocity and resistance experienced by the drafting swimmer.

A passive tow experiment was performed measuring R-T for a female (Height: 1.73 m, Mass: 60 kg) actively swimming both in open water and at two positions behind a lead swimmer. The lead swimmer was male of unknown height and mass and was free swimming. Since the drafting swimmer required a towline to extend out in front of them, it was not possible to tow them directly behind the lead swimmer. Therefore, the tow was performed with lateral spacing between the two swimmers, with the aim to take advantage of the lead swimmer's wave system. The drafting swimmer was towed with the head at the hips and the feet of the lead swimmer (figure 7.13). Four measurements were performed for each condition.

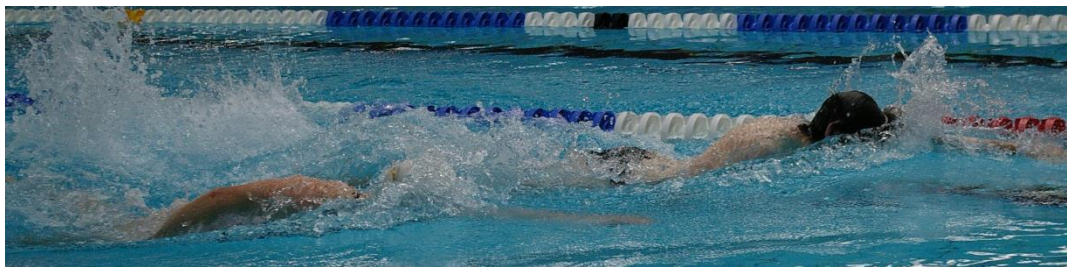


Figure 7.13. Lead swimmer (right) and drafting swimmer (left). The drafting swimmer is being towed with R-T measured and the lead swimmer is free swimming.

Figure 7.14 displays the bootstrapped mean distributions of the R-T measured for the free swimming and two drafting conditions. The R-T data has been non-dimensionalised using equation 2.2 with surface area. Drafting with the head at the feet of the lead swimmer was found to make no difference to the measured R-T. Drafting with the head at the hips of the lead swimmer produced a reduction in R-T of 19.3%, with a confidence of 98%, determined from a permutation test.

Simulation Case Studies

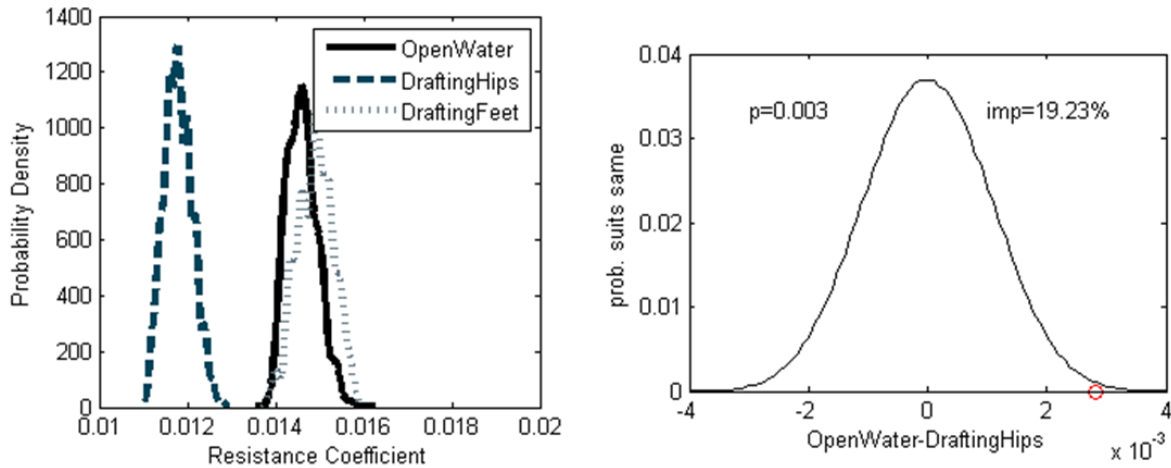


Figure 7.14. Bootstrapped distributions of the measured R-T for free swimming and the two drafting conditions (left). Permutation test, identifying the confidence in the measured difference between the open water condition and drafting with the head at the hips.

It is necessary to convert the measured R-T reduction to a reduction in passive resistance. It is assumed the absolute reduction in R-T is only a reduction in resistance and not an increase in propulsion. Therefore, there was a reduction in active resistance of 6.2 N (measured reduction in R-T) at 1.6 m s⁻¹. This equates to a reduction of 5 N in passive resistance assuming a thrust deduction of 0.8. With a simulated passive resistance of 84.4 N at 1.6 m s⁻¹, this equates to a passive resistance reduction of 5.9%.

A race simulation was performed for the female participant over the distance of a 10 Km with and without a passive resistance reduction of 5.9%. A fixed stroke rate of 35 cycles/min was set. These conditions were simulated with and without fatigue modelling (Table 7.2). In a 10Km race, there are no turn phases with a push-off, therefore no turns were simulated. The 5.9% reduction in passive resistance equates a work done saving of 4.1% and 3.1%, with and without fatigue modelling respectively. This information may provide open water swimmers with a tactical advantage, allowing them to conserve energy in the former portion of a race, which can be utilised to achieve faster swimming speeds at the finish.

Table 7.2. Simulated race time and work done for a 10000 m freestyle race.

Condition	Race Time (s)	Work Done (KJ)
10K No Drafting, No Fatigue	7737	2556
10K With Drafting, No Fatigue	7565	2451
10K No Drafting, With Fatigue	7461	2681
10K Drafting, With Fatigue	7219	2599

7.6 Summary

The race simulation has been used to simulate the effect of changes to swimming resistance on race time for a male and female 100 m freestyle race. The resistance changes were applied to only underwater resistance, only surface resistance and both surface and underwater resistance. By modelling fatigue, the race time effects of the various resistance changes are amplified.

Changes in swimming resistance, such as that achieved by hair removal, different swimming suits, and cap and goggle arrangements, are quantified using the passive tow and push-off glide experiments. In a hair removal study, a 9.5% reduction in total resistance is measured using both experimental methods for an individual male participant. This resistance change would equate to a 100 m race time saving of 2.75s or 0.99s, assuming the saving affects the full race or just the underwater phases. Suit testing is performed for a male and female participant using the push-off glide experiment. A maximum resistance difference between suits of 5.7% and 7.6% is measured for the male and female respectively. Attributing these resistance changes to the underwater portion of a 100 m race, results in race time difference of 0.65 s and 1.05 s respectively, identifying the importance of selecting the correct suit. The difference between good and bad cap and goggle arrangements is quantified from an underwater passive tow. A non-significant 2.1 % difference in underwater resistance between good and bad arrangements is measured. This resistance change would equate to a race time difference of 0.17 s and 0.27 s for males and females respectively.

The race time effect of an imbalance in the freestyle arm stroke is investigated. Imbalance coefficients from 1 (no imbalance) to 0.7 are simulated for a 100 m freestyle race, for males and females. The race time effect for the range of imbalances is determined. By incorporating the fatigue model, the race time

Simulation Case Studies

effect of removing an imbalance becomes less. This is due to the fatigue model simulating the finite power of a swimmer, and therefore when an imbalance is removed, the overall stroke rate is reduced to ensure the propulsive does not increase. A race time saving of 0.4 s and 0.65 s is identified for imbalance coefficients of 0.9 and 0.95 determined for athletes K and P from SwimSIM testing.

Using the fatigue model, various pacing strategies are investigated for a 200 m freestyle race. A range of stroke rate gradients are input, describing the change stroke rate throughout a race. An optimum gradient of -0.48 cycles/min/length is identified for both males and females. This suggests swimming fast at the beginning of a race, and slowing as the race progresses, produces the fastest race time. However, inaccuracy in the decay of available power throughout a race is suggested may have an impact on the optimum strategy identified. Therefore, more accurate swimming specific *maximum available power*, *anaerobic capacity*, and its decay relationship are required.

The resistance effect of drafting behind a swimmer has been quantified with an active tow experiment. A swimmer was towed in open water and at various positions behind a lead swimmer. A passive resistance reduction of 5.9% was determined when the drafting swimmer swims with their head adjacent to the hips of the lead swimmer. A 10000 m marathon swimming event has been simulated, with and without this 5.9% reduction, to determine the work done saving as a result of drafting. This simulation was performed with and without fatigue modelling. A 5.9% resistance saving resulted a work done saving of 4.1% and 3.1% without and with fatigue modelling.

These case studies have highlighted the potential use of a race simulation as outlined in this thesis. For the first time, the key questions identified in Chapter 1 have been addressed. This information allows the personnel involved in the preparation of a swimmer to appreciate the potential race time savings that can be made if these interventions are achieved. Implementing change in an elite athlete is a difficult task, and without evidence the commitment to change is likely to be weak. Therefore, the race simulation combined with the experimental methods to measure changes to resistance and propulsion, provides the evidence that is required. In additions, the ability to prioritise a range of potential interventions and exclude unrealistic aims can be used to

influence the long term development of swimmers. This process allows the hydrodynamic performance of a swimmer through a training cycle to be monitored and also enables target setting. This could be in the form of an R-T threshold at a specific tow speed, which could be achieved through improved technique or increased power. Using the race simulation, improvements to R-T measured in training could be used to set race time targets. This will also serve as continued development and validation of the simulation.

8 Conclusions

8.1 Simulation

The complexity of the forces acting on a swimmer requires a new approach to understanding the factors that relate to swimming race time. The current state of the art, a swimming force model SWUM, is successful in the modelling the individual segment forces experienced by a swimmer for a range of stroke input motions. However, this approach neglects the components of resistance experienced by a swimmer, the likely cause of an error in the simulated free swimming speed. In addition, this approach does not model a swimming race and therefore cannot be used to analyse the race time effects of changes to resistance and propulsion measured from experimental testing.

8.1.1 The Simulation Concept

A simulation approach based on resistive forces, determined from naval architecture theory, and propulsive forces determined from a simple arm model and fish propulsion theory is adopted. This is combined with a race phase algorithm, which controls the resistance and propulsion models, to simulate the motion of a swimmer in the various phases of a swimming race.

The motion of the swimmer in surge is modelled with a one degree-of-freedom equation of motion, using resistive and propulsive forces to predict acceleration, from which velocity and distance are determined. A first order time stepping model is used.

8.1.2 Propulsion Models

A single element arm model is used to predict the arm propulsion. Only drag force is considered. The force along the arm is determined numerically in thin strips. The onset velocity along the arm is determined from a vector addition of the arm tangential velocity and the forward velocity of the swimmer. The horizontal force component is the propulsion. Arm power is determined from the torque and the rotational speed of the arm. The motion of the arm is determined from video data of swimmers performing freestyle. A generic motion is assumed to model all swimmers. An imbalance in propulsion from

Conclusions

left to right is simulated by slowing one arm down during the in-water phase and speeding it up in the out of water phase, providing a reduction in propulsion without a change in stroke rate.

Freestyle flutter kick and underwater undulatory swimming are modelled using large amplitude elongated body theory. Input motion is determined from manual digitisation of video data of an individual swimmer. The same kinematics are scaled with height to achieve the correct swimmer size and kicking amplitude. The kinematic data was acquired for a fixed kicking frequency and therefore where simulating other frequencies the kicking amplitude is scaled assuming a fixed Strouhal number.

8.1.3 Fatigue Model

A fatigue model is generated assuming aerobic and anaerobic energy sources. Aerobic capacity is assumed infinite since the majority of swimming events are relatively short. Anaerobic energy is finite and depletes as work is done by the propulsion models. Anaerobic power is assumed directly proportional to the stored anaerobic energy. A PI control algorithm controls stroke rate to ensure the propulsive power does not exceed available power.

8.1.4 Experimental Measurement of Resistance

To quantify swimming resistance and propulsion, experimental methods have been developed. A tow system, which tows a swimmer at a fixed speed and measures force, has been constructed. When performing a passive tow, resistance is measured; when performing an active tow, resistance minus thrust is measured. Statistical methods, bootstrapping and permutation are used to gain insight into the variability of measured resistance, and quantify confidence in the differences measured between two conditions.

Changes in swimming resistance are quantified by performing a passive tow experiment. An alternative simpler experimental process has been developed where the resistance of the swimmer is derived from the rate of deceleration during a push-off glide. A repeatability study of both methods was performed by measuring the change in resistance associated with wearing drag shorts, for three male and three female participants. This study identified that the push-off glide experiment has sufficient precision to determine small changes in

resistance with five repeat tests. The passive tow experiment in both the validation study and a hair removal study, shows greater precision, however at the expense of a more complex experimental setup and a longer measurement period. Both methods have shown that with five repeat tests, a 1.8% difference in resistance can be resolved with 95% and 70% confidence for the passive tow and push-off glide experiments respectively. Where variability in the data is high or changes in resistance become small, both methods would benefit from a larger number of repeat tests.

8.1.5 Resistance Model

Through the SwimSIM testing program, a large resistance database has been created. Passive resistance from towing on the surface and underwater, for a range of heights and masses, for both males and females, has been determined. A weak correlation between resistance and slenderness was found for both males and females, on the surface and underwater. The variation in resistance for a single athlete was found to be greater than the variation across a population of swimmers. Reasons for this variability are likely due to variation in swimmer attitude, affecting projected area, across tests. In addition, surface penetration is known to affect wave making resistance, therefore identifying another likely source of resistance variation. Future testing of passive swimming resistance needs to account for swimmer attitude and projected area, if an accurate relationship between slenderness and passive resistance is desired. Due to the low number of swimmers tested for underwater passive resistance, the relationship between slenderness and resistance is very sensitive to the data from individual swimmers; therefore, a larger dataset is desirable to increase the robustness of the underwater passive resistance prediction. However, comparison of the passive resistance data with published values shows similar magnitudes.

Using Thin Ship Theory, the wave resistance for a range of slenderness's and Froude numbers is determined. A relationship of increasing wave resistance with decreasing slenderness is found and a typical resistance hump relationship with increasing Froude number. Visual comparison of the predicted wave system from Thin Ship Theory and that of the wave pattern from an equivalent passive tow, identify similar wave patterns but potential over prediction of wave amplitude by Thin Ship Theory. This may due to the

Conclusions

incapability of Thin Ship Theory to model wave breaking, which occurs commonly around a swimmer. This may result in an over prediction of wave making resistance.

The skin friction resistance is determined for a range of heights and velocities, identifying a decrease in skin friction resistance for an increase in either height or velocity, causing an increase in Reynolds number.

Viscous pressure resistance is determined as the difference between total passive resistance and wave making resistance plus skin friction. Therefore a dataset of viscous pressure resistance is determined for males and females on the surface and underwater. However, this dataset possess the weak correlation with slenderness as a result of the original passive resistance data.

With all surface and underwater resistance components known for a population of swimmers, a resistance prediction is possible. The resistance prediction compares well to literature. Contributions from wave, viscous pressure and skin friction resistance are 60%, 31% and 9% respectively at 2 m s^{-1} for a swimmer of height 1.79 m and mass 75 kg. An independent study measuring the surface and underwater resistance of a male participant, whose data has not contributed to the resistance model, found the surface resistance prediction was very close; however, the underwater resistance prediction was 20% less than measured, but followed a similar trend. An uncertainty analysis, accounting for bias and precision, finds a predicted uncertainty of 22%, 32%, 37% and 36% for female surface, male surface, female underwater and male underwater conditions respectively.

Active resistance differs from passive resistance, due to the dynamic motion of the body and the added resistance due to the interaction between the propulsive and non-propulsive parts of the body. A novel approach to measuring active resistance, the naval architecture based approach, is compared to the conventional velocity perturbation method, by testing an individual male participant. A thrust deduction is used to describe the ratio between the active and passive resistance. Both methods predict similar thrust deduction values, however the naval architecture based approach has a smaller error. A thrust deduction value for freestyle of 0.8 is determined and assumed constant for all conversions of passive to active resistance. Testing of a greater number of participants is required to increase the confidence in the measured

thrust deduction, and to gain a better understanding of the thrust deduction for underwater undulatory swimming.

8.2 Simulation Setup and Validation

Combining the resistance and propulsion models, surface and underwater swimming is simulated. A verification and validation process identified by Sargent (2005) and Robinson (1997b) was adopted. White-box validation ensured the individual models correctly simulate the various resistive and propulsive forces and black-box validation ensured the combined models simulate the correct swimming motion.

8.2.1 White Box Validation

To compare the simulated propulsive forces with experimental data of active swimming, a towed scenario is simulated providing simulated R-T. To ensure the individual resistance models achieve the correct thrust, the area parameters are scaled. This is achieved by scaling arm length and width, for the arm model, and leg width for the large amplitude elongated body theory model. This was performed comparing the mean simulated and experimental R-T for five athletes performing arms only freestyle, two athletes performing legs only freestyle, and two athletes performing underwater undulatory swimming. However, it is found by scaling the model parameters to match the simulated and experimental R-T, the magnitude of oscillations in the simulated R-T are significantly larger than the experimental R-T. It is proposed that the experimental R-T undergoes attenuation from losses in the human body and damping/elasticity in the experimental equipment and attachment to the swimmer. Therefore to compare the time varying experimental and simulated R-T, the simulated data is filtered to simulate a similar smoothing process. This does not affect the physical processes of the simulation; it merely allows the comparison of experimental and simulated R-T.

With appropriate filtering the simulated time varying R-T for arms only freestyle compares well with experimental data. For freestyle flutter kick and underwater undulatory swimming, the simulated time varying R-T, from large amplitude elongated body theory, differs from the experimental data. When simulating the wake component only, two propulsive phases are produced in one kicking

Conclusions

cycle, where in reality only one propulsive phase is measured. When incorporating body reaction forces the time varying R-T moves more towards a single propulsive and resistive phase in a stroke cycle, however the shapes of force trace are not similar. As suggested by Lighthill (1971), a more realistic force trace may be achieved if the resistive force along the body is included. This may be more appropriate for human swimming, where the knee bend during a kick likely produces a resistive force, not modelled by large amplitude elongated body theory.

8.2.2 Black Box Validation

Simulated free swimming speed for a range of stroke rates, for males and females of different heights and masses, is performed and compared to race data of world championship finalists. The simulated swimming speed is generally less than achieved in a race for the corresponding stroke rate; however, the error is least for stroke rates around 50 cycles/min. This is a result of setting up the propulsion models using experimental R-T data from less elite athletes, under fatigue during training, who only performed stroke rates close to 50 cycles/min. For different stroke rates, it is likely that technique change occurs, changing the lift and drag characteristics of the arm pull, for a given stroke rate. Since technique cannot be changed during a simulation, races with a large variation in stroke rate will be less accurately modelled. To achieve the correct swimming speed for a given stroke rate, the arm and leg widths are scaled.

The effect of changes to resistance and swimming speed are investigated on an individual male participant. Surface passive resistance and maximum effort free swimming speed, with and without a resistance adding device, are measured. A 41% increase in total resistance results in a 21% reduction in swimming speed. Simulating both resistance cases results in a 16% reduction in swimming speed, a 5% error. Reasons for this error are suggested to be a technique change due to the added resistance, occurring in reality but not simulated, and fatigue of the swimmer. Further tests are required with a larger number of participants to improve understanding of how resistance affects swimming speed and to validate the simulated response.

A swimming race is simulated. The velocity of the swimmer during each surface and underwater phase is simulated, according to predefined stroke rates, and arm width is scaled to achieve the correct swimming speed. The time, distance and velocity effect of the dive and turns are incorporated without being physically modelled. Comparison of the simulated output with race data identifies similar split times and a correct final race time.

8.2.3 Simulating Fatigue

The fatigue of a swimmer is modelled in a race situation. The predefined stroke rates of the race simulation are reduced if the propulsive power exceeds the available power determined by the fatigue model. However to achieve the stroke rates and swimming speeds experienced in a real 50 m freestyle race, the maximum anaerobic power was increased by 9%. Additionally, the anaerobic capacity was increased by 430% to achieve the correct decay in stroke rate and swimming speed. Reasons for the required increases in available power and capacity are attributed to the non-swimming specific human power and energy data, and over-simplification of the arm propulsion model. The data determined from literature is based on cycle ergometer tests of non-elite athletes. With swimming using different muscle groups to cycling, it is proposed fatigue may happen more slowly since a larger proportion of a human muscle mass is utilised during swimming, and therefore the specific energy and power (by body mass) quoted by the literature may be disproportionately small for swimming. Additionally, to achieve the required horizontal component of force from the arm propulsion model, the arm width is scaled, increasing propulsive power. In reality the complex motion of the arm, from multiple segments and generation of lift and drag forces will require less propulsive power for a given propulsive force than a single segment drag only approach. Both of these factors may contribute to the over-prediction of required power or the under prediction of available power; however, further research on the energetic cost of freestyle is necessary to ensure fatigue is modelled accurately.

8.3 Simulation Case Studies

8.3.1 Race time effect to changes in resistance

With the process established to predict race time and model swimming speed and fatigue throughout a race, a 100 m freestyle race is simulated. This is performed for a male and a female athlete for a range of changes in resistance, with and without fatigue modelling. These resistance changes are applied to only underwater resistance, only surface resistance and both surface and underwater resistance. Modelling fatigue increases the race time impact of changes to resistance.

Real changes to swimming resistance are quantified using the passive tow and push-off glide experiments. The simulated 100 m freestyle race times for various resistance changes are used to determine potential race time impacts. Hair removal on a male participant provides a 9.5% reduction in total resistance, equating to a 100 m race time saving of 2.75s or 0.99s, if the resistance reduction influences the whole race or underwater phases only. Suit testing identifies a difference in resistance between suits of 5.7% and 7.6% for males and females respectively. These equate to race time changes of 0.65 s and 1.05 s when applied to the underwater phase, identifying the importance of suit selection. Good and bad cap and goggle arrangements provide a resistance change of 2.1% equating to a race time impact of 0.17 s and 0.27 s for males and females, when applied to the underwater phases of a race.

8.3.2 Stroke Imbalance

A range of stroke imbalances are simulated for a 100 m freestyle race, to determine the race time impact of a stroke imbalance, with and without fatigue modelling. The race time impact of removing an imbalance is reduced when fatigue is modelled, since the finite power of a swimmer requires the overall stroke rate to be reduced when an imbalance is removed. This process identifies potential race time savings of 0.4 s and 0.65 s for measured imbalances in athletes K and P from SwimSIM testing

8.3.3 Pacing Strategies

Various pacing strategies are investigated for a 200 m freestyle race. Stroke rate gradients are used to describe the change stroke rate throughout a race. An optimum gradient of -0.48 cycles/min/length is identified for both males and females, with an average race stroke rate of 44 and 45 cycles/min. However, inaccuracy in the decay of available power throughout a race is suggested may have an impact on the optimum strategy identified. Therefore, more accurate swimming specific energy and power information is required.

8.3.4 Energy return from drafting in open water swimming

A 5.9% reduction in passive resistance has been quantified, using a tow experiment, for drafting in an open water swimming race. The optimum position identified was drafting with the head next to the hips of a lead swimmer, taking advantage of the lead swimmers wave system. Simulating this resistance reduction in a 10000 m race, with and without fatigue modelling, identified a reduction in work done of 3.1% and 4.1% respectively. Knowing this information will enable open water swimmers to adopt the optimum position to achieve maximum resistance reduction, saving energy for the majority of a race, which could be advantageous in the final portion of the race.

8.4 Closing Remarks

This study has shed light on the complexities of the forces involved in swimming, and the coupling of the physiological and hydrodynamic problem. By developing a model to predict swimming speed and work done throughout a race, combined with a model to simulate the fatigue of a swimmer, for the first time, the race time effect of changes to the resistive and propulsive forces can be estimated. This experimental and simulation approach, provides quantitative information allowing coaches to make more informed decisions on the preparation of a swimmer for a race

Further work is required in the following areas, to improve simulation accuracy.

- More accurate total resistance measurements, accounting for body attitude, for a range of body slenderness.

Conclusions

- Better understanding of the relationship between the passive and active resistance during both freestyle and underwater undulatory swimming.
- Time varying propulsive force and power of a freestyle arm stroke.
- The reactive and resistive forces along the body during freestyle flutter kick and underwater undulatory swimming.
- The anaerobic and aerobic power and energy consumed during swimming.
- The relationship between anaerobic energy and available power during fatigue while performing freestyle.

Appendices

Appendix 1

Final version of race simulation code.

1.1 Race Model

```

clc;clear all;close all force
tic
cd engine

swimmer_input_parameters
for j=1:size(input.swimmer,1)

    input_parameters                % Load input
parameters
    resistance        %%%%% Check Resistance Factors!!!!
% Load resistance model
    experimental_data                % Load
experimental data
    race_phases                    % Load race
phases

    %% Waitbar

    title_str=['Run ',num2str(j),' of
',num2str(size(input.swimmer,1)),' - ',batch_title];

    wb =
waitbar(0,'1','Name',title_str,'CreateCancelBtn','setappdata(gcf,'canceling',1)');
    setappdata(wb,'canceling',0)

    %% %%%%%%%%%%%%% Time Stepping Race Model
%%%%%%%%%%%%

    tStart = tic;

    while stot(i)<input.dist(j)

        if getappdata(wb,'canceling')
            break
        end

        dt=input.arm_model_time_step(j);
        if stot(i)>input.dist(j)-0.2 && dt>0.001
            dt=0.001;                % adjust time step
size for final 0.1m of race to ensure exact race distance is achieved
        end

        %         arm_power(i+1)=0;
        ds=V(i).*dt;
        stot(i+1)=stot(i)+ds;

```

Appendix 1

```
waitbar(stot(i)/input.dist(j),wb,sprintf('Race Distance
Calculated (m)      %.1f',stot(i)))

%% Energy Model
if P>4000
    P_log(i+1)=P_log(i);
else
    P_log(i+1)=P;
end
energy_model % Accumulates the work
done by the swimmer to determine fatigue, anaerobic and aerobic output
potentials

%% Phase Model

phase_model % Determines the phase
of the race the swimmer is in and switches on/off the relevent
resistance and propulsion models

if input.plot_motion(j) == 1
    animation
end

%% Kinetic Model

kinetic_model

%% Propulsive Efficiency for Surface Phase

propulsive_efficiency

t=t+dt;
i=i+1;
time(i)=t; % Accumulating a
time line
end

tElapsed(j) = toc(tStart);

%% Output

output_data % Collect
important data in an output structure
save_data % Save the output
data in a results folder

clearup
delete(wb)

%% Segment Force Calculation
if input.segment_force(j)==1
    segment_force
end

end
%% End Plot
for j=1:size(output,2)
    plot_results
```

```

end
    arm_work_tot=sum(arm_power);
toc

```

1.2 Swimmer Input Parameters

```

% Name, Height, Mass, UUS Start Frequency, UUS Turn Frequency,
% Surface Stroke rate (strokes/min), Arm Width Scale Factor, Arm
% Length, Race Distance, Thrust Factor, Surface Resistance Factor, Tow
% Speed, Entry Speed, Turn Speed, Arm Model Time Step, Lighthill Time
% Step,
% Finish Time Step, Dive Distance, Start Distance, Turn Time, Turn out
% Distance,
% Leg Kick Beat Ratio, Plot motion logic, Segment force Calc Logic,
% Thrust reduction to create imbalance, Underwater Resistance factor,
% Wave Resistance factor, experimental_data_logic,
% Gender Logic(Male=1, Female=0), Arm Strip Length, flutter kick
% amplitude,
% Arm model logic, leg model logic

batch_title=('imbalance_0_9_fatigue_male');

input.swimmer(1,:)={'Athlete o 100m, ',1.95,88,2.0,2.00, [48.5
48.5 44 47 46 46 46
46],1.5,0.79,100.0,1,1.00,0.00,4.00,3,0.01,0.01,0.01,3.5,11.57,1.36,8.
51,6,0,0,0.90,1.00,1,0,1,0.01,0.4,1,1,'Imbalance no fatigue'};

input.name=char(input.swimmer(:,1));
input.height=cell2mat(input.swimmer(:,2));
input.mass=cell2mat(input.swimmer(:,3));
input.UUS_kickfreq_start=cell2mat(input.swimmer(:,4));
input.UUS_kickfreq_turn=cell2mat(input.swimmer(:,5));
input.strokerate=input.swimmer(:,6);
input.armwidth=0.067.*input.height.*cell2mat(input.swimmer(:,7));
for i=1:size(input.swimmer,1)
    if cell2mat(input.swimmer(i,29))==1;
        input.arm_length(i)=0.1.*input.height(i)+0.67;
    %     input.arm_length(i)=0.056.*input.height(i)+0.683;
    % scaling relationship for arm length to ensure the correct thrust
    % with respect to height is achieved.
    else
        input.arm_length(i)=0.18.*input.height(i)+0.45;
    %     input.arm_length(i)=0.1538.*input.height(i)+0.357;
    end
end
input.dist=cell2mat(input.swimmer(:,9));
input.thrust_factor=cell2mat(input.swimmer(:,10));
input.surface_resistance_factor=cell2mat(input.swimmer(:,11));
input.Tow_Speed=cell2mat(input.swimmer(:,12));
input.entry_speed=cell2mat(input.swimmer(:,13));
input.turn_speed=cell2mat(input.swimmer(:,14));
input.arm_model_time_step=cell2mat(input.swimmer(:,15));
input.lighthill_time_step=cell2mat(input.swimmer(:,16));
input.finish_time_step=cell2mat(input.swimmer(:,17));
input.dive_dist=cell2mat(input.swimmer(:,18));
input.startd=cell2mat(input.swimmer(:,19));
input.turn_time=cell2mat(input.swimmer(:,20));
input.turnout=cell2mat(input.swimmer(:,21));

```

Appendix 1

```
input.leg_kickfreq=cell2mat(input.swimmer(:,22));
% 6 BEAT LEG KICK DEFINED HERE
input.plot_motion=cell2mat(input.swimmer(:,23));
input.segment_force=cell2mat(input.swimmer(:,24));
input.arm_imbalance=cell2mat(input.swimmer(:,25));
input.underwater_resistance_factor=cell2mat(input.swimmer(:,26));
input.wave_resistance_factor=cell2mat(input.swimmer(:,27));
input.experimental_data_logic=cell2mat(input.swimmer(:,28));
input.gender=cell2mat(input.swimmer(:,29));
input.arm_strip_length=cell2mat(input.swimmer(:,30));
input.fk_amp=cell2mat(input.swimmer(:,31));
input.arms=cell2mat(input.swimmer(:,32));
input.legs=cell2mat(input.swimmer(:,33));
input.comment=char(input.swimmer(:,34));
```

1.3 Model Input Parameters

```
%% Swimmer Parameters
S=0.20247*(input.height(j)^0.725)*(input.mass(j)^0.425); %
DuBois D; DuBois EF: A formula to estimate the approximate surface
area if height and weight be known. Arch Int Med 1916 17:863-71.
human_density=[1060 1043]; % kg/m^3 [Male
Female]
if input.gender(j)==1 %
evalute human density based on inputted gender
human_density_eval=human_density(1);
else
human_density_eval=human_density(2);
end
swimmer_volume=input.mass(j)/human_density_eval; %
Volume calculation
Projected_Area_max_factor=2;
Projected_Area=Projected_Area_max_factor*swimmer_volume/input.height(j
);
slenderness=input.height(j)/swimmer_volume^(1/3); %
Slenderness calculation = Length/Volume^(1/3). This value is used to
determine resistance component coefficients from the resistance
database

arm_strip_length=input.arm_strip_length(j);
% arm_strip_length=0.01;
arm_points=(0:arm_strip_length:input.arm_length(j));
clear arm_strips
for ii=1:length(arm_points)-1
arm_strips(ii)=mean([arm_points(ii),arm_points(ii+1)]);
end
clear ii
clear arm_width cd_arm added_mass_arm
% clear it just in case data is left over from a previous run.
arm_width(1:length(arm_points))=input.armwidth(j); % arm width
along the arm.
flat plate assuming the hand produces drag based propulsion
http://www.engineeringtoolbox.com/drag-coefficient-d\_627.html
cd_arm(1:length(arm_points))=1.3;
added_mass_arm(1:length(arm_points))=1.364;
addedmasscoef=1.2; % Added mass
coefficient
buoyancy=500; % Bouyancy expressed
as newtons per meter
```

```

%% Fluid Parameters
water_temp=26;
temp=(0:10:100)';
density=[999.9 999.7 998.2 995.7 992.2 988.1 983.2 977.8 971.8 965.3
958.4]';
kinematic_viscosity=[1.787 1.307 1.004 0.801 0.658 0.553 0.475 0.413
0.365 0.326 0.294]'*10^-6;
fluid=[temp density kinematic_viscosity];
ro=interp1q(fluid(:,1),fluid(:,2),water_temp); % Pool water density
mu=interp1q(fluid(:,1),fluid(:,3),water_temp); % Pool water kinematic
viscosity
%% Lighthill Parameters and initial conditions
% input motion from joint angles
load kindata
Axz=kindata.Axz;
points=Axz(1, :, 1);
increment=diff(points);
segments=(increment./2)+points(1:end-1);
% centroids of the segments based on the position of the points
original.freq=1.6867;
original.amp=0.4577;
original.height=1.71;
original.scale_factor=1.5;
original.s=0.2*original.scale_factor;

A = exist('UUS_data.mat', 'file');

if A==0

% X DATA

x_lighthill_data=reshape(Axz(2, :, :), size(Axz, 2), size(Axz, 3))';

% Eliminate movement in the X direction
x_motion_shift=x_lighthill_data(:, end)-x_lighthill_data(1, end);
% movement in the x direction of the arms used to correct the overall
motion of the body so that it is stationary
for a=1:size(x_lighthill_data, 2)
x_lighthill_data(:, a)=x_lighthill_data(:, a)-x_motion_shift;
end
% where the dataset is not complete linearly interpolate to add
additional data points between the end and the beginning
additional_steps=32;
x_lighthill_data_correction_step=(x_lighthill_data(end, :)-
x_lighthill_data(1, :))./additional_steps;
for a=1:additional_steps
x_lighthill_data_correction(a, :)=x_lighthill_data(end, :)-
x_lighthill_data_correction_step.*a;
end
x_lighthill_data(end+1:end+additional_steps, :)=x_lighthill_data_correc
tion;
% enlarge data set size and filter middle section to eliminate
discontinuity
no_cycles=5;
% number of repeated cycles to fit
for a=1:no_cycles-1;

x_lighthill_data_large(1:size(x_lighthill_data, 1), :)=x_lighthill_data;

```

Appendix 1

```
x_lighthill_data_large((a*size(x_lighthill_data,1)+1):(a+1)*size(x_lighthill_data,1)),:)=x_lighthill_data;
end
% Phase Vector
phase_UUS=(360*no_cycles/size(x_lighthill_data_large,1):360*no_cycles/size(x_lighthill_data_large,1):360*no_cycles);
% Filtered x data
x_sample_rate=1/0.02;
x_cutoff_freq=2;
x_order=2;
[b,a] = butter(x_order,(x_cutoff_freq/(x_sample_rate*2)),'low');
for q=1:size(x_lighthill_data_large,2)
    x_lighthill_data_large_filt(:,q)=
    filtfilt(b,a,x_lighthill_data_large(:,q));
end

c=[001 067 089;[050 061 067].*2;[0 114 117].*1.1;010 150 169;151 158
069]./255);
line_weight=3;
font_size=10;
marker_size=10;
h=figure;
set(h,'Position',[400 100 350 290]);
plot(x_lighthill_data_large(:,1000),'-','color','k','linewidth',line_weight)
hold on
plot(x_lighthill_data_large_filt(:,1000),'--','color',c(3,:),'linewidth',line_weight)
xlim([0 400])
k=legend('Raw','Filtered','location','northwest');
set(k,'FontSize',font_size);
xlabel('Frame','FontSize',font_size)
ylabel('X displacement (m)','FontSize',font_size)

% Z DATA

z_lighthill_data=reshape(Axz(3, :, :), size(Axz,2), size(Axz,3))';

% Eliminate movement in the Z direction due to camera movement and swimmer depth change
z_motion_shift(1:size(z_lighthill_data,2))=z_lighthill_data(1,end);
for a=1:size(z_lighthill_data,1)
    z_lighthill_data(a,:)=z_lighthill_data(a,:)-z_motion_shift;
end

% where the dataset is not complete linearly interpolate to add additional data points between the end and the beginning
z_lighthill_data_correction_step=(z_lighthill_data(end,:)-z_lighthill_data(1,:))./additional_steps;
for a=1:additional_steps
    z_lighthill_data_correction(a,:)=z_lighthill_data(end,:)-z_lighthill_data_correction_step.*a;
end
z_lighthill_data(end+1:end+additional_steps,:)=z_lighthill_data_correction;

% enlarge data set size and filter middle section to eliminate discontinuity
for a=1:no_cycles-1;
```

```

z_lighthill_data_large(1:size(z_lighthill_data,1),:)=z_lighthill_data;

z_lighthill_data_large((a*size(z_lighthill_data,1)+1):((a+1)*size(z_lighthill_data,1)),:)=z_lighthill_data;
end

% Filtered z data
z_sample_rate=1/0.02;
z_cutoff_freq=2;
z_order=2;
[b,a] = butter(z_order, (z_cutoff_freq/(z_sample_rate*2)), 'low');
for q=1:size(z_lighthill_data_large,2)
    z_lighthill_data_large_filt(:,q)=
    filtfilt(b,a,z_lighthill_data_large(:,q));
end

save('UUS_data','x_lighthill_data_large_filt','z_lighthill_data_large_filt','x_lighthill_data','z_lighthill_data','phase_UUS','no_cycles');

else
    load UUS_data
end

% X Data Height Rescale

% lighthill_height=max(max(x_lighthill_data_large_filt))-
min(min(x_lighthill_data_large_filt));
% determine the height of the lighthill data
lighthill_height=points(end);
lighthill_scale_factor=1.411*input.height(j)/lighthill_height; %
Determine the swimming length of the swimmer as a ratio of height;
generate scale factor for lighthill data. 1.441 is a factor to convert
standing height to height with stretched out arms and pointed toes
x_lighthill_data_large_filt=x_lighthill_data_large_filt.*lighthill_scale_factor; % Scale the
lighthill input data to ensure the correct height is achieved

%% Amplitude rescale according to height

z_lighthill_amplitude=max(z_lighthill_data_large_filt(:,1))-
min(z_lighthill_data_large_filt(:,1)); % maximum vertical displacement
of the feet
amp_height_ratio=original.amp/original.height;
z_lighthill_amplitude_scale_factor=input.height(j)*amp_height_ratio/z_lighthill_amplitude;
z_lighthill_data_large_filt=z_lighthill_data_large_filt.*z_lighthill_amplitude_scale_factor;

%% UUS Feet Motion Plot Check
%% segment information

s_height_ratio=original.s/original.height;
s=input.height(j)*s_height_ratio; % Scale "s" directly
proportional to height. s is the cross-sectional width of the body. It
is assumed constant.
m=0.25*pi*ro.*s.^2;

```

Appendix 1

```
W(1,1:size(z_lighthill_data,2)+1)=zeros;

lighthill_UUS_initial_conditions

%% Leg Kick Data
kick.NS=kindata.NS(1:3);
kick.L=kindata.L(1:3);
kick.points=kindata.Axz(1,1:(sum(kick.NS)+1),1);
kick.increment=diff(kick.points);
kick.segments=(kick.increment./2)+kick.points(1:end-1);

kick.x_fit_uncorrected=x_lighthill_data_large_filt(:,1:(sum(kick.NS)+1));
kick.z_fit_uncorrected=z_lighthill_data_large_filt(:,1:(sum(kick.NS)+1));
kick.x_motion_shift=kick.x_fit_uncorrected(:,end);
kick.z_motion_shift=kick.z_fit_uncorrected(:,end);

phase_leg_kick=(360*no_cycles/size(kick.x_fit_uncorrected,1):360*no_cycles/size(kick.x_fit_uncorrected,1):360*no_cycles);

for a=1:size(kick.x_fit_uncorrected,2)
kick.x_fit(:,a)=kick.x_fit_uncorrected(:,a)-kick.x_motion_shift;
end

for a=1:size(kick.z_fit_uncorrected,2)
kick.z_fit(:,a)=kick.z_fit_uncorrected(:,a)-kick.z_motion_shift;
end

% Motion Scaling to achieve correct leg length and kicking amplitude

kick.x_factor=0.53*input.height(j)/abs(max(kick.x_fit(:,1)));
kick.x_fit=kick.x_fit.*kick.x_factor;

kick.amp=max(kick.z_fit(:,1))-min(kick.z_fit(:,1));
kick.desired_amp=input.fk_amp(j); %
desired_kicking_amplitude(m)
kick.z_factor=kick.desired_amp/kick.amp;
kick.z_fit=kick.z_fit.*kick.z_factor;

kick.s=s/2*1.5/original.scale_factor;
kick.m=0.25*pi*ro.*kick.s.^2;

leg_phase=180;
lighthill_L1_initial_conditions
lighthill_L2_initial_conditions

%% Model parameters

input_velocity=(0:0.001:10)';

%% Energy Model Initial Conditions

exp_data_power_factor=1.2;
exp_data_capacity_factor=5.3;

% exp_data_power_factor=1.09;
% exp_data_capacity_factor=4.3;
```

```

if input.gender(j)==1;
    E_glycolytic_capacity=242*input.mass(j)*exp_data_capacity_factor;
%1.2388e+006*input.mass; % Anaerobic capacity (J) based on the work
done for a 50m sprint, assuming only anaerobic energy and the full
capacity was consumed
else
    E_glycolytic_capacity=158*input.mass(j)*exp_data_capacity_factor;
%1.2388e+006*input.mass*0.77; % Female anaerobic capacity, relative to
mass, is 77% of male, Reference: 'Gender difference in anaerobic
capacity: role of aerobic contribution'
end

% currently assuming aerobic power is constant. However in reality it
will decrease with fatigue due to depleating blood sugar etc. Values
taken from Reference: 'Gender difference in anaerobic capacity: role
of aerobic contribution'
if input.gender(j)==1;
    P_aero_initial=3.4*input.mass(j); % New values
obtained from max vo2 tests. previous values (below) were from tests
lasting 30s where max vo2 capacity would not have been reached
% P_aero_initial=1.9*input.mass(j);
else
    P_aero_initial=3.1*input.mass(j);
% P_aero_initial=1.77*input.mass(j);
end

if input.gender(j)==1;
    max_P_glycolytic=13.3*input.mass(j)*exp_data_power_factor; %
Reference: 'Gender difference in anaerobic capacity: role of aerobic
contribution'
else
    max_P_glycolytic=10.2*input.mass(j)*exp_data_power_factor;
end

E_glycolytic=E_glycolytic_capacity;
E_glycolytic_log(1)=E_glycolytic_capacity;

max_power_available_log=zeros(60000,1);
max_power_available_average_log=zeros(60000,1);
max_power_available_log(1)=P_aero_initial+max_P_glycolytic;
max_power_available_average_log(1)=P_aero_initial+max_P_glycolytic;
power_filt=zeros(60000,1)';

passive_power_factor_log=ones(60000,1);
power_factor_log=zeros(60000,1);
power_factor_time_averaged_log=zeros(60000,1);
power_factor=1;
power_factor_log(1)=power_factor;
power_factor_time_averaged_log(1)=power_factor;
power_factor_cycle=1;
power_factor_temp=1;

p_out=zeros(60000,1);
I_out=zeros(60000,1);
D_out=zeros(60000,1);

error=zeros(60000,1);

```

Appendix 1

```
power_leg_total=0;
arm_power=0;
UUS_power_output.total=0;
surface=0;

% initial strokerate
temp_strokerate=cell2mat(input.strokerate(j));
strokerate=temp_strokerate(1);

%% Initial Conditions
i=1; % Initial calculation
cycle number
t=0;
strokerate_log=zeros(60000,1);
stot=zeros(60000,1)+input.dive_dist(j);
slen=input.dive_dist(j);
V=ones(60000,1).*input.entry_speed(j);
% Preallocating the time varying matrices
acc=zeros(60000,1);
acc=NaN(60000,1);
% Tx=zeros(100000,1);
Tz=NaN(60000,1);
SV=NaN(60000,1);
time=zeros(60000,1);
% P=NaN(60000,1);
force=NaN(60000,1);
E=zeros(60000,1);
z=NaN(60000,1);
Hands=NaN(60000,4);
% arm_power=zeros(60000,1);
V(1)=input.entry_speed(j); %
ATM the entry speed into the water (m/s)
acc(1)=0;
T(1)=0;
Tx=zeros(60000,1);
Tx(1)=0;
R_T_calculated(1)=0;
L1_THRUST=0;
L2_THRUST=0;
Hand1x=0;
Hand2x=0;
Hand1z=0;
Hand2z=0;
arm_power(1)=0;
arm1x_force=0;
arm2x_force=0;
Pd=zeros(60000,1);
Pe=zeros(60000,1);
perp_fluid_mom_kick=[];
perp_fluid_mom_UUS=[];
work=0;
P=0;
P_log=zeros(60000,1);
time_averaged_power_log=zeros(60000,1);
time_averaged_averaged_power_log=zeros(60000,1);
arm1_torque_log=zeros(60000,1);
arm1x_force_log=zeros(60000,1);
arm2x_force_log=zeros(60000,1);
lighthill_log=0; % just an arbitrary initial value to allow
lighthill_log to exist when UUS is not performed
```

```

%% Arm Model
arm_phase_shift=0.524;
alpha1=[0 0];
% Right arm pointing forwards
alpha2=[pi-arm_phase_shift pi-arm_phase_shift];
% Left arm pointing backwards
arm_motion_data;
stroke_time1=interp1(arm_data,arm1_time_vector,alpha1(1),'linear','extrap');
stroke_time2=interp1(arm_data,arm2_time_vector,alpha2(1),'linear','extrap');
arm_phase_time=stroke_time2-stroke_time1;
%
stroke_time2=interp1(arm_data,arm2_time_vector,alpha2(1),'linear','extrap')-12*input.arm_model_time_step(j); % phase shift to get arms in phase. This is a problem that needs addressing.
%
stroke_time2=interp1(arm_data,arm2_time_vector,alpha2(1),'linear','extrap')-25*input.arm_model_time_step(j); % phase shift to get arms in phase. This is a problem that needs addressing.
% stroke_time2=interp1(arm_data,arm_time_vector,alpha2(1));
arm_x_pos=0.34*input.height(j); % for animation purposes

```

1.4 Arm Motion Data

```

% Unsteady Arm Motion Data
arm_data=[2.07 4.92 9.43 15.44 22.52 30.31 39.52 51.88
66.71 81.47 95.77 110.05 124.10 137.35 149.28 160.29 170.14
180.76 195.28 212.19 229.27 246.38 263.48 280.58 297.69 314.78
331.72 345.56 353.04 356.22 358.24 360.00]./(180/pi); % time
accurate

x_sample_rate=1/0.02;
x_cutoff_freq=20;
x_order=2;
[b,a] = butter(x_order,(x_cutoff_freq/(x_sample_rate*2)),'low');

arm_data_filt= filtfilt(b,a,arm_data);

diff_arm_data=diff(arm_data);
diff_arm_data_filt=diff(arm_data_filt);

arm2_time_vector=(0:60/strokrate/(length(arm_data)-1):60/strokrate);

if input.arm_imbalance(j)<1

arm1_time_vector=(0:60/(strokrate*input.arm_imbalance(j))/(length(arm_data)-1):60/(strokrate*input.arm_imbalance(j)));
else
arm1_time_vector=arm2_time_vector;
end

```

1.5 Resistance Model

```

%% Resistance Model
%% Surface Resistance

```

Appendix 1

```
% Velocity
Vi=input_velocity; % Input velocity
range
Fn=Vi/sqrt(9.81*input.height(j)); % Froude
number
Re=Vi*input.height(j)/mu; % Reynolds
Number

% Skin Friction Resistance
cf=0.075./((log10(Re)-2).^2); % ITTC 1957 Corelation
line for frictional resistance coefficient. Used for all geometries.

% Wave Resistance
cw_data % Load
Thin Ship Theory Cw data
if input.gender(j)==1

cw=interp1(slenderness_cw,cw_input',slenderness,'spline')';%.*0.55;
% wave resistance curve for the given slenderness against the velocity
vector from thin ship theory. next stage is to asociate with input
velocity vector
else
    cw=interp1(slenderness_cw,cw_input',slenderness,'spline')';%.*0.3;
% wave resistance curve for the given slenderness against the velocity
vector from thin ship theory. next stage is to asociate with input
velocity vector
end
vel_cw=fn_data.*sqrt(9.81*input.height(j));
cw_surface=interp1(vel_cw,cw,Vi,'spline'); % plot
spline through data to provide resistance for the input velocity
points. However it does not extrapolate effectively so need to fix the
data outside the thin ship theory range.

min_cw_cutoff_speed=1.3;
a=[max(find(Vi<min_cw_cutoff_speed)) min(find(Vi>vel_cw(end)))];
% find the indices of begining and end of the thin ship velocity range
within the input velocity
% cw_surface(1:a(1))=cw(1); %
Outside the range of the thin ship theory cw data, use the end data
points of cw for the remaining Vi range
cw_surface(1:a(1))=cw(max(find(vel_cw<min_cw_cutoff_speed)));
cw_surface(a(2)+1:end)=cw(end);

% Pressure Resistance
cp_data % Load
experimental data
if input.gender(j)==1 %
evaluate the cp value from the fit to the experimental data; for
slenderness and gender

cp_surface(1:length(Vi),:)=polyval(cp_fit_male_surface,slenderness);
else
    cp_surface(1:length(Vi),:)=
polyval(cp_fit_female_surface,slenderness);
end

% Total Surface Resistance
```

```

Rf_s=cf.*0.5.*ro.*S.*Vi.^2;
Rw_s=cw_surface.*0.5.*ro.*S.*Vi.^2;
Rp_s=cp_surface.*0.5.*ro.*S.*Vi.^2;
R_surface=[Vi
((Rf_s+Rp_s)*input.underwater_resistance_factor(j)+Rw_s*input.wave_res
istance_factor(j))*input.surface_resistance_factor(j)];

%%% Underwater Glide Resistance

% Pressure Resistance
if input.gender(j)==1 %
evaluate the cp value from the fit to the experimental data; for
slenderness and gender

cp_underwater(1:length(Vi),:)=polyval(cp_fit_male_underwater,slenderne
ss);
else
cp_underwater(1:length(Vi),:)=
polyval(cp_fit_female_underwater,slenderness);
end

% Total Underwater Resistance
Rf_u=cf.*0.5.*ro.*S.*Vi.^2;
Rp_u=cp_underwater.*0.5.*ro.*S.*Vi.^2;
R_underwater=[Vi (Rf_u+Rp_u)*input.underwater_resistance_factor(j)];

```

1.6 Energy Model

```

work=work+P*dt; % work done accumulation

%%% Energy Capacity Calculation

P_aero=P_aero_initial;

% E_glycolytic=E_glycolytic+P_aero; % Fixed Power
E_glycolytic=E_glycolytic+P_aero*dt-P*dt; % Depleting Power
E_glycolytic_log(i)=E_glycolytic;

if E_glycolytic>E_glycolytic_capacity
E_glycolytic=E_glycolytic_capacity; % Preventing anaerobic
recovery to be greater than anaerobic capacity
end

if E_glycolytic<0 % Preventing negative
anaerobic capacity
E_glycolytic=0;
end

max_power_available=P_aero+E_glycolytic/E_glycolytic_capacity*max_P_gl
ycolytic;
max_power_available_log(i)=max_power_available;

% Time Averaged available power. Smoothes transition from surface and
underwater phases
available_power_av_period=1;
average_time_steps=available_power_av_period/dt;

```

Appendix 1

```
if i<average_time_steps+1
% if averaging period is longer than the model has run for, make the
averaging period the time the model has run for
    average_time_steps=i-1;
end

max_power_available_average=mean(max_power_available_log(i-
average_time_steps:i));
max_power_available_average_log(i)=max_power_available_average;

%% Double Time Averaged Power Calculation

power_av_period=1;
average_time_steps=power_av_period/dt;

if i<average_time_steps+1
% if averaging period is longer than the model has run for, make the
averaging period the time the model has run for
    average_time_steps=i-1;
end

time_averaged_power=mean(P_log(i-average_time_steps:i));
time_averaged_power_log(i)=time_averaged_power;

time_averaged_averaged_power=mean(time_averaged_power_log(i-
average_time_steps:i)); % second average - less phase shift
time_averaged_averaged_power_log(i)=time_averaged_averaged_power;

% Filter
sample_rate=1/dt;
cutoff_freq=1;
order=2;
[b,a] = butter(order, (cutoff_freq/(sample_rate*2)), 'low');
if i>3*order
    a=filtfilt(b,a,time_averaged_power_log(1:i));
    power_filt(i)=a(i);
else
    power_filt(i)=time_averaged_power_log(i);
end

%% PID Control

power_threshold=1;
% if power_filt(i)>max_power_available_average*power_threshold
% if the available power is less than the required power, produce a
power factor 0 < 1 to reduce the strokerate, to reduce the required
power
if i>3
    Kp=0.05;
    Ki=0.3;
    Kd=0.00;

    % Filter
    if i>3*order+1
        sample_rate=1/dt;
        cutoff_freq=3;
        order=2;
        [b,a] = butter(order, (cutoff_freq/(sample_rate*2)), 'low');
```

```

        a=filtfilt(b,a,(abs(power_filt(1:i)-
max_power_available_average_log(1:i)'.*power_threshold).^ (1/3)).*sign(
power_filt(1:i)-
max_power_available_average_log(1:i)'.*power_threshold));
        error_phase_shift=3*order;
        error(i)=a(end-error_phase_shift);
        if error(i)<0
            error(i)=0;
        end
    else
        error(i)=(abs(power_filt(i)-
max_power_available_average*power_threshold)^(1/3))*sign(power_filt(i)
-max_power_available_average*power_threshold);
        if error(i)<0
            error(i)=0;
        end
    end

    p_out(i)=Kp*error(i);
    I_out(i)=Ki*trapz(time(1:i),error(1:i));

    if i>3
        D_out(i)=Kd*mean((diff(error(i-3:i))./diff(time(i-3:i))));
    end

    pid(i)=p_out(i)+I_out(i)+D_out(i);

    pid_power_factor(i)=1-
pid(i)/temp_strokerate((floor(stot(i)/50)+1));
    power_factor_temp=pid_power_factor(i);

else
    power_factor_temp=1;
end

%% Power Factor
power_factor=power_factor_temp;

%% Power Factor Override

if power_factor<0.1
    power_factor=0.1;
end

%% Power Factor Log

power_factor_log(i)=power_factor;

```

1.7 Phase Model

```

temp_strokerate=cell2mat(input.strokerate(j));
% strokerate=temp_strokerate((floor(stot(i)/50)+1));
strokerate=temp_strokerate((floor(stot(i)/50)+1))*power_factor;
strokerate_log(i)=strokerate;
%
if slen<50
    slen=slen+ds;
else

```

Appendix 1

```
slen=0.0;
t=t+input.turn_time(j);

V(i)=input.turn_speed(j);
% V(i+1)=input.turn_speed(j);
lighthill_UUS_initial_conditions

alpha=[0 0];
% Right arm pointing forwards
alpha2=[pi-arm_phase_shift pi-arm_phase_shift];
% Left arm pointing backwards

stroke_time1=0;%interp1(arm_data,arm1_time_vector,alpha(1),'linear','
extrap');

stroke_time2=interp1(arm_data,arm2_time_vector,alpha2(1),'linear','ext
rap');
arm_phase_time=stroke_time2-stroke_time1;

lighthill_L1_initial_conditions
lighthill_L2_initial_conditions
end

if (stot(i)<input.startd(j)) % Initiate
Start Phase
    surface=0;
    UUS_kickfreq=input.UUS_kickfreq_start(j);
    UUS_thrust_model
    R=R_underwater;
    if i>3 % wait three
time steps to remove transient effects
    % Tx(i+1)=THRUST_FEET;
    Tx(i+1)=UUS_THRUST;
% P=UUS_power_output.total;
    P=abs(UUS_power_output.total); %
Instantaneous Power for UUS
    end
end

if ((stot(i)>=input.startd(j)) && (stot(i)<50)) ||
((slen>=input.turnout(j)) && (stot(i)>50)) % Initiate Surface Phase
    surface=1;
    R=R_surface;
    if input.arms(j)==1
        arm_thrust_model
        % if i==3934;
        % break
        % end
    end
    if input.legs(j)==1
        leg_kick_thrust_model
    end

Tx(i+1)=(arm1x_force+arm2x_force)*input.thrust_factor(j)+L1_THRUST_FEE
T+L2_THRUST_FEET;
    P=abs(power_leg_total)+abs(arm_power);
end

if((stot(i)>input.startd(j)) && (slen<=input.turnout(j)) &&
(stot(i)>50)) % Initiate Turnout Phase
```

```

    surface=0;
    UUS_kickfreq=input.UUS_kickfreq_turn(j);
    if slen>1 % glide for 1 m off the wall before initiating the UUS
thrust model
        UUS_thrust_model
            % P=UUS_power_output.total;
            P=abs(UUS_power_output.total); %
Instantaneous Power for UUS
            Tx(i+1)=UUS_THRUST;
        end
        R=R_underwater;
end

Tz(i+1)=Hand1z+Hand2z;

```

8.5 Kinetic Model

```

% Kinetic Model
if Tx(i+1)>2000 || Tx(i+1)<-2000
    Tx(i+1)= Tx(i);
end

R_Time_Step(i+1)=interp1q(R(:,1),R(:,2),V(i));
acc(i+1)=(Tx(i+1)-
(R_Time_Step(i+1)/thrust_deduction))/(input.mass(j)*addedmasscoef);
% acc(i+1)=((Tx(i+1)-
R_Time_Step(i+1))/thrust_deduction)/(input.mass(j)*addedmasscoef);
V(i+1)=acc(i+1)*dt+V(i);

if V(i+1)<input.Tow_Speed(j);
    V(i+1)=input.Tow_Speed(j);
end

Pe(i+1)=V(i+1)*interp1q(R(:,1),R(:,2),V(i));
E(i+1)=V(i+1)*interp1q(R(:,1),R(:,2),V(i))*dt;

R_T_calculated(i+1)=R_Time_Step(i+1)/thrust_deduction-Tx(i+1);

```

1.8 UUS Thrust Model

```

% UUS Thrust Model
% MOTION INPUT - Vertical Position of points along body with time
%% Amplitude scaling for a constant frequency amplitude ratio
z_lighthill_amplitude=max(z_lighthill_data_large_filt(:,1))-
min(z_lighthill_data_large_filt(:,1));
freq_amp_ratio=original.freq/original.amp; % taken from the
original data
z_lighthill_amplitude_scale_factor=freq_amp_ratio/(UUS_kickfreq/z_ligh
thill_amplitude);

%% New Body Position

```

Appendix 1

```
d(2)=d(1)+UUS_kickfreq*360*dt*power_factor;
% Interpolant for position within stroke

if d(2)>phase_UUS(end)
    lighthill_UUS_initial_conditions
    d(2)=d(1)+UUS_kickfreq*360*dt*power_factor;
% Power factor NEW
end

z_lighthill(2,:)=interp1(phase_UUS,z_lighthill_data_large_filt.*z_ligh
thill_amplitude_scale_factor,d(2));
x_lighthill(2,:)=interp1(phase_UUS,x_lighthill_data_large_filt,d(2));

d(1)=d(2);

%% Thrust Calculation
[UUS_THRUST,UUS_SIDEFORCE,z_lighthill,x_lighthill,momentum_body,calc_C
,THRUST_BODY,THRUST_FEET,perp_fluid_mom_external_temp,UUS_power_output
,w_output,dzdt_output,dxdt_output,dzda_output,dxda_output,increment_ne
w,segment_new,thrust_length,momentum_length]=lighthill(z_lighthill,x_l
ighthill,kindata,increment,dt,segments,m,i,V,momentum_body,calc_C,perp
_fluid_mom_UUS,input.segment_force,UUS_power_output,momentum_length);

%% Output Logging
lighthill_log.thrust.total(i+1)=UUS_THRUST;
lighthill_log.thrust.body(i+1)=THRUST_BODY;
lighthill_log.thrust.feet(i+1)=THRUST_FEET;
lighthill_log.thrust.momentum_body(i+1)=momentum_body(2);

UUS_power.total(i+1)=UUS_power_output.total;
UUS_power.feet(i+1)=UUS_power_output.feet;
UUS_power.body(i+1)=UUS_power_output.body;
lighthill_log.w(i+1,:)=w_output;
lighthill_log.dzdt_log(i+1,:)=dzdt_output;
lighthill_log.dxd_t_log(i+1,:)=dxdt_output;
lighthill_log.dzda_log(i+1,:)=dzda_output;
lighthill_log.dxda_log(i+1,:)=dxda_output;
lighthill_log.momentum_length(i+1,:)=momentum_length(1,:);
lighthill_log.thrust_length_log(i+1,:)=thrust_length(1,:);

lighthill_log.z_lighthill(i+1,:)=z_lighthill(1,:);
lighthill_log.x_lighthill(i+1,:)=x_lighthill(1,:);

increment_new_log(i+1,:)=increment_new;
lighthill_log.segment_new_log(i+1,:)=segment_new;

if input.segment_force==1
    perp_fluid_mom(i,:)=perp_fluid_mom_external_temp;
end
```

1.9 Leg Kick Thrust Model

```
% Leg Kick Thrust Model
%% MOTION INPUT - X & Z coordinates of points along body with time
% Leg 1 interpolant
L1(2)=L1(1)+(input.leg_kickfreq(j)/2*strokerate/60)*360*dt;
```

```

if L1(2)>phase_leg_kick(end)
    lighthill_L1_initial_conditions
    L1(2)=L1(1)+(input.leg_kickfreq(j)/2*strokerate/60)*360*dt;
end

% Leg 1 position interpolation
L1_z(2,:)=interp1q(phase_leg_kick,kick.z_fit,L1(2))./1.3;
% divisor is to scale the UUS kinematic data down to realistic leg
kick data for freestyle/backstroke
L1_x(2,:)=interp1q(phase_leg_kick,kick.x_fit,L1(2));
L1(1)=L1(2);

% Leg 2 interpolant
L2(2)=L2(1)+(input.leg_kickfreq(j)/2*strokerate/60)*360*dt;
if L2(2)>phase_leg_kick(end)
    lighthill_L2_initial_conditions_run
% use different initial conditions since phase shift only needs to be
applied at the beginning
    L2(2)=L2(1)+(input.leg_kickfreq(j)/2*strokerate/60)*360*dt;
end

% Leg 2 position interpolation
L2_z(2,:)=interp1q(phase_leg_kick,kick.z_fit,L2(2))./1.3;
L2_x(2,:)=interp1q(phase_leg_kick,kick.x_fit,L2(2));
L2(1)=L2(2);

[L1_THRUST,L1_SIDEFORCE,L1_z,L1_x,L1_calc_A,L1_calc_C,L1_THRUST_BODY,L
1_THRUST_FEET,L1_perp_fluid_mom_external_temp,L1_power]=lighthill(L1_z
,L1_x,kick,kick.increment,dt,kick.segments,kick.m,i,V,L1_calc_A,L1_cal
c_C,perp_fluid_mom_kick,input.segment_force);
[L2_THRUST,L2_SIDEFORCE,L2_z,L2_x,L2_calc_A,L2_calc_C,L2_THRUST_BODY,L
2_THRUST_FEET,L2_perp_fluid_mom_external_temp,L2_power]=lighthill(L2_z
,L2_x,kick,kick.increment,dt,kick.segments,kick.m,i,V,L2_calc_A,L2_cal
c_C,perp_fluid_mom_kick,input.segment_force);

% thrust_leg_total(i+1)=L1_THRUST+L2_THRUST;
thrust_leg_total(i+1)=L1_THRUST_FEET+L2_THRUST_FEET;
power_leg_total=L1_power.total+L2_power.total;

```

1.10 LAEBT Model

```

function
[THRUST,SIDEFORCE,z_lighthill,x_lighthill,momentum_body,calc_C,THRUST_
BODY,THRUST_FEET,perp_fluid_mom,power,w,dzdt,dxdt,dzda,dxda,increment_
calc,segments_calc,THRUST_LENGTH,momentum_length] =
lighthill(z_lighthill,x_lighthill,kindata,increment,dt,segments,m,i,V,
momentum_body,calc_C,perp_fluid_mom,segment_force_calc,power,momentum_
length)

%% Analysis of Body Shape and Motion

increment_calc=sqrt((diff(z_lighthill(2,:)).^2)+(diff(x_lighthill(2,:))
).^2)); % increment between points along the body calculated instead
of using the original defined values which have been changed due to
filtering the kinematic data.
segments_calc=increment_calc./2+cumsum(increment_calc)-increment_calc;
% calculate segment centroids

```

Appendix 1

```
dzda=diff(z_lighthill(2,:))./increment_calc;
% Slope along the body wrt z
dxda=diff(x_lighthill(2,:))./increment_calc;
% Slope along the body wrt x

dzdt_points=(z_lighthill(2,:)-z_lighthill(1,:))./dt;
% dz/dt from numerical differentiation of z points
dxdt_points=((x_lighthill(2,:)-x_lighthill(1,:))./dt)+V(i);
% dx/dt from numerical differentiation of x points with swimmer
velocity deducted

z_lighthill(1,:)=z_lighthill(2,:);
x_lighthill(1,:)=x_lighthill(2,:);

dzdt=(diff(dzdt_points)./2)+dzdt_points(1:end-1);
% dz/dt of the z segments between the z points
dxdt=(diff(dxdt_points)./2)+dxdt_points(1:end-1);
% dx/dt of the x segments between the x points

w=(dzdt.*dxda)-(dxdt.*dzda);
%
%% Thrust Calculation

THRUST_FEET=m*w(1)*dzdt(1)-0.5*m*(w(1)^2)*dxda(1);
% Reaction force due to rate of change of momentum in the wake
momentum_body(2)=trapz(segments_calc,m.*w.*-dzda);
% Integrate momentum per unit length along the body. Positive momentum
is in the diection of swimming (left to right)

if momentum_body(1)==0;
    THRUST_BODY=0;
else
    THRUST_BODY=(momentum_body(2)-momentum_body(1))/dt;
%
end
THRUST=THRUST_FEET-THRUST_BODY;
%

momentum_body(1)=momentum_body(2);

%% Thrust per unit length along the body

momentum_length(2,:)=m.*w.*-dzda;

if momentum_length(1,:)==0;
    THRUST_LENGTH=zeros(1,length(segments_calc));
else
    THRUST_LENGTH=(momentum_length(2,:)-momentum_length(1,:))./dt;
end

momentum_length(1,:)=momentum_length(2,:);

%% Side Force Calculation

calc_C(2)=trapz(segments,m.*w.*dxda);
% integrate the force along the body with respect to segment position
calc_D=(calc_C(2)-calc_C(1))/dt;
SIDEFORCE=-m*w(end)*V(i+1)-0.5*m*(w(end)^2)*dzda(end)-calc_D;
```

```

%% Lighthill Segment force Calculation

perp_fluid_mom=m.*w;
% Perpendicular momentum per unit length along the body

%% Lighthill Power Calculation

power.feet=m*(w(1)^2)*dzdt(1)-0.5*m*(w(1)^3);
% Same as thrust from feet with w raised to power 2 and no component
taken

power.momentum_body_local(2,:)=perp_fluid_mom;
if power.momentum_body_local(1,')==zeros
% Rate of change of momentum calculation
    power.force_body(1:length(segments))=zeros;
else
    power.force_body=(power.momentum_body_local(2,:)-
power.momentum_body_local(1,:))./dt;
end

power.momentum_body_local(1,:)=power.momentum_body_local(2,:);

% power.body_local=power.force_body.*w;
power.body_local=abs(power.force_body).*abs(w);
% Power per unit length. Take the magnitude of the vectors since power
is required from the swimmer to accelerate and decelerate the segment
power.body=trapz(segments_calc,power.body_local);
% Integrate power along the body
power.total=power.feet+power.body;

end

```

1.11 Arm Thrust Model

```

%% Arm Thrust Model

alpha1(1)=alpha1(2);
alpha2(1)=alpha2(2);

stroke_time1=stroke_time1+dt;
stroke_time2=stroke_time2+dt;

%% Time Vector Definition to create an imbalance between left and
right

arm1_time_vector_in=(length(find(arm_data_filt<pi))/length(arm_data)*6
0/(strokerate*input.arm_imbalance(j))/length(find(arm_data_filt<pi)):l
ength(find(arm_data_filt<pi))/length(arm_data)*60/(strokerate*input.ar
m_imbalance(j))/length(find(arm_data_filt<pi)):length(find(arm_data_fi
lt<pi))/length(arm_data)*60/(strokerate*input.arm_imbalance(j)));
arm1_time_vector_out=(arm1_time_vector_in(end)+length(find(arm_data_fi
lt<pi))/length(arm_data)*60/(strokerate*input.arm_imbalance(j))/length
(find(arm_data_filt<pi)):(60/strokerate-
(arm1_time_vector_in(end)+length(find(arm_data_filt<pi))/length(arm_da
ta)*60/(strokerate*input.arm_imbalance(j))/length(find(arm_data_filt<p
i))))/(length(find(arm_data_filt>pi))-1):60/strokerate);

```

Appendix 1

```
arm2_time_vector=(60/strokerate/length(arm_data):60/strokerate/length(
arm_data):60/strokerate);

%% New arm position

arm_interp_method='spline';

if input.arm_imbalance(j)<1
% if no imbalance is specified, use arm2 time vector, as it is the
same
    if alpha1(2)<pi

alpha1(2)=interp1(arm1_time_vector_in,arm_data_filt(find(arm_data_filt
<pi)),stroke_time1,arm_interp_method,'extrap');
        else

alpha1(2)=interp1(arm1_time_vector_out,arm_data_filt(find(arm_data_fil
t>pi)),stroke_time1,arm_interp_method,'extrap');
        end
    else
        stroke_time1=stroke_time2-arm_phase_time/power_factor;
        if stroke_time1<0
            stroke_time1=stroke_time1+60/strokerate;
        end

alpha1(2)=interp1(arm2_time_vector,arm_data_filt,stroke_time1,arm_inte
rp_method,'extrap');
    end

alpha2(2)=interp1(arm2_time_vector,arm_data_filt,stroke_time2,arm_inte
rp_method,'extrap');

alpha1_log(i,:)=alpha1;
alpha2_log(i,:)=alpha2;

%% Reset when arm completes a full revolution

if input.arm_imbalance(j)<1
    if alpha1(2)>=2*pi                                % Interpolant -
Position of arm throughout a stroke cycle in terms of time
        stroke_time1=stroke_time1-60/strokerate;

alpha1(2)=interp1(arm1_time_vector_in,arm_data_filt(find(arm_data_filt
<pi)),stroke_time1+dt,arm_interp_method,'extrap');

alpha1(1)=interp1(arm1_time_vector_in,arm_data_filt(find(arm_data_filt
<pi)),stroke_time1,arm_interp_method,'extrap');
        power_factor_cycle=power_factor_temp;
    end
else
    if alpha1(2)>=2*pi
        stroke_time1=stroke_time1-60/strokerate;

alpha1(2)=interp1(arm2_time_vector,arm_data_filt,stroke_time1+dt,arm_i
nterp_method,'extrap');

alpha1(1)=interp1(arm2_time_vector,arm_data_filt,stroke_time1+dt,arm_i
nterp_method,'extrap');
        power_factor_cycle=power_factor_temp;
```

```

    end
end

if alpha2(2)>=2*pi % Interpolant - Position of
arm throughout a stroke cycle in terms of time
    stroke_time2=stroke_time2-60/strokerate;

alpha2(2)=interp1(arm2_time_vector,arm_data_filt,stroke_time2+dt,arm_i
nterp_method,'extrap');

alpha2(1)=interp1(arm2_time_vector,arm_data_filt,stroke_time2,arm_inte
rp_method,'extrap');
end
%% Vector Calculation to determine arm vector position and velocity
vectors along the arm

% Advance Velocity
vel_unit=[1 0]/norm([1 0]);
vel_advance=vel_unit*V(i);

% Arm 1
    arm1=[input.arm_length(j)*cos(alpha1(2))
input.arm_length(j)*sin(alpha1(2))];
    arm_unit1=arm1/norm(arm1);
    arm_norm1=[-input.arm_length(j)*sin(alpha1(2))
input.arm_length(j)*cos(alpha1(2))];
    arm_norm_unit1=arm_norm1/norm(arm_norm1);

    for k=1:length(arm_points)
% Calculate the individual velocity vectors and scalors along the arm
        arm.arm_vel_resultant1(k,:)=(alpha1(2)-
alpha1(1))/dt*arm_points(k)*arm_norm_unit1+vel_advance;
%         arm_vel_resultant_mag(i)=norm(arm_vel_resultant)

arm.arm_vel_resultant_norm1(k,:)=dot(arm.arm_vel_resultant1(k,:),arm_n
orm_unit1)*arm_norm_unit1;

arm.arm_vel_resultant_norm_mag1(k)=dot(arm.arm_vel_resultant1(k,:),arm
_norm_unit1);

arm.arm_vel_resultant_X_mag1(k)=dot(arm.arm_vel_resultant_norm1(k,:),-
vel_unit);
    end

% Arm 2
    arm2=[input.arm_length(j)*cos(alpha2(2))
input.arm_length(j)*sin(alpha2(2))];
    arm_unit2=arm2/norm(arm2);
    arm_norm2=[-input.arm_length(j)*sin(alpha2(2))
input.arm_length(j)*cos(alpha2(2))];
    arm_norm_unit2=arm_norm2/norm(arm_norm2);

    for k=1:length(arm_points)
% Calculate the individual velocity vectors and scalors along the arm
        arm.arm_vel_resultant2(k,:)=(alpha2(2)-
alpha2(1))/dt*arm_points(k)*arm_norm_unit2+vel_advance;
%         arm_vel_resultant_mag(i)=norm(arm_vel_resultant)

arm.arm_vel_resultant_norm2(k,:)=dot(arm.arm_vel_resultant2(k,:),arm_n
orm_unit2)*arm_norm_unit2;

```

Appendix 1

```
arm.arm_vel_resultant_norm_mag2(k)=dot(arm.arm_vel_resultant2(k,:),arm
_norm_unit2);

arm.arm_vel_resultant_X_mag2(k)=dot(arm.arm_vel_resultant_norm2(k,:),-
vel_unit);
    end
%%
arm_velocity_log(i,1)=arm.arm_vel_resultant_norm_mag1(end);
arm_velocity_log(i,2)=arm.arm_vel_resultant_norm_mag2(end);
average_tip_vel(i)=strokerate/60*2*pi*input.arm_length(j);

%% Fluid Phase Model to simulate the arm transitioning between water
and air

if alpha1(2)>pi && alpha1(2)<2*pi
    ro1=0; % This should be the density
of air (1.23 kgm^-3), but all simulations up to this point have been
for zero density so will keep it at zero for the mean time.
else
    ro1=ro; % Pool water density
end

if alpha2(2)>pi && alpha2(2)<2*pi
    ro2=0; % This should be the density
of air (1.23 kgm^-3), but all simulations up to this point have been
for zero density so will keep it at zero for the mean time.
else
    ro2=ro; % Pool water density
end

%% Arm 1 force model
arm1_pressure_points=(0.5*ro1*(arm.arm_vel_resultant_norm_mag1).^2).*s
ign(arm.arm_vel_resultant_norm_mag1);
arm1x_pressure_points=(0.5*ro1*(arm.arm_vel_resultant_X_mag1).^2).*sig
n(arm.arm_vel_resultant_norm_mag1);
arm1_force=trapz(arm_points,arm1_pressure_points.*arm_width.*cd_arm.*a
dded_mass_arm);
arm1_torque=trapz(arm_points,arm1_pressure_points.*arm_width.*cd_arm.*
added_mass_arm.*arm_points);
arm1x_force=trapz(arm_points,arm1x_pressure_points.*arm_width.*cd_arm.
*added_mass_arm);
arm1_COE=arm1_torque/arm1_force;
power1=arm1_torque*(strokerate/60)*2*pi;

arm1_torque_log(i)=arm1_torque;

arm1x_force_log(i)=arm1x_force;

%% Arm 2 force model
arm2_pressure_points=(0.5*ro2*(arm.arm_vel_resultant_norm_mag2).^2).*s
ign(arm.arm_vel_resultant_norm_mag2);
arm2x_pressure_points=(0.5*ro2*(arm.arm_vel_resultant_X_mag2).^2).*sig
n(arm.arm_vel_resultant_norm_mag2);
arm2_force=trapz(arm_points,arm2_pressure_points.*arm_width.*cd_arm.*a
dded_mass_arm);
arm2_torque=trapz(arm_points,arm2_pressure_points.*arm_width.*cd_arm.*
added_mass_arm.*arm_points);
arm2x_force=trapz(arm_points,arm2x_pressure_points.*arm_width.*cd_arm.
*added_mass_arm);
```

```

arm2_COE=arm2_torque/arm2_force;
power2=arm2_torque*(strokerate/60)*2*pi;

arm2x_force_log(i)=arm2x_force;

%% Power and Work calculation
arm_power=power1+power2; %
propulsive power from both arms (watts)
arm_work(i+1)=arm_power*dt; % arm work
per time step
Pd(i+1)=arm_power;

```

1.12 UUS Initial Conditions

```

% Lighthill UUS initial conditions
d(1)=0; % to start the UUS
model in the middle of the dataset to ensure the jump does not effect
the start
if d(1)<phase_UUS(1)
    d(1)=phase_UUS(1)*1.01; % the phase value
used to interpolate the leg coordinate data MUST be within the phase
vector data. To ensure this, lowest possible phase value has been
multiplied by 1.01.
end
z_lighthill(1,:)=interp1(phase_UUS,z_lighthill_data_large_filt.*z_ligh
thill_amplitude_scale_factor,d(1));
x_lighthill(1,:)=interp1(phase_UUS,x_lighthill_data_large_filt,d(1));

momentum_body(1)=0;
calc_C(1)=0;
UUS_power_output.momentum_body_abs(1)=0;
UUS_power_output.momentum_body_local(1,1:length(segments))=zeros;
momentum_length(1,:)=zeros(1,length(segments));

```

1.13 Leg Kick Initial Conditions

```

% Lighthill Leg Kick Initial Conditions
L1(1)=leg_phase;
if L1(1)<phase_leg_kick(1)
    L1(1)=phase_leg_kick(1)*1.01; % the phase value
used to interpolate the leg coordinate data MUST be within the phase
vector data. I.e. greater than the smallest value in the phase
vector. To ensure this, lowest possible phase value has been
multiplied by 1.01. This problem could be solved by using a higher
order interpolation method at the expense of a higher computational
cost.
end
L1_z(1,:)=interp1q(phase_leg_kick,kick.z_fit,L1(1))./4;
L1_x(1,:)=interp1q(phase_leg_kick,kick.x_fit,L1(1));

L1_calc_A(1)=0;
L1_calc_C(1)=0;
L1_THRUST_FEET=0;

```


Appendix 2

Passive resistance data used in the resistance model in Chapter 5.

Female - Surface Passive Resistance Data

Height (m)	Mass (kg)	Slenderness	Speed (ms ⁻¹)	Passive Resistance (N)	Ct
1.71	61.00	4.41	2.20	198.88	0.0479
1.71	61.00	4.41	2.17	218.68	0.0542
1.71	61.00	4.41	2.20	166.51	0.0401
1.71	61.00	4.41	2.22	162.97	0.0386
1.71	61.00	4.41	2.18	215.73	0.0530
1.71	61.00	4.41	2.20	202.12	0.0487
1.71	61.00	4.41	2.20	169.80	0.0409
1.71	61.00	4.41	2.21	166.52	0.0398
1.71	61.00	4.41	2.18	177.68	0.0436
1.71	61.00	4.41	2.18	185.98	0.0457
1.71	61.00	4.41	2.19	188.74	0.0459
1.71	61.00	4.41	2.19	188.52	0.0459
1.71	61.00	4.41	2.21	178.73	0.0427
1.71	61.00	4.41	2.17	193.68	0.0480
1.71	61.00	4.41	2.20	178.16	0.0429
1.71	61.00	4.41	2.20	177.69	0.0428
1.71	61.00	4.41	2.19	186.54	0.0454
1.71	61.00	4.41	2.21	170.86	0.0408
1.71	61.00	4.41	2.21	171.93	0.0411
1.71	61.00	4.41	2.21	173.12	0.0414
1.71	61.00	4.41	1.85	112.60	0.0384
1.71	61.00	4.41	1.85	130.50	0.0445
1.71	61.00	4.41	1.85	140.40	0.0479
1.71	61.00	4.41	1.85	137.50	0.0469
1.71	61.00	4.41	1.86	147.70	0.0498
1.71	61.00	4.41	1.86	156.80	0.0529
1.71	61.00	4.41	1.87	129.80	0.0433
1.84	76.00	4.41	1.85	117.20	0.0345
1.84	76.00	4.41	1.85	121.30	0.0357
1.84	76.00	4.41	1.85	109.80	0.0323
1.84	76.00	4.41	1.85	120.20	0.0354
1.84	76.00	4.41	1.85	116.00	0.0342
1.84	76.00	4.41	1.86	110.80	0.0323
1.84	76.00	4.41	1.86	114.70	0.0334
1.71	62.80	4.36	1.85	118.30	0.0398
1.71	62.80	4.36	1.85	124.80	0.0420
1.71	62.80	4.36	1.85	118.50	0.0399
1.71	62.80	4.36	1.86	117.20	0.0390
1.71	62.80	4.36	1.86	115.60	0.0385
1.71	62.80	4.36	1.86	119.40	0.0398
1.71	62.80	4.36	1.86	115.10	0.0383
1.71	62.80	4.36	1.86	117.70	0.0392
1.71	62.80	4.36	1.87	105.60	0.0348
1.78	77.35	4.24	1.49	83.20	0.0384
1.78	77.35	4.24	1.50	81.90	0.0373
1.78	77.35	4.24	1.50	80.80	0.0366
1.68	57.00	4.41	1.35	72.90	0.0488
1.68	57.00	4.41	1.35	71.50	0.0478
1.68	57.00	4.41	1.35	65.90	0.0441
1.68	52.00	4.56	1.42	60.80	0.0381
1.68	52.00	4.56	1.41	59.60	0.0379
1.68	52.00	4.56	1.41	61.10	0.0389
1.68	52.00	4.56	1.42	58.50	0.0367

Appendix 2

Male - Surface Passive Resistance Data

Height (m)	Mass (kg)	Slenderness	Speed (ms ⁻¹)	Passive Resistance (N)	Ct
1.83	83.00	4.27	2.15	183.88	0.0388
1.83	83.00	4.27	2.16	194.15	0.0406
1.83	83.00	4.27	2.19	184.00	0.0374
1.83	83.00	4.27	2.11	184.17	0.0403
1.83	83.00	4.27	2.18	192.57	0.0395
1.83	83.00	4.27	2.16	196.31	0.0410
1.83	83.00	4.27	2.17	175.33	0.0363
1.83	83.00	4.27	2.17	179.15	0.0371
1.83	83.00	4.27	2.20	174.52	0.0352
1.83	83.00	4.27	2.17	185.02	0.0383
1.83	83.00	4.27	2.18	174.69	0.0358
1.83	83.00	4.27	2.17	172.58	0.0357
1.83	83.00	4.27	2.18	182.59	0.0375
1.82	84.00	4.24	2.19	227.94	0.0463
1.82	84.00	4.24	2.12	304.40	0.0659
1.82	84.00	4.24	2.14	294.95	0.0627
1.82	84.00	4.24	2.12	295.25	0.0639
1.82	84.00	4.24	2.14	276.44	0.0588
1.82	84.00	4.24	2.18	215.50	0.0441
1.82	84.00	4.24	2.18	221.41	0.0454
1.82	84.00	4.24	2.16	236.68	0.0494
1.82	84.00	4.24	2.16	244.65	0.0510
1.82	84.00	4.24	2.14	260.27	0.0553
1.82	84.00	4.24	2.15	272.24	0.0573
1.82	84.00	4.24	2.13	273.87	0.0588
1.82	84.00	4.24	2.16	255.65	0.0533
1.82	84.00	4.24	2.16	247.24	0.0516
1.82	84.00	4.24	2.15	253.89	0.0535
1.82	84.00	4.24	2.20	181.08	0.0364
1.82	84.00	4.24	2.17	237.00	0.0490
1.82	84.00	4.24	2.19	225.15	0.0457
1.82	84.00	4.24	2.18	201.56	0.0413
1.82	84.00	4.24	2.19	191.09	0.0388
1.82	84.00	4.24	2.18	201.64	0.0413
1.82	84.00	4.24	2.20	198.66	0.0400
1.78	66.00	4.50	1.67	125.08	0.0491
1.78	66.00	4.50	1.67	119.76	0.0470
1.78	66.00	4.50	1.66	123.65	0.0491
1.78	66.00	4.50	1.66	119.65	0.0475
1.78	66.00	4.50	1.67	119.00	0.0467
1.78	66.00	4.50	1.67	126.53	0.0496
1.78	66.00	4.50	1.67	124.09	0.0487
1.78	66.00	4.50	1.67	125.05	0.0491
1.78	66.00	4.50	1.67	135.70	0.0532
1.78	66.00	4.50	1.66	136.56	0.0542
1.78	66.00	4.50	1.67	128.09	0.0503
1.78	66.00	4.50	1.66	136.56	0.0542
1.78	66.00	4.50	1.69	106.03	0.0406
1.78	66.00	4.50	1.66	122.00	0.0484
1.78	66.00	4.50	1.68	115.20	0.0447
1.78	66.00	4.50	1.68	119.20	0.0462
1.78	66.00	4.50	1.68	115.87	0.0449
1.78	66.00	4.50	1.67	110.52	0.0434
1.78	66.00	4.50	1.68	111.48	0.0432
1.78	66.00	4.50	1.68	105.90	0.0411
1.78	66.00	4.50	1.68	110.97	0.0430
1.78	66.00	4.50	1.67	115.71	0.0454
1.75	71.00	4.31	1.84	139.70	0.0444
1.75	71.00	4.31	1.84	134.00	0.0426

1.75	71.00	4.31	1.84	120.30	0.0382
1.75	71.00	4.31	1.84	122.50	0.0389
1.75	71.00	4.31	1.84	119.60	0.0380
1.75	71.00	4.31	1.84	133.00	0.0423
1.75	71.00	4.31	1.85	125.50	0.0394
1.75	71.00	4.31	1.85	126.10	0.0396
1.88	74.40	4.56	1.84	142.00	0.0419
1.88	74.40	4.56	1.84	130.10	0.0384
1.88	74.40	4.56	1.85	119.20	0.0348
1.88	74.40	4.56	1.85	124.20	0.0363
1.88	74.40	4.56	1.85	136.80	0.0400
1.88	74.40	4.56	1.85	108.70	0.0318
1.88	74.40	4.56	1.85	114.20	0.0334
1.88	74.40	4.56	1.85	110.00	0.0321
1.88	74.40	4.56	1.85	119.60	0.0349
1.93	86.00	4.46	1.83	135.90	0.0375
1.93	86.00	4.46	1.83	148.80	0.0410
1.93	86.00	4.46	1.84	142.20	0.0388
1.93	86.00	4.46	1.84	135.70	0.0370
1.93	86.00	4.46	1.84	131.40	0.0358
1.93	86.00	4.46	1.84	136.20	0.0372
1.93	86.00	4.46	1.84	136.60	0.0373
1.82	77.00	4.36	1.67	110.80	0.0401
1.82	77.00	4.36	1.84	131.00	0.0391
1.82	77.00	4.36	1.84	125.60	0.0375
1.88	74.40	4.56	1.94	122.70	0.0325
1.75	81.00	4.12	1.90	130.80	0.0369
1.78	66.00	4.50	2.14	153.20	0.0366
1.78	66.00	4.50	2.16	134.00	0.0314
1.78	66.00	4.50	2.16	135.30	0.0317
1.78	66.00	4.50	2.16	131.10	0.0307
1.78	66.00	4.50	2.10	124.80	0.0310
1.78	66.00	4.50	2.16	138.40	0.0325
1.78	66.00	4.50	2.15	127.00	0.0301
1.78	66.00	4.50	2.15	132.90	0.0315
1.78	66.00	4.50	2.17	130.40	0.0303
1.78	66.00	4.50	2.16	125.70	0.0295
1.78	66.00	4.50	2.16	133.40	0.0313
1.78	66.00	4.50	2.16	123.50	0.0290
1.78	66.00	4.50	2.16	120.60	0.0283
1.78	66.00	4.50	2.16	124.10	0.0291
1.78	66.00	4.50	2.16	116.60	0.0273
1.78	66.00	4.50	2.13	115.80	0.0279
1.78	66.00	4.50	2.13	112.90	0.0272
1.78	66.00	4.50	2.17	119.30	0.0277
1.78	66.00	4.50	2.17	117.90	0.0274
1.78	66.00	4.50	2.17	118.10	0.0274
1.78	66.00	4.50	2.17	120.60	0.0280
1.78	66.00	4.50	2.16	121.60	0.0285
1.75	81.00	4.12	1.59	115.00	0.0463
1.75	81.00	4.12	1.58	115.00	0.0469
1.75	81.00	4.12	1.58	118.60	0.0483
1.93	83.50	4.50	1.59	112.60	0.0417
1.93	83.50	4.50	1.59	122.60	0.0454
1.93	83.50	4.50	1.59	116.50	0.0431
1.93	83.50	4.50	1.59	117.10	0.0433
1.88	77.00	4.51	1.56	152.90	0.0620
1.88	77.00	4.51	1.59	93.60	0.0365
1.88	77.00	4.51	1.58	96.60	0.0382
1.88	77.00	4.51	1.58	102.80	0.0406

Appendix 2

Female - Underwater Passive Resistance Data

Height (m)	Mass (kg)	Slenderness	Speed (ms ⁻¹)	Passive Resistance (N)	Ct
1.71	61.00	4.41	2.22	143.56	0.0340
1.75	70.00	4.31	1.91	78.10	0.0231
1.75	70.00	4.31	1.94	85.30	0.0245
1.75	70.00	4.31	1.94	88.50	0.0254
1.75	70.00	4.31	1.94	74.10	0.0213
1.75	70.00	4.31	1.95	79.00	0.0225
1.75	70.00	4.31	1.95	80.50	0.0229
1.75	70.00	4.31	1.96	76.00	0.0214
1.75	70.00	4.31	1.95	77.40	0.0220
1.75	70.00	4.31	1.95	79.00	0.0225
1.75	70.00	4.31	1.96	81.40	0.0229
1.75	70.00	4.31	1.93	74.70	0.0217
1.75	70.00	4.31	1.96	76.60	0.0216
1.75	70.00	4.31	1.96	74.30	0.0209
1.75	70.00	4.31	1.95	76.10	0.0216
1.75	70.00	4.31	1.96	77.70	0.0219
1.75	70.00	4.31	1.95	74.60	0.0212
1.75	70.00	4.31	1.97	72.00	0.0201
1.75	70.00	4.31	1.96	75.00	0.0211
1.75	70.00	4.31	1.94	74.10	0.0213
1.75	70.00	4.31	1.96	78.70	0.0221
1.75	70.00	4.31	1.92	73.00	0.0214
1.75	70.00	4.31	1.96	73.20	0.0206
1.75	70.00	4.31	1.97	72.10	0.0201
1.75	70.00	4.31	1.94	72.40	0.0208
1.75	70.00	4.31	1.95	73.70	0.0210
1.75	70.00	4.31	1.94	79.00	0.0227
1.75	70.00	4.31	1.95	77.80	0.0221
1.75	70.00	4.31	1.95	72.60	0.0206
1.75	70.00	4.31	1.96	75.00	0.0211
1.75	70.00	4.31	1.95	70.40	0.0200
1.75	70.00	4.31	1.95	66.30	0.0188
1.75	70.00	4.31	1.95	73.60	0.0209
1.75	70.00	4.31	1.91	71.40	0.0212
1.75	70.00	4.31	1.95	81.20	0.0231
1.75	70.00	4.31	1.96	76.50	0.0215
1.75	70.00	4.31	1.96	77.00	0.0217
1.75	70.00	4.31	1.94	73.90	0.0212
1.75	70.00	4.31	1.97	76.00	0.0212
1.75	70.00	4.31	1.97	68.90	0.0192
1.75	70.00	4.31	1.97	68.50	0.0191
1.75	70.00	4.31	1.97	70.50	0.0196
1.75	70.00	4.31	1.97	72.70	0.0203
1.75	70.00	4.31	1.97	71.20	0.0198
1.75	70.00	4.31	1.96	71.60	0.0201
1.75	70.00	4.31	1.93	64.90	0.0188
1.75	70.00	4.31	1.97	71.10	0.0198
1.75	70.00	4.31	1.93	65.00	0.0189
1.75	70.00	4.31	1.96	67.60	0.0190
1.75	70.00	4.31	1.96	68.10	0.0192
1.75	70.00	4.31	1.93	63.80	0.0185
1.75	70.00	4.31	1.92	65.80	0.0193
1.75	70.00	4.31	1.97	73.90	0.0206
1.75	70.00	4.31	1.97	70.80	0.0197
1.75	70.00	4.31	1.97	72.70	0.0203
1.75	70.00	4.31	1.96	73.90	0.0208
1.75	70.00	4.31	1.96	79.50	0.0224
1.75	70.00	4.31	1.94	67.80	0.0195
1.75	70.00	4.31	1.97	74.00	0.0206

1.75	70.00	4.31	1.97	75.80	0.0211
1.75	70.00	4.31	1.96	74.10	0.0209
1.75	70.00	4.31	1.97	76.80	0.0214
1.75	70.00	4.31	1.92	72.20	0.0212
1.75	70.00	4.31	1.95	78.80	0.0224
1.68	57.00	4.41	1.36	65.20	0.0430
1.68	57.00	4.41	1.38	63.80	0.0408
1.68	57.00	4.41	1.36	70.40	0.0464
1.68	57.00	4.41	1.38	63.70	0.0408
1.68	57.00	4.41	1.38	66.50	0.0426
1.68	57.00	4.41	1.38	64.20	0.0411
1.68	57.00	4.41	1.37	69.00	0.0448
1.68	57.00	4.41	1.39	61.30	0.0387
1.68	57.00	4.41	1.39	61.50	0.0388
1.68	57.00	4.41	1.38	61.10	0.0391
1.68	52.00	4.56	1.06	30.40	0.0342
1.68	52.00	4.56	1.45	47.40	0.0285
1.68	52.00	4.56	1.42	52.00	0.0326
1.68	52.00	4.56	1.45	48.00	0.0289
1.68	52.00	4.56	1.41	53.60	0.0341
1.68	52.00	4.56	1.43	48.00	0.0297
1.68	52.00	4.56	1.43	53.20	0.0329
1.68	52.00	4.56	1.32	39.70	0.0288
1.68	52.00	4.56	1.44	53.30	0.0325
1.68	52.00	4.56	1.45	50.00	0.0301
1.68	52.00	4.56	1.45	52.70	0.0317
1.68	52.00	4.56	1.46	50.00	0.0297
1.57	50.00	4.32	1.68	46.90	0.0224
1.57	50.00	4.32	1.46	38.50	0.0244
1.57	50.00	4.32	1.41	44.80	0.0304
1.57	50.00	4.32	1.44	38.30	0.0249
1.57	50.00	4.32	1.40	46.80	0.0323
1.57	50.00	4.32	1.45	39.50	0.0254
1.57	50.00	4.32	1.41	45.40	0.0308
1.57	50.00	4.32	1.40	46.90	0.0323
1.57	50.00	4.32	1.45	37.90	0.0243
1.57	50.00	4.32	1.40	45.70	0.0315
1.57	50.00	4.32	1.42	43.70	0.0293
1.57	50.00	4.32	1.40	46.30	0.0319

Appendix 2

Male - Underwater Passive Resistance Data

Height (m)	Mass (kg)	Slenderness	Speed (ms ⁻¹)	Passive Resistance (N)	Ct
1.83	83.00	4.27	2.19	131.94	0.0268
1.82	84.00	4.24	2.20	184.19	0.0370
1.75	81.00	4.12	1.90	129.30	0.0364
1.75	81.00	4.12	1.90	128.50	0.0362
1.75	81.00	4.12	1.90	136.60	0.0385
1.75	81.00	4.12	1.89	138.90	0.0395
1.75	81.00	4.12	1.91	125.30	0.0349
1.75	81.00	4.12	1.89	126.40	0.0360
1.75	81.00	4.12	1.91	126.00	0.0351
1.75	81.00	4.12	1.91	132.40	0.0369
1.75	81.00	4.12	1.91	132.80	0.0370
1.75	81.00	4.12	1.89	118.60	0.0338
1.88	85.00	4.36	1.94	95.70	0.0241
1.88	85.00	4.36	1.90	88.50	0.0232
1.88	85.00	4.36	1.95	90.40	0.0225
1.88	85.00	4.36	1.95	85.70	0.0213
1.88	85.00	4.36	1.96	77.90	0.0192
1.88	85.00	4.36	1.95	82.80	0.0206
1.88	85.00	4.36	1.96	81.90	0.0202
1.88	85.00	4.36	1.94	84.90	0.0213
1.88	85.00	4.36	1.95	81.00	0.0202
1.88	85.00	4.36	1.96	81.80	0.0201
1.88	85.00	4.36	1.96	83.30	0.0205
1.88	85.00	4.36	1.93	81.80	0.0208
1.88	85.00	4.36	1.96	82.40	0.0203
1.88	85.00	4.36	1.95	81.40	0.0203
1.88	85.00	4.36	1.95	79.90	0.0199
1.88	85.00	4.36	1.94	80.00	0.0201
1.88	85.00	4.36	1.93	81.00	0.0206
1.88	85.00	4.36	1.96	77.70	0.0191
1.88	85.00	4.36	1.95	80.50	0.0200
1.88	85.00	4.36	1.95	85.40	0.0212
1.88	85.00	4.36	1.94	81.60	0.0205
1.88	85.00	4.36	1.93	77.20	0.0196
1.88	85.00	4.36	1.95	77.60	0.0193
1.88	85.00	4.36	1.96	79.70	0.0196
1.88	85.00	4.36	1.92	91.90	0.0236
1.88	85.00	4.36	1.94	92.70	0.0233
1.88	85.00	4.36	1.94	87.70	0.0220
1.88	85.00	4.36	1.95	83.80	0.0209
1.88	85.00	4.36	1.94	81.60	0.0205
1.88	85.00	4.36	1.95	81.20	0.0202
1.88	85.00	4.36	1.95	78.10	0.0194
1.88	85.00	4.36	1.94	86.50	0.0217
1.88	85.00	4.36	1.94	83.10	0.0209
1.88	85.00	4.36	1.94	86.40	0.0217
1.88	85.00	4.36	1.95	82.10	0.0204
1.88	85.00	4.36	1.95	81.70	0.0203
1.88	85.00	4.36	1.95	82.60	0.0206
1.88	85.00	4.36	1.96	80.10	0.0197
1.88	85.00	4.36	1.93	81.60	0.0207
1.88	85.00	4.36	1.96	81.90	0.0202
1.88	85.00	4.36	1.94	81.10	0.0204
1.88	85.00	4.36	1.95	88.80	0.0221
1.88	85.00	4.36	1.96	84.50	0.0208
1.88	85.00	4.36	1.95	81.80	0.0204
1.88	85.00	4.36	1.90	70.40	0.0185
1.88	85.00	4.36	1.94	81.50	0.0205
1.88	85.00	4.36	1.94	82.80	0.0208

1.88	85.00	4.36	1.92	78.20	0.0201
1.88	85.00	4.36	1.95	81.80	0.0204
1.88	85.00	4.36	1.96	80.00	0.0197
1.88	85.00	4.36	1.95	84.40	0.0210
1.88	85.00	4.36	1.93	84.20	0.0214
1.88	85.00	4.36	1.96	82.30	0.0203
1.88	85.00	4.36	1.95	84.50	0.0210
1.88	85.00	4.36	1.95	88.40	0.0220
1.88	85.00	4.36	1.96	84.40	0.0208
1.88	85.00	4.36	1.96	85.20	0.0210
1.88	85.00	4.36	1.96	83.70	0.0206
1.88	85.00	4.36	1.94	91.00	0.0229
1.88	85.00	4.36	1.94	90.30	0.0227
1.88	85.00	4.36	1.95	89.40	0.0222
1.88	85.00	4.36	1.96	85.50	0.0211
1.75	81.00	4.12	1.60	84.90	0.0337
1.75	81.00	4.12	1.61	81.60	0.0320
1.75	81.00	4.12	1.61	82.00	0.0322
1.75	81.00	4.12	1.62	82.30	0.0319
1.75	81.00	4.12	1.62	84.90	0.0329
1.75	81.00	4.12	1.62	83.30	0.0323
1.75	81.00	4.12	1.61	85.50	0.0335
1.75	81.00	4.12	1.62	83.70	0.0324
1.75	81.00	4.12	1.61	90.10	0.0354
1.75	81.00	4.12	1.63	81.10	0.0310
1.93	83.50	4.50	1.60	101.80	0.0372
1.93	83.50	4.50	1.61	91.30	0.0329
1.93	83.50	4.50	1.62	91.00	0.0324
1.93	83.50	4.50	1.62	90.60	0.0323
1.93	83.50	4.50	1.63	87.50	0.0308
1.93	83.50	4.50	1.63	84.70	0.0298
1.93	83.50	4.50	1.62	91.40	0.0326
1.93	83.50	4.50	1.64	85.10	0.0296
1.93	83.50	4.50	1.63	89.00	0.0313
1.93	83.50	4.50	1.62	91.40	0.0326
1.93	83.50	4.50	1.62	90.10	0.0321
1.93	83.50	4.50	1.61	94.20	0.0340
1.88	77.00	4.51	1.62	61.10	0.0230
1.88	77.00	4.51	1.63	62.50	0.0232
1.88	77.00	4.51	1.62	67.30	0.0253
1.88	77.00	4.51	1.60	69.90	0.0269
1.88	77.00	4.51	1.62	64.10	0.0241
1.88	77.00	4.51	1.63	61.80	0.0229
1.88	77.00	4.51	1.64	57.90	0.0212
1.88	77.00	4.51	1.63	60.00	0.0223
1.88	77.00	4.51	1.63	66.40	0.0247

Appendix 3

Wave resistance coefficient lookup table, for a range of human geometry slenderness, determined from Thin Ship Theory

slenderness V	3.51	3.68	3.85	4.04	4.24	4.45	4.69	4.95	5.24	5.58	5.96
1.00	0.1000	0.0951	0.0894	0.0833	0.0765	0.0794	0.0620	0.0547	0.0475	0.0404	0.0337
1.11	0.0606	0.0566	0.0529	0.0496	0.0463	0.0490	0.0395	0.0360	0.0322	0.0284	0.0243
1.21	0.0528	0.0475	0.0430	0.0385	0.0346	0.0354	0.0277	0.0246	0.0218	0.0189	0.0163
1.32	0.0487	0.0436	0.0392	0.0348	0.0309	0.0313	0.0240	0.0210	0.0182	0.0156	0.0132
1.42	0.0460	0.0409	0.0365	0.0321	0.0283	0.0286	0.0217	0.0188	0.0162	0.0138	0.0115
1.53	0.0462	0.0407	0.0360	0.0313	0.0273	0.0273	0.0206	0.0177	0.0151	0.0127	0.0105
1.63	0.0473	0.0415	0.0365	0.0316	0.0274	0.0272	0.0203	0.0173	0.0146	0.0122	0.0100
1.74	0.0475	0.0417	0.0367	0.0317	0.0275	0.0273	0.0202	0.0171	0.0144	0.0119	0.0097
1.84	0.0462	0.0407	0.0359	0.0310	0.0269	0.0269	0.0198	0.0168	0.0140	0.0116	0.0094
1.95	0.0437	0.0387	0.0342	0.0297	0.0258	0.0259	0.0190	0.0161	0.0135	0.0111	0.0090
2.05	0.0406	0.0360	0.0319	0.0278	0.0242	0.0244	0.0179	0.0152	0.0127	0.0105	0.0086
2.16	0.0372	0.0330	0.0293	0.0257	0.0224	0.0226	0.0167	0.0142	0.0119	0.0098	0.0079
2.26	0.0338	0.0301	0.0268	0.0235	0.0205	0.0208	0.0153	0.0130	0.0110	0.0091	0.0074
2.37	0.0306	0.0273	0.0243	0.0213	0.0187	0.0190	0.0141	0.0119	0.0101	0.0084	0.0068
2.47	0.0276	0.0247	0.0221	0.0194	0.0170	0.0173	0.0128	0.0109	0.0092	0.0077	0.0062
2.58	0.0249	0.0224	0.0200	0.0176	0.0155	0.0158	0.0117	0.0100	0.0085	0.0070	0.0058
2.68	0.0225	0.0202	0.0181	0.0160	0.0141	0.0143	0.0107	0.0091	0.0078	0.0064	0.0053
2.79	0.0204	0.0183	0.0164	0.0146	0.0128	0.0131	0.0097	0.0084	0.0071	0.0059	0.0048
2.89	0.0184	0.0166	0.0149	0.0133	0.0117	0.0120	0.0089	0.0077	0.0065	0.0054	0.0045
3.00	0.0168	0.0151	0.0136	0.0121	0.0107	0.0109	0.0082	0.0070	0.0060	0.0050	0.0041

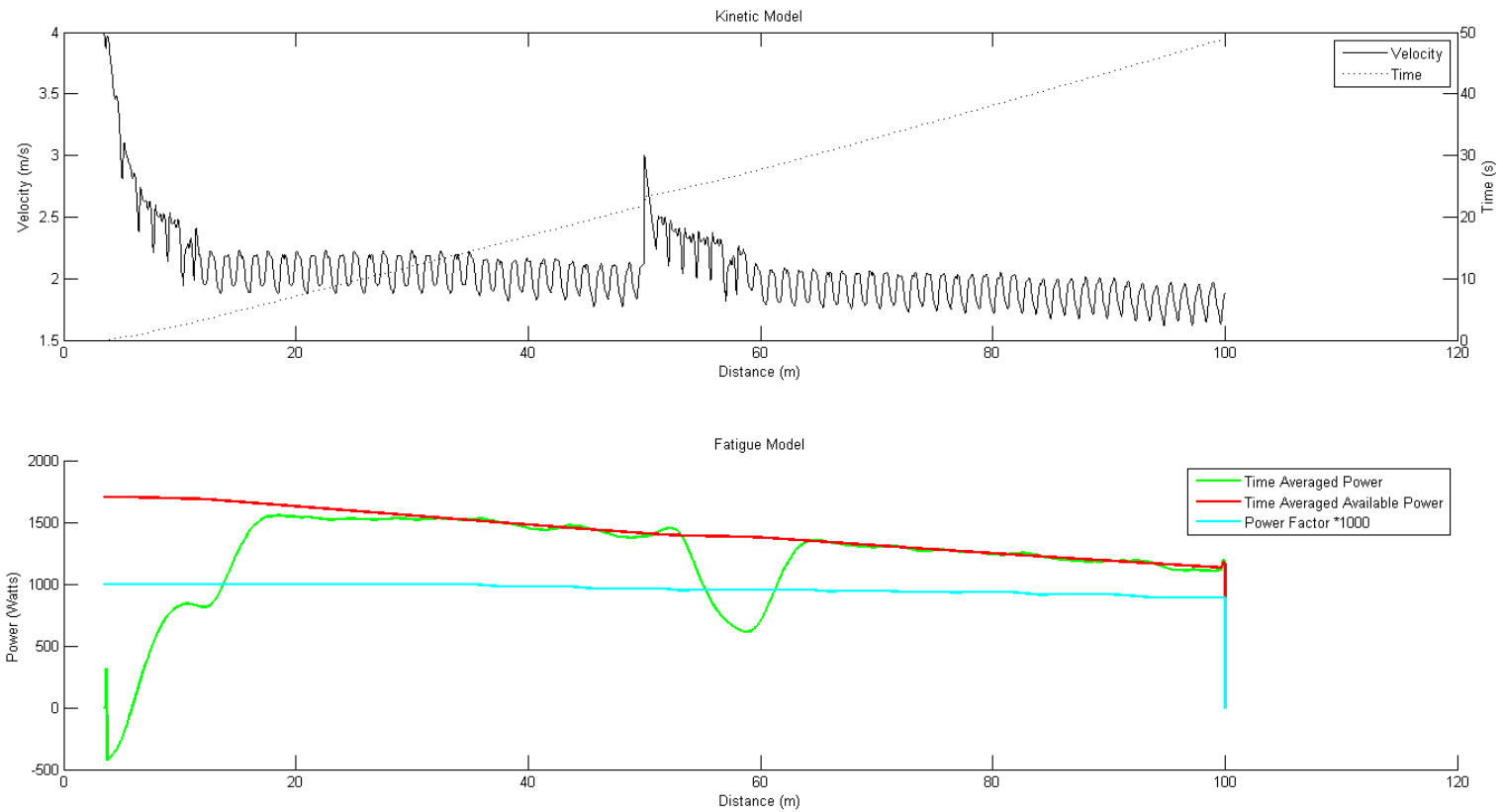
Appendix 4

A key to identify the origin of the experimental data used in Chapter 6. This provides the necessary information to access the data from the SwimSIM database.

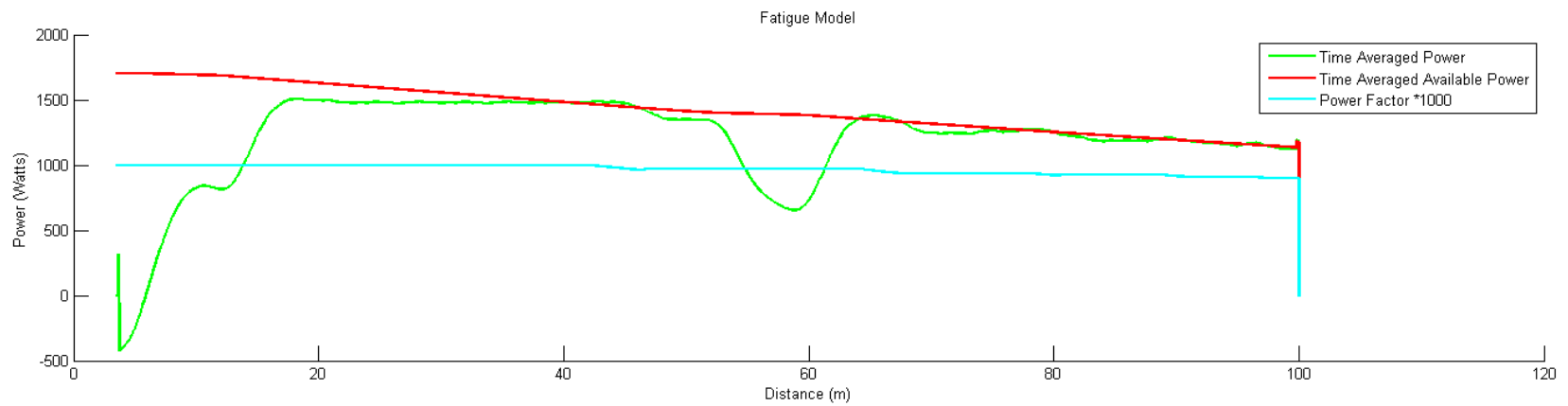
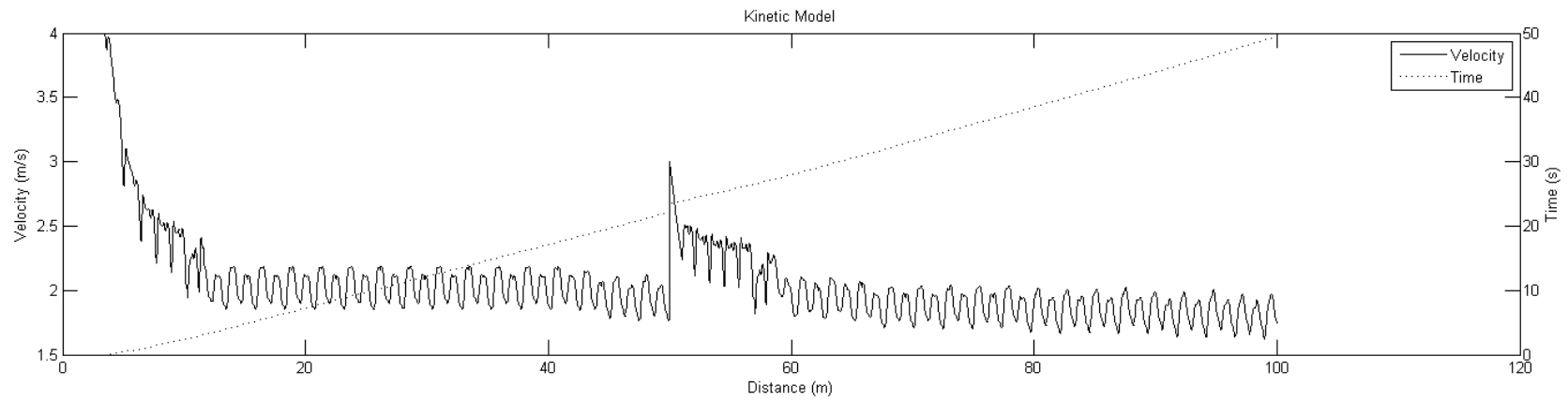
Run ID – SwimSIM Database	Gender	Height (m)	Mass (kg)	Protocol	Speed (ms ⁻¹)	R-T (N)
2011-Jan-6_Athlete_K_003	M	1.93	86	Freestyle Arms only	1.98	92.4
2010-Dec-17_Athlete_M_006	F	1.84	76	Freestyle Arms only	1.68	53.7
2011-Jan-5_Athlete_N_004	F	1.71	62.8	Freestyle Arms only	1.67	42
2010-Dec-17_Athlete_O_009	M	1.75	71	Freestyle Arms only	2.02	101.1
2010-Dec-17_Athlete_P_011	M	1.883	74.4	Freestyle Arms only	1.98	75.5
2010-Dec-17_Athlete_O_008	M	1.75	71	Freestyle Legs only	1.99	134.9
2010-Dec-17_Athlete_O_010	M	1.75	71	Freestyle Legs only	1.99	133.9
2010-Dec-17_Athlete_P_009	M	1.883	74.4	Freestyle Legs only	1.95	123.6
2010-Dec-17_Athlete_P_012	M	1.883	74.4	Freestyle Legs only	1.94	128.4
2010-Dec-17_Athlete_K_005	M	1.93	86	Freestyle Full Stroke	2.03	66
2010-Dec-17_Athlete_M_003	F	1.84	76	Freestyle Full Stroke	1.63	18.6
2011-Oct-14_Athlete_N_003	F	1.71	62.8	Freestyle Full Stroke	1.87	38.6
2010-Dec-17_Athlete_O_006	M	1.75	71	Freestyle Full Stroke	2.03	68.3
2010-Dec-17_Athlete_P_005	M	1.883	74.4	Freestyle Full Stroke	2.01	45
Athlete F Run 46	M	1.82	84	UUS - Low	2.02	136.84
Athlete F Run 48	M	1.82	84	UUS - High	2.02	109.54
Athlete G Run 45	F	1.71	61	UUS - Low	2.02	137.99
Athlete G Run 47	F	1.71	61	UUS - High	2.02	116.16
2012-Dec-17_Athlete_DB	M	1.88	90	All Chute Testing Data	-	-

Appendix 5

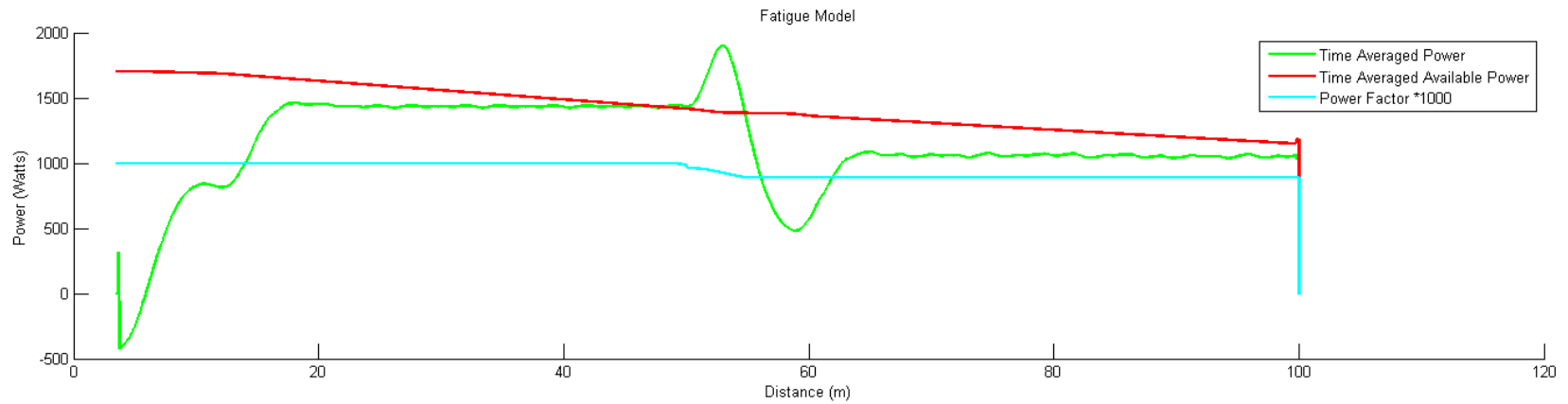
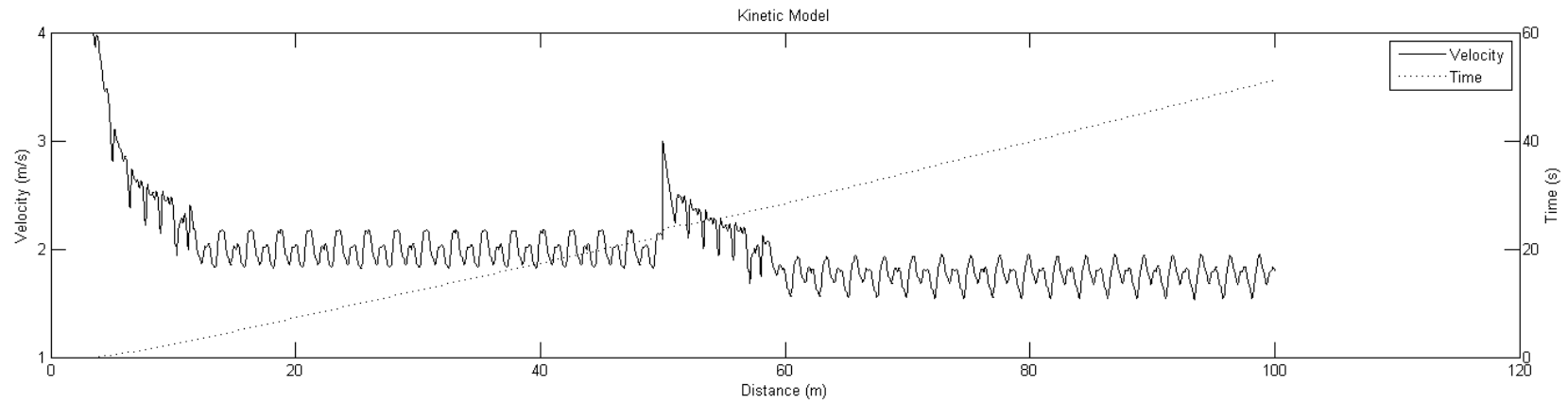
Example race simulation data – Male Imbalance Study, with fatigue modelling.



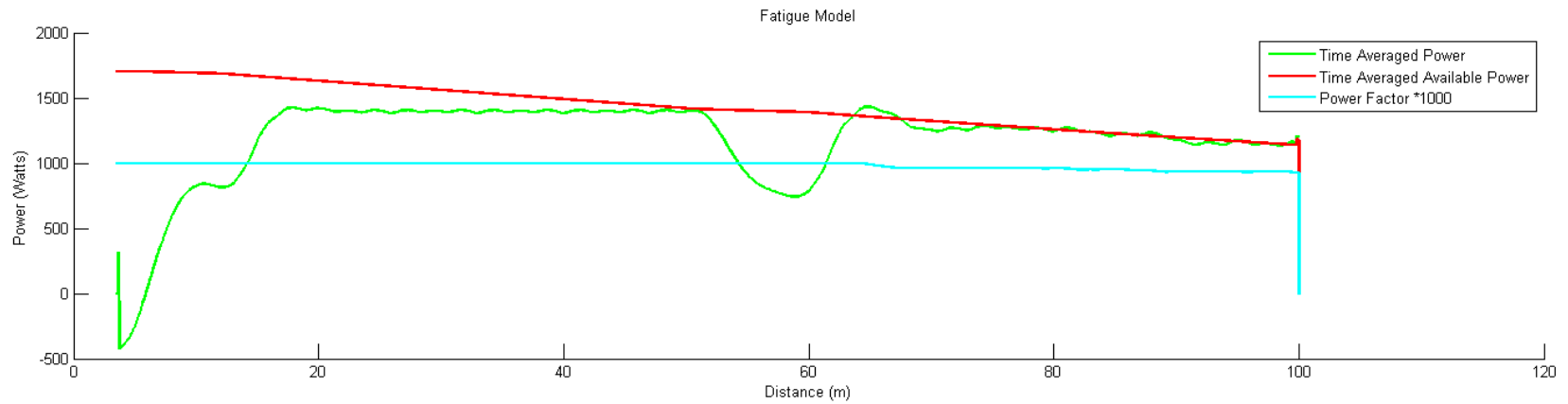
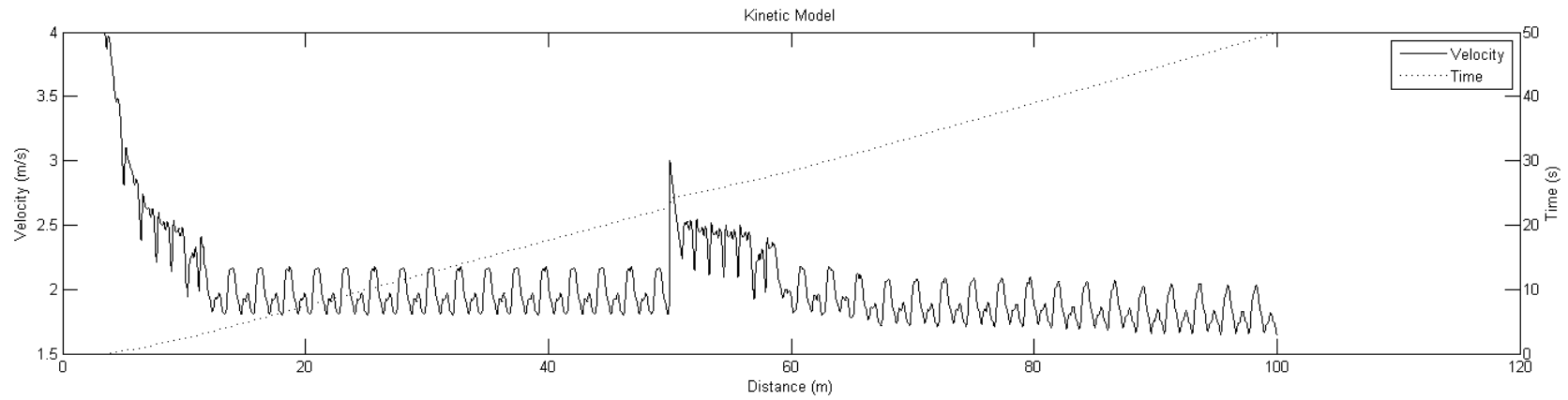
Male 100 m Freestyle – Imbalance Coefficient 1.0



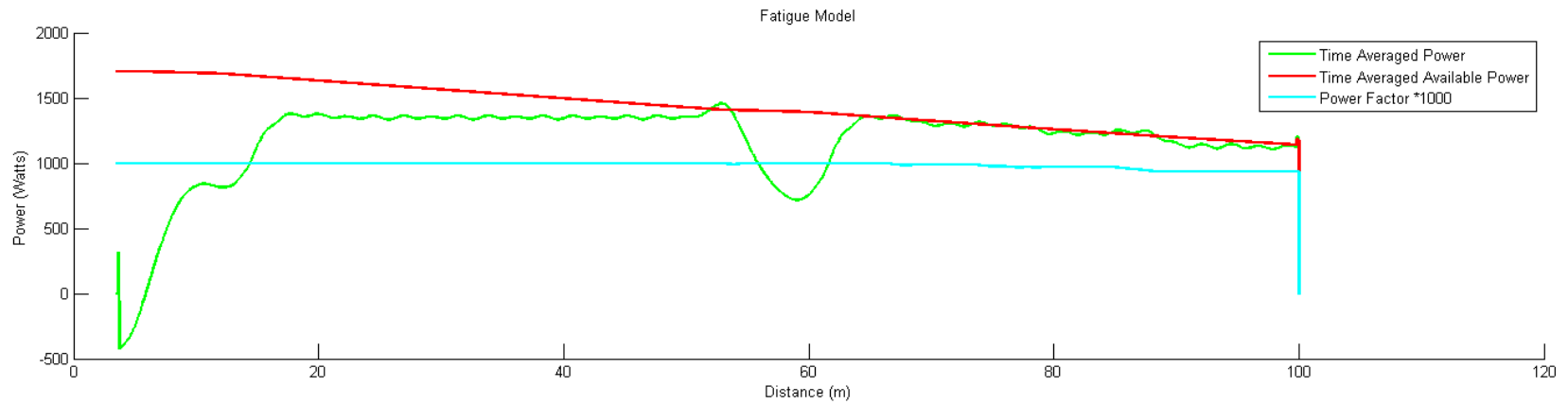
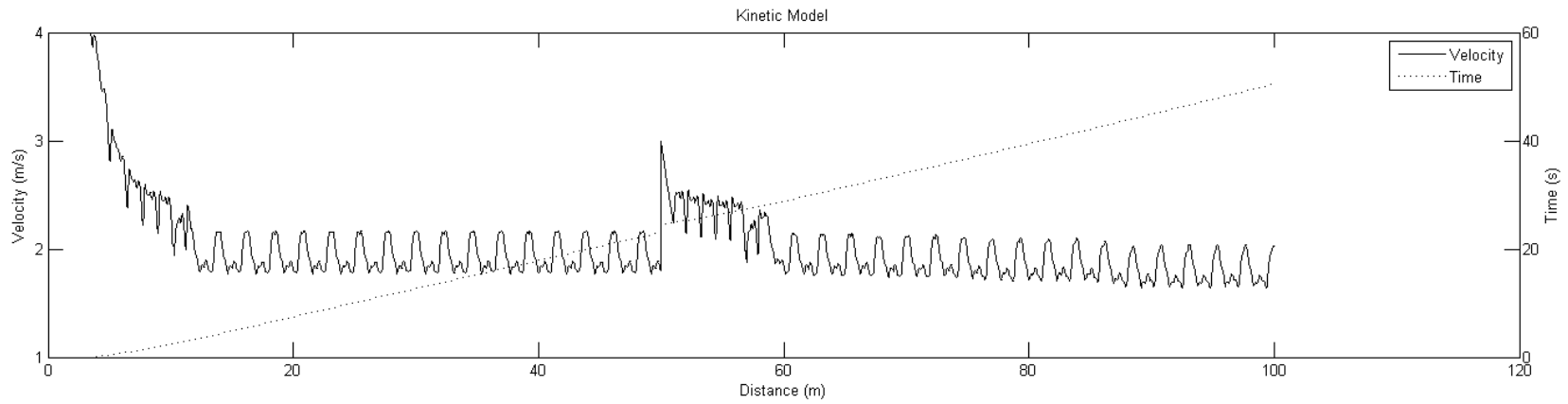
Male 100 m Freestyle - Imbalance Coefficient 0.95



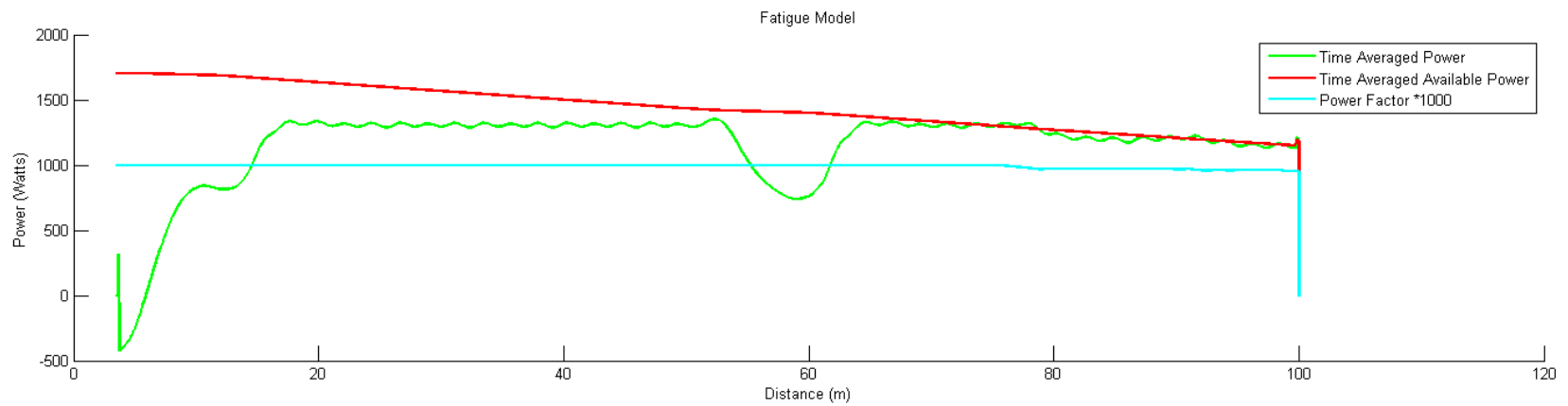
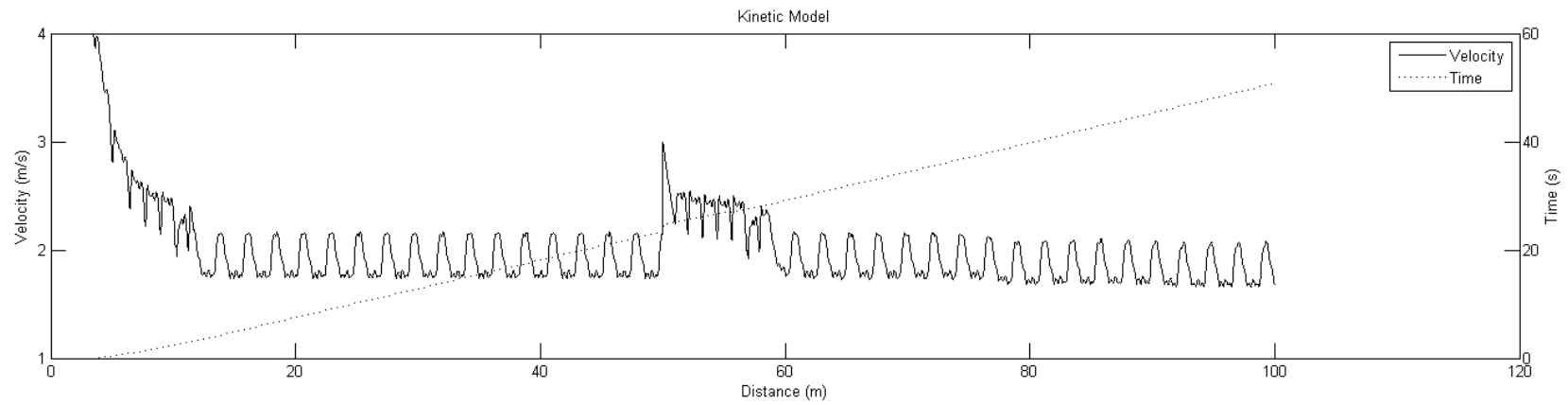
Male 100 m Freestyle - Imbalance Coefficient 0.9



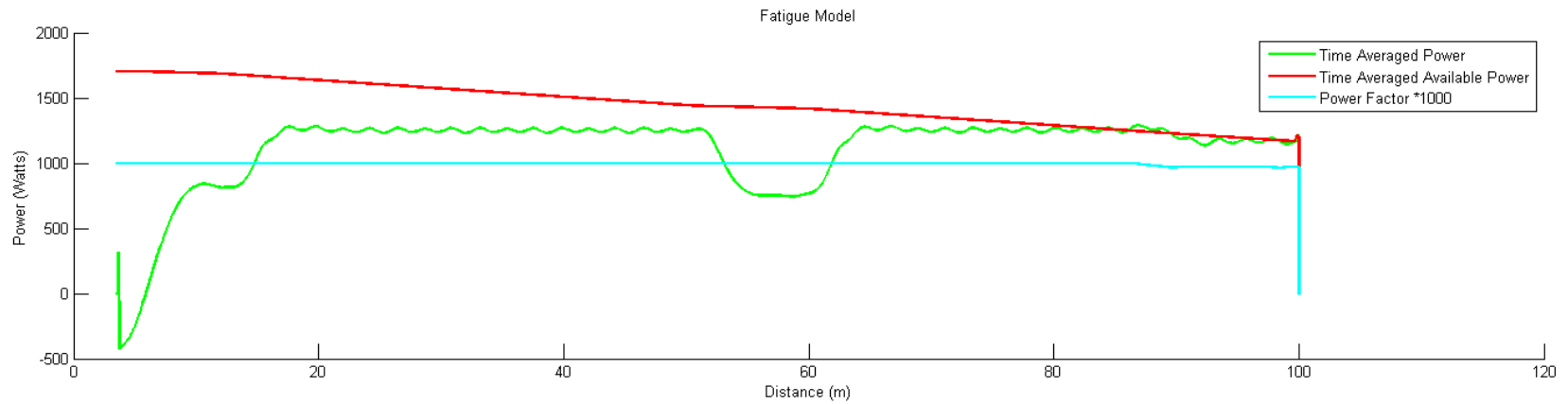
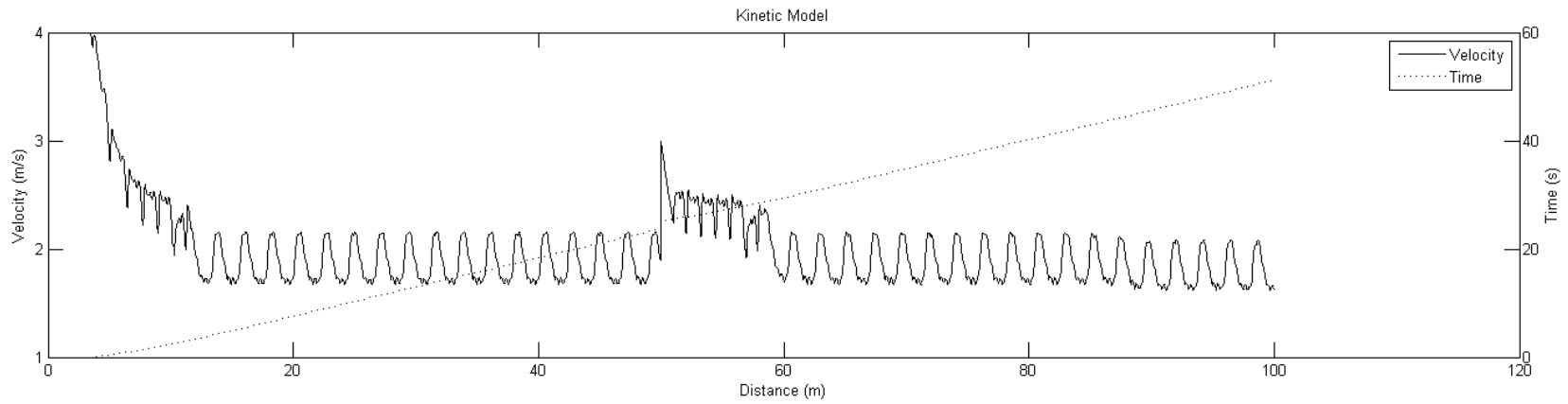
Male 100 m Freestyle - Imbalance Coefficient 0.85



Male 100 m Freestyle - Imbalance Coefficient 0.8



Male 100 m Freestyle - Imbalance Coefficient 0.75



Male 100 m Freestyle - Imbalance Coefficient 0.7

References

- Akis, T., 2004. Experimental and analytical investigation of the mechanics of crawl stroke swimming. *Mechanics Research Communications* 31, 243–261.
- Anderson, J.D., 1985. *Fundamentals of Aerodynamics*, 5th ed. McGraw-Hill Higher Education.
- Arellano, R., 1999. Vortices and propulsion. In: *Applied Proceedings of the XVII International Symposium on Biomechanics in Sports: SWIMMING*. pp. 53 – 65.
- Babb, R.J., 1994. Instrumentation for a Low Drag Hydrodynamic Test Vehicle. In: *Electronic Engineering in Oceanography - Sixth International Conference*. Institute of Oceanographic Sciences Deacon Laboratory, UK, Southampton, pp. 24 – 29.
- Bai, K.J., 1977. The added mass of two-dimensional cylinder heaving in water of finite depth. *Journal of Fluid Mechanics* 81, 85–105.
- Baker, J.S., McCormick, M.C., Robergs, R.A., 2010. Interaction among Skeletal Muscle Metabolic Energy Systems during Intense Exercise. *Journal of nutrition and metabolism* 2010, 1–13.
- Banks, J., 2013. “Modelling the propelled resistance of a freestyle swimmer using Computational Fluid Dynamics”, PhD thesis. University of Southampton, Southampton.
- BERGER, M., 1999. Determining propulsive force in front crawl swimming: a comparison of two methods. *Journal of sports sciences* 37–41.
- Berger, M.A.M., Groot, G. De, Hollander, A.P., 1995. Hydrodynamic Drag and Lift Forces on Human Hand/Arm Models. *Journal of biomechanics* 28.
- Billat, V., 1996. Use of blood lactate measurements for prediction of exercise performance and for control of training. *Sports Medicine* 3, 157–175.
- Bixler, B., Pease, D., Fairhurst, F., 2007. The accuracy of computational fluid dynamics analysis of the passive drag of a male swimmer. *Sports biomechanics / International Society of Biomechanics in Sports* 6, 81–98.
- Bixler, B., Riewald, S., 2002. Analysis of a swimmer’s hand and arm in steady flow conditions using computational fluid dynamics. *Journal of biomechanics* 35, 713–7.
- Blasius, H., 1908. Grenzschichten in Flüssigkeiten mit kleiner reibung. *Zeitschrift für angewandte Mathematik and Physik* 56.
- Brannigan, M., Adali, S., 1981. Mathematical modelling and simulation of a tennis racket. *Medicine and science in sports and exercise* 13, 44–53.

References

- Childress, S., 1981. *Mechanics of swimming and flying*. Cambridge University Press.
- Clements, R., 1959. An Analysis of Ship Model Correlation Data Using the 1957 ITTC Line. *Transactions of the Royal Institute of Naval Architects* 101, 373-402.
- Cossor, J., Mason, B., 2001. Swim start performances at the Sydney 2000 Olympic Games. *Proceedings of XIX Symposium on Biomechanics in Sport*.
- Date, J.C., Turnock, S.R., 2000. Computational fluid dynamics estimation of skin friction experienced by a plane moving through water. *Transactions of the Royal Institute of Naval Architects* 142, 116-135.
- Deschodt, V.J., Arsac, L.M., Rouard, a H., 1999. Relative contribution of arms and legs in humans to propulsion in 25-m sprint front-crawl swimming. *European journal of applied physiology and occupational physiology* 80, 192-9.
- Dhawan, S., Engineer, I., 1953. Direct measurements of skin friction. NACA Washington.
- Doyle, J.C., Francis, B.A., Tannenbaum, A.R., 2009. *Feedback Control Theory* (Dover Books on Engineering). Dover Publications Inc.
- DuBois, D., DuBois, E., 1916. A formula to estimate the approximate surface area if height and weight be known. *Archives of Internal Medicine* 17, 863-871.
- Eyer, L., Bartholdi, P., 1999. Variable stars: which Nyquist frequency? *Astronomy and Astrophysics Supplement Series*.
- FINA, 2011. FINA Requirements For Swimwear Approval [WWW Document]. URL <http://www.fina.org/H2O/docs/rules/FRSA.pdf>
- FINA, 2012. Facility Rules 2 - Swimming Pools [WWW Document]. URL http://www.fina.org/H2O/index.php?option=com_content&view=article&id=365:fr-2-swimming-pools&catid=88:facilities-rules&Itemid=184
- Fish, F., 1993. Power output and propulsive efficiency of swimming bottlenose dolphins (*Tursiops truncatus*). *Journal of Experimental Biology* 193, 179-193.
- Fish, F., 1994. Influence of Hydrodynamic-Design and Propulsive Mode on Mammalian Swimming Energetics. *Australian Journal of Zoology* 42, 79.
- Gadd, G.E., Hogben, N., 1965. The determination of wave resistance from measurements of the wave profile. NPL Ship Division Report No. 70.
- Gardano, P., Dabnichki, P., 2006. On hydrodynamics of drag and lift of the human arm. *Journal of biomechanics* 39, 2767-73.

- Gourgoulis, V., Aggeloussis, N., Vezos, N., Kasimatis, P., Antoniou, P., Mavromatis, G., 2008. Estimation of hand forces and propelling efficiency during front crawl swimming with hand paddles. *Journal of biomechanics* 41, 208–15.
- Hatze, H., 1981. A comprehensive model for human motion simulation and its application to the take-off phase of the long jump. *Journal of Biomechanics* 14.3, 135–142.
- Hesterberg, T., Moore, D., Monaghan, S., 2010. Bootstrap methods and permutation tests. In: *Introduction to the Practice of Statistics*. W. H. Freeman, Boston, pp. 14.1–14.70.
- Hill, D., Smith, J., 1993. Gender difference in anaerobic capacity: role of aerobic contribution. *British journal of sports medicine* 27.
- Hoar, W., Randall, D., 1978. *Locomotion, Volume 7: Fish Physiology*. Academic Press.
- Hochstein, S., Blickhan, R., Kunze, S., Brücker, C., Buchner, M., 2009. “Flow around a human underwater undulatory swimmer”, Department Report. University of Jena, Jena.
- Hoerner, S., 1965. *Fluid-Dynamic Drag: Theoretical, Experimental and Statistical Information*, 2nd ed. Hoerner Fluid Dynamics.
- Hoffman, J., 2002. *Physiological Aspect of Sport Training and Performance*. Human Kinetics, Champaign.
- Hollander, A.P., De Groot, G., Van Ingen Schenau, G.J., Toussaint, H.M., De Best, H., Peeters, W., Meulemans, A., Schreurs, A.W., 1986. Measurement of active drag during crawl arm stroke swimming. *Journal of sports sciences* 4, 21–30.
- Insel, M., 1990. “An Investigation Into the Resistance Components of High Speed Displacement Catamarans”, PhD thesis. University of Southampton, Southampton.
- Insel, M., Molland, A.F., Wellicome, J.F., 1994. “Wave Resistance Prediction of a Catamaran by Linearised Theory”, Department report. Faculty of Naval Architecture and Ocean Engineering, Istanbul Technical University, TURKEY.
- Keys, M., Lyttle, A., Blanksby, B.A., Cheng, L., 2010. A Full Body Computational Fluid Dynamic Analysis of the Freestyle Stroke of a Previous Sprint Freestyle World Record Holder. In: *11th International Symposium of Biomechanics and Medicine in Swimming*. Oslo, Norway., pp. 105–107.
- Kolmogorov, S.V., Duplishcheva, O.A., 1992. Active Drag, Useful Mechanical Power Output and Hydrodynamic Force Coefficient in Different Swimming Strokes at Maximal Velocity. *Journal of Biomechanics* 25, 311–318.

References

- Krzywicki, H., Chinn, K., 1966. Human body density and fat of an adult male population as measured by water displacement. *The American Journal of Clinical Nutrition* 20.4, 305–310.
- Lauder, M. a, Dabnichki, P., 2005. Estimating propulsive forces--sink or swim? *Journal of biomechanics* 38, 1984–90.
- Lees, A., 2002. Technique analysis in sports: a critical review. *Journal of Sports Sciences* 20.10, 37–41.
- Lighthill, M.J., 1960. Note on the swimming of slender fish. *Journal of Fluid Mechanics* 9, 305–317.
- Lighthill, M.J., 1969. *Mathematical Biofluidmechanics*. University of Cambridge, Cambridge.
- Lighthill, M.J., 1971. Large-Amplitude Elongated-Body Theory of Fish Locomotion. *Proceedings of the Royal Society B: Biological Sciences* 179, 125–138.
- Liu, H., 1999. A Numerical Study of Undulatory Swimming. *Journal of Computational Physics* 155, 223–247.
- Lyttle, A., 2000. “Hydrodynamics of the human body during the freestyle tumble turn”, PhD Thesis. Department of Human Movement and Exercise Science, The University of Western Australia.
- Lyttle, A., Elliott, C., 1998. The effect of depth and velocity on drag during the streamlined glide. *Journal of Swimming Research* 13, 15–22.
- Maglischo, E.W., 2002. *Swimming Fastest*, 3rd ed. Human Kinetics, Champaign.
- Marinho, D., 2009. “The Study Of Swimming Propulsion Using Computational Fluid Dynamics A three-dimensional analysis of the swimmer ’ s hand and forearm A three-dimensional analysis of the swimmer ’ s hand and forearm”, PhD Thesis. Universidade de Trás-os-Montes e Alto Douro Vila Real.
- Mason, B., Cossor, J., 2001. Swim turn performances at the Sydney 2000 Olympic Games. *Proceedings of XIX Symposium on Biomechanics in Sport*.
- Mason, B., Formosa, D., 2009. A COMPARISON BETWEEN THE VALUES OBTAINED FROM ACTIVE DRAG ANALYSIS COMPARED TO FORCES PRODUCED IN TETHERED SWIMMING. *International Society of Biomechanics in Sport Proceedings Archive*. Vol. 1. No. 1.
- Mason, B., Formosa, D., Rollason, S., 2007. A comparison between the values obtained from active drag analysis compared to forces produced in tethered swimming. *International Society of Biomechanics in Sport Proceedings Archive*. Vol. 1. No. 1.

- Mason, B.R., Formosa, D.P., Toussaint, H.M., 2010. A Method to Estimate Drag over a Range of Swimming Velocities which may be used to Evaluate the Stroke Mechanics of a Swimmer. In: *Biomechanics and Medicine in Swimming XI*. pp. 124 – 126.
- Matsuuchi, K., Miwa, T., Nomura, T., Sakakibara, J., Shintani, H., Ungerechts, B.E., 2009. Unsteady flow field around a human hand and propulsive force in swimming. *Journal of biomechanics* 42, 42–7.
- Michell, J., 1898. XI. The wave-resistance of a ship. *The London, Edinburgh, and Dublin Philosophical Magazine and Journal of Science* 45.272, 106–123.
- Minetti, A.E., Machtsiras, G., Masters, J.C., 2009. The optimum finger spacing in human swimming. *Journal of biomechanics* 42, 2188–90.
- Molland, A.F., Turnock, S.R., Hudson, D.A., 2011. *Ship Resistance and Propulsion: Practical Estimation of Ship Propulsive Power*. Cambridge University Press, London, pp. 51–57.
- Naemi, R., Easson, W.J., Sanders, R.H., 2009. Hydrodynamic glide efficiency in swimming. *Journal of science and medicine in sport / Sports Medicine Australia* 13, 444–451.
- Nakashima, M., 2007. Mechanical Study of Standard Six Beat Front Crawl Swimming by Using Swimming Human Simulation Model. *Journal of Fluid Science and Technology* 2, 290–301.
- Nakashima, M., 2009. Simulation Analysis of the Effect of Trunk Undulation on Swimming Performance in Underwater Dolphin Kick of Human. *Journal of Biomechanical Science and Engineering* 4, 94–104.
- Nakashima, M., Kiuchi, H., Nakajima, K., 2010. Multi Agent/Object Simulation in Human Swimming. *Journal of Biomechanical Science and Engineering* 5.4, 380–387.
- Nakashima, M., Satou, K., Miura, Y., 2007. Development of Swimming Human Simulation Model Considering Rigid Body Dynamics and Unsteady Fluid Force for Whole Body. *Journal of Fluid Science and Technology* 2, 56–67.
- NASA, 1978. *Anthropometry for Designers* Anthropology Staff/Webb Associates. pp. 7–78.
- NECHITA, F., 2009. BIOMECHANICS IN SPORT. *Bulletin of the Transilvania* 2.51, 135–138.
- Newman, J., 1977. *Marine hydrodynamics*. MIT Press.
- Patton, J., Vogel, J., Mello, R., 1982. Evaluation of a maximal predictive cycle ergometer test of aerobic power. *European journal of applied physiology and occupational physiology* 49, 131–140.

References

- Perrine, J.J., Edgerton, V.R., 1978. Muscle force-velocity and power-velocity relationships under isokinetic loading. *Medicine and science in sports* 10, 159-66.
- Picasso, B., Bertetto, A., Ruggiu, M., 2001. Fish and ships: can fish inspired propulsion outperform traditional propeller based systems? In: *Proceedings of Marine Technology Symp.* Szczecin, Poland.
- Polidori, G., Tajar, R., Fohanno, S., Mai, T.H., Lodini, a, 2006. Skin-friction drag analysis from the forced convection modeling in simplified underwater swimming. *Journal of biomechanics* 39, 2535-41.
- Pollock, M. L., Laughridge, E.E., Coleman, B., Linnerud, A.C., Jackson, A., 1975. Prediction of body density in young and middle-aged women. *Journal of applied physiology* 38, 745-749.
- Pripstein, L.P., Rhodes, E.C., McKenzie, D.C., Coutts, K.D., 1999. Aerobic and anaerobic energy during a 2-km race simulation in female rowers. *European journal of applied physiology and occupational physiology* 79, 491-4.
- Proakis, J.G., Ingle, V.K., 2011. *Essentials of Digital Signal Processing Using MATLAB.* Nelson Engineering.
- Robinson, S., 1997a. Simulation model verification and validation: increasing the users' confidence. *Proceedings of the 29th conference on Winter simulation.*
- Robinson, S., 1997b. Simulation model verification and validation: increasing the users' confidence. *Proceedings of the 29th conference on Winter simulation.*
- Rouboa, A., Silva, A., Leal, L., Rocha, J., Alves, F., 2006. The effect of swimmer's hand/forearm acceleration on propulsive forces generation using computational fluid dynamics. *Journal of biomechanics* 39, 1239-48.
- Sargent, R., 2005. Verification and validation of simulation models. *Proceedings of the 37th conference on Winter simulation* 130-143.
- Sharp, R., Hackney, A., Cain, S., 1988. The effect of shaving body hair on the physiological cost of freestyle swimming. *Journal of Swimming Research* 4, 9 - 13.
- Shuter, B., Aslani, A., 2000. Body surface area: Du Bois and Du Bois revisited. *European journal of applied physiology* 82, 250-4.
- Sidelnik, N.O., Young, B.W., 2006. Optimising the freestyle swimming stroke: the effect of finger spread. *Sports Engineering* 9, 129-135.

- Silva, A., Rouboa, A., 2008. Analysis of drafting effects in swimming using computational fluid dynamics. *Journal of Sports Science and Medicine* 7.1, 60-66.
- Sprigings, E., Neal, R., 2000. An insight into the importance of wrist torque in driving the golfball: a simulation study. *Journal of Applied Biomechanics* 16.4, 356-366.
- Stern, F., Muste, M., Beninati, M., Eichinger, W., 1999. Summary of experimental uncertainty assessment methodology with example. IIHR Report, Iowa Institute of Hydraulic Research, The University of Iowa, Iowa City.
- Takagi, H., 1998. A Hydrodynamic Study of Active Drag in Swimming. *The Japan Society of Mechanical Engineers* 42, 171-177.
- Taunton, D.J., Turnock, S.R., Hudson, D.A., Webb, A., Banks, J., 2013. Predicting wave drag of swimmers using slender body theory, Department Report. Fluid Structure Interactions, University of Southampton, Southampton.
- Taunton, D.J., Turnock, S.R., Hudson, D.A., Webb, A.P., Banks, J., 2012. Predicting wave drag of swimmers using slender body theory, Department Report. Fluid Structure Interactions, University of Southampton, Southampton.
- Toussaint, H., 2002. Wave drag in front crawl swimming. *ISBS-Conference Proceedings* 279-282.
- Toussaint, H.M., Roos, P.E., Kolmogorov, S., 2004. The determination of drag in front crawl swimming. *Journal of Biomechanics* 37, 1655-1663.
- Toussaint, H.M., Truijens, M., Elzinga, M.J., Van De Ven, A., De Best, H., Snabel, B., De Groot, G., 2002. Effect of a Fast-skin "Body" Suit on Drag during Front Crawl Swimming. *Sports Biomechanics* 1, 1-10.
- Toussaint, H.M., Van den Berg, C., Beek, W.J., 2002. "Pumped-up propulsion" during front crawl swimming. *Medicine and science in sports and exercise* 34, 314-9.
- Triantafyllou, G., 1993. Optimal thrust development in oscillating foils with application to fish propulsion. *Journal of Fluids and Structures* 7, 205-224.
- Triantafyllou, M.S., Triantafyllou, G.S., Gopalkrishnan, R., 1991. Wake mechanics for thrust generation in oscillating foils. *Physics of Fluids A: Fluid Dynamics* 3, 28-35.
- Tupper, E.C., Rawson, K.J., 2001. *Basic Ship Theory*, 5th ed. Butterworth-Heinemann.
- Vennell, R., Pease, D., Wilson, B., 2006. Wave drag on human swimmers. *Journal of Biomechanics* 39, 664-671.

References

- Verbraecken, J., Van de Heyning, P., De Backer, W., Van Gaal, L., 2006. Body surface area in normal-weight, overweight, and obese adults. A comparison study. *Metabolism: clinical and experimental* 55, 515–24.
- Vogel, S., 1940. *Life in Moving Fluids: The Physical Biology of Flow*, Second Edition. Princeton University Press, Princeton.
- Von Loebbecke, A., Mittal, R., Fish, F., Mark, R., 2009a. A comparison of the kinematics of the dolphin kick in humans and cetaceans. *Human movement science* 28, 99–112.
- Von Loebbecke, A., Mittal, R., Fish, F., Mark, R., 2009b. Propulsive efficiency of the underwater dolphin kick in humans. *Journal of biomechanical engineering* 131, 054504.
- Von Loebbecke, A., Mittal, R., Mark, R., Hahn, J., 2009. A computational method for analysis of underwater dolphin kick hydrodynamics in human swimming. *Sports biomechanics / International Society of Biomechanics in Sports* 8, 60–77.
- Weihs, D., 2006. Semi-infinite vortex trails, and their relation to oscillating airfoils. *Journal of Fluid Mechanics* 54, 679.
- Winter, D., 1979. Biomechanics of human movement. *Medical Physics* 8, 528.
- Yu, J., Yi, C., 2009. Analysis of Relationship between Efficiency and Motion Parameters of Robotic Fish. 2009 International Conference on Intelligent Human-Machine Systems and Cybernetics 401–404.
- Zaïdi, H., Taïar, R., Fohanno, S., Polidori, G., 2008. Analysis of the effect of swimmer's head position on swimming performance using computational fluid dynamics. *Journal of biomechanics* 41, 1350–8.